Development of Novel Silk Fibroin/Carboxymethyl Cellulose Based Electrospun Nanofibrous Scaffolds for Bone Tissue Engineering Application

Bhisham Narayan Singh

Department of Biotechnology and Medical Engineering
National Institute of Technology Rourkela

DEVELOPMENT OF NOVEL SILK FIBROIN/CARBOXYMETHYL CELLULOSE BASED ELECTROSPUN NANOFIBROUS SCAFFOLDS FOR BONE TISSUE ENGINEERING APPLICATION

Dissertation submitted in partial fulfillment
of the requirements of the degree of
Doctor of Philosophy

in

Biotechnology and Medical Engineering

by

Bhisham Narayan Singh

(Roll Number: 511BM605)

based on the research carried out
under the supervision of

Prof. Krishna Pramanik

January, 2017

Department of Biotechnology and Medical Engineering
National Institute of Technology Rourkela

Department of Biotechnology and Medical engineering
National Institute of Technology Rourkela

January 5, 2017

Certificate of Examination

Roll Number: 511BM605

Name: Bhisham Narayan Singh

Title of Dissertation: Development of Novel Silk Fibroin/Carboxymethyl Cellulose Based Electrospun Nanofibrous Scaffolds for Bone Tissue Engineering Application

We the below signed, after checking the dissertation mentioned above and the official record book (s) of the student, hereby state our approval of the dissertation submitted in partial fulfillment of the requirements of the degree of *Doctor of Philosophy* in *Biotechnology and Medical engineering* at *National Institute of Technology Rourkela*. We are satisfied with the volume, quality, correctness, and originality of the work.

…….	…….
Krishna Pramanik Principal Supervisor	*Amit Biswas* Member (DSC)
…….	…….
A.Thirugnanam Member (DSC)	*Samir Kumar Patra* Member (DSC)
…….	…….
Utpal Bora (Examiner)	*Mukesh Kumar Gupta* (HOD)

…….
Subhankar Paul
Chairman (DSC)

Department of Biotechnology and Medical Engineering
National Institute of Technology Rourkela

Prof. Krishna Pramanik
Professor

January 5, 2017

Supervisor's Certificate

This is to certify that the work presented in this dissertation entitled " Development of Novel Silk Fibroin/Carboxymethyl Cellulose Based Electrospun Nanofibrous Scaffolds for Bone Tissue Engineering Application " by "Bhisham Narayan Singh", Roll Number 511BM605, is a record of original research carried out by him/her under our supervision and guidance in partial fulfillment of the requirements of the degree of *Doctor of Philosophy* in *Biotechnology and Medical Engineering*. Neither this dissertation nor any part of it has been submitted for any degree or diploma to any institute or university in India or abroad.

……

Prof. Krishna Pramanik
(Principal Supervisor)

Dedicated To

MY GRANDMOTHER

Declaration of Originality

I, Bhisham Narayan Singh, Roll Number 511BM605 hereby declare that this dissertation entitled “Development of Novel Silk Fibroin/Carboxymethyl Cellulose Based Electrospun Nanofibrous Scaffolds for Bone Tissue Engineering Application” represents my original work carried out as a doctoral student of NIT Rourkela and, to the best of my knowledge, it contains no material previously published or written by another person, nor any material presented for the award of any other degree or diploma of NIT Rourkela or any other institution. Any contribution made to this research by others, with whom I have worked at NIT Rourkela or elsewhere, is explicitly acknowledged in the dissertation. Works of other authors cited in this dissertation have been duly acknowledged under the section "Bibliography". I have also submitted my original research records to the scrutiny committee for evaluation of my dissertation.

I am fully aware that in case of any non-compliance detected in future, the Senate of NIT Rourkela may withdraw the degree awarded to me on the basis of the present dissertation.

January 5, 2017
NIT Rourkela

Bhisham Narayan Singh

ACKNOWLEDGEMENT

It is often said that the roots of hard work are bitter but its fruits are sweet. After toiling hard for four long years, I have finally been able to relish my sweets of success by submitting my dissertation. Its time I penned down my gratitude towards all the wonderful people who have joined hands in making this long time dream come true. My heartfelt thanks to my guide, Prof. Krishna pramanik for her kind support and she also provided me space to chase my own ideas. She has been a good critic towards my work and dissertation which has helped me to complete my experiments and write my thesis in the best possible manner. I believe my triumph in my future career is the best way to express my appreciation towards her.

I thank my sponsoring agency, Department of Biotechnology, Government of India, New Delhi for their complete and continual financial support through the project period. I am grateful to my institute for providing essential equipment and chemical facilities. I also thank our Sponsored Research Cell (SRICCE) for helping us manage our funding and innumerable purchases. I thank my doctoral scrutiny committee chairman Dr. Subhankar Paul (Dept.of.Biotechnology & Medical Engg) and members Dr.Amit Biswas (Dept.of.Biotechnology & Medical Engg), Dr. A. Thirugnanam (Dept.of.Biotechnology & Medical Engg) and Dr. Samir kumar patra (Dept.of. Life science), and Head of the Department Dr. Mukesh gupta for their constant monitoring and valuable comments which have helped to complete this dissertation successfully. I also wish to express my sincere gratitude to all the faculty members and staff of my department for extending their warm support.

I would like to thank my dear friends Kanchan, Satya, Vadolia, Nadeem Siddiqui, Niladrinath Panda, Arvind kumar, Parinita Agrawal, Anurag, Om das, Rasmi ranjan and Amit kumar and many more who have been with me through the bittersweet moments of my stay.

Abstract

Bone Tissue Engineering (TE) has been evolved as a promising mean to repair and regenerate defect and/or diseased bone tissues through the development of artificial extracellular matrix made from biopolymers. Silk fibroin based biomaterials are considered ideal for developing scaffolds for TE applications. The present research aims to develop novel biomimetic silk fibroin (SF) and carboxymethyl cellulose (CMC) based nanofibrous scaffold by free liquid surface electrospinning method. Randomly oriented electrospun nanofibrous scaffolds were developed from SF/CMC blends. Among the different blend ratios, 98:2 w/w of SF/CMC_2 is the optimal achieving a set of superior scaffold properties in comparison to pure SF scaffold. The scaffolds were characterized for morphology (SEM, AFM), structural (XRD, FT-IR), surface property (% water uptake and contact angle measurement) and mechanical strength. The average fiber diameter was obtained as 227.8 ± 87 nm. The scaffold exhibited higher water uptake capacity, hydrophilicity and bioactivity showing uniform nucleation of Ca/P over the surface with controlled particle size of $\leq$ 100 nm than the pure bombyx mori SF scaffolds. Though the tensile strength of pure SF (12.7 ± 1.5 MPa) was slightly reduced by the addition of CMC (10.54 ± 1.3 MPa), the scaffold still possess sufficient strength to support many types of bone tissue regeneration. In vitro cell culture study has confirmed the cell supportive property of the scaffold as evident from cell attachment, cell proliferation, cell penetration and cellular metabolic activity of hMSCs which was derived from umbilical cord blood over the scaffold. The developed calcified SF/CMC_2 blend scaffold possess good osteogenic property as confirmed by ALP activity, biomineralization ability, GAG secretion, osteocalcin, RUN X2 and collagen type1 expression. The osteogenic potential of SF/CMC scaffold was further enhanced by incorporating nano-bioglass thereby SF/CMC/nBG composite scaffold was developed. The surface roughness of SF/CMC/nBG (5 - 20 wt%) scaffolds was linearly increased with nano-bioglass content. Among the various concentration of nBG, SF/CMC loaded with 10%nBG shows optimal tensile strength of 7.591 ± 1.23 MPa and tensile strain at break of 9.62 ± 0.85 %. The ALP activity of hMSCs on SF/CMC/10nBG was significantly ($p<0.05$) higher than SF/CMC_2 throughout the culture period. The OCN expression on SF/CMC/10%nBG was observed to be 4.1 fold higher than SF/CMC_2 and 2.3 fold higher than calcified SF/CMC_2 nanofibrous scaffold. Hence, SF/CMC/10%nBG composite scaffold is proven to provide better osteogenic platform for hMSCs. An effort has further been given to

improve the angiogenic property of SF/CMC/nBG composite scaffolds by incorporating Cu^{2+} ion. Among the scaffolds with varied compositions, SF/CMC/Cu_1-5%nBG exhibited superior osteogenic and angiogenic property. Though a slightly higher OCN expression was observed over SF/CMC/$Cu_{0.5}$-5%nBG composite scaffold than SF/CMC/Cu_1-5%nBG, the difference in the expression was not statistically significant. However, SF/CMC/Cu_1-5%nBG shows higher VEGF expression representing its superior angiogenic property than SF/CMC/$Cu_{0.5}$-5%nBG scaffold. Thus, copper doped nano bioglass incorporated SF/CMC/Cu_1-5%nBG composite nanofibrous matrix was proven to be a potential artificial extracellular matrix with enhanced bioactivity, osteogenic and angiogenic properties which might be a promising scaffold for future bone tissue regeneration.

Keywords: Silk fibroin; Electrospinning; Carboxymethyl cellulose; Tissue engineered scaffold; Bioactive glass; Osteogenesis; Angiogenesis; Biomineralization.

CONTENTS

Supervisor's Certificate

Dedication

Declaration of Originality

Acknowledgement

Abstract

List of Figures ……iv

List of Tables ……..x

Abbreviation ……xi

CHAPTER 1: General Introduction

1.1 Background and significance of study ….1

1.2 Strategies for Tissue regeneration 2

1.3 Applications of tissue engineering 3

1.4 Tissue engineered scaffold 3

1.4.1 Properties of scaffold 3

1.4.2 Biomaterials for scaffold development 6

1.4.3 Scaffold fabrication techniques 9

1.4.4 Stem cells for tissue engineering 13

1.4.6 Bone 14

1.4.7 Silk fibroin as ideal biopolymer for tissue regeneration 16

1.4.8 Future prospects of tissue engineering 17

1.4.9 Thesis outline…….. 17

CHAPTER 2: Literature Review

2.1 Current status, prospects and challenges of bone tissue engineering 19

2.2 Ideal biomaterials for bone tissue engineering 20

2.3 Silk fibroin based polymer-polymer blend scaffold 22

2.4 Silk fibroin based polymer-ceramic composite scaffold 26

CHAPTER 3: Scope and Objective……30

CHAPTER 4: Materials and Methods

4. 1 Materials 33
4.1.1 Preparation of scaffold 33
4.1.2 Cell culture study 33
4.2 Methods 33
4.2.1 Preparation of regenerated silk fibroin 33
4.2.2 Preparation of electrospun SF nanofibrous scaffold 34
4.2.3 Development of electrospun SF/CMC blend nanofibrous scaffold 34
4.2.4 Synthesis of nano-bioglass and copper doped nano-bioglass 35
4.2.5 Development of electrospun SF/CMC/nBG composite nanofibrous scaffold 35
4.2.6 Development of electrospun SF/CMC/Cu-nBG composite nanofibrous scaffold 36
4.3 Characterization of nano-bioglass 36
4.3.1 Morphology 36
4.3.2 Bioactivity 36
4.3.3 Structural and functional characterization 37
4.4 Characterizations of scaffolds 37
4.4.1 Rheological behaviour 37
4.4.2 Morphological study 37
4.4.3 Structural and functional analysis 38
4.4.4 Surface roughness analysis 38
4.4.5 Mechanical strength measurement 38
4.4.6 Contact angle measurement 39
4.4.7 Equilibrium water uptake capacity measurement 39
4.4.8 In vitro biodegradation of scaffolds 39
4.4.9 In vitro bioactivity study 39
4.5 In vitro cell study 40
4.5.1 Isolation and culture of hMSCs 40
4.5.2 Cell seeding and culture 40
4.5.3 Cell morphology and cell attachment 40
4.5.4 Cell viability 41
4.5.5 Cell distribution and cytoskeleton organization 41
4.5.6 Osteogenic differentiation potential 42
4.5.7 Angiogenic potential analysis 44
4.6 Statistical analysis 45
CHAPTER 5: Results and Discussion

CHAPTER 5A: Development and characterization of SF/CMC blend scaffold

5.1.1 Preparation & characterization of electrospun pure SF and cross-linked SF nanofibrous scaffolds 46

5.1.2 Development of SF/CMC nanofibrous scaffold 51

5.1.3 Characterization of SF/CMC scaffold 53

5.1.4 In vitro bioactivity analysis 59

5.1.5 In vitro biodegradation of scaffold 63

5.1.6 In-vitro cell culture study 65

5.1.7 Osteogenic differentiation 72

CHAPTER-5B: Synthesis and Characterisation of nano-bioglas and Copper-doped nano-bioglass

5.2.1 Synthesis and characterization of nano-bioglass 78

5.2.2 In vitro apatite forming ability of nano-bioglass 80

5.2.3 Synthesis and characterization of copper doped nano-bioglass 83

5.2.4 In vitro apatite forming ability of copper doped nano-bioglass 85

CHAPTER 5C: Development of nano-bioglass incorporated electrospun SF/CMC composite nanofibrous scaffold

5.3.1 Fabrication and characterization of SF/CMC/nBG nanofibrous composite scaffold 91

5.3.2 In vitro bioactivity analysis 101

5.3.3 In vitro biodegradation of scaffold 104

5.3.4 In-vitro cell culture study 105

5.3.5 Osteogenic differentiation 111

CHAPTER 5D: Development of copper doped nano bioglass incorporated SF/CMC composite scaffolds

5.4.1 Fabrication and characterization of SF/CMC/Cu-nBG nanofibrous composite scaffold 115

5.4.2 In vitro bioactivity 119

5.4.3 In vitro biodegradation of scaffold 122

5.4.4 In-vitro cell culture study 123

5.4.5 Osteogenic differentiation 128

CHAPTER 6: Summary and Conclusion 137

References 142

List of Figures

Chapter 5

Figure 5.1	The graphs showing the effect of concentration of SF solution (A) and distance between the electrodes (B) on the fiber formation. Effect of SF concentration on viscosity (C).	47
Figure 5. 2	(A) SEM images of electrospun SF nanofiber generated from different SF concentration (10 -14%) SF solutions at 16 cm distance between the electrodes. (B) SEM images of electrospun SF nanofiber formed from 10 wt% solutions at varying distances between the electrodes.	48
Figure 5.3	SEM images of cross-linked electrospun SF scaffold.	49
Figure 5.4	XRD spectrum (A), FT-IR spectrum (B) and Load Vs Extension curve (C) for electrospun pure SF scaffold.	51
Figure 5.5	Rheological behavior of the pure SF and SF/CMC blend solutions at different shear rate.	52
Figure 5.6	FESEM images of electrospun SF (a), SF/CMC_1 (b) and SF/CMC_2 (c) scaffolds.	54
Figure 5.7	(A) XRD and (B) FT-IR spectrum of SF, SF/CMC1 and SF/CMC2 nanofibrous scaffolds.	55
Figure 5.8	(A) Load Vs Extension curve for SF and SF/CMC_2 scaffolds in dry and wet condition. (B) Distribution of tensile strength and tensile strength at break of SF and SF/CMC_2 scaffold.	56
Figure 5.9	The AFM images of fabricated SF (A) and SF/CMC_2 (B) nanofibrous scaffolds.	57
Figure 5.10	(A) Swelling behaviour at different time interval observed with SF and SF/CMC_2 in PBS solution. (B) Variation of contact angle measured with SF and SF/CMC_2 scaffolds.	59
Figure 5.11	(A) FESEM images of pure and calcified SF, calcified SF/CMC_1 and calcified SF/CMC_2 after SBF treatment for 7 days (a, d). (B) Illustration of *in situ* mineralization of calcified SF/CMC_1 and blend scaffolds.	61
Figure 5.12	XRD (A) and FTIR (B) spectrum of pure and calcified SF, calcified SF/CMC_1 and calcified SF/CMC_2 after incubation in SBF for a week.	63
Figure 5.13	AFM images of (A) calcified SF and (B) calcified SF/CMC_2 after treatment in SBF for 7 days. Observed degradation behaviour of SF and SF/CMC_2 scaffolds by soaking in PBS (C) and enzymatic solution (D) for 28 days.	64
Figure 5.14	(A) Morphological changes of hMSCs (a) MNCs, (b) after passage 1, (c) after	66

passage 2 and (d) after passage 3 as observed under phase contrast microscope at magnification 10X and scale bar 50μm. (B) Multilineage differentiation potential of hMSCs assessed by alizarin red S staining (a), Alcian blue staining (b) and Oil red staining (c).

Figure 5.15 FESEM images of hMSCs on gelatin (A), SF (B) and calcified SF/CMC_2 (C) after 12 h of culture. FESEM micrographs of cells cultured on gelatin (D), SF (E) and calcified SF/CMC_2 (F) after 7 days. FESEM images of cells cultured on gelatin (G), SF (H) and calcified SF/CMC_2 (I) on day 14. 68

Figure 5.16 Cell proliferation and distribution are visualized under confocal microscope on gelatin (A), SF (B) and calcified SF/CMC_2 (C) after culture for 7 days, and gelatin (D), SF (E and calcified SF/CMC_2 (F) after culture for 14 days. 69

Figure 5.17 MTT assay of hMSCs cultured on gelatin, SF and calcified SF/CMC_2. 70

Figure 5.18 (A) Calcein AM and EthD-1 staining of hMSCs cultured for 7 days on Gelatin (a), SF (b) and calcified SF/CMC_2 (c). (B) 3D laser scanning confocal images were observed while live/dead staining (Z stacks) of hMSCs cultured for 7 days on Gelatin (a), SF (b) and calcified SF/CMC_2 (c). Green signals indicate viable cells and red signal for dead cells. 71

Figure 5.19 Estimation of intracellular GAG secreted by hMSCs cultured in the osteogenic media for 7 and 14 days of culture over gelatin, SF and calcified SF/CMC_2. 72

Figure 5.20 Alkaline phosphatase (ALP) activity in hMSCs cultured on the gelatin, SF and calcified SF/CMC_2 in osteogenic culture medium over time (n=3). 73

Figure 5.21 (A) Alizarin red S staining of hMSCs cultured over gelatin, SF and calcified SF/CMC_2 for 7 and 14 days. (B) FESEM images and EDX spectra of mineral deposition of SF and calcified SF/CMC_2 cultured for 7 days. (C) Alizarin Red S staining assay for quantitative evaluation of hMSCs mineralization on nanofibrous scaffolds after 14 days of culture. 75

Figure 5.22 Immuno-cytochemistry for RunX2 and osteocalcin on hMSCs cultured on gelatin, pure SF and calcified SF/CMC_2 scaffolds. (A) Confocal images showing RunX2 expressions of hMSCs on day 7 and day 14 (B) Confocal images for osteocalcin expressions were observed in hMSCs on day 7 and day 14 in the osteogenic culture medium. Integrated density evaluation for RunX2 and osteocalcin are depicted in graphs (C) and (D) respectively. Scale bar = 25 μm. (E) The osteoblastic differentiation of hMSCs on nanofibrous scaffolds was assessed by measuring the mRNA expression of Runx2, osteocalcin and type1 collagen (F). 77

Figure 5.23 Showing the morphology of nBG by FESEM (A) and TEM images (B). HRTEM images (C) and SAED pattern (D) of nanobioglass. 79

Figure 5.24 Showing the XRD diffractogram (A) and FT-IR spectra (B) of nano-bioglass. 80

Figure 5.25 Showing the FESEM image (A), HRTEM image (B) and SAED pattern (C) for the developed nBG after SBF treatment. 81

Figure 5.26 Showing the XRD diffractogram (A), FT-IR spectra (B) and EDS spectra (C) of nano-bioglass before and after SBF treatment. 81

Figure 5.27 The graph showing the rate of ion release from nBG during the 7 days of SBF treatment. 83

Figure 5.28 FESEM and EDX images showing the morphology and elemental composition of $Cu_{0.5}$-nBG (A) and Cu_1-nBG (B). TEM image and SAED pattern of $Cu_{0.5}$-nBG(C) and Cu_1-nBG (D). 84

Figure 5.29 Showing the XRD diffractogram (A) and FT-IR spectra (B) of the synthesized two varieties of copper doped nano-bioglasses. 85

Figure 5.30 FESEM images showing the morphology of $Cu_{0.5}$-nBG (A) and Cu_1-nBG (B) after SBF treatment. HRTEM image and SAED pattern of $Cu_{0.5}$-nBG(C) and Cu_1-nBG (D) after SBF treatment. 86

Figure 5.31 Showing the XRD diffractogram (A), FT-IR spectra (B), EDX analysis(C) and EDX analysis (D) of copper doped $Cu_{0.5}$-nBG and Cu_1-nBG bioglasses after 7 days of SBF treatment. 87

Figure 5.32 The graphs showing the rate of ion release from $Cu_{0.5}$-nBG and Cu_1-nBG during the 7 days of SBF treatment. 88

Figure 5.33 Showing the FESEM (A) and TEM(B) images of fabricated SF/CMC/0%nBG, SF/CMC/5%nBG, SF/CMC/10%nBG and SF/CMC/20%nBG nanofibrous scaffolds. 92

Figure 5.34 XRD diffractogram(A) and FT-IR spectrum (B) showing the change in structural and functional conformation of the fabricated SF/CMC/0%nBG, SF/CMC/5%nBG, SF/CMC/10%nBG and SF/CMC/20%nBG nanofibrous scaffolds due to the incorporation of nano-bioglass. 94

Figure 5.35 (A) Load Vs Extension curve for composite scaffolds in dry condition. (B) Distribution of tensile strength and tensile strength at break of SF/CMC/0%nBG, SF/CMC/5%nBG, SF/CMC/10%nBG and SF/CMC/20%nBG scaffolds in dry condition. (C) Load Vs Extension curve for composite scaffolds SF/CMC/0%nBG, SF/CMC/5%nBG, SF/CMC/10%nBG and SF/CMC/20%nBG in wet condition. (D) Distribution of tensile strength and tensile strength at break of SF/CMC/0%nBG, SF/CMC/5%nBG, SF/CMC/10%nBG and SF/CMC/20%nBG scaffolds in wet condition. 96

Figure 5.36 Surface roughness of fabricated SF/CMC/5%nBG, SF/CMC/10%nBG and SF/CMC/20%nBG composite scaffolds. 97

Figure 5.37 Swelling behavior at different time interval observed with SF/CMC/0%nBG, SF/CMC/5%nBG, SF/CMC/10%nBG and SF/CMC/20%nBG composite nanofibrous scaffolds in PBS solution. 99

Figure 5.38 FESEM images of SF/CMC/0%nBG, SF/CMC/5%nBG, SF/CMC/10%nBG and SF/CMC/20%nBG composite matrices after SBF treatment for 7 days (A). EDX spectra depict the mineral deposition over SF/CMC/0%nBG (B) and SF/CMC/10%nBG (C) after 7 days of SBF treatment. 101

Figure 5.39 Showing the XRD spectrum(A) and FT-IR spectrum(B) of SF/CMC/0%nBG, SF/CMC/5%nBG, SF/CMC/10%nBG and SF/CMC/20%nBG after incubation in SBF for 7 days 103

Figure 5.40 Observed degradation behaviour of SF/CMC/0%, SF/CMC/5%nBG, SF/CMC/10%nBG and SF/CMC/20%nBG scaffolds by soaking in enzyme (A) and PBS solution (B) for 28 days. 104

Figure 5.41 FESEM images of hMSCs cultured over the SF/CMC/0%nBG and SF/CMC/10%nBG scaffolds after 12 hour (A) ,7 days (B) & 14 days (C). 106

Figure 5.42 hMSCs proliferation and distribution are visualized under confocal microscope on SF/CMC/0%nBG (A and C) and SF/CMC/10%nBG (B and D) on 7 and 14 days of culture, Nuclei of the cells were stained with DAPI (blue) and actin filaments with phalloidin (green). 107

Figure 5.43 Live/dead confocal microscopy images (A) and MTT reduction assay (B) of hMSCs cultured on SF/CMC/0%nBG(control) and SF/CMC/10%nBG nanofibrous scaffolds. 109

Figure 5.44 Estimation GAG secreted by hMSCs cultured in osteogenic media during 7 and 14 days of culture over SF/CMC/0%nBG and SF/CMC10%nBG nanofibrous scaffolds. 110

Figure 5.45 Alkaline phosphatase (ALP) activity in hMSCs on SF/CMC/0%nBG and SF/CMC/10%nBG in an osteogenic culture medium over time (n=3). 111

Figure 5.46 (A) Alizarin red S staining of SF/CMC/0%nBG and SF/CMC/10%nBG nanofibrous scaffolds cultured for day 7 (a) and day 14 (b). (B) Alizarin Red S staining assay for quantitative evaluation of hMSCs mineralization on SF/CMC/0%nBG and SF/CMC/10%nBG nanofibrous scaffolds after 14 days of culture. 112

Figure 5.47 Immunocytochemistry for Runx2 and osteocalcin expression by hMSCs cultured on SF/CMC/0%nBG and SF/CMC/10%nBG nanofibrous scaffolds. (A) Confocal 114

images for Runx2 expressions (A) and Confocal images for osteocalcin expressions of hMSCs on day 7 and day 14 in the osteogenic culture medium. Integrated density evaluation for RunX2 and osteocalcin were shown in graphs (C) and (D) respectively. The osteogenic differentiation of hMSCs on SF/CMC and SF/CMC/10nBG scaffolds was assessed by RT-PCR for Runx2, osteocalcin and collagen type1 (E) expression after 14 days of culture.

Figure 5.48 FESEM, TEM and SAED pattern images of fabricated SF/CMC/0%nBG, SF/CMC/$Cu_{0.5}$-5%nBG, SF/CMC/$Cu_{0.5}$-10%nBG, SF/CMC/Cu_1-5%nBG and SF/CMC/ Cu_1-10%nBG scaffolds. 117

Figure 5.49 (A) XRD diffractogram and (B) FT-IR spectra of SF/CMC/0%nBG, SF/CMC/$Cu_{0.5}$-5%nBG, SF/CMC/$Cu_{0.5}$-10%nBG, SF/CMC/Cu_1-5%nBG and SF/CMC/ Cu_1-10%nBG nanofibrous scaffolds. 119

Figure 5.50 FESEM images of SF/CMC/0%nBG, SF/CMC/$Cu_{0.5}$-5%nBG, SF/CMC/$Cu_{0.5}$-10%nBG, SF/CMC/Cu_1-5%nBG and SF/CMC/Cu_1-10%nBG scaffolds after SBF treatment for 7 days (A-E). 120

Figure 5.51 (A) XRD diffractogram and (B) FTIR Spectra of SF/CMC/0%nBG, SF/CMC/$Cu_{0.5}$-5%nBG, SF/CMC/$Cu_{0.5}$-10%nBG, SF/CMC/Cu_1-5%nBG and SF/CMC/ Cu_1-10%nBG nanofibrous scaffolds after SBF treatment for 7 days. 121

Figure 5.52 Observed degradation behaviour of *SF/CMC, SF/CMC/$Cu_{0.5}$-5%nBG, SF/CMC/$Cu_{0.5}$-10%nBG, SF/CMC/Cu_1-5%nBG and SF/CMC/ Cu_1-10%nBG* scaffolds by soaking in enzyme (A) and PBS solution (B) for 28 days. 122

Figure 5.53 (A) Live/dead confocal microscopy images and (B) MTT reduction assay of hMSCs cultured on SF/CMC, SF/CMC/$Cu_{0.5}$-5%nBG, SF/CMC/$Cu_{0.5}$-10%nBG, SF/CMC/Cu_1-5%nBG and SF/CMC/ Cu_1-10%nBG nanofibrous scaffolds. 124

Figure 5.54 FESEM images of hMSCs cultured on the SF/CMC/0%nBG, SF/CMC/5%nBG, SF/CMC/$Cu_{0.5}$-5%nBG and SF/CMC/Cu_1-5%nBG scaffolds after 12 hour, 7 and 14 days of culture in DMEM media supplemented with FBS. 125

Figure 5.55 hMSCs proliferation & distribution are visualized under confocal microscope over SF/CMC/0%nBG, SF/CMC/5%nBG, SF/CMC/$Cu_{0.5}$-5%nBG & F/CMC/Cu_1-5%nBG after 14 days of culture. 126

Figure 5.56 Estimation GAG secreted by hMSCs cultured in osteogenic media during 7 and 14 days of culture over over SF/CMC/0%nBG, SF/CMC/5%nBG, SF/CMC/$Cu_{0.5}$-5%nBG and SF/CMC/Cu_1-5%nBG. 128

Figure 5.57 Alkaline phosphatase (ALP) activity in hMSCs on SF/CMC/0%nBG, SF/CMC/5%nBG, SF/CMC/$Cu_{0.5}$-5%nBG and SF/CMC/Cu_1-5%nBG nanofibrous scaffolds in an osteogenic culture medium over time (n=3). 129

Figure 5.58 Showing the microscopic images of Alizarin red S staining of SF/CMC/0%nBG, SF/CMC/5%nBG, SF/CMC/$Cu_{0.5}$-5%nBG and SF/CMC/Cu_1-5%nBG nanofibrous scaffolds cultured for 14 days (A). Alizarin Red S staining assay for quantitative evaluation of mineralization on SF/CMC/0%nBG, SF/CMC/0.5Cu-5nBG and SF/CMC/1Cu-5nBG nanofibrous scaffolds after 14 days of culture. 130

Figure 5.59 Immunocytochemistry for Runx2 & osteocalcin expression in hMSCs cultured on SF/CMC/0%nBG, SF/CMC/5%nBG, SF/CMC/$Cu_{0.5}$-5%nBG & SF/CMC/Cu_1-5%nBG scaffolds. Confocal images for Runx2 (A) &Osteocalcin expressions (b) observed in hMSCs on day 7 & 14 in the osteogenic medium. Integrated density evaluation for RunX2 and osteocalcin were shown in graphs (C) & (D) respectively. (E) The osteogenic differentiation of hMSCs on the scaffolds was assessed by RT-PCR for Runx2 & osteocalcin expression after 14 days of culture. 133

Figure 5.60 Confocal images for HIF-1α expression in hMSCs seeded on SF/CMC/0%nBG, SF/CMC/5%nBG, SF/CMC/$Cu_{0.5}$-5%nBG and SF/CMC/Cu_1-5%nBG nanofibrous nano composite scaffolds cultured for day 7 (A) and 14 (B). 135

Figure 5.61 Relative VEGF expression in hMSCs seeded over SF/CMC/0%nBG, SF/CMC/5%nBG, SF/CMC/$Cu_{0.5}$-5%nBG and SF/CMC/Cu_1-5%nBG nanofibrous scaffolds during 7 days culture period. 136

List of Table

Chapter 1

Table 1. 1	Advantage and disadvantage of various scaffold fabrication techniques	11
Table 1. 2	Various component of extracellular matrix of bone and its role	15
Table 1. 3	Bone cells and their function	16

Chapter 2

Table 2. 1	Various biopolymers and its application in tissue engineering.	21
Table 2. 2	Various silk fibroin-biopolymer blend based scaffold and its application in tissue engineering	25
Table 2.3	Silk fibroin based composite scaffold and their advantages	28

Chapter 4

Table 4.1	Selected primer sequence for the gene of interest and house-keeping gene	45

Chapter 5

Table 5. 1	Mean contact angle measurement of SF and SF/CMC_2 nanofibrous scaffolds	58
Table 5. 2	Fiber diameter of electrospun composite mats and viscosity of various solutions prepared for fabrication of the respective electrospun mats	92
Table 5. 3	Mean contact angle measurement of nanofibrous scaffolds	98
Table 5. 4	Composition of various composite nanofibrous scaffold	116
Table 5. 5	Average fiber diameter and average pore size of various composite nanofibrous scaffolds with and without Cu-nBG	118
Table 5.6	Comparison of results	136

List of Abbreviations

AFM	Atomic Force Microscope
ALP	Alkalaine Phosphatase
CAD	Computer Aided Designing
hMSCs	Human Mesenchymal Stem Cells
ECM	Extra Cellular Matrix
FT-IR	Fourier Transformer Infrared Spectroscopy
HFIP	Hexa Fluro Isopropanol
DMEM	Dulbecco's Modified Eagle Medium
GAG	Glycosaminoglycan
MNCs	Mononuclear Cells
MTT	3-(4,5-Dimethylthiazol-2-yl]-2,5-tetrazolium bromide
PBS	Phosphate Buffer Saline
RH	Relative Humidity
UCB	Umbilical Cord Blood
OD	Optical Density
SF	Silk Fibroin
RUNX 2	Runt Related Transcription Factor
SEM	Scanning Electron Microscope
TEM	Transmission Electron Microscopy
OCN	Osteocalcin
CMC	Carboxymethyl Cellulose
FESEM	Field Emission Scanning Electron Microscope
nBG	Nano-Bioglass
NHS	N-hydroxysuccinimide
MTT	3-[4,5-dimethyltriazol-2-y1]-2,5-diphenyl tretrazolium

$NaHCO_3$	Sodium Bicarbonate
Na_2SO_4	Sodium Sulphate
PI	Propidium Iodide
RT-PCR	Reverse Transcription Polymerase Chain Reaction
FITC	Fluorescein Isothiocyanate
HIF-1α	Hypoxia-Inducible Factor 1α
Col I	Collagen Type I
VEGF	Vascular Endothelial Growth Factor
ELISA	Enzyme Linked Immunosorbent Assay
XRD	X-ray Diffraction
UTS	Universal Testing Machine
FBS	Fetal Bovine Serum
TE	Tissue Engineering

CHAPTER 1: General Introduction

1.1 Background and significance of study

Bone tissue related defects, wounds and diseases predominantly due to the consequences of trauma, infection and degenerative bone defects and diseases are of major apprehension in the field of human health [1-2]. In USA, around 1 million bone injury cases is reported to occur every year and an alarming increase in bone related defects and diseases is expected to arise worldwide in future [3]. Presently, orthopaedic reconstruction procedure has been dramatically increased, that triggers the high demand for advanced bone reconstruction technology. The current modern clinical alternatives for orthopaedic reconstructive surgery are includes autografts, allograft, and xenografts [4-5]. These bone substitutes have several limitations such as limited supply, immunogenic, zoonotic disease transfer and donor site morbidity which are of major concern [6-7]. Such intrinsic problems associated with the currently available clinical strategy lead to the evolution of bone tissue engineering as a promising clinical alternative in the last decade. The aim of this interdisciplinary tissue engineering field is to replace, maintain and restore damage tissues through the development of bioactive, biodegradable and biocompatible functionalized three dimensional (3D) scaffolds made of natural or synthetic biopolymers [8-9].

The key challenges for bone tissue engineering is to develop scaffold with desired physico-chemical properties such as biomimetic, non-immunogenicity, desired mechanical strength, desirable biodegradation, porosity, swelling behaviour and to guide tissue regeneration [10]. The surface modification of the scaffold to produce biologically active matrix is another important aspect which improves the cell adhesion, proliferation and differentiation of host cells [11]. Bone tissue extracellular matrix is composed of collageneous fibers and inorganic substances like carbonated hydroxyapatite as biological mineral, which provides properties like hardness, rigidity and strength [12]. To achieve biomimetic properties of bone extracellular matrix, use of potential biopolymers, inorganic ceramics like hydroxyapatite, beta-tricalciumphosphate and bioglass and their composites are of prime interest. In this context, silk fibroin, a natural polymer widely used in textile industry has drawned attention of the researchers worldwide in last two decades for use in medical and tissue engineering field because of its excellent property like mechanical strength, biodegradability, biocompatibility and desired oxygen and water permeability [13-15]. However, SF alone

cannot meet all the desired property of the tissue engineered scaffold, as it lacks hydrophilicity, bioactivity, osteoconductivity, swelling, flexibility and lack of bioactive cell signalling molecule [16]. Therefore, many researchers have been given effort to prepared SF blends like SF/chitosan, SF/chitin, and SF/PLA to improve the property of SF [17-20]. Besides SF biomaterial, Cellulose derivatives like carboxymethyl cellulose, cellulose acetate, hydroxyethyl cellulose and bacterial cellulose have been reported to be good candidates to fabricate scaffolds for tissue engineering application in bone regeneration, postinjury brain, blood vessels, artificial liver and cardiac cell construct development [21-25]. Furthermore, development of biopolymer/ceramic composite scaffold has gained significant interest over the last decade for bone tissue engineering applications. Besides exploring potential scaffolding material, fabrication of scaffold with nanostructure is important aspect as it mimics the extracellular matrix the structure and provide suitable template for cell attachment, proliferation and differentiation. In this context electrospinning is considered as the suitable fabrication technique that can produce nanofiber from polymeric blend and their composite solution. Thus the present research focused on the development of silk fibroin/carboxymethyl cellulose based composite nanofibrous scaffolds as potential artificial extracellular matrix for bone tissue engineering application.

1.2 Strategies for Tissue regeneration

Langer and Vacanti defined tissue engineering as an interdisciplinary field that applies the principles of engineering and the life sciences towards the development of biological substitutes that can restore, maintain or improve tissue or organ function [26-27]. Tissue engineering emerges as a clinical alternative in response to the problem related with the tissue damage or loss due to trauma or diseases. Tissue engineering deals with the creation of scaffold, which allows cell growth and proliferation in vitro and in vivo as well as degraded in time with tissue regeneration [28]. The biocompatible and biodegradable scaffold will degrade completely and prevent any chronic inflammation at the site of implantation. The scaffold should promote angiogenesis or vasculogenesis for the development of vascular network throughout the scaffold matrix for supplying oxygen, nutrient, growth factor and removal of degraded waste of scaffold while tissue regeneration. The design of surrogate

extracellular matrix with appropriate structural framework embedded with suitable bioactive agent is essential to guide cells behaviour and organize tissue regeneration in vivo.

1.3 Applications of tissue engineering

Tissue engineering (TE) is emerging as a low cost and long term alternative clinical treatment method for tissue damage and organ failure. The technique involves the implantation of natural, synthetic, or semi-synthetic polymeric biological substitute that mimic tissue or organ and led to regeneration of functional tissue or organ. Tissue engineering is used to develop extracellular matrix to coax differentiated or undifferentiated cells into desired cell type and its important application of includes bone [29-30], cartilage [31-32], skin [33], ligament [34], tendon [34], neural [35], liver [36], cardiovascular [37] and muscle tissue [38-40] related diseases [41]. The global medical and market potential attracted significant research & development academic and corporate interest in the field of tissue engineering.

1.4 Tissue engineered scaffold

In TE scaffold is a three dimensional temporary structure which supports cell attachment, proliferation and differentiation. Scaffold should be biocompatible, bioactive and biodegradable in nature [42]. Scaffold material, its structure or design and surface property are some of the crucial factors which guide cell attachment, proliferation and cell fate determination for desired tissue regeneration. Furthermore, the by-product of scaffold degradation should not be toxic, inflammatory and should be quickly removed from the site of implantation.

1.4.1 Properties of scaffold

Microscopic topography

The microscopic and ultrafine structural properties of scaffold play vital role in regulating cell behaviour, cell migration into scaffold and influencing cell phenotype while tissue regeneration [43-44]. The irregular fibrous structures can facilitate cell adhesion and penetration into the scaffold [43]. The biomimetic architecture of human body consists of collagen fibers as natural extracellular matrices (ECM) with 50-500 nm diameter range [45].

Thus the nanofibrous architecture of scaffold is one of the essential considerations in scaffold development for tissue engineering applications.

Pore size

Structure and size of pore is an important consideration in the fabrication of scaffolds in TE. Scaffolds must possess interconnected pores to facilitate cell growth, migration, diffusion of nutrients and removal of waste [46-47]. If the pore size is too small it limit the cell migration, diffusion of nutrient, removable of waste while if too large it will limit the cell attachment, cell seeding, mechanical strength and thus scaffolds with too small or too large pore size are not suitable for tissue regeneration. The pore sizes for scaffold varies depending on the type of applications such as for bone tissue engineering pore size lie in the range of 50-300 μm, whereas for cartilage tissue engineering the range is 150–300 μm [48-49]. The minimum pore size for significant bone tissue regeneration is 75-100 μm [49-50].

Porosity

Scaffold must be porous and having optimum porosity, as porosity play important role in regulating cell migration, diffusion of nutrients and removal of degraded waste [51-52]. Furthermore, porosity influences directly or indirectly mechanical properties of scaffold, thus the scaffold should have optimum porosity within the construct [53].

Mechanical property

The scaffold supports the tissue regeneration from the time of cell seeding to the remodelling of scaffold at the site of implantation by the host tissue [54]. While application in the case of bone and cartilage tissue, the scaffold matrix must provide enough mechanical support to endure in vivo stress and loading [54]. Also the mechanical property should be optimized so that it can stimulate lineage specific cell differentiation [55]. The material selection for scaffold fabrication is also important consideration for tissue regeneration, as the scaffold should have adequate strength to support complete tissue regeneration without failure [54].

Hydrophilicity

The affinity of scaffold for water and getting wet is defined as hydrophilicity. The wetting affinity of scaffold material influences cell adhesion, spreading, proliferation, differentiation

and diffusion of nutrients within the cell-seeded construct [48]. The hydrophilicity of scaffold is determined by measuring contact angle. The cell response to scaffold material surface is governed by the adsorption of protein and cell secreted extracellular matrix [48]. Proteins tend to adsorb quickly on hydrophobic surface in comparison to hydrophilic surface. Thus scaffold material should have optimum contact angle [48].

Surface roughness

Surface roughness is one of the crucial factors that regulates cell adhesion, proliferation and phenotype expression [48]. The roughness of material surface can be classified as macro-roughness (100 µm - millimetres), micro-roughness (100 nm - 100 µm) and nanoroughness (less than 100 nm) [48]. Different types of cells have different response depending on surface roughness of the scaffold. However, osteoblast cells show favourable behaviour over scaffold with macro-roughness [48].

Biocompatibility

Biocompatibility of scaffold refers to its ability to interact with the host tissue without causing any inflammatory or harmful reaction. The degraded product of the scaffold should be non-toxic for the successful tissue regeneration at the site of implantation.

Biodegradation

The scaffold material should be selected by taking into consideration of its rate of degradation and resorption while tissue regeneration [54]. Moreover, the rate of degradation and resorption should be optimized, so that the scaffold maintains its physical properties for at least 6 months [54]. The scaffold should allow cells to proliferate, migrate and differentiate in a controlled way while the scaffold matrix degrades and it should leaves enough space for new tissue growth and vascularisation [54].

Bioactivity

The development of biocompatible, biodegradable and bioactive scaffold with suitable porosity and mechanical property is of prime goal in tissue engineering application. The bioactivity of scaffold determine its ability to integrate or bonding with host tissue at the site of implantation [56]. Therefore, In case of bone tissue engineering it is desirable to determine

apatite forming ability of scaffold material for predicting bioactivity of the material [56]. The osteoconductive and osteoinductive property of scaffold are essential for bone tissue engineering. Thus the development of scaffold with innate osteoconductive and osteoinductive property is of prime goal in bone tissue engineering application.

1.4.2 Biomaterials for scaffold development

Material selection for tissue engineered scaffold development is one of the most important strategies in tissue engineering as it determines the rate of degradation and remodelling while host tissue regeneration [57]. An appropriate scaffolding material should possess some of the crucial properties like biocompatibility, biodegradability, bioresorbable, desired physico-chemical properties and desired mechanical strength for successful tissue regeneration [57-59]. Although a number of implantable metal and ceramic based structures has been developed earlier but since these materials fail to meet the criteria of biodegradability thus not suitable for tissue regeneration application [57-58]. Although there are various ceramic materials such as tri calcium phosphate and bioglass with biodegradability, bioactivity and biocompatibility properties but these materials are difficult to process into complex structure and also highly brittle. Thus ceramic material alone cannot fulfil the prerequisite for tissue engineering application [57-58]. However, polymeric material either natural or synthetic can be used alone or in combination to develop complex structure as polymers are ductile and can be processed into various shapes. Thus to fulfil various strategies for developing smart scaffolding material polymers and ceramics are combined to form composite to achieve prerequisite for successful tissue engineering application.

Natural polymer

Natural polymers derived from animal or plant sources are considered as the most suitable scaffolding material for TE including bone tissue engineering application. Natural polymers like collagen [60], chitosan [61-62], silk fibroin [63-64], cellulose and its derivatives [65] and gelatin [66-67] are considered as suitable material for the development of scaffold, as these materials offer superior cell adhesion, spreading and proliferation properties. Natural biopolymers are of great interest for the researchers because of their low toxicity, biocompatibility, low cost, large availability and renewability. Also well known chemical structure of biopolymer provides opportunity to develop advanced functionalized scaffolds

and well known biosynthetic pathway offers to genetically modify the biopolymer structure and function to make them more potential for tissue engineering application [65].

Synthetic polymers

Biodegradable and biocompatible synthetic polymers offer various advantageous properties such as tuneable mechanical property, defined degradation kinetics, can be modified with desired chemical functional moieties and also can be fabricated in to various shapes thereby making them suitable for various biomedical applications [68-69]. Synthetic biopolymer offer extensive applications in making resorbable sutures, drug delivery and orthopaedic fixations such as screws, pins, rods and plates [68]. Selection of synthetic polymers for tissue engineering application is one of the important parameters as the biopolymers like poly(glycolic acid), poly(lactic acid) and their copolymers resulted in to release of acidic products while biodegradation, which resulted in inflammatory reaction and thus failure of tissue regeneration occurs [68]. Thus synthetic biopolymer, which offers nontoxic degraded product during biodegradation are of preferred choice for tissue engineering application. To fulfil desired characteristic of scaffold for application in tissue engineering various synthetic polymers, natural polymers and ceramics were used alone or in combination for successful tissue regeneration.

Bioceramics

Various bio-ceramics like hydroxyapatite (HAp) [70], tri-calcium phosphate (TCP) [71-72], biphasic calcium phosphate (BCP) [73], bioglass [74] and wollastonite [75] have been the choice of many researcher for the development of 3D structure by adding with biopolymers for bone tissue engineering applications [76]. However matching mechanical properties of ceramic based scaffold with native bone remains a challenge as these ceramics based matrices are highly brittle and thus limit their clinical application. Presently various ceramic based products are available for various clinical applications such as dental, maxillofacial and orthopaedic. But there is of great need to identify smart biomaterials to overcome the limitations such as brittleness of ceramics based product, lack of bioactivity in case of polymeric scaffold, toxic product produced through degradation of synthetic polymers and lack of osteoconductivity of polymeric scaffolds. Thus the development of ceramic-

biodegradable polymer composites is of great interest in bone tissue engineering to achive desirable mechanical property.

Hydroxyapatite $Ca_{10}(PO_4)_6(OH)_2$ is an important biomaterial constituent of bone and teeth. It is used in the replacement of hip joints, heart valves etc. Due to its similarity with bone material at chemical and crystallographic structure hydroxyapatite, is used as bio-active material in bone tissue engineering [77]. Hydroxyapatite can be synthesized by using chemical source of calcium like calcium nitrate or by using natural source of calcium like egg shell. Using natural source will minimize the impurities like silica in the material. Concentrations of reactant were determined by the fact that Ca/P ratio for hydroxyapatite equal to 1.67 [78]. Bioactive glass and other class of ceramic material are able to stimulate bone regeneration better than other bioactive ceramic materials. Although in vivo study reveals that bioactive glass possess ability to bond with bone much faster in comparison of other bioactive ceramics. Also in vitro studies shows that its osteogenic property are due to the product formed after its dissolution which stimulate stem cell at genetic level to form bone [79-80]. Professor Hench made a biodegradable glass with Na_2O-CaO-SiO_2-P_2O_5 system having high calcium content. Hench developed a glass having composition 46.1 mol% SiO_2, 24.4 mol% Na_2O, 26.9 mol% CaO and 2.6 mol% P_2O_5, later called as 45S5 Bioglass [81-82]. Dissolution of glass leads to the formation of carbonated hydroxyapatite on the surface of glass. carbonated hydroxyapatite is similar to bone mineral, and interact with collagen fibrils that leads to formation of mineralized bone extra cellular matrix [82]. Soluble silica and calcium ions stimulate osteoprogenetor cells to produce bone matrix [83]. Dissolution rate of glass were regulated by varying its composition and thus can be used for long term regeneration therapy as well as short term regeneration therapy. Various types of bioactive glasses developed are conventional silicates (45S5 Bioglass), phosphate based glasses, and borate based glasses, which were made by either melt-down method or by sol-gel method.

Biocomposites

The ideal scaffolds for bone tissue engineering must possess appropriate pore size, porosity, mechanical strength, biodegradability, biocompatibility and ability to integrate with host bone tissue. However polymeric scaffold alone fails to provide proper mechanical strength,

bioactive environment for cell differentiation and structural feature for bone tissue regeneration. Thus in recent years, composite materials gained tremendous attention to fulfil the properties like bioactivity, biocompatibility, biodegradability and mechanical strength for successful bone tissue regeneration. Composites are fabricated by using two or more different materials like polymers (silk fibroin, chitosan, and gelatin etc) and ceramics (hydroxyapatite, bioglass and tricalcium phosphate etc). Bioceramics in polymers-ceramics composite improves its osteogenic differentiation potential, upregulated various osteogenic genes such as collagen type 1, osteocalcin, runt-related transcription factor, bone sialoprotein and alkaline phosphatase activity. Thus bioceramic based polymeric composite may provide suitable platform for bone tissues regeneration.

1.4.3 Scaffold fabrication techniques

Artificial extracellular matrices (scaffold) with three dimensional architecture have gained widespread application in tissue engineering due to their nano-scale topography, biomimetic property and ability to direct specific tissue regeneration. As of now there are various techniques available to fabricate scaffold such as electrospinning, freeze drying, phase separation, rapid prototyping and particulate leaching [84]. But the numbers of challenges are still need to overcome for developing a functional smart matrix for successful bone tissue regeneration. Apart from the fabrication of scaffold by using various techniques, surface modification of scaffold is also desirable to improve cell attachment, migration, proliferation and differentiation. Various methods and its merits and demerits are listed out in Table 1.1 [85]. The most important methods are described below.

Particulate leaching

Artificial extracellular matrix (scaffold) provide appropriate surface for cell attachment, proliferation and help in tissue regeneration. Pore size and porosity of scaffold are one of the crucial factors which determine specific surface area for cell adherence and tissue in-growth [86]. Particulate leaching technique involves preparation of polymer solution with well distributed salt particles with uniform diameter followed by evaporation of solvent leaving behind polymer matrix [87]. The polymer –salt composite is then soaked in water to remove salt through leaching. The porogens particle size, amount and shape determine pore size and porosity of developed scaffold by particulate leaching method [84].

Melt molding

Melt molding method involves the filling of mould with polymer powder and porogens of specific diameter followed by heating above the glass transition temperature of polymer under applied pressure. This leads to binding of polymeric materials together and then porogens are leached out using non-solvent. Finally porous scaffold with appropriate morphology and shape are fabricated. However the major disadvantage of melt molding method includes high processing temperature and residual porogens.

Freeze drying

Freeze drying a drying process based on the principle of sublimation is used to fabricate porous structure and to convert solution with useful labile material into solid form with good stability [84]. It has wide application in food science, pharmaceutical, enzyme stabilization and biomedical applications [88]. Freeze drying process mainly consists of three steps freezing of solution at low temperature (-20°C to -80°C), followed by primary drying at -110°C under low pressure (high vacuum) [88]. The porous structure with proper interconnectivity is obtained from polymeric solution through freeze drying. The pore size, distribution and interconnectivity of pores can be controlled through the controlling rate of freezing and direction of solidification [84]. However, it's a time consuming process but avoids high temperature and separate leaching step as involved in other process such as melt molding, particulate leaching etc [84].

Freeze gelation

The freeze gelation technique based on freezing of polymeric solution followed by use of non-solvent to generate phase separation in polymeric solution, which finally leads to development of porous scaffold [84]. While freeze gelation two distinct phase develop one having high polymer concentration and other is polymer deficient [84]. As the temperature lowered liquid-liquid phase separations occur and quenched to form solid phase and the solvent phase, where the solvent phase is finally removed by extraction, evaporation and sublimation to fabricate three dimensional porous structures [84]. Polymeric nanofiber can also be fabricated using phase separation method however selection of solvent and phase separation temperature is crucial factor for nanofiber formation [84].

Table 1.1 Advantage and disadvantage of various scaffold fabrication techniques

Techniques	Advantages	Disadvantages	References
Solvent casting/ Particulate leaching	Control over Porosity, pore size and crystallinity	Limited mechanical property, residual solvents and porogen material	[89]
Porogen leaching	Controlled over porosity and pore geometry	Inadequate pore sizeand pore interconnectivity	[90]
Gas forming	Free of harsh organic solvents, control over porosity and pore size	Limited mechanical property, inadequate pore interconnectivity	[84]
Self-assembly	Control over organization of biomolecule, fiber diameter, porosity	Complicated and elaborated process, high cost of synthesis of biomaterial	[91]
Electrospinning	Control over porosity, pore size and fiber diameter	Limited mechanical property, pore size decrease with fiber thickness	[92]
Phase separation	No decrease in the activity of the molecule	Difficult to control precisely scaffold morphology	[93]
Rapid prototyping	Excellent control over geometry, porosity, no supporting material require	Limited polymer type highly expensive equipment	[54, 94]
Fiber mesh	Large surface area for cell attachment, rapid nutrient diffusion	Lack the structure stability	[95]
Fiber bonding	High surface to volume ratio, high porosity	Poor mechanical property, limited applications to other polymers	[96]
Melting molding	Independent control over porosity and pore size	Required high temperature for non-amorphous polymer	[97-98]
Membrane lamination	Provide 3D matrix	Lack required mechanical strength, inadequate pore interconnectivity	[99]
Freeze drying	High temperature & leaching not required	Small pore size and long processing time	[85, 100]

Self assembly

Self assembly technique is based on organization of the natural or synthetic molecule in to nanofibrous structure. The method is based on interaction between hydrophilic and hydrophobic domain of amphiphilic peptides, which further assemble into nanofibrous structure through weak non covalent bonding such as hydrogen bond, van der waals interaction, ionic interaction etc. Apart from peptides synthetic polymer molecule can also be used to fabricate nanofiber by self assembly method. The major advantage of self assembly

method is fabrication of nanofiber from aqueous solution and avoids organic solvent, thus reduce the cytotoxicity. However, this technique is very complicated.

Electrospinning

Electrospinning is a versatile technique used to fabricate polymeric fibers with diameters either in nanoscale or microscale range. Electrospinning technique is classified as needle based electrospinning and free liquid surface electrospinning both are operated at high electric voltage. The needle based electrospinning machine consists of a syringe pump, high voltage electric source and collector, where free liquid surface electrospinning consists of spinning electrode tray, high voltage source and collector electrode. In needle based electrospinning high voltage is applied to a syringe filled with polymer solution and under high electric field polymer solution electrospun and deposited on collector positioned at appropriate distance. In free liquid surface electrospinning spinning electrode carries thin layer of solution over its surface and under high electric field polymer solution electrospun over collector positioned at appropriate distance. In both the cases when charge repulsion under high electrical field overcomes the surface tension a charged jet of polymer solution formed. Finally, the solvent get evaporated under dehumidified condition leading to the formation of electrospun fibers over the collector. Although electrospinning is the simplest method to fabricate nanofibrous scaffold, it needs further improvement in order to fabricate scaffolds for complex tissues 3D in particular.

Rapid prototyping

Rapid prototyping (RP) is computer controlled technique used to produce three dimensional scaffolds by using layer by layer deposition method [84]. Rapid prototyping is also called as solid free form technique. The RP method is based on computer assisted design (CAD) and computer assisted manufacturing technique [87]. It allows fabrication of scaffold with better control of internal and external macroshape in comparison to other fabrication techniques [87]. Rapid prototyping uses images of site of wound and create CAD model, which is further reduced to a thin slices to utilize it to deign appropriate three dimensional architecture [84]. Finally three dimensional structures are developed by layer by layer deposition of polymeric or polymer composite solution using rapid prototyping [84]. This is the most suitable technique to fabricate scaffold with appropriate deign or architecture for complex tissue

regeneration. The comparison of various scaffold fabrication technique are shown in table [1.1].

1.4.4 Stem cells for tissue engineering

In recent years great interest has been shown by the researchers in stem cell research and derivation of its potential applications in tissue regeneration and other biomedical applications [101]. The development of tissue engineered construct *in vitro* requires three dimensional scaffolds seeded with cells derived from patient native tissue. However, the invasive method of cell collection and disease carrying possibilities limit their application [102]. Therefore stem cells such as embryonic stem cells and mesenchymal stem cells from various sources has gained much attention in recent years for tissue engineering applications [102-103].

Embryonic stem cells

Embryonic stem cells are isolated from blastocyst before uterine implantation and are maintained for longer culture duration [101]. The embryonic stem cells can be characterized by analysing various markers such as CD324, CD90, CD117 and CD326 [104]. The important characteristics of embryonic stem cells are their ability to maintain undifferentiated stage for longer period, capable of self renewal, lead to formation of teratoma and ability to differentiate into all three germ layer [101-102]. Though embryonic stem cells are one of the prominent cell types for the development of tissue engineered constructs, the formation of teratoma and teratocarcinoma limits their applications in tissue engineering [102].

Mesenchymal stem cells (hMSCs)

Mesenchymal stem cells are post-natal stem cells and having capability to differentiate into various cell types such as chondrocytes, osteoblasts, adipocytes, muscle cells and neural cells [105]. hMSCs shows expression of a unique cell surface markers such as STRO-1, CD29, CD73, CD90, CD105, CD146 and Octamer-4, whereas negative for hematopoietic stem cell marker such as CD14, CD45 and CD34 [106]. Bone marrow mesenchymal stem cells having colony forming ability, fibroblast like morphology and capable to differentiate both *in vitro* and *in vivo* without any specific treatment into osteoblast cells. Also hMSCs leads to form

mineralized nodule when cultured with a specific medium. Various animal models were used and bone tissue regeneration capability of hMSCs was observed [105]. Also ceramic carriers loaded with hMSCs shows significant improvement in bone tissue regeneration and thus confirm its therapeutic application [105].

Umbilical cord blood derived mesenchymal stem cells shows ability to differentiate into cells of multi-lineage fate such as adipocytes, osteoblasts, hepatocytes and neuronal cells [105]. Also the gene expression profile and cell surface marker was observed to be similar of hMSCs gene expression [105]. In animal models, umbilical cord blood derived mesenchymal stem cells shows in vivo differentiation capability and immunocompatibility with host tissue even in xenotransplantation as they are immunologically younger [107-108]. Thus cord blood derived mesenchymal stem cells would also be used as prominent therapeutics stem cell source for bone tissue engineering application.

1.4.6 Bone

Bone tissue is a mineralized, dynamic, highly vascularised and have the capacity to heal and remodel [109]. Besides providing structural support to the body, it also acts as mineral reservoir, withstands body load, protect internal body structure and supports muscular activity [53, 109]. Thus any diseases or injury to bone may alter the body function and lifestyle. The present available treatment for bone tissue related injury or diseases are mostly consisting of titanium or stainless steel based bone graft or autografts, allografts and xenografts. However metal based bone grafts have several limitations such as poor integration with host tissue and failure due to fatigue loading, which are of major concern. Whereas natural bone tissue based graft from various sources suffer from non-availability, possibilities of immune rejection and pathogen transmission from donor to host [53]. Even though ceramic based bone substitutes offer more favourable environment for bone tissue regeneration but their application are limited due to low tensile strength and brittleness [53]. Hence for satisfactory and successful bone tissue injury recovery, a much more advanced alternative therapeutics is of great demand and tissue engineering could be a possible solution.

Structure and composition of bone

Bone tissue extracellular matrix consists of two major components, a biomineral component constituted of hydroxyapatite, which covers 65% to 70% of the extracellular matrix and an organic component consisting of proteoglycans, glycoproteins, bone sialoproteins and bone gla proteins which cover 25% to 30% of the extracellular matrix. Various components of extracellular matrix of bone and its role highlighted in Table 1.2.

Table 1.2: Various component of extracellular matrix of bone and its role

Bone Extracellular matrix constituent	Functions and properties	Reference
Collagen I	Responsible for matrix calcification and skeletal framework construction	[110]
Byglican, Decorin	Control collagen fiber growth and diameter, participate in mineralization of bone matrix	[111]
Osteonectin	Hydroxyapatite nucleation and bind with calcium and collagen and help in resorption of bone tissue and remodelling	[112]
Thrombospondin	Glycoprotein binds calcium and hydroxyapatite, facilitate adhesion of cells through RGD-independent fashion	[113-114]
Fibronectin	Help in osteoblast adhesion, attachment	[115]
Osteopontin	Helps in remodelling of bone tissue	[112]
Bone sialoprotein	Bone sialoprotein; major constituent of cement line of bone tissue	[112]
Osteocalcin	late marker of osteogenic phenotype, regulate mineralization of matrix and remodelling of bone tissue	[116-117]

Types of bone and bone cells

Bone tissue is classified depending upon its architectural forms as cancelous or spongy bone, which covers 20% of the total skeleton and cortical or compact bone which covers 80% of the total skeleton. Cortical bone posses 10% porosity, whereas cancelous bone posses around 50-

90% porosity. Thus, cortical bone posses 20 times higher ultimate compressive strength than cancelous bone. Bone tissue is a mineralized connective tissue which is made up of mineral phase mainly hydroxyapatite, organic phase and various bone cells such as osteoblast, osteocytes and osteoclasts [118]. However the role of bone cells is not well understood through they play vital role in coupling bone resorption to bone formation [118]. Each type of bone cells have particular functions and thus play important role in maintenance of a healthy bone [53]. The characteristics and functions of bone cells are detailed in Table 1.3.

Table 1.3: Bone cells and their function

Cell type	Morphological characteristics	Function	Reference
Osteoblasts	Cuboidal in shape and polarized cell	Regulate bone extracellular matrix deposition and mineralization,	[119-121]
Osteocytes	Stellate shaped	Calcification of the bone matrix, blood calcium homeostasis,	[122]
Osteoclasts	Multinucleated and polarized cells	Mediate bone resorption	[123]

1.4.7 Silk fibroin as ideal biopolymer for tissue regeneration

Silk is a natural biopolymer used in the textile industry from centuries because of its luster and mechanical property. Various organisms such as members of class Arachnida and of order Lepidoptera produces silk [14, 124]. These organisms produces silk fibroin (SF) to provide structural framework in cocoon formation, nest building and protection of eggs [14]. Silk fibroin protein consists of beta-sheet structure and rich in hydrophobic domains with short side chain amino acid, which allows tight packing of stacked anti-parallel chains of the protein [14]. The hierarchical molecular structure of silk fibroin consists of large hydrophobic domains interspaced with smaller hydrophilic domains, which provide excellent assembly of silk fibroin and higher tensile property [14]. Silk fibers from *B.Mori* used as suture material in medical feild for centuries, thus silk fibroin have been widely investigated as promising biomaterial for tissue engineering applications [14]. The flexibility of silk fibers makes it suitable for the development of scaffold for load bearing bone tissue regeneration [125]. The superior mechanical characteristic of silk fibroin scaffold as compared of other natural polymers scaffolds makes silk fibroin as suitable candidate for bone tissue engineering applications [126]. Silk fibroin possess various important characteristics such as

biocompatibility, biodegradability, solubility in aqueous/organic solvent, ease to process into various forms of structure (film, nanofiber, porous) and tuneable mechanical strength, which make it suitable biopolymer for wide application in biomedical and tissue engineering [14]. However due to lack of bioactivity, hydrophilicity and osteoconductivity property, silk fibroin alone is not able to offer suitable template for bone tissue regeneration. Therefore, it is of great need to fabricate calcified SF or composite SF scaffolds combined with biocermics is of paramount importance.

1.4.8 Future prospects of tissue engineering

Tissue engineering is emerging as one of the potential science and technology applications to restore, maintain or replace the damaged and/or diseased tissues of different type. However in current scenario, it needs to be far broader in coming future, which not only deals with the development of engineered tissue to reduce organ transplantation but also accelerate the novel drug development. Although some of the tissue engineered products have been approved by the Food and Drug Administration and more than 70 corporate companies and government research agencies are spending 600 million dollar per year for the development of novel tissue engineered products [8, 127]. The production of tissue engineered product at large scale requires efficient technique to isolate, culture and maintenance of cells for longer duration, optimization and development of smart scaffolds, and development of suitable bioreactor to mimic body tissue environment and capable to scale-up [8]. Thus in future, tissue engineering will emerge as a potential clinical treatment method as compared to traditional clinical approaches to cure not only bone but other tissue defects and diseases as well.

1.4.9 Thesis outline

The entire thesis wsork has been organised in six chapters as follows: **Chapter 1-** deals with the general introduction on the topic including the principle of tissue engineering and its application to bone TE by overcoming the limitations associated with the current clinical approaches, extracellular matrix and its role, strategies employed to fabricate and develop smart polymeric matrices for bone tissue engineering. **Chapter 2-** presents the literature review covering fundamental concept and recent advancement in silk fibroin, cellulose and its derivatives based scaffold fabrication for bone tissue engineering application. It also

covers the possible ways to improve or modify bio-relevant properties as well as material characteristic of silk fibroin scaffold for its successful application in bone tissue regeneration. **Chapter 3-** describes the scope and objective of the research work. **Chapter 4-** presents materials and methods adopted to fabricate silk fibroin and carboxymethyl cellulose based composite nanofibrous scaffold incorporated with nano-bioglass and copper doped nano-bioglass. It covers various methods adopted to evaluate physical, chemical and biological characterization of developed scaffolds. **Chapter 5-** presents the result and discussion of experimental work, which is sub-divided into the following parts: **Chapter 5A** deals with the development of SF and SF/CMC blend scaffolds and their characterization for physical, chemical and biological property. **Chapter 5B** describes the synthesis and characterization of nano-bioglass. **Chapter 5C** reports on the further improvement of osteogenic potential of SF/CMC nanofibrous scaffold by incorporation of nano-bioglass. **Chapter 5D** deals with improvement of osteogenic and angiogenic potential of SF/CMC composite scaffold loaded with copper doped nano-bioglass. **Chapter 6-** presents a brief summary and conclusion of the experimental work along with suggested future study.

CHAPTER 2: Literature Review

2.1 Current status, prospects and challenges of bone tissue engineering

Bone tissue defects and diseases because of the consequences of trauma, degeneration infection, deformity etc affecting human life style as well as death are of major concern in health sector. Every year, more than 700,000 total joint replacement are performed only in the US [128], whereas, 50% of total osteoporotic hip fracture has been projected to occur in Asia alone by 2050 [129]. In India, approximately 26 million osteoporosis patients was reported in 2010 and was expected to reach 36 million by 2013 [130]. It has been reported that more than 51 million peoples had been diagnosed with some form of arthritis, according to the National Health Interview Survey [131]. This prevalence is higher than many well known diseases. Current clinical treatment strategies for cartilage tissue and subchondral bone damage like mosaicplasty, autologous chondrocytes implantation (ACI) and marrow stimulation technique have varying success rates, but average long-term results are unsatisfactory thereby eventually pain continues [132-133].

The various clinical approaches such as artificial prosthesis, surgical reconstruction and other bone grafts (allografts, autografts and xenografts) are currently used to treat various bone tissue defects. However due to some of the major limitations of such approaches like corrosion of prosthesis, immunogenic reaction, disease transmission, donor morbidity and lack of donor limits their applications. In this context the reparative ability of bone tissue leads to adopt various tissue engineering strategies to develop alternative clinical treatment options [134]. For this appropriate molecular and macroscopic architectural framework of regenerated tissue are essential factors of consideration in tissue engineering approaches. Bone tissue engineering particularly deals with the development of living tissues *in vitro* through growing cells over bioactive degradable scaffolds. Thus it is important to understand cell behaviour over the scaffold surface, role of scaffolding material to guide tissue specific differentiation of cells and their assembly into 3D functional tissue [8]. In addition fabrication and design of scaffold are also crucial factors which determine the successful development of functional tissue construct. Selection of ideal biomaterial is crucial mainstay of tissue engineering as it plays key role in guiding bone tissue regeneration, angiogenesis and growth of nerves under the orchestrate activity of specific cell signalling molecule [8].

2.2 Ideal biomaterials for bone tissue engineering

The ideal scaffold material should mimic the body extracellular matrix to support cell adhesion, cell proliferation and differentiation leading to tissue regeneration [54, 135]. Scaffolding material and fabrication technology play critical role in designing and development of appropriate functional three dimensional artificial extracellular matrices. Developed scaffold should have high porosity, appropriate pore size, biodegradability, biocompatibility, bioactivity, needed to degrade with regeneration of damaged tissue parallelly, should provide high surface area for cell adhesion, proliferation and migration, adequate mechanical strength, ability to deliver active molecules to guide cell proliferation and tissue specific differentiation [136-138]. Natural and synthetic biopolymer alone or in combination are the primary scaffolding material, as these can be easily molded into appropriate architecture, facilitate surface modification to improve cell interaction and biomineralization for bone tissue engineering application [139]. For successful bone tissue regeneration polymeric materials are reported to be reinforced with bioceramic to achieve scaffold with enhanced osteogenic potential or other desirable properties [140].

For tissue engineering application it is of great need to fabricate scaffold from bioactive biodegradable material that provide physical and chemical cues to guide cell adhesion, proliferation, differentiation and assembly into appropriate three-dimensional structure similar to native tissue [141]. The basic requirements of the biomaterials used for fabrication of scaffold are biocompatible, suitable mechanical strength and bioactivity. However to meet such requirement single polymeric materials cannot fulfil the desirable prerequisite for tissue regeneration [141]. Therefore, multi-polymeric material system might be a suitable strategy to design and fabricate functional biomaterial [141]. The potential biopolymers have been explored for TE application in recent decades includes silk fibroin [142], chitosan [143], collagen [144], and so on. Whereas bioceramics such as hydroxyapatite, beta-tricalcium phosphate and bioglass at both micro and nano scale are reported as suitable bioceramics for making composite with biopolymer [145]. Further, interaction between bioceramics and polymer matrix at nano scale provides enhanced mechanical and functional properties to polymeric nanocomposites [141]. In fact, natural bone tissue extracellular matrix are made up of organic/inorganic composite material of collagen and apatite, thus composite materials are

appropriate choices to design and fabricate scaffold for bone tissue engineering [146]. To optimize or adjust the properties of scaffolding biopolymers to apply in tissue engineering application, a wide variety of approaches are considered for their modification. The biopolymer surfaces have been physically and chemically modified with bioactive agents after the processing condition, which consequently provides bio-modulating or biomimetic microenvironment for tissue regeneration [141, 147]. Thus, various approaches has been adopted to modify the surface of scaffolding materials in order to achieve desired surface characteristic for improvement of tissue regeneration.

Various surface treatment techniques such as plasma treatment [148], ion sputtering [149], oxidation and corona discharge [150] has been considered as potential methods of modifying surface characteristic of polymeric material without much affecting their bulk properties [141]. Furthermore, to improve apatite nucleation or deposition polymeric surface was functionalized with calcium ion using calcium chloride solution [151]. The surface of scaffolding materials were conjugated with extracellular matrix component or peptide sequence like Arg-Gly-Asp (RGD sequence) to achieve superior cell adhesion [152]. The incorporation of RGD sequence improved the scaffold bio-responsive surface site for integrin receptors of cells that eventually facilitated integrin mediated cell adhesion process. Biopolymers such as silk fibroin and chitosan used as scaffolding materials were also reported to be cross-linked using carbodimide chemistry to graft cell adhesive peptides and to improve physico-chemical, biological and degradation properties [153-154]. Various natural and synthetic biopolymers and its application listed out in table 2.1.

Table 2.1: Various biopolymers and its application in tissue engineering.

Sl. No.	Biopolymer	Application	References
1	Silk Fibroin	Bone, cartilage and hepatic tissue engineering, Drug delivery	[15, 155-157]
2	Chitosan	Bone and cartilage tissue engineering, Drug delivery, wound healing	[143, 158-159]
3	Chitin	Bone, cartilage and dental tissue engineering, wound healing, drug delivery	[158, 160]
4	Starch	Bone tissue engineering, biomolecules and	[161-162]

		cell delivery	
5	Pectin	Bone tissue engineering, drug delivery	[163]
6	Cellulose	Bone and vascular tissue engineering,	[164]
7	Carboxymethyl cellulose	Bone tissue engineering, drug delivery	[165-166]
8	Gelatin	Bone, cartilage and nerve tissue engineering	[167-169]
9	Polyvinyl alcohol (PVA)	Cartilage and orthopaedic application	[170]
10	Poly(caprolactone) (PCL)	Bone tissue engineering, drug delivery	[171]
11	Poly(3-hydroxybutyrate)	Bone and cartilage tissue engineering, peripheral nerve regeneration	[172-173]
12	Poly(dioxanone)	Cardiovascular and Vascular tissue engineering	[174-175]
13	Poly(glycolic-co-lactic acid)	Bone tissue engineering	[176]
14	Poly(lactic acid)	Bone, cartilage and neural tissue engineering	[35, 177-178]
15	Poly(glycolic acid)	Bone, cartilage and musculoskeletal tissue engineering	[42, 179-180]

2.3 Silk fibroin based polymer-polymer blend scaffold

Silk fibroin is a unique biomaterial with various superior characteristics such as biocompatibility [181], biodegradability [182] and tuneable mechanical properties [183], which offer suitable platform for cells adhesion, proliferation and migration. Silk fibroin can be dissolved in both aqueous as well as in organic solvent and can be molded in to various structures such as film, fiber and porous architecture for various tissue engineering applications [184-186]. Non-woven silk fibroin mats having higher surface area and roughness, which provide superior surface topography thereby improving cell attachment phenomenon while tissue regeneration. Electrospinning technique is the most commonly used to fabricate non-woven mats. Park et al (2004) reported successful electrospinning of silk

fibroin (SF) and chitosan (CS) blend prepared in formic acid and demonstrated about significant conformational changes of the as-spun SF/CS blend nanofiber with improved β-sheet content [187]. Chen et al (2012) also reported on fabrication of biomimetic SF/CS nanofiber and observed osteogenic potential of SF/CS blend nanofibrous scaffold [188]. Fabrication of porous SF/CS based scaffold with interconnected porous structure, suitable antimicrobial, degradation and mechanical property for tissue engineering especially cartilage was also reported [19]. Fan et al (2008) fabricated silk cable-reinforced silk fibroin based hybrid scaffold and observed to be suitable candidate for ligament tissue engineering, as it support proliferation and differentiation of co-culture mesenchymal stem cell/anterior cruciate ligament fibroblast cell [189]. Twisted structure developed using degummed silk fiber provides appropriate mechanical integrity (maximum load of 2337 ± 72 N, elastic modulus of 354 ± 26 N/mm and strain at failure of 38.6 ± 2.4 %) closer to native ligament tissue, thus play vital role in ligament tissue regeneration [190]. Navakovik et al. developed six-cord silk fiber with appropriate configuration for enhanced tissue infiltration and ligament tissue regeneration [191].

Various components derived from natural extracellular matrix such as gelatin, collagen, chondroitin sulphate etc are of prime interest of researchers for development of suitable scaffold for tissue engineering applications. Fabrication of silk fibroin and gelatin blend nanofiber with improved mechanical and biological property was reported to be suitable template for vascular tissue engineering application as it support proliferation of umbilical vein endothelial cells proliferation [192]. Sung et al (2008) reported fabrication of silk fibroin and collagen based biomimetic nanofibrous scaffold, which support cell attachment and spreading of fibroblast cell and observed to be potential material for wound dressing and tissue engineering applications [193]. Hu et al (2010) developed silk fibroin and hyaluronic acid based non-chemical cross-linked hydrogel with improved mesenchymal stem cell attachment and proliferation potential and observed to be suitable candidate for tissue engineering application [194]. Also various researchers developed silk fibroin and plant derived biopolymer such as starch, cellulose, pectin, carboxymethyl cellulose etc based blend scaffold for tissue engineering and other biomedical applications. Cellulose and its derivative based biomaterials are used for various applications such as carrier for immobilization of enzymes, hemodialysis and drug releasing scaffolds [195-197].

Cellulose and its derivatives has wide application in hard and soft tissue engineering such as bone regeneration, cardiac tissue engineered construct, artificial liver and connective tissue regeneration [151]. Also cellulose based biomaterial performance can be improved by functionalization with small amount of cations [198]. Kundu et al (2011) reported fabrication of silk fibroin and carboxymethyl cellulose based film with improved properties such as hydrophilicity, surface roughness, transparent, mechanical flexibility, swelling ratio, homogeneous and biocompatibility and thus observed to be potential biomaterial for biotechnological application [199]. Numata et al (2014) demonstrated fabrication of silk fibroin and pectin based hydrogel with suitable mechanical property, biocompatibility, biodegradability and elasticity and suggested to be suitable for various biomedical applications [200]. Electrospun nanofibrous tubular matrices offer suitable structural integrity and withstand arterial pressure similar to native arterial pressure of blood vessel, thus could be successfully used for vascular tissue engineering applications [201]. Electrospun tubular silk fibroin scaffold from silk fibroin dissolved in formic acid can resist pressure up to 575 mmHg, which is higher than the upper physiological and pathological pressure of 120 mmHg and 180-220 mmHg, makes it suitable for vascular grafts [202]. Also anticoagulant property of scaffolding matrices play important role in development of scaffold for vascular tissue engineering applications. Silk fibroin based matrices treated with chlorosulphonic acid in pyridine develop antithrombogenicity property and thus observed to be suitable artificial extracellular matrices for vascular tissue regeneration [203].

However, silk fibroin and natural polymer blends offer various advantages but even though there is various disadvantages like poor crystallinity of SF/CS based porous scaffold, poor thermal stability of SF/gelatin, high hydrophilicity of SF/collagen, water insolubility of SF/chitin and poor mechanical property of SF/hyaluronic acid. Thus researchers were also developed SF and synthetic polymer blends based scaffold for tissue engineering applications. Wang et al (2009) developed Polylactide/SF/Gelatin based fibrous tubular scaffold by electrospinning with appropriate mechanical strength of 2.21 ± 0.18, suitable biocompatibility with 3T3 mouse fibroblast, induce minor inflammatory reaction in vivo and thus proposed to be suitable candidate for vascular tissue engineering applications [17]. Poly L-lactic acid/SF/Gelatin based multilayer electrospun scaffold with desirable pliability,

porosity, and breaking strength, also observed to be biocompatible and biodegradable and suitable for tissue engineering applications [18].

Fibroblast growth factor releasing SF/ Poly(glycolic-co-lactic acid) based knitted scaffold, was reported to support mesenchymal stem cell proliferation and tenogeneic differentiation and thus observed to be suitable substratum for ligament/tendon tissue engineering applications [34]. Mcclcure et al (2009) demonstrate fabrication of PCL/SF based nanofibrous scaffold with various suitable properties such as mechanical strength, biocompatibility and biodegradability for vascular tissue engineering applications [204]. Bhattacharjee et al also demonstrated development of SF/PCL based nanofibrous scaffold with superior biocompatibility, biomineralization, biodegradability, ECM deposition, Alkaline phosphatase activity and suitable mechanical property for bone tissue engineering [205]. However, it has been reported that SF based polymeric scaffold lacks proper bioactivity and osteoconductivity, which limits its application as suitable biomaterial for bone tissue engineering application [16]. Thus it has been observed that silk fibroin matrices of various forms like film, fiber and porous structure are suitable for cell adhesion and proliferation but poor bioactivity and osteoconductivity property limits their applications [16]. Thus, currently development of silk fibroin based composite scaffolds with improvised bioactivity, hydrophilicity and osteoconductivity are of paramount importance for bone tissue engineering applications. Various silk fibroin and other polymer blend based scaffold and its application was listed out in Table 2.2.

Table 2.2: Various silk fibroin-biopolymer blend based scaffold and its application in tissue engineering.

Sl. No.	Polymer-Polymer blend	Morphologic form	Application	References
1	Silk fibroin/Chitosan	Nanofiber, porous	Bone and cartilage tissue engineering	[188]
2	Silk fibroin/Gelatin	Nanofiber, cable	Vascular and ligament tissue engineering	[189, 192]
3	Silk fibroin/Collagen	Nanofiber	Wound dressing and tissue engineering	[193]

4	Silk fibroin/ Hyaluronic acid	Hydrogel	Tissue engineering and other biomedical applications	[194]
5	Silk fibroin/Pectin	Hydrogel	Various biomedical applications	[200]
6	Silk fibroin/Carboxymethyl cellulose	Film	Various biotechnological application	[199]
7	Polylactide/SF/Gelatin	Tubular	Vascular tissue engineering	[17]
8	PLA/SF/Gelatin	Nanofibrous	Various tissue engineering application	[18]
9	SF/PLGA	Knitted	Ligament/tendon tissue engineering	[34]
10	PCL/SF	Nanofibrous	Various tissue engineering application	[204]
11	SF/PCL	Nanofibrous	Bone tissue engineering	[205]

2.4 Silk fibroin based polymer-ceramic composite scaffold

Various researchers have reported the limitation of bioactivity and osteogenic property (osteoconductivity and osteoinductivity) of polymeric scaffolds [16]. However after investigation of cell behaviour and its lineage specific differentiation over polymer-ceramic based composite scaffold, researchers have demonstrated the improvement of cell adhesion, cell proliferation and differentiation when scaffold matrices were reinforced/added with bioceramic [206-207]. Thus, there is a growing interest for the development of ceramic-biopolymer composites for successful bone tissue regeneration. Biocermics such as hydroxyapatite, beta-tricalcium phosphate and bioglass play vital role in enhancement of osteoblast proliferation and differentiation [208-210]. Ceramic-biopolymer composites have been used for coating of metallic implant surface and to filling bone defects of dental and other bone tissues during orthopaedic surgery, thereby improved implant integration with host bone were achieved [16]. Till date researchers are not yet completely understood the exact signalling cascade in response of hydroxyapatite but yet various report on signalling

mechanism such as ERK/SOX9, BMP/Smad, Wnt, TGF-β, MAPK and Notch pathways upon interaction of mesenchymal stem cells in response of hydroxyapatite were reported [211]. Silk fibroin based porous scaffold incorporated with hydroxyapatite through alternate soaking method of $CaCl_2$ and Na_2HPO_4 or by mixing hydroxyapatite with silk fibroin solution has shown improved or higher bone tissue regeneration capability as compared to unmodified silk fibroin scaffolds [212]. Cao et al. developed 3% hydroxyapatite-silk fibroin reinforced calcium phosphate cement/silk fibroin scaffold with enhanced compressive strength of 50.2 ± 1.9 MPa [213]. Silk fibroin/gelatin/nano-hydroxyapatite (nHAp) composite scaffold with appropriate pore size, 50% – 60% porosity and mechanical property prepared by freeze drying was also reported to support proliferation and attachment of mouse pre-osteoblast cells [214]. Such SF/gelatin/nHAp based porous scaffold may be suitable for bone tissue engineering applications.

Silk fibroin and hydroxyapatite based composite hydrogel shows higher compression modulus as well as improved osteogenic potential due to scaffold reinforcement and osteoconductivity properties [215]. However for load bearing bone tissue engineering application hydroxyapatite based scaffold was also reported, where SF was used as sacrificial polymer and observed to be suitable for bone tissue engineering application as it support proliferation and differentiation of bone marrow derived mesenchymal stem cells [216].

Electrospun silk fibroin and hydroxyapatite as well as hydroxyapatite loaded with BMP-2 based nanofibrous composite offered improved growth of mesenchymal stem cells growth and their osteogenic differentiation. However BMP-2 loaded hydroxyapatite shows better osteogenic potential than hydroxyapatite alone in silk fibroin based composite matrices [63]. Kim et al. developed 20 wt% hydroxyapatite loaded silk fibroin based composite electrospun scaffold with superior mechanical properties [217].

However, bioactive glass as another class of bioceramics shows higher bioactivity and degradation properties as compared to hydroxyapatite and beta-tricalcium phosphate, thus it led to better bonding of bioglass based composite scaffold with host tissues [218]. Also dissolution of bioglass led to availability of bone trace element such as Si, which is reported to stimulate osteogenesis and improvised bone tissue regeneration [219]. Silk fibroin coated

mesoporous bioglass scaffold shows improved cytocompatibility, mechanical properties, degradation and osteogenic potential for bone tissue engineering applications [220]. Trace metal ion (copper, cobalt, strontium etc.) releasing bioactive glass was also reported to be suitable for development of scaffold with osteogenic and angiogenic potential [221-223]. C Wu et al demonstrated development of copper containing mesoporous bioactive glass scaffolds with enhanced osteogenic and angiogenic potential for bone tissue engineering. Similarly, cobalt doped mesoporous bioglass scaffold was also demonstrated to be suitable candidate for with enhanced osteogenic and angiogenic potential for bone tissue engineering applications [222]. However silk fibroin and nano-bioglass based nanofibrous scaffold has so far not been developed and investigated for bone tissue engineering applications. Table 2.3 depicts the various silk fibroin based composite scaffolds with improved properties reported earlier.

Table 2.3: Silk fibroin based composite scaffolds and their advantages

Sl. No.	Scaffold content	Type of scaffold	Advantage and application	References
1	SF/Hydroxyapatite (By alternate soaking method)	Porous	Biocompatible, biodegradable & osteogenic, suitable for bone tissue engineering	[212]
2	SF/Gelatin/nHAp	Porous	Biocompatible, support attachment & proliferation of mouse pre-osteoblast, suitable for Bone tissue engineering.	[214]
3	SF/Hap	Hydrogel	Biocompatible, higher compression modulus as well as improved osteogenic potential	[215]
4	Hap/SF (SF used as sacrificial polymer)	Porous	High compressive strength (152 MPa), biocompatible and support osteogenic differentiation of bone marrow derived mesenchymal stem cell. Suitable for load bearing bone tissue regeneration.	[216]
5	SF/Calcium polyphosphate	Porous	Higher compressive strength (2.4 MPa), biocompatible and enhanced biodegradation, suitable for bone tissue regeneration	[224]
6	Bilayered SF/SF/nanoCaP	Porous	Compressive strength in wet 0.4 MPa, support rabbit MSCs growth and	[225]

			proliferation *in vitro*, In vivo study shows bone tissue and vessel formation after implantation in rabbit knee.	
7	SF/BMP-2/nHAp	Nanofiber	Improved mesenchymal stem cells growth and osteogenic differentiation, BMP-2 loaded scaffold shows better osteogenic potential than SF/nHAP scaffold lacking BMP-2.	[63]
8	Bioglass/SF	Porous	Improved cytocompatibility, mechanical properties, degradation and osteogenic potential for bone tissue engineering applications	[220]
9	SF/mesoporous bioglass	Porous	Compressive strength of 0.9 MPa, low contact angle (71.2°), improved bioactivity, good biocompatibility and ALP activity, osteogenic differentiation of human mesenchymal stem cells.	[226]
10	Copper containing Mesoporous bioglass scaffold	Porous	Pore size in range of 300-500 µm, possess multifunctional property such as osteogenic and angiogenic potential, antibacterial properties	[226]
11	Cobalt doped 1393 Bioactive glass scaffold	Porous	Suitable compressive strength (4.2 MPa) for cancelous bone, bioactive, osteogenic, angiogenic, suitable for soft bone tissue engineering applications.	[227]

CHAPTER 3: Scope and Objectives

The incidence of bone tissue related disorders across the globe increases rapidly and the current clinical treatments are not satisfactory that led to serious concern in field of health sector. In recent years, bone tissue engineering has been emerged as a promising tool for the treatment of bone tissue defects and diseases through the development of functionalized bioactive scaffold via synergistic combination of suitable biomaterials. However, due to several factors application of bone tissue engineering has not yet been successfully practiced at clinical level. In this context the development of scaffold matrix from appropriate biomaterial is the backbone of TE. Silk fibroin derived from silk cocoon is considered as promising biopolymer because of its biocompatibility, biodegradability, robust mechanical strength and wound healing properties. However, Silk fibroin scaffold possess poor bioactivity and osteoconductivity property which limits their applications in bone TE. Which opens up the tremendous scope for developing silk fibroin based composite scaffolds to meet the desired scaffold property for bone tissue regeneration applications. Therefore, the present research focuses on the development of a novel silk fibroin based composite nanofibrous scaffold for bone tissue engineering application by overcoming the prevailing limitation associated with silk fibroin.

The specific objectives of this present research work are.

i. To develop nanofibrous silk fibroin/carboxymethyl cellulose blend scaffolds by electrospinning method

ii. To synthesise and characterize nano-bioglass and copper doped nano-bioglass
iii. To improve bioactivity and osteogenic potential by incorporating nano-bioglass into SF/CMC scaffold

iv. To improve angiogenic potential by incorporating copper doped nano-bioglass.
v. To assess biocompatibility, bioactivity, osteogenic and angiogenic potential of the developed scaffolds by *in vitro* cell study

Scope of the research work

1. **Preparation and characterization of silk fibroin-carboxymethyl cellulose based biomimetic scaffolds**

   As discussed earlier, silk fibroin is a unique biomaterial with various superior properties such as biocompatibility, biodegradability and tuneable mechanical properties. Inspite of these favourable properties, silk fibroin lacks bioactivity, hydrophilicity, flexibility and osteoconductive property that limit its applications in bone tissue engineering. Carboxymethyl cellulose (CMC), a highly hydrophilic semi-synthetic natural polymer has chelating abilities, biocompatibility, biodegradable, and finds widespread applicability in wound dressing, skin and bone tissue engineering applications. Therefore, this phase of research work focuses on the improvement of bioactivity and osteogenic ability of SF by preparing SF/CMC blend nanofibrous scaffold by electrospinning. Finally, developed SF/CMC nanofibrous scaffold was characterized for its physic-chemical property, biocompatibility, bioactivity and its osteogenic potential.

2. **Synthesis of nano-bioglass and copper doped nano-bioglass**

   It has been reported earlier that bioglass can improve bioactivity of biopolymeric scaffolds and could facilitate integration with surrounding bone tissue in vivo. Thus it is hypothesized that incorporation of nano-bioglass may improve the cell supportive property of SF/CMC scaffold. So this phase of research work, deals with the synthesis of nano-bioglass and copper doped nano-bioglass by sol-gel method. Synthesised nano-bioglass was further characterized for particle size, morphology and elemental composition. Biodegradation and ion releases are the advantageous phenomenon of bioglass for bone tissue regeneration, as Si, Ca and Cu ions having gene activating potential. Thus, bioactivity and ion release property were further analysed after soaking it for desired time interval in simulated body fluid.

3. Development of loaded SF/CMC/nano-bioglass composite nanofibrous scaffold

The present work aims to develop a novel SF/CMC/nano-bioglass composite nanofibrous scaffold matrix as a bioactive template with enhanced osteogenic potential for bone tissue regeneration. Considering bioactivity of nano-bioglass, mechanical property of silk fibroin and hydrophilicity, flexibility and chelating abilities of CMC are aimed to bring these properties on common template for the development of scaffold with more robust property for bone tissue engineering. It is further postulated that the dissolution of bioglass results in higher calcium and phosphate ion concentration in surrounding environment, which was further chelated by hydroxyl/carboxyl group of scaffold material thereby leading to the deposition of nano-hydroxyapatite across the nanofibrous matrix. Developed nanofibrous scaffolds were evaluated in terms of physicochemical, mechanical property and biomineralization. The biocompatibility, bioactivity, Glycosamino glycan deposition, and osteogenic differentiation ability of the developed scaffolds were investigated *in vitro*.

4. Development of copper doped nano-bioglass loaded SF/CMC composite nanofibrous scaffold

The angiogenesis of the scaffold is important for the development of vascular network throughout the scaffold matrix that facilitates the supply of oxygen, nutrient, and growth factor and removal of wastes of the degraded scaffold while tissue regeneration. Thus it is essential to design surrogate extracellular matrix with appropriate structural framework with suitable bioactive agent to direct cells towards tissue regeneration in vivo. Thus, this phase of research work focused on the development of copper doped nano-bioglass incorporated SF/CMC composite nanofibrous scaffold. The developed scaffold was further characterized for physic-chemical properties, mechanical property and bioactivity under physiological conditions. In addition, the biocompatibility, osteogenic differentiation and angiogenic ability of the developed scaffolds was investigated *in vitro.*

CHAPTER 4: Materials and Methods

4. 1 Materials

4.1.1 Preparation of scaffold

Bombyx mori silk cocoons were obtained from Central Tasar Research and Training Institute (Jharkhand, India). Tetraethyl orthosilicate (TEOS), triethyl phosphate (TEP), calcium nitrate tetrahydrate (Ca $(NO_3)_2$. $4H_2O$), *N*,*N*-(3-dimethylaminopropyl)-*N′*-ethyl carbodimide (EDC), *N* hydroxysuccinimide (NHS), 2-(*N* morpholino) ethanesulfonic acid (MES), NaCl, KCl, $CaCl_2$, $MgCl_2$, K_2HPO_4, $NaHCO_3$, Na_2SO_4, dialysis tube, *Protease XIV* (from *streptomyces griseus*) and carboxymethyl cellulose as sodium salt (molecular weight ≈ 700kDa and degree of substitution ~ 0.65 - 0.85)were purchased from Sigma - Aldrich Company Ltd. Lithium bromide (LiBr), sodium carbonate (Na_2CO_3), formic acid (98%), ethanol, dimethyl sulfoxide (DMSO), sodium hydroxide (NaOH), di-sodium hydrogen phosphate (Na_2HPO_4), ethanol (C_2H_5OH), nitric acid and formic acid were obtained from Merck India Ltd.

4.1.2 Cell culture study

Dulbecco's Modified Eagle Medium (DMEM), fetal bovine serum (FBS), trypsin (0.25%), antibiotic – antimycotic solution, alexa-Fluor 488 conjugated phalloidin, Live/Dead staining kit, anti-RUNX2 antibody, anti-osteocalcin antibody and FITC-conjugated secondary antibody, TRIzol, high-capacity cDNA reverse transcription Kit, SYBER green RT-PCR kit, osteogenic culture media (dexamethasone (DEX), staurosporine, α-MEM, L-glutamine, L-ascorbate and β-glycerophosphate (βGP)) and phosphate buffer solution were purchased from Invitrogen, USA. Bovine serum albumin (BSA), SIGMAFASTTM p-nitrophenyl phosphate (pNPP) tablets, paraformaldehyde, Triton X-100, 4'6-Diamidino-2-phenyindole (DAPI), MTT assay kit, Alizarin red S (ARS) solution, and cetylpyridinium chloride (CPC) were purchased from Sigma - Aldrich Company Ltd.

4.2Methods

4.2.1 Preparation of regenerated silk fibroin

Bombyx mori cocoons were chopped and degummed in 0.02M aqueous Na_2CO_3 solution for 20 min at 100^0C followed by washing with distilled water for two to three times to remove the sericin and other impurities [228]. After degumming silk fibers were dried at 37^0C for overnight. Degummed silk fibers were dissolved in a 9.3M LiBr aqueous solution at 45^0C for 2 to 3hr resulted in a 10 wt% solution. Above obtained solution was then transferred carefully

into dialysis cassette (molecular weight cut-off of 10000 Da) and dialyzed against deionized water for 2 to 3 days to remove LiBr ions. The solutions were then centrifuged at 5000 rpm to remove un-dissolved impurities and aggregates. Finally, the obtained solutions were dried and used for further study.

4.2.2 Preparation of electrospun SF nanofibrous scaffold

The SF was dissolved in formic acid to obtain homogeneous solutions of various concentrations such as 10wt%, 12wt% and 14wt%. The prepared solutions were electrospun by using Free liquid surface electrospinning machine (NS Lab 200, ELMARCO), at 45 kV voltage, 40% relative humidity of electrospinning chamber and 12 rpm of wire based spinning electrode at 20±2 °C [229]. The solution was filled in cylindrical tray and thin wire (200 µm) based spinning electrode was placed in solution. The distance between collector and spinning electrode was set at 12, 14, and 16 cm. The electrospun mats at various distances (12 - 16 cm) were collected and kept in dessicator at 37°C. The obtained SF nanofibrous scaffolds were further cross-linked with 3 wt% EDC-NHS [2:1 (w/w)] in ethanol: water (95:5 v/v)] solution [210]. The cross-linked nanofibrous scaffold was then rinsed twice with deionized water to remove residual cross-linking reagent and vacuum dried at room temperature. The cross-linked scaffolds were further used for various characterizations.

4.2.3 Development of electrospun SF/CMC blend nanofibrous scaffold

Four different batches with varied compositions of SF/CMC (100/0, 99/1, 98/2 and 97/3 (w/w)) blend solutions (10 wt%) were prepared by dissolving appropriate amount of SF and CMC powder in 98% formic acid with stirring to make well dispersed homogenous solutions. The nanofibers were generated from these blends at 12 cm and 68 kV of applied electric potential as described above in section 4.2.2. The different composite scaffolds are designated as SF, SF/CMC_1, SF/CMC_2 and SF/CMC_3 for 100/0, 99/1, 98/2 and 97/3 (w/w) of SF/CMC compositions respectively. The electrospun SF/CMC nanofibrous scaffolds were cross-linked with 3 wt% EDC-NHS [2:1 (w/w)] in ethanol: water (95:5 v/v)] solution and further treated with 0.1 M $CaCl_2$ solution overnight at 40°C. The cross-linked scaffolds were rinsed thoroughly with deionized water to remove ions like chlorine and residual cross-linking reagent, followed by drying under vacuum at room temperature for 24 h. The different composite scaffolds treated with $CaCl_2$ were designated as calcified SF_1, SF/CMC_1

and SF/CMC_2 corresponding to SF, SF/CMC (99:1 w/w) and SF/CMC (98:2 w/w) respectively. The gelatin nanofibrous scaffold was also fabricated by electrospinning of 10 wt% gelatin solution under similar electrospinning conditions was use as control.

4.2.4 Synthesis of nano-bioglass and copper doped nano-bioglass

Nano-bioactive glass (nBG) was synthesized by an acid mediated sol-gel method [230]. In brief, the molar composition considered for nBG was 60% SiO_2, 36% CaO, and 4% P_2O_5. Bioglass sol was prepared by hydrolysing 4.53 ml of tetraethyl orthosilicate in water and pH of sol was adjusted with 2M HNO_3. Solution was stirred till a clear sol was formed. Then 3.022 gm of calcium nitrate tetrahydrate and 0.195 ml of triethyl phosphate were dissolved in obtained sol. The prepared sol was kept in an oven at 45°C for gelling and aged for 3-4 days. Finally, the gels were freeze dried and part of the obtained powder was stabilised at 600°C for 2hr. The rate of heating for calcination of synthesized bioglass was fixed at 30°C/min. The copper doped nano–bioactive glass (Cu-nBG) based on 58S bioglass was prepared by an acid mediated sol-gel method. The Cu-nBG with 0.5 mol% ($Cu_{0.5}$-nBG) and 1 mol% (Cu_1-nBG) copper were synthesized by using tetraethyl orthosilicate, calcium nitrate tetrahydrate, triethyl phosphate and copper nitrate trihydrate in water and pH was adjusted with 2M HNO_3 at room temperature. Finally, the obtained sol was kept at 45°C for gelling followed by ageing for 3-4 days in an oven. The gels were freeze dried and stabilized at 600°C with heating rate of 30°C/min for 2hr.

4.2.5 Development of electrospun SF/CMC/nBG composite nanofibrous scaffold

The 10 wt% SF/CMC (98:2 (wt %)) solution was prepared by dissolving appropriate amount of SF and CMC in formic acid. Different bathes of 10 wt% SF/CMC/nBG composite solutions were prepared by adding different amount of nBG (5 wt% to 20 wt% nBG) to SF/CMC (98:2) solution. The nanofibrous SF/CMC/nBG scaffolds were fabricated by electrospinning followed as described in section 4.2.2. Each of the composite solution was alternately tested by filling 25 ml of the solution in rotatory spinning electrode tray at 70kV applied voltage and 16 cm distance. The resulting nanofibrous mat was immersed in 3 wt% EDC+NHS [2:1 (w/w)] in [(95:5 v/v (Ethanol:water)] solution followed by washing with deionized water to remove residual cross-linking reagent. The obtained cross-linked scaffolds were then dried in dehumidified chamber at 37°C.

4.2.6 Development of electrospun SF/CMC/Cu-nBG composite nanofibrous scaffold

The 10 wt% SF/CMC/Cu-nBG composite solutions were prepared by adding different amount (5wt% and 10 wt%) of $Cu_{0.5}$-nBG and Cu_1-nBG respectively in SF/CMC (98:2) solution. Finally prepared solutions were electrospun at 70kV applied voltage and 16 cm distance. Finally deposited composite nanofibrous scaffolds were cross-linked with 3 wt% EDC+NHS [2:1 (w/w)] in [(95:5 v/v (Ethanol:water)] solution for 12 hr. After cross-linking scaffolds were washed thoroughly with deionised water and dried in desiccators. Thus obtained scaffolds were used for further study.

4.3 Characterization of nano-bioglass

4.3.1 Morphology

The morphology of nBG powder with and without copper doped was examined by using Field emission scanning electron microscope (FE-SEM, Nova NanoSEM 450) [231]. Before imaging, the nBG particles were sputter coated with gold for 2.5 min. The average particle size was calculated by counting at least 100 different particles based on FESEM images using image J software. Elemental composition of nBG was determined by energy dispersive X-ray analysis (EDX) (Bruker, Germany). FEI Tecai^{TM} transmission electron microscope (TEM TF-30, Netherland) working at 300kV was used to examine the existence of bioactive glasses in nano-scale range [232].

4.3.2 Bioactivity

Bioactivity of nBG was studied in simulated body fluid (SBF) for 7 days. The SBF having pH of 7.35 – 7.40 was prepared according to the procedure described elsewhere [233]. In brief, nBG was soaked in SBF in separate batch at a concentration of 1mg ml^{-1}. Ten millilitre solutions were taken out from each batch after interval of 3, 5 and 7 days. The solutions were filtered through 0.2 micron syringe filter and then analysed for ionic species concentration by inductively coupled plasma optical emission spectrophotometer (ICP – OES, Perkin Elmer optima 5300 DV) [234-235]. Finally the soaked nano – bioglass powders were collected, washed with acetone and dried for overnight at 400°C in hot air oven. The obtained SBF

treated nBG powder was used for FE-SEM, XRD and FT-IR study to evaluate hydroxyapatite formation.

4.3.3 Structural and functional characterization

X-ray diffraction (XRD) of nBG was performed by X-ray Diffractometer (Rigaku Japan/Ultima-IV) using Cu-Kα radiation (λ = 0.1542 A0). X-ray diffraction (XRD) curves were recorded with an X'celerator counter at a scanning rate of 5°/min with a step size of 0.03° within a scanning region of 2θ = 10–70°. Fourier transform infrared spectroscopy (FTIR, Shimadzu AIM-8800, Japan) was used to obtained the FTIR spectra in transmittance mode under the mid infrared region (4000 – 400 cm^{-1}). This is used to study molecular composition and functional groups in SF/CMC based scaffold and nano-bioglass [236].

4.4 Characterizations of scaffolds

4.4.1 Rheological behaviour

The rheological property of the SF, SF/CMC and SF/CMC/nBG solutions were measured by rotational cone (diameter = 30 mm; angle = 5.4°) and plate viscometer (Bohlin Visco-88, Malvern, UK) with a linear increment in shear rate from 0.1-1000 s^{-1} at 25°C. A constant gap of 0.15 mm was maintained between cone and the plate throughout the study. The data was analyzed with Bohlin visco-8 software using Moore model [237]. For each experiment, three samples were used and result was reported as the average and standard deviation of obtained viscosities.

4.4.2 Morphological study

Characterization of the developed SF, SF/CMC, SF/CMC/nBG and SF/CMC/Cu-nBG scaffold was done before and after the *in-vitro* mineralization. Nanofibrous scaffolds with 0.5×0.5 cm^2 sizes were sputter coated with gold, and observed under field emission scanning electron microscope (FESEM) (NOVA NANO SEM, USA) for morphological assessment [231, 238]. The average fiber diameters were measured from ten different FESEM images of ≥5000 magnification using Image J software. A minimum of 50 pores were considered for calculating the average pore size of the developed scaffolds by using Image J software. Energy dispersive X-ray analysis (EDX) was used to ensure the presence of bioglass reinforcement within the scaffolds. FEI Tecai™ transmission electron microscope (TEM TF-

30, Netherland) working at 300kV was used to examine the presence of bioactive glasses in composite scaffold [232, 239].

4.4.3 Structural and functional analysis

X-ray diffraction (XRD) of nanofibrous scaffolds (1.0 × 1.0 cm) were performed by X-ray Diffractometer (Rigaku Japan/Ultima-IV) using Cu-Kα radiation (λ = 0.1542 A0). X-ray diffraction (XRD) curves were recorded with an X'celerator counter at a scanning rate of 5°/min with a step size of 0.03° within a scanning region of 2θ = 10–70°. The nature of interactions among the functional groups of the prepared scaffolds and their interaction with nBG were determined using Fourier transforms infrared (FTIR) spectroscopic analysis (FTIR, Shimadzu AIM-8800, Japan) operated in the transmittance mode in 4000–400 cm-1 region. Hydraulic press was used to pelletize the scaffold specimens by mixing them with dry KBr powder. The prepared mixture was pressed into transparent disks like structure and used for FT-IR analysis [236].

4.4.4 Surface roughness analysis

The topography or roughness of the developed nanofibrous scaffold surface was studied using a scanning probe microscope operated in atomic force microscopy (AFM, NTEGRE (NTMDT)) semi-contact mode at microscopic level [236]. In this technique, the probe tip made up of quartz is attached to a flexible micro-fabricated 225 μm long silicon cantilever with a spring constant of 3 N/m, the deflection of which is measured by optical method. The reflected light beam is focused to a particular position by moving the surface of the scaffold and a constant force is maintained between the surfaces that produces topographical images.

4.4.5 Mechanical strength measurement

Universal testing machine (Instron 3369, Bioplus, USA) was used to determine the tensile strength and tensile strain at break of the developed nanofibrous scaffolds both in dry and wet conditions. The scaffolds were cut into small rectangular shapes (30×5×0.05 ± 0.03 mm^3) and loaded between the clamps of the tensile tester. Tensile testing was performed with a load cell of 1000 N at cross head speed of 5 mm/min [236]. For measurement in wet condition, the samples loaded between the clamps were immersed in bioplus bath filled with 3 litres SBF solution maintained at 37±1 °C. The value reported is the average of measurement taken with three specimens.

4.4.6 Contact angle measurement

The contact angle of the nanofibrous scaffolds (1×1 cm^2) was measured using K100MK3 tensiometer (Kruss GmbH, Hamburg, Germany) operating at 6 mm/min detection speed and 3 mm/min measuring speed [240]. Three specimens were used for single set of scaffold and the average result was reported. All the measurement was done at room temperature and water was used as the solvent for measuring contact angle.

4.4.7 Equilibrium water uptake capacity measurement

The water uptake capacity was measured by immersing small pieces (2×2 cm^2) of pre-weighed dried nanofibrous scaffolds in PBS solution at room temperature. After particular time interval of 2 h to 24 h specimen was removed and then weighed. By dividing the difference in weight before (*wD*) and after the soaking (*wT*) by the original dry specimen weight (*wD*), we obtained the equilibrium water uptake percentage of the scaffolds using equations 1 [241].

$$water\ uptake\% = \frac{wT - wD}{wD} \times 100 \text{ ..... } \textbf{(1)}$$

4.4.8 *In vitro* biodegradation of scaffolds

The initial dry weight of the nanofibrous scaffold samples were weighed and noted as (W_o) The nanofibrous scaffolds were incubated at 37°C in *Protease XIV* (from S*treptomyces griseus*) solution (1.0 mg/ml) prepared in PBS solution as well as in PBS without enzyme [242]. After incubation for particular designated time period (3 days to 28 days) scaffolds were taken out, washed with deionised water and lyophilized. Finally percentage of degradation was calculated using initial weight (W_O) and final weight (W_F) of scaffolds by using equation 2.

$$Percentage\ of\ degradation = \frac{Wo - WF}{Wo} \times 100 \text{ ..... } \textbf{(2)}$$

4.4.9 *In vitro* bioactivity study

In vitro bioactivity of the scaffold was assessed by incubating 1×1 cm^2 sizes of scaffolds in 20 ml simulated body fluid (SBF) for 7 days. SBF was prepared following the earlier reported method by adding NaCl (7.995 g), KCl (0.224 g), $CaCl_2 \cdot 2H_2O$ (0.368 g), $MgCl_2 \cdot 6H_2O$ (0.305 g), K_2HPO_4 (0.174 g), NaHCO3 (0.349 g), and $Na_2SO_4 \cdot 10\ H_2O$ (0.161 g) to 1 L of distilled

water in the same order as mentioned [243]. The pH of the fluids was adjusted to 7.4 at 36.5 °C. After 7 days, the scaffolds were taken out, gently rinsed in distilled water and dried at room temperature. FESEM was used to observe the apatite deposition over the scaffold surface and elemental composition was determined using EDX.

4.5 *In vitro* cell study

4.5.1 Isolation and culture of hMSCs

Umbilical cord blood (UCB) was collected from the local Ispat General Hospital, Rourkela, India with prior consent of the full-term delivery patients. The Institutional Ethical Board approved the collection procedure. The mononuclear cells (MNCs) were isolated from UCB following the Ficoll Hypaque method described in literature [244]. The isolated mononuclear cells (MNC_s) from umbilical cord blood cultured in complete media (Dulbecco's Modified Eagle Medium supplemented with 10% FBS and 1% antibiotic solution) [245]. The culture condition was 37°C, 5% CO_2 with 80% relative humidity in CO_2 incubator. During culture period, cell culture medium was replaced with fresh medium, also non adherent cells were washed out. The adhered cells were cultured for 4 – 6 passages, mean while non-adherent cells were completely removed. The cells were characterized for multilineage differentiation potential using osteogenic [236], chondrogenic [246] and adipogenic [247] culture medium.

4.5.2 Cell seeding and culture

Disk shaped scaffold specimens of 6 mm in diameter were sterilized in 75% ethanol overnight and then extensively rinsed with PBS. The scaffolds were incubated for overnight in complete medium in 24-well plate and hMSCs (10^5cells/cm^2) were seeded on the scaffolds after 24 hr of incubation. The cell seeded scaffolds were incubated at 37 °C for 4-6 h to allow cell adhesion. After the cell attachment, the cell seeded nanofibrous scaffolds were cultured for two weeks in complete media, at 37°C in humidified atmosphere containing 5% CO_2 [236].

4.5.3 Cell morphology and cell attachment

The cell attachment and cell morphology of hMSCs seeded on each of the prepared nanofibrous scaffolds were monitored during 7 to 14 days of culture under FESEM. For FESEM study, the cultured cell-seeded scaffolds were fixed with 2.5% glutaraldehyde for 20

min and dehydrated consecutively for 5 min using gradient ethanol concentrations (30%, 50%, 70%, 90% and 100% (v/v) in water). After drying at room temperature, the scaffolds were sputter coated with gold and observed under FESEM [248].

4.5.4 Cell viability

MTT assay

The metabolic activity of the cells seeded on the scaffolds (10^4 cells/cm^2) was done by MTT assay during 7 days of culture period following the standard protocol described elsewhere [249]. After 3, 5, and 7 days, the culture medium (complete media) was removed and rinsed with 100 µl PBS and 100 µl MTT solution (0.5 mg/ml) was added to each well (96 wells plate) and incubated for 4 hr at 37 °C in 5% CO_2. After incubation, MTT solution was replaced with 100 µl of DMSO and finally the absorbance was measured at 490 nm using UV-Visible spectrophotometer (Double beam spectrophotometer 2203, Systronics).

Fluorescent Microscopy

The cell viability of hMSCs seeded over scaffolds (10^5 cells/cm^2) was done by live/dead staining during culture period. The cell seeded scaffolds were incubated for 20 min in live/dead staining solution (calcein AM and EthD-1) and then observed under confocal microscope (Leica TCS SP5 X Super continuum) [250].

4.5.5 Cell distribution and cytoskeleton organization

Morphological, cytoskeleton organisation and cellular distribution were assessed by confocal microscopy. The hMSCs seeded scaffolds were fixed with 4% paraformaldehyde for 30 min and incubated in 3% BSA for another 30 min. The fixed specimens were permeabilized using 0.1% Triton X-100 for 5 min and then incubated with Alexa-Fluor 488 conjugated phalloidin at room temperature for 15 min in dark condition. After rinsing with PBS and staining with DAPI for 15 min, the specimens were mounted over the glass slides and the images were taken by Leica TCS SP5 X Super continuum Confocal Microscope [245]. The penetration and proliferation of hMSCs within the scaffolds were determined from the 3D-Z-stack images composed by arranging all Z-sections developed during the scanning of cell-seeded scaffolds under the confocal microscope.

4.5.6 Osteogenic differentiation potential

Alkaline Phosphatase assay (ALP)

The osteogenic differentiation activity of hMSCs (10^4 cells/cm^2) seeded on the nanofibrous scaffolds and cultured in osteogenic media (complete media, which additionally supplemented with 5 mM β-glycerol phosphate, 50 mg/mL ascorbic acid-2-phosphate and 1 nM dexamethasone) were quantitatively estimated by measuring alkaline phosphatase (ALP) secretion by the cultured hMSCs using pNPP solution as the reaction substrate for ALP. 50 µl of Lysis solution (0.5% TritonX-100) and subsequently, 200 µl of 1 mg/ml p-NPP solution were added to each well and incubated for 1.5 h at 37 °C. The absorbance was later measured at 405 nm after 7 and 14 days using UV-Visible spectrophotometer (Double beam spectrophotometer 2203, Systronics) [236].

***In-vitro* biomineralization**

The formation of mineralized nodules on the cell-seeded nanofibrous scaffolds cultured in osteogenic media was confirmed by FESEM analysis and alizarin red assay. Alizarin red S stain (ARS) solution was prepared by dissolving 0.5 g ARS in 25 ml MiliQ water and pH of the solution was adjusted to 4.1-4.3 by adding 10% NH_4OH. The cell-seeded scaffolds after culturing in osteogenic media for 7 days and 14 days of culture duration was taken out washed twice with PBS and fixed with 2.5% glutaraldehyde for 2 hr and 1 ml ARS solution was added to each well. The specimens were incubated at 37 °C for 1 h and then washed in MiliQ water to remove excess dye adsorbed on the scaffold surface. Biomineralization of hMSCs on the SFC nanofibrous scaffolds was qualitatively evaluated by examining the intensity of the red colour developed on the scaffold surface by using inverted phase contrast microscope (Axiovert 40 CFL) at 20X magnification. The degree of biomineralization was estimated through calcium quantification which involved the aspiration of ARS stain from specimen by incubating with 500 µL of cetylpyridinium chloride (CPC) for 1 hr and recording the absorbance at 550 nm [251] using UV-Visible spectrophotometer (Double beam spectrophotometer 2203, Systronics).

Estimation of GAG (Glycosamino glycan)

The hMSCs seeded (10^5 cells/cm^2) scaffolds were cultured in osteogenic differentiation media (complete media suplimented with 5 mM β-glycerol phosphate, 50 mg/mL ascorbic acid-2-phosphate and 1 nM dexamethasone) for two weeks.

On day 7 and 14, intracellular GAG was removed from the hMSCs seeded scaffold by digestion with papain digestion solution (125 μg/mL of papain, 5 mM L-cystein, 100 mM Na_2HPO_4, 5 mM EDTA) at pH 6.8, 65°C for 3 hrs. The total GAG content on scaffolds was determined by BlyscanTM assay (Biocolor) following the manufacturer's protocol [252]. Finally the absorbance recorded at 656 nm using UV-Visible spectrophotometer (Double beam spectrophotometer 2203, Systronics) and matched with a standard calibration curve to determine the GAG content.

Osteocalcin and RUNX2 expression using Immunocytochemistry

The hMSCs seeded scaffolds were cultured in osteogenic media and analysed both qualitatively and quantitatively for the expression of RUNX2 transcription factor (Runt-related transcription factor 2) and osteocalcin differentiation markers by immunocytochemistry. The scaffolds were fixed with 4% paraformaldehyde for 15 min and rinsed well in PBS, followed by permeabilization with 0.5% TritonX-100 for 5 min at room temperature. The permeabilized scaffolds were rinsed with 1X PBS and incubated for 30 min at RT in 3% BSA solution. After blocking the non-specific sites, each specimen was separately incubated with anti-RUNX2 antibody and anti-osteocalcin for 1 h at RT followed by thorough washing. FITC-conjugated secondary antibody (1:200) was then added to it and incubated for 30 min. Counter staining with DAPI was performed for 5-10 min after washing in 1X PBS and image was taken by confocal microscopy [236]. Finally quantitative analysis of the osteocalcin and Runx2 expression from confocal images was done by using Image J software.

Expression of osteogenic specific genes

The RUNX2 transcription factor, osteocalcin and type1 collagen (Col1) gene expressions of the hMSCs (10^5 cells/cm^2) seeded on the SF and SFC nanofibrous scaffolds were quantitatively evaluated in real time quantitative polymerase chain reaction (RT-PCR). After two weeks of culture in osteogenic medium, cell-scaffold construct was immersed in TRIzol and homogenised by vortexing to isolate RNA. These isolated RNAs were converted to cDNA using High-capacity cDNA Reverse Transcription Kit according to the manufacturer's instructions. A SYBER Green RT-PCR kit was used for quantitative estimation of gene expression. The $2^{\Delta\Delta ct}$ relative quantification method was used for the estimation of gene expression. The relative expressions of each gene were normalized against Ct value of the

house-keeping gene [236]. The selected primer sequence for the gene of interest and house-keeping gene are shown in Table 4.1.

Table 4.1: Selected primer sequence for the gene of interest and house-keeping gene

Genes	5'-3'	Primers
Runx2	Forward	GTCTCACTGCCTCCCTTCTG
	Reverse	CACACATCTCCTCCCTTCTG
Osteocalcin	Forward	GTGACGAGTTGGCTGACC
	Reverse	TGGAGAGGAGCAGAACTGG
Type 1 collagen	Forward	GACCTCTCTCCTCTGAAACC
	Reverse	AACTGCTTTGTGCTTTGGG
B-actin	Forward	TTCCAGTCCTTCCTG
	Reverse	GCCCGACTCGTCATACTC

4.5.7 Angiogenic potential analysis

Hypoxia-inducible factor 1α (HIF1α) expression analysis via immunocytochemistry

The hMSCs seeded scaffolds were cultured for 7 and 14 days and then stained for HIF1α expression analysis. The cultured scaffold was taken out and washed twice with PBS after 7 and 14 days followed by the incubation for 2-4 min in 0.5% TritonX 100 solution. Then permeabilized scaffold was washed twice with PBS and incubated in BSA solution (2%) for 15 min. After blocking the non-specific sites, scaffolds were washed twice with PBS and incubated with HIF1α antibody (mouse antihuman antibody 1:200) for 20 min. Then the scaffold was washed twice with PBS and incubated with FITC-conjugated secondary antibody (1:200) for 10 min. The FITC stained specimens were washed twice with PBS and stained with DAPI for 5-10 min. Finally, the samples were washed twice with PBS and image was taken by using Leica TCS SP5 X Super continuum confocal microscopy. Finally quantitative analysis of the HIF1α expression from confocal images was done by using Image J software.

VEGF Immunoassay

The *in vitro* release of VEGF by hMSCs (1 × 105) seeded scaffold was quantified on day 7 of culture by using a human VEGF ELISA kit (Abcam 100662). On day 7 culture media from 12 well plates were collected from each well and added to each well of a pre-coated ELISA plate. Finally ELISA for VEGF release was done according to the manufacturer protocol [253].

4.6 Statistical analysis

The experiments were done in triplicate, and data were presented as mean ± SD. Statistical significance was determined by one way ANOVA. 'p' Value less than 0.05 was considered as significant.

CHAPTER 5: Results and Discussion

CHAPTER 5A: Development and characterization of SF/CMC blend scaffold

Silk fibrin (SF) of *Bombyx mori* origin is one of the most attractive natural biopolymers was investigated for developing tissue engineering scaffolds over the past decade because of its several inherent properties such as tuneable mechanical strength and biological properties namely biocompatibility and biodegradability [254]. However, SF lacks adequate hydrophilicity [255-256], flexibility [257], bioactivity and osteoconductivity [16] which limit its use in TE. The blending of SF with other polymers has received considerable attention of the researchers to improve physico-chemical and biological property of SF [258].

Carboxymethylcellulose (CMC), a natural polymer (polysaccaharade) is highly hydrophilic, biodegradable, biocompatible, non-toxic and has mucoadhesive and chelating properties because of which it has widespread applications in biomedical and pharmaceutical industries [259-261]. Recently, CMC has been considered as an attractive candidate for potential application as wound dressing, artificial bone and skin [262].

Considering the above, CMC was chosen as blending polymer with silk fibroin. Besides material property, fabrication of scaffold with nanofiber architecture is another important aspect, which can mimic the body tissue. In this context, electrospinning has been evolved as the most suitable method for the generation of polymer nanofibers so far [263]. Therefore, research work in this phase of thesis work focuses on the development of a novel SF/CMC blend electrospun nanofibrous scaffolds for bone tissue engineering application. The scaffolds were subjected to morphological, physico-chemical and various *in vitro* biological characterisations to prove their potentiality to act as cell career for bone tissue regeneration. The result and discussion of these experimental studies is presented in this chapter.

5.1.1 Preparation & characterization of electrospun pure SF and cross-linked SF nanofibrous scaffolds

Preparation of pure SF nanofibers

The concentration of polymer solution has a great influence on its spinnability, thereby affects the formation of nanofiber and its morphology [264]. Therefore, the effect of SF polymer concentration on fiber formation and morphology was investigated at varying concentration range of 8 - 14 wt% to establish the optimal polymer concentration that favours fiber formation. The electrospinning condition was maintained at 45 kV and 16 cm distance between the electrodes. As indicated in figure 5.1A, the fiber diameter was increased with

increase in polymer solutions and the nanofiber generation was most favourable in the polymer concentration between 10 wt% to 12 wt%.

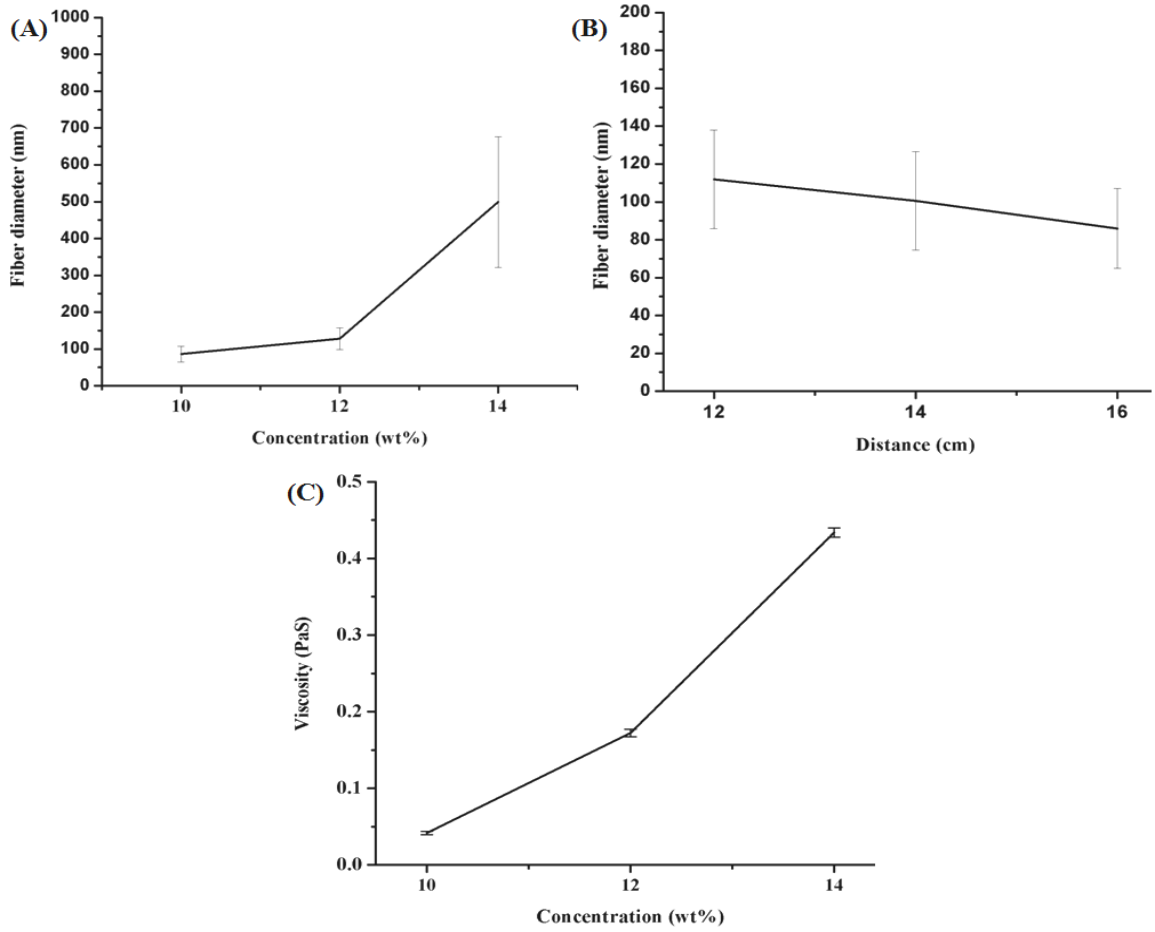

Figure 5.1: The graphs showing the effect of concentration of SF solution (A) and distance between the electrodes (B) on the fiber formation. Effect of SF concentration on viscosity (C). Average fiber diameter decreases with increasing distance between the electrodes and increases with increasing solution concentration. The nanofiber generation was favourable in the concentration between 10 wt% - 12 wt%. 10% SF solution was established as the optimal solution generating nanofibers with average fiber diameter of 86 ± 21 nm.

It has been observed that as the concentration of SF solution increases from 10 wt% to 12 wt%, the average fiber diameter of electrospun SF mat increased from 86 ± 21 nm to 128 ± 29 nm. There was no fiber formation observed at lower polymer concentration of 8 wt%. At this concentration, the solution was not spinnable which may be due to its very low viscosity

(Figure 5.1C). Furthermore, the polymer solution was difficult to electrospun at higher polymer concentration beyond 12wt% as the solution is too viscous and obtained fiber diameter (499±178 nm) was higher than those generated at lower concentrations. Overall, 10% SF solution was the optimal concentration providing continuous fiber formation and superior fiber diameter. The SF nanofiber formation was also drastically changed when the distance between the electrodes was varied from 12cm to 18cm (Figure 5.1B). SF solution with 10 wt% concentration shows linear decrement in average fiber diameter from 112 ± 26 nm to 86 ± 21 nm as the distance between electrode increases from 12cm to 16 cm. The fiber formation either below (12cm) or above (18cm) 16cm was not favourable which was on the basis of either fiber diameter or continuous fiber generation.

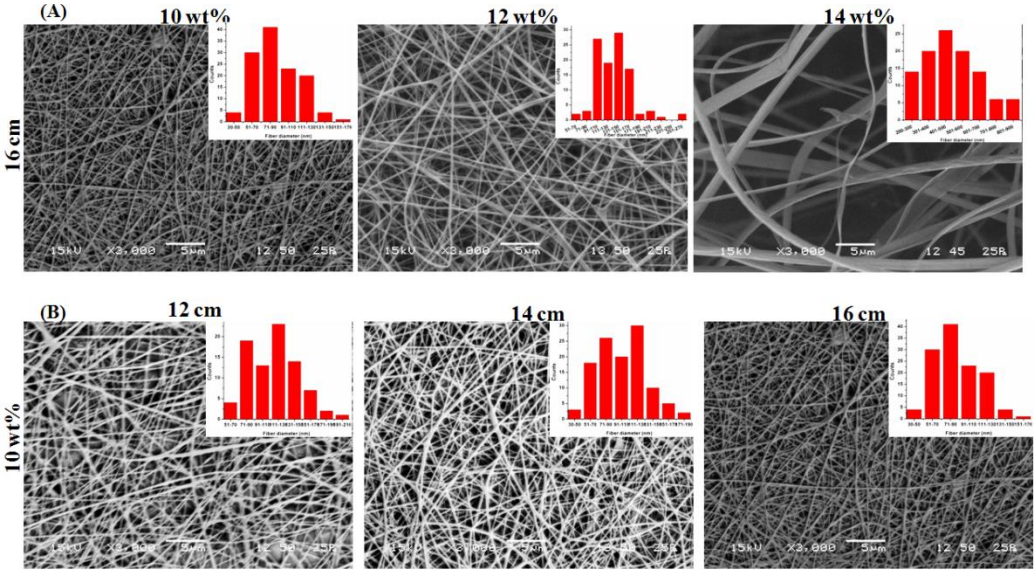

Figure 5.2: (A) SEM images of electrospun SF nanofiber generated from different SF concentration (10 -14%) SF solutions at 16 cm distance between the electrodes. (B) SEM images of electrospun SF nanofiber formed from 10 wt% solutions at varying distances between the electrodes. Decrease in fiber diameter of SF nanofiber with increase in distance between the electrodes is noticed. Also 10wt% solution shows lowest average fiber diameter (86 ± 21 nm) at 16 cm distance between the electrodes.

Figure 5.2 shows the morphological structure of the electrospun SF nanofiber. The SF nanofiber obtained from various solution (10 wt% to 14 wt %) shows random fiber distribution. From Figure 5.2A it has been observed that fiber diameter increases with increasing solution concentration, where 14 wt% SF nanofibers was not successfully electrospun and posse's fiber with higher fiber diameter. Figure 5.2B shows uniform and

continuous deposition of 10 wt% SF nanofiber at various distances between the electrodes. The fiber diameter was also observed to be reduced as the distance between the electrodes increases. Thus 10 wt% SF solution electrospun at 16cm was observed to be appropriate to fabricate nano-scale fibers for tissue engineering applications.

Preparation & Characterisation of cross-linked SF nanofibrous scaffold

Cross-linking is important for the development of scaffold as it improves the chemical, thermal and mechanical stability of scaffold. EDC/NHS is a non-toxic cross-linking agent which was extensively studied and reported to improve the flexibility and tensile strength of SF scaffold. The cross-linking method using EDC/NHS has been successfully applied to recombinant human collagen matrix to produce bio-artificial grafts, that have been evaluated in a phase I clinical trial [265]. Thus, developed nanofibrous SF scaffold was cross-linked with EDC/NHS solution.

Morphological study

SEM images as shown in Figure 5.2, reveals that the generated nano fibers from cross-linked SF solution were closely packed and intertwined. Due to cross-linking well defined pores with varying pore sizes were formed compare to un-cross-linked SF scaffold.

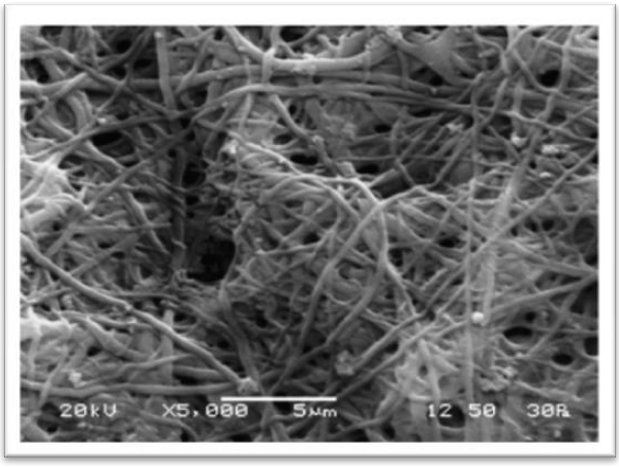

Figure 5.3: SEM images of cross-linked electrospun SF scaffold. The nanofiber was observed to be closely packed and intertwined after cross-linking, which provides stability to the nanofibrous mat. Due to cross-linking well defined pores were formed in the scaffold.

Structural and functional characterization

The structural and functional property of scaffold determined by XRD and FT-IR is important for designing functional scaffold for tissue engineering application [266-267]. These properties determine the stability and mechanical property of the scaffold. The assessment of any conformational or phase change that might have occurred in the developed SF scaffold due to cross-linking was done by XRD. Silk fibroin exhibits conformations such as random coil, silk I and silk II as major molecular structures. Silk II conformation commonly thought to be constituted of β-sheet and endows silk nanofiber with superior mechanical properties. The assessment of conformational property of scaffolds was done from XRD diffractogram of the scaffolds as shown in Figure 5.4 (A). The peaks at 20.8º (2θ) and 24.3º (2θ) indicate the silk II conformation [268] contributing to superior stability and mechanical properties of the nanofiber. A weak peak at 27.6º (2θ) indicates the silk I structure [229, 268-269].

The presence of characteristic functional groups in SF scaffolds was confirmed by FT-IR analysis as shown in Figure 5.4(B). As indicated, the amide I, amide II and amide III conformations of pure SF correspond to the characteristic peaks at 1627 cm^{-1}, 1519 $cm^{-1}$and 1236 cm^{-1} respectively after cross-linking with EDC/NHS [270]. Thus, it confirms that the SF scaffold possess β-sheet conformation which improves its mechanical properties.

Mechanical strength

The mechanical properties of the scaffold play important role in neo bone tissue regeneration. Scaffold must have desired mechanical properties that facilitate osteogenic differentiation of cells over the scaffold. The mechanical property such as tensile strength and tensile strain at break of the prepared cross-linked scaffold was measured. The ultimate tensile strength (UTS) of SF nanofibrous scaffolds obtained from 10 wt% SF solution was 13.68 ± 1.2 MPa, whereas the corresponding tensile strain at break was 10.48 ± 2.6% (Figure 5.4 (C)). Thus, the β-sheet conformation as assessed by XRD analysis augments the tensile property of SF nanofibrous mat.

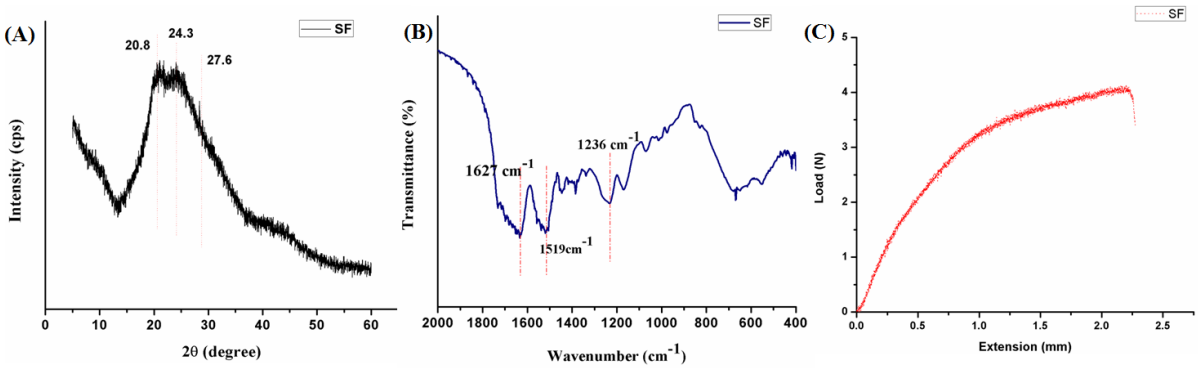

Figure 5.4: XRD spectrum (A), FT-IR spectrum (B) and Load Vs Extension curve (C) for cross-linked electrospun pure SF scaffold

5.1.2 Development of SF/CMC nanofibrous scaffold

The SF/CMC blend nanofibrous scaffolds were prepared by electrospinning with varied compositions of SF/CMC (100/0, 99/1, 98/2 and 97/3 (w/w)) blend solutions. The scaffolds are designated as SF (100/0), SF/CMC_1 (99/1), SF/CMC_2 (98/2) and SF/CMC_3 (97/3). The prepared blend solutions and scaffolds were further characterized by using various techniques.

Rheological behavior of SF/CMC blend solution

The rheological property of polymer solution is an important factor which governs successful electrospinning and morphology of generated fiber [271]. Thus, the rheological behaviour of the prepared pure SF and SF/CMC blend solutions was studied by viscosity measurement under varied shear stress as the flow behaviour depends on the composition and stability of polymer blends. Figure 5.5 shows the shear thinning or thickening property of the pure SF and blend with CMC. The pure SF solution viscosity was determined to be 0.042 PaS and exhibits non-newtonian flow behaviour, as shear thickening occurred at lower shear rate followed by shear thinning behaviour at higher shear rate. The viscosity of SF/CMC_1 blend solution was 0.032 PaS and exhibited similar trend as SF solution, whereas SF/CMC_2 (0.092 PaS) solution showed faster shear thickening at lower shear rate and slower shear thinning behaviour at higher shear rate. Thus, pure SF and SF/CMC (99/1 and 98/2 w/w) blend solutions show similar behaviour of shear thickening and shear thinning as of natural silk dope[272].

The polymeric chains of SF/CMC_2 solution might be organised either parallel or entangled due to the suppression of repulsive forces between the negative charges of polymeric chains at low pH of formic acid [273-275] resulting in increased viscosity and shear thickening behaviour was observed at lower shear rate of SF/CMC solutions. Whereas, as the concentration of CMC increased (> 2 wt%) shear thickening started early with lower shear rate followed by early shear thinning after reaching maximum shear viscosities. Thus, SF/CMC_3 solutions with 3 wt% CMC content possess viscosity of 0.173 PaS and exhibited higher shear thinning behaviour at lower shear rate due to the strong interaction between SF and CMC, which leads to increasing the solution inertia and hinders the electrospinning[276]. Therefore, SF/CMC_2 is more favourable because of the spinnability of the blend solution containing the maximum CMC content which is expected to provide higher hydrophilicity, biomineralization activity and the flexibility of the scaffold.

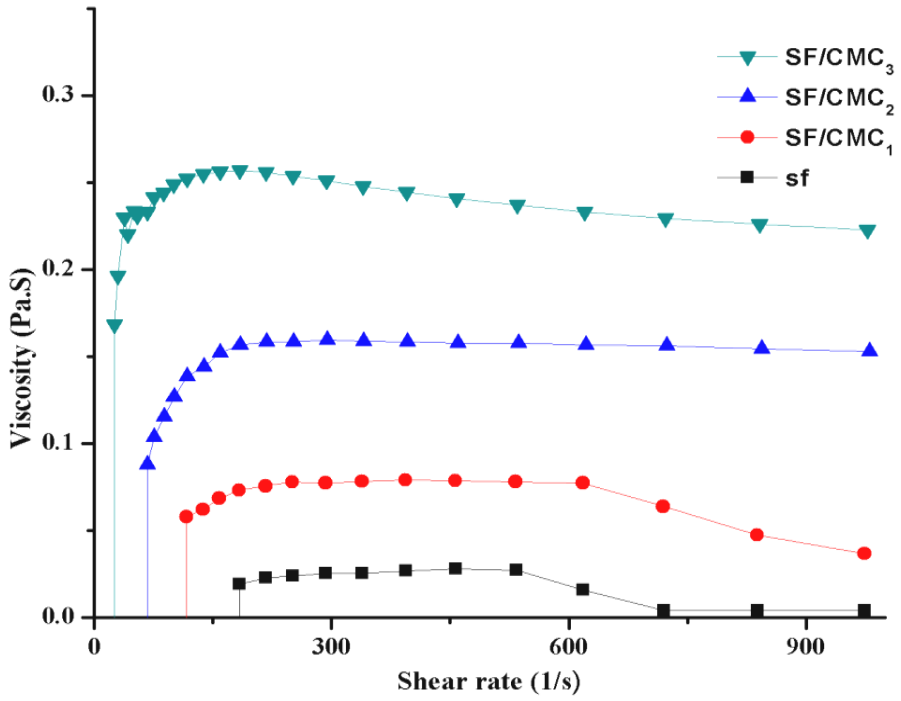

Figure 5.5: (A) Rheological behaviour of the pure SF and SF/CMC blend solutions at different shear rate. Both SF and SF/CMC blend solutions show non-newtonian fluid behaviour. The viscosity of SF/CMC blends solution is observed to be increases with increasing CMC content.

5.1.3 Characterization of SF/CMC scaffold

Morphological study

The microstructures of SF, SF/CMC_1 and SF/CMC_2 scaffolds were assessed by FESEM image analysis as shown in Figure 5.6. The FESEM image shows the irregular distribution of nanofibers in the form of non-woven mats. The SF/CMC_3 blend failed to produce nanofibers because the solution was highly viscous owing to the increased CMC content in it. The fiber diameter was increased with the gradual addition of CMC as shown in Figure 5.6A. The majority of SF/CMC nanofibers are within 100 - 300 nm diameter range, where pure SF exhibits an average diameter of 146.6 ± 38.3 nm. The average fiber diameter of SF/CMC_1 and SF/CMC_2 shows a linear increment of average diameters from 183.7 ± 82 nm to 227.8 ± 87 nm respectively. Thus the developed SF/CMC_1 and SF/CMC_2 scaffolds possess fiber diameter favourable to cell adhesion as the range of body tissue fiber diameter is 50 - 500 nm [45].

The average pore size for SF, SF/CMC_1 and SF/CMC_2 was measured to be 3.5 ± 1.6 µm, 4.2 ± 1.3 µm and 4.7 ± 1.9 µm respectively. Thus, the pore size of scaffold was increased with increase in fiber diameter of electrospun mat [175]. The SF/CMC electrospun scaffolds were cross-linked with 3 wt% EDC-NHS [2:1 (w/w)] in ethanol: water (95:5 v/v)] solution as a post-treatment step. Silk fibroin protein consists of both carboxyl and amino groups, whereas CMC a polysaccharide also contains carboxyl and hydroxyl groups. When the polymeric scaffold is soaked in cross-linking solution swelling occurs, which provides sufficient space for the rearrangement of molecular chains. EDC activates the carboxylic acid residues of CMC and amide bonds are formed by nucleophilic attack of free amine groups of SF on the activated carboxylic groups (Figure 5.6D). Whereas NHS is used in combination with EDC, to prevent quick hydrolysis of *O*-acylisourea intermediate group, through the formation of stable NHS-ester intermediate [210, 277-278]. Thus, EDC/NHS solution helps cross-linking of SF/CMC scaffold through covalent bonding.

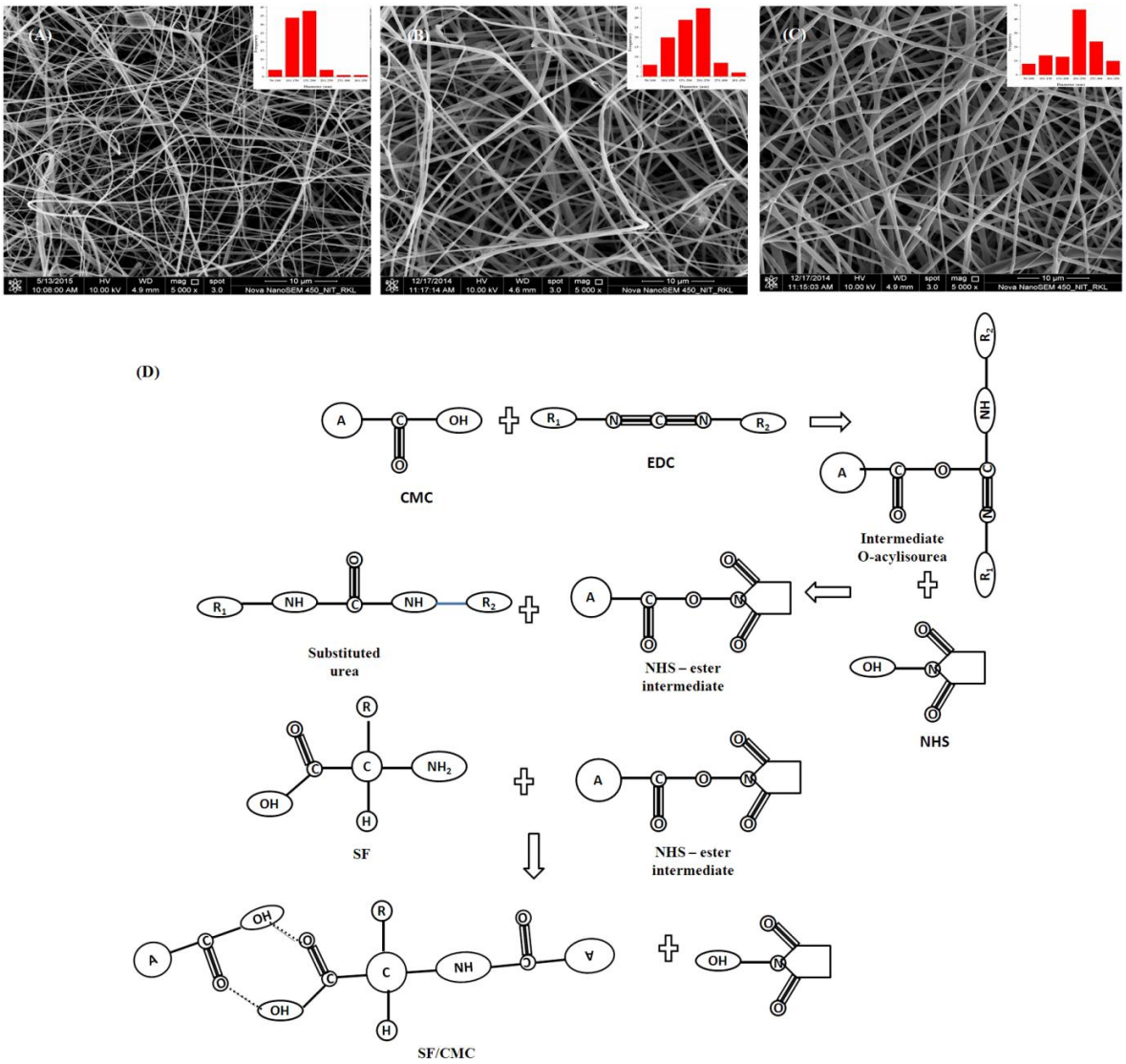

Figure 5.6: FESEM images of electrospun SF (A), SF/CMC$_1$ (B) and SF/CMC$_2$ (C) scaffolds. The fiber diameter of SF/CMC nanofiber increases with increasing CMC content is noticed. The pore size of the scaffolds in turn increased with increase in fiber diameter. (D) Schematic diagram of SF/CMC cross-linking using EDC/NHS.

Structural and Functional analysis

XRD diffractogram representing the changes in chemical structure in SF/CMC blend scaffold is depicted in Figure 5.7A. The peaks at 20.8º (2θ) and 24.3º (2θ) (Figure 2A-a) indicate the anti parallel β-sheet (silk II) conformation [268] contributing to superior stability and mechanical properties of the nanofibers [279]. A weak peak appeared at 27.6º (2θ) indicates the repeated β-turn (silk I) structure [229, 268-269]. Moreover, the diffractogram clearly shows the change in the respective peak intensity of the SF scaffolds with gradual addition of CMC and this phenomenon is possibly due to the interactions between the amide groups of

SF and the hydroxyl/carboxyl groups of CMC chains. The peak intensity for silk I and silk II conformation was reduced as the CMC content increased from 1 wt% to 2 wt% due to amorphous characteristic of CMC [280].

The characteristic functional groups in SF, SF/CMC_1 and SF/CMC_2 are represented by FTIR spectra as shown in Figure 5.7 (B). The characteristic peaks of amide I, amide II and amide III of SF were observed at 1627 cm^{-1}, 1519 cm^{-1} and 1236 cm^{-1} respectively [270]. The peaks at 1627 cm^{-1} , 1519 cm^{-1} and 1236 cm^{-1} in SF/CMC_2 became intensified, indicating the ability of CMC in facilitating the conformational transition from random coils to β-sheets by forming additional intermolecular hydrogen bonds between the carboxyl groups of CMC and amide groups of SF. However, the peak intensified and narrowed at 1236 cm^{-1} in SF/CMC_2 is attributed to the overlapping of amide III band with the acetyl ester band of CMC [281].

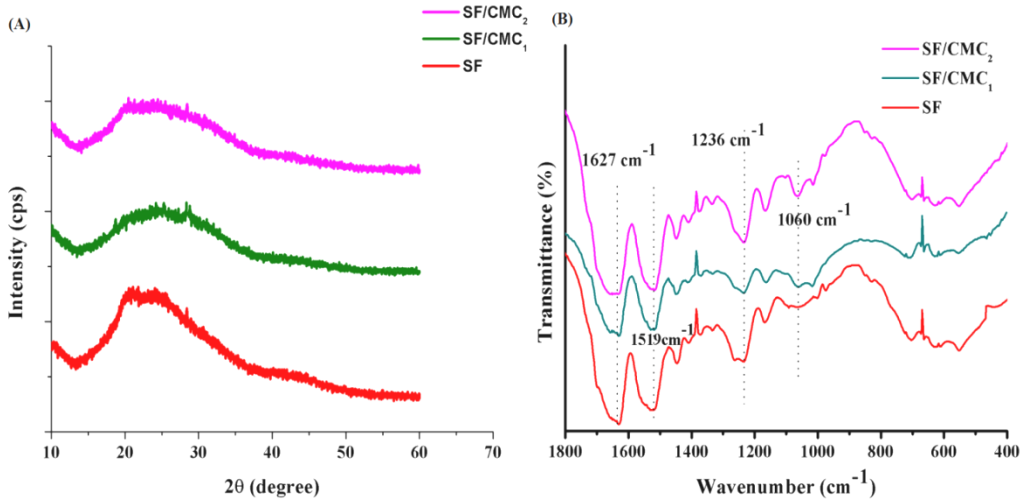

Figure 5.7: (A) XRD and (B) FT-IR spectrum of SF, SF/CMC1 and SF/CMC2 nanofibrous scaffolds. The peak at 1060 cm^{-1} is dominated by the incorporation of CMC.

The FT-IR peak at 1060 cm^{-1} is due to >CH-O-CH_2 stretching of CMC[282]. The peak intensity at 1060 cm^{-1} in SF/CMC_2 was observed to be higher as compared to SF/CMC_1, which is due to higher content of CMC in SF/CMC_2.

Mechanical property

The ultimate tensile strength (UTS) of SF and SF/CMC blend nanofibrous scaffolds in dry and wet states are depicted in Figure 5.8. The UTS of pure SF was measured as 12.7 ± 1.5 MPa and 10.54 ± 1.3 MPa that of SF/CMC_2 in dry state, whereas the corresponding values in

wet state were 3.82 ± 0.7 MPa and 3.46 ± 0.6 MPa respectively. The lower tensile strength shown by polymer blend scaffold may be attributed to its higher fiber diameter as compared to SF [283]. A slight variation in UTS observed with both the scaffolds in wet state suggests that the addition of CMC can improve mineralization without much affecting the mechanical property of the scaffold. Moreover, in wet state, the tensile strain at break of SF/CMC_2 was measured to be 18.37 ± 3.8 %, which is quite higher than the pure SF scaffold (8.36 ± 3.3 %) that reflects the higher flexibility of the blend scaffold. The corresponding increase in tensile strain with addition of 2 wt% of CMC is 118%. Thus, the addition of 2 wt% CMC to SF may improve the cell retention ability and increase the number of cell penetration inside the scaffold during cell-seeding [284]. Furthermore, SF/CMC_1 exhibits tensile strength of 9.15 ± 0.19 MPa and 2.71 ± 1.3MPa in dry and wet state, however tensile strain at break in dry and wet state was measured to be 2.19 ± 0.13 % and 3.97 ± 1.08 %. The stiffness of SF and SF/CMC_2 was measured to be 253.031 ± 41.3 MPa and 580.36 ± 58 MPa respectively. The higher stiffness of the developed SF/CMC_2 scaffold as compared to SF might be due to the formation of strong covalent bond between SF and CMC after cross-linking with EDC/NHS.

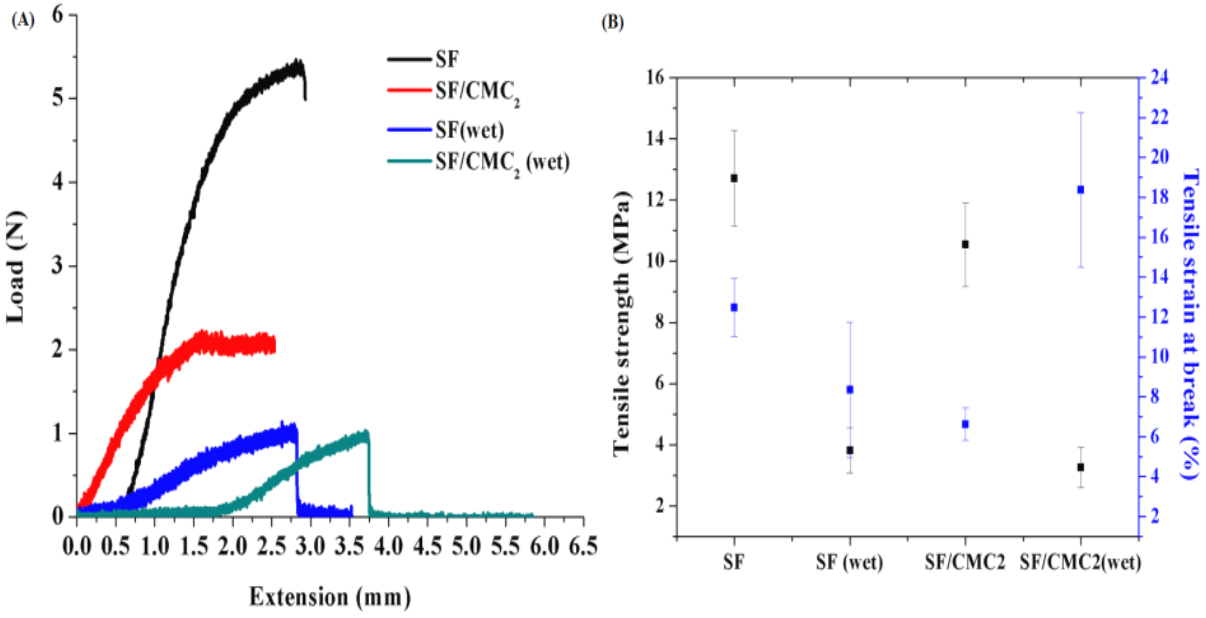

Figure 5.8: (A) Load Vs Extension curve for SF and SF/CMC_2 scaffolds in dry and wet condition. (B) Distribution of tensile strength and tensile strength at break of SF and SF/CMC_2 scaffold. The tensile strain at break of SF solution was improved by the addition of CMC. However, the tensile strength of SF/CMC_2 scaffold was slightly reduced due to its higher fiber diameter.

Thus it has been concluded that CMC at 1wt% is not sufficient to improve flexibility of SF scaffold, this might be due to weak intermolecular interaction between silk fibroin and CMC, which was also observed from amide I, amide II and amide III peaks of SF/CMC_1 in FT-IR spectra (Figure 5.7B).

Surface roughness analysis

The surface roughness is an important characteristic which influences cellular adhesion and differentiation over the scaffold [48]. Moreover, surface roughness has direct impact on cell morphology, proliferation and phenotype expression both *in vitro* and *in vivo* [48]. The surface roughness of the prepared scaffolds was measured by AFM analysis as shown in Figure 5.9. Both SF and SF/CMC_2 nanofibrous mat had a microrough surface with the average surface roughness (Ra) of 0.142 µm and 0.101 µm respectively representing the suitability of the scaffolds for successful tissue regeneration providing desired cellular interaction and protein adsorption [285-286].

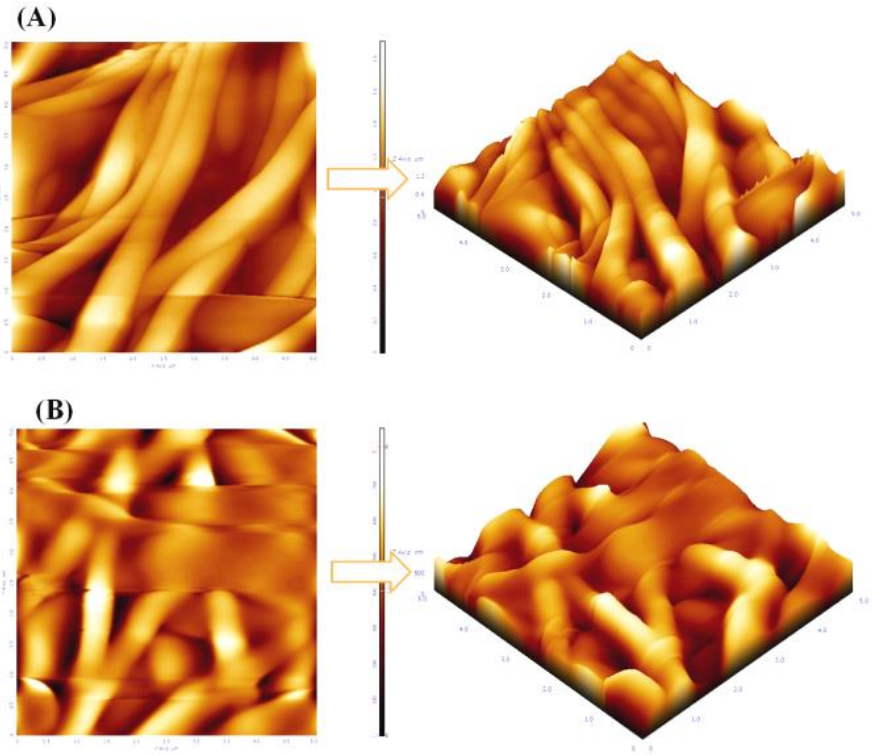

Figure 5.9: The AFM images of fabricated SF (A) and SF/CMC_2 (B) nanofibrous scaffolds. The AFM images clearly show the formation of ridges and grooves that augment the surface roughness of nanofibrous mat.

Hydrophilicity and swelling behaviour

Hydrophilicity of scaffold is a key factor which governs cell adhesion [287], cell spreading and differentiation over the scaffold [48]. The surface hydrophilicity of the scaffold was assessed by measuring the contact angle through spreading behaviour of water over the surface of scaffold [48, 288]. Table 5.1 shows mean contact angle measurements of the prepared scaffolds, where the mean advancing contact angle (MACA) and mean receding contact angles (MRCA) (a measure of wettability and de-wettability) of SF/CMC_2 is lower than pure SF scaffold representing the higher hydrophilicity of the blend scaffold.

Table 5.1: Mean conta angle measurement of SF and SF/CMC_2 nanofibrous scaffolds

Scaffolds	**MACA [°]**	**MRCA [°]**	**Hysteresis [°]**
SF	64.2 ± 4.2	36.9 ± 3.8	26.6 ± 3.0
SF/CMC_2	57.4 ± 0.3	18.5 ± 1.8	38.9 ± 3.2

This phenomenon is also corroborated from Figure 5.10B, where the receding contact angles for SF/CMC_2 attained 0º after certain time period, whereas the measured value is around 30º for SF scaffold. The mean contact angle hysteresis plays an important role in the intrusion and extrusion of body fluids through the scaffolds. This will further augment the cell adhesion property of SF/CMC_2 scaffolds in comparison to pure SF, as the optimum contact angle of the surface for cell adhesion is reported in the range between 55° and 75° [289]. The increase in hysteresis of SF/CMC_2 in comparison to pure SF scaffold indicates an increased in surface roughness or chemical in- homogeneity along the contact line.

The water uptake (Figure 5.10 A) determined for SF/CMC_2 is in the range of 361% - 417% which is higher than the control (180% - 270%). This suggests the better uptake capacity of nutrients into the interior of the SF/CMC_2 scaffold thereby an enhanced cell migration and proliferation is expected to be achieved during the culture of cell scaffold construct. The cell adhesion, proliferation and tissue integration are greatly influenced by the hydrophilicity of the scaffolds [290]. Thus the addition of a small amount of CMC improves the hydrophilic property of SF based nanofibrous scaffolds, thus facilitates biofluid transport, cell migration, prevention from dehydration, exudates accumulation across the wound and maintenance of microenvironment and pH [42, 291].

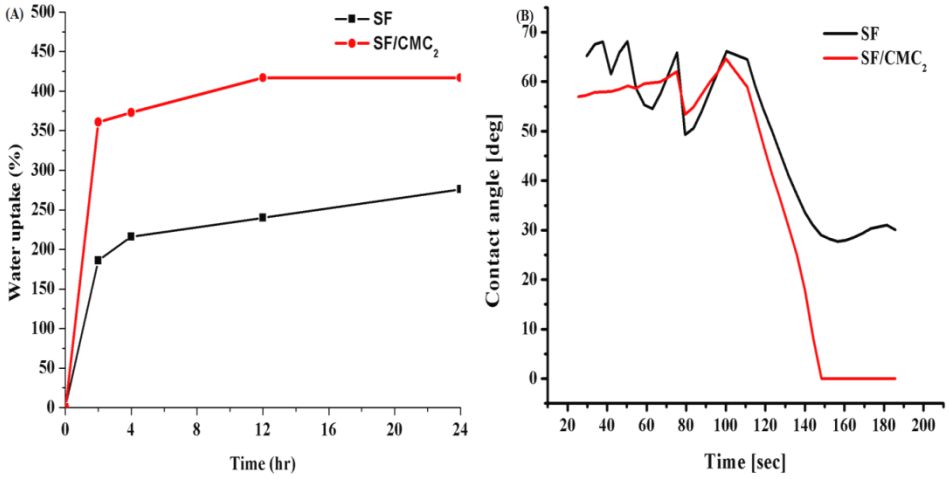

Figure 5.10: (A) Swelling behaviour at different time interval observed with SF and SF/CMC_2 in PBS solution. (B) Variation of contact angle measured with SF and SF/CMC_2 scaffolds. The results represent the superior hydrophilic and water uptake capacity of SF/CMC_2 than the control.

5.1.4 *In vitro* bioactivity analysis

Osteogenic property is one of the key factors for the neo bone tissue regeneration, which is assessed by measuring the deposition of apatite crystals over the scaffold surface [292]. The bioactivity of scaffold was assessed by using simulated body fluid with ion concentration similar to human blood plasma [293]. Also it was reported that the negatively charged or neutral surface hinders osteoblast attachment and spreading as compared to positively charged surface [294]. So, calcified SF/CMC scaffold was prepared to neutralize the negatively charged carboxylate group of SF/CMC scaffold thereby improved biomimetic potential [151, 295]. The bioactivity of pure and calcified SF, calcified SF/CMC_1 and calcified SF/CMC_2) was assessed by SBF treatment for 7 days at room 37°C. After *in vitro* mineralization, the scaffold surfaces were observed under

FESEM (Figure 5.11A-a, b). As revealed by the FESEM images, the scaffold surfaces were rough indicating the nucleation of Ca/P crystals on the scaffolds. Furthermore, the varied extent of roughness observed with different scaffolds indicates the different level of Ca/P nucleation. As for example, the surfaces of pure and calcified SF nanofibers were hardly rough suggesting its marginal biomineralization ability (random and weak) in forming Ca/P crystals. However, calcified SF/CMC_1 and SF/CMC_2 (Figure 5.11 A-c, d) demonstrated higher nucleation sites with uniform and spherical Ca/P crystal formations of sizes ≤ 100 nm.

Figure 5.11B illustrates in situ mineralization of calcified SF/CMC nanofibrous scaffolds. The mineralization of the nanofibers can be attributed to the formation of free hydroxyl groups/carboxyl groups during the electrospinning of SF/CMC blends in formic acid (derivatizing solvent for CMC) contributing to the increased number of Ca^{2+} ion nucleation sites on the nanofibers. After that, PO_4^{3-} ions from surrounding SBF solution was adsorbed by calcium ion resulting in the formation of nanosized Ca/P crystals in SBF (1X) solutions [296-297]. The gradual increase in CMC content augments the content of free hydroxyl groups/ carboxyl groups and thus calcified SF/CMC_2 exhibits the highest mineralization. The biomineralization of electrospun SF/CMC based nanofibrous scaffold shows a controlled nucleation of Ca-P crystal. Whereas, when the scaffold was coated with CMC, most of the Ca^{2+} nucleation sites were exposed to SBF leading to the uncontrolled mineralization of scaffold. Furthermore, in electrospinning under high shear rate (in range of 104 1/s) polymeric chains of SF and CMC get entangled or parallelly aligned [298], because of which CMC was well distributed over the surface as well as within the fiber leading to the exposure of Ca^{2+} nucleation sites on the scaffold surface in controlled manner. The controlled mineralization of matrix provides superior osteogenic differentiation of hMSCs in comparison to the matrix with uncontrolled biomineralization [299]. Thus too low or too much mineralization is not favourable for human bone tissue regeneration.

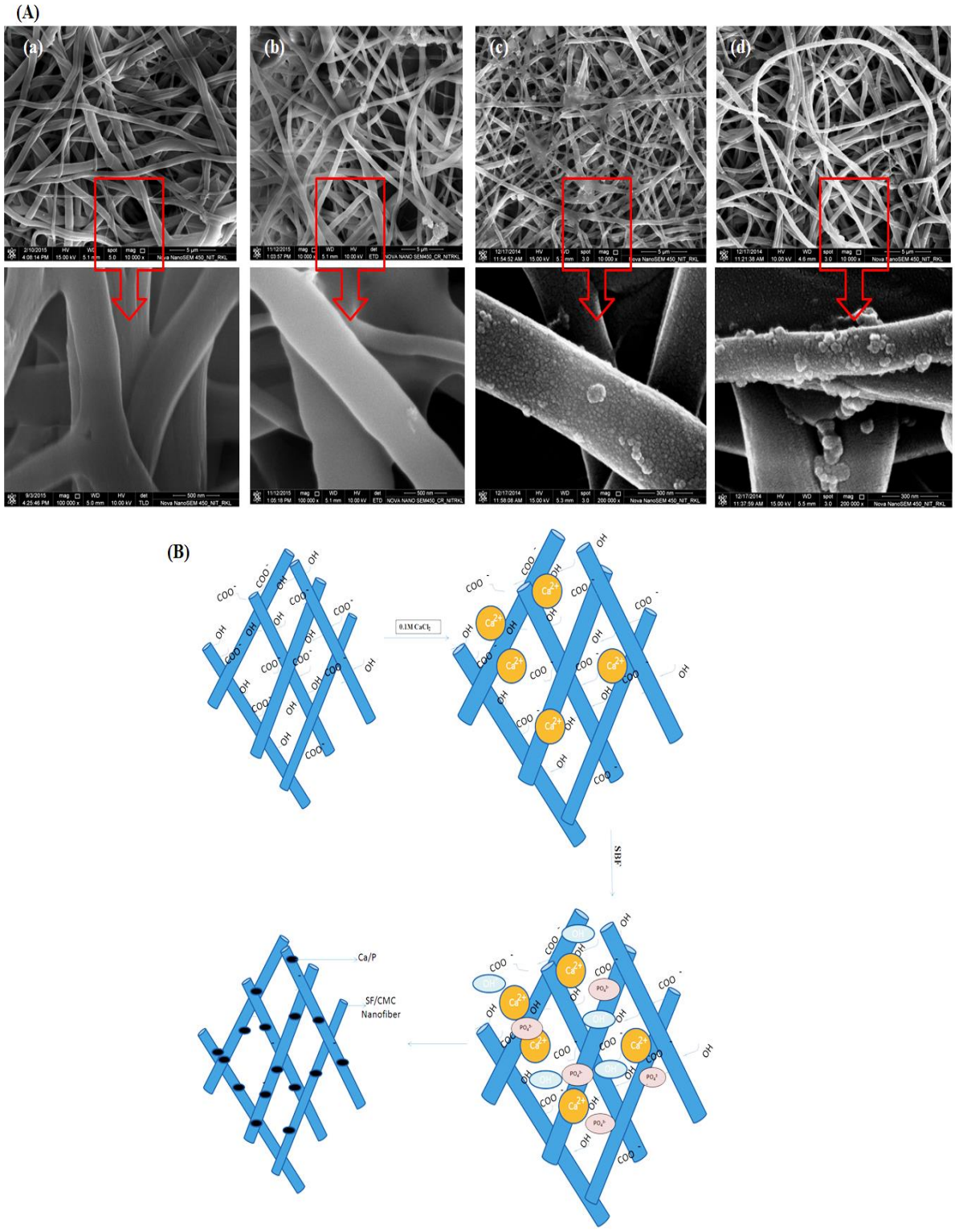

Figure 5.11: (A) FESEM images of pure and calcified SF, calcified SF/CMC$_1$ and calcified SF/CMC$_2$ after SBF treatment for 7 days (a, d). (B) Illustration of *in situ* mineralization of calcified SF/CMC$_1$ and blend nanofibrous scaffolds. Incorporation of CMC led to the uniform nanosized Ca/P mineralization of the SF scaffold. In comparison, SF/CMC$_2$ exhibits superior biomineralization activity than its counterpart SF/CMC$_1$ scaffold and the control.

Structural and functional analysis of biomineralized scaffold

After 7 days of SBF treatment, X-ray diffractogram (Figure 5.12A) depicts Ca/P bone like apatite formation over the scaffolds, where calcified SF/CMC_2 shows prominent peak at 2θ equal to 31.8°, 45.52º, 56.37º and 66.36º in close proximity with reference spectrum for hydroxyapatite as compared to other scaffolds. Thus, it has been confirmed that, calcified SF/CMC_2 offers higher mineralization in comparison to calcified SF/CMC_1 and SF, whereas pure SF shows minimal level of mineralization. This confirms our hypothesis that the addition of CMC can enhance the mineralization property, which was further investigated by FT-IR analysis with mineralised nanofibrous scaffold.

As observed in FT-IR spectra (Figure 5.12B) the Ca/P deposition on the scaffolds is reflected by the characteristic peak at 1062 cm^{-1} corresponding to the P-O asymmetric stretching mode of vibration of PO_4^{-3} group [300-301]. The P-O stretching mode has been observed at 1012 cm^{-1} and 976 cm^{-1} which correspond to major band for phosphate group. The peaks observed at about 610 cm^{-1} and 568 cm^{-1} are due to O-P-O bending and stretching respectively [301-302]. The absorbed CO_2 corresponding to 1400-1450 cm^{-1} peak indicates the deposition of carbonated Ca/P on the nanofibers. Since the characteristic peak for deposited Ca/P was observed much more prominent in calcified SF/CMC_2 (Figure 5.12B) in comparison to other scaffolds thus indicating that CMC plays significant role in the improvement of biomineralization of nanofibrous scaffold. Most of the peaks observed with calcified SF/CMC_2 show more peak broadening in comparison to calcified SF and calcified SF/CMC_1 with time, thereby indicates that the calcified SF/CMC_2 supports superior mineralization and intermolecular bonding with developed Ca/P [303].

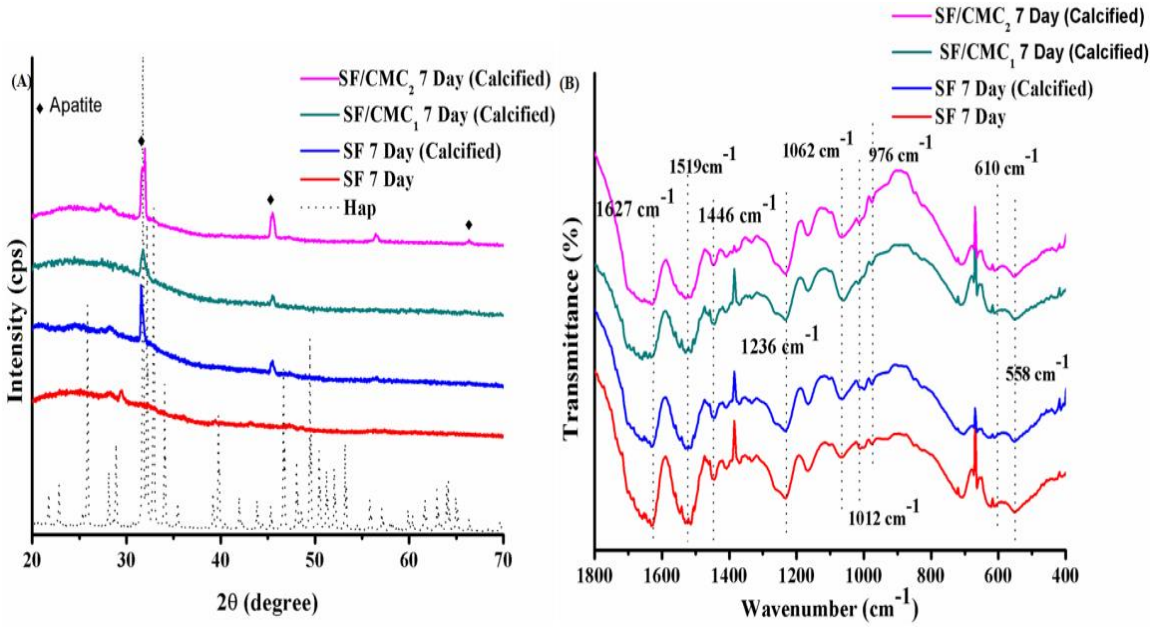

Figure 5.12: XRD (A) and FTIR (B) spectrum of pure and calcified SF, calcified SF/CMC$_1$ and calcified SF/CMC$_2$ after incubation in SBF for a week. The prominent peaks at 2θ=31.8° in XRD diagram and peaks at 1062 cm^{-1} , 1012 cm^{-1} and 976 cm^{-1} in FT-IR diagram confirm the apatite like deposition on the scaffold surface. Overall, the bioactivity of SF scaffold is shown to be remarkably enhanced by the incorporation of CMC and trend is SF/CMC$_2$ > SF/CMC$_1$ >SF scaffolds

Surface roughness analysis of biomineralized SF and SF/CMC$_2$ scaffold

The structure and surface morphology of calcified SF/CMC$_2$ scaffolds after biomineralization were examined by AFM analysis and the results were compared with calcified SF as the control. An enhanced Ca/P deposition and improved surface roughness were exhibited by the calcified SF/CMC$_2$ than that observed with calcified SF, as revealed by the AFM images (Figure 5.13A, B). As indicated calcified SF shows comparatively smooth surface with average surface roughness of 0.247 µm whereas calcified SF/CMC$_2$ possess the average roughness of 0.322 µm. The growth of Ca/P crystals over calcified SF/CMC$_2$ improves its surface roughness and thus, it may promote better adhesion, proliferation and differentiation of hMSCs [304].

5.1.5 *In vitro* biodegradation of scaffold

Biodegradation of scaffold is one of the major strategies in tissue engineering approaches for neo tissue regeneration [305]. The scaffold should have controlled degradation rate so that it matches with the new tissue formation [53]. More importantly, the degradation was reported

to be a major concern when scaffold is made of silk based material [13]. Thus, the developed SF and SF/CMC_2 nanofibrous scaffolds were investigated for biodegradation in both PBS and protease XIV enzymatic solutions. Figure 5.13 shows the biodegradation behaviour of both the scaffolds in PBS (Figure 5.13C) and enzymatic solution (Figure 5.13D).

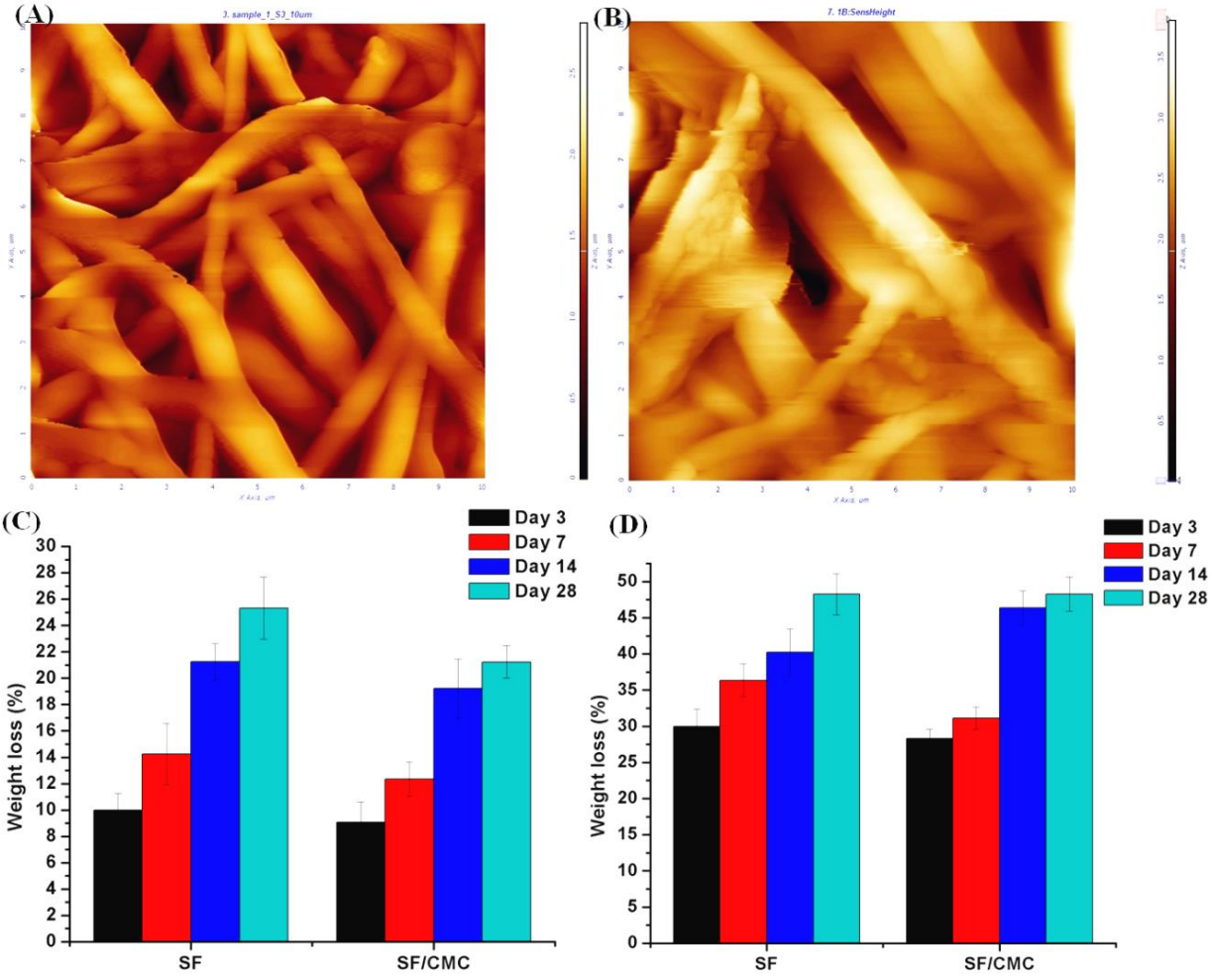

Figure 5.13: AFM images of (A) calcified SF and (B) calcified SF/CMC_2 after treatment in SBF for 7 days. Observed degradation behaviour of SF and SF/CMC_2 scaffolds by soaking in PBS (C) and enzymatic solution (D) for 28 days. The AFM images show the higher surface roughness of SF/CMC_2 which confirms the improvement of biomineralization ability of SF based scaffold with the incorporation of CMC.

From these studies it has been observed that SF scaffold was degraded faster and up to 45% to 50% degradation occurred in presence of enzyme, where as in PBS it degraded slower

showing 26% - 28% degradation. The SF/CMC_2 scaffold shows a slightly lower degradation rate of 20% to 22% and 42% to 47% in PBS and in presence of enzyme respectively.

5.1.6 In-vitro cell culture study

Isolation, culture and differentiation of hMSCs

The isolated mononuclear cells from Umbilical cord blood (UCB) by Ficoll hypaque method were cultured upto 4 to 6 passages to produce hMSCs which were used to evaluate biological property of the developed scaffolds. The mononuclear cells were observed to be spherical in morphology (Figure 5.14A-a), whereas after culturing for various passages, cells were observed to be spindle shape fibroblast like in morphology (Figure 5.14A (b-d)). The isolated hMSCs also show multilineage differentiation potential such as osteogenic, chondrogenic and adipogenic, which has been assayed by Alizarin red S, Alcian blue and Oil red staining assays respectively during 14 days of culture (Figure 5.14B). The osteoblastic differentiation of hMSCs in osteogenic culture media was confirmed by mineralized calcium nodule deposition stained in bright orange-red colour [306-307]. The adipogenic differentiation of hMSCs is confirmed by the presence of lipid vacuole as observed in Figure 5.14B-c [306-307]. Whereas, chondrogenic differentiation of hMSCs was confirmed by glycosaminoglycans deposition [308].

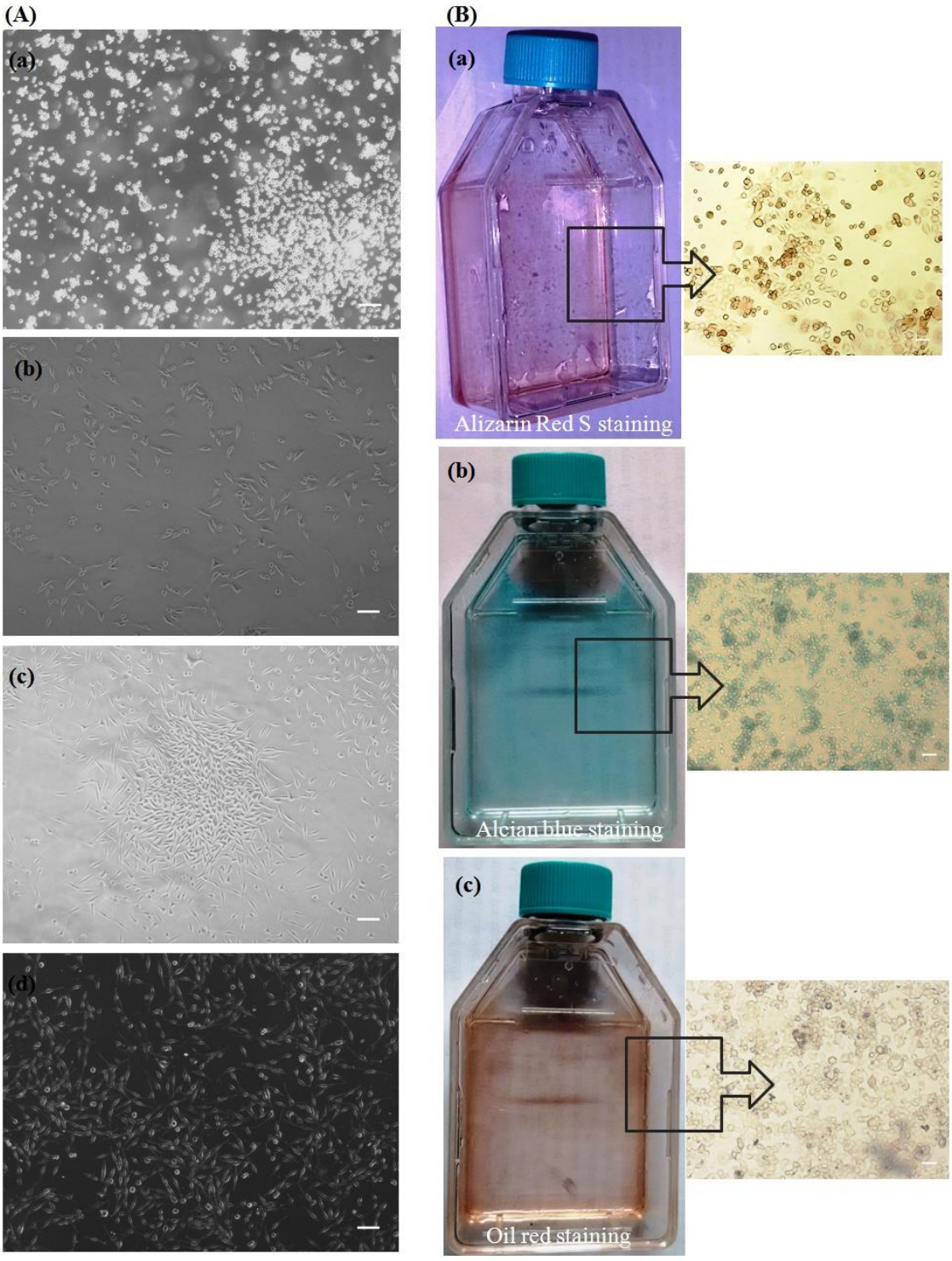

Figure 5.14: (A) Morphological changes of hMSCs (a) MNCs, (b) after passage 1, (c) after passage 2 and (d) after passage 3 as observed under phase contrast microscope at magnification 10X and scale bar 50µm. Initially the cells are found to be spherical in shape and slowly changed to fibroblast like morphology. (B) Multilineage differentiation potential of hMSCs assessed by alizarin red S staining (a), Alcian blue staining (b) and Oil red staining (c).

Cell adhesion and cell morphology

Cell adhesion and cellular morphology are the important indicators which reflect the affinity of the cells to the scaffold thereby forming the cell scaffold construct and finally neo tissue regeneration [309]. These cell supportive properties of the pure SF and calcified SF/CMC_2 composite nanofibrous scaffolds were evaluated in term of cellular attachment, spreading and proliferation of hMSCs cultured on the scaffold surface. A positive control was taken by culturing hMSCs on gelatin nanofiber. As can be seen from the FESEM images (Figure 5.15A-C), the hMSCs attached to the scaffolds attained a more or less elliptical shape after 12 h of culture thereby demonstrating their initial signs of spreading. The measured aspect ratios for gelatin (2.23 ± 0.46) and silk fibroin (2.08 ± 0.04) scaffolds are comparable whereas a lower aspect ratio of 1.725 ± 0.091 was shown by calcified SF/CMC_2 scaffold. The lower aspect ratio of cells over calcified SF/CMC_2 was expected due to the negatively charged carboxylate group of CMC [294] and the effect was gradually reduced with time due to the progress of the mineralization over the surface of SF/CMC scaffold. After 7 days (Figure 5.15D-F), most of the cells were appeared elongated and spindle like in morphology over SF, whereas cells over gelatin was less elongated. On 14^{th} day (Figure 515G-I), the cells were observed to be proliferated and a strong cell attachment was evident from filopodia protrusions from cell surface thereby formation of a monolayer was observed over the surface of the scaffolds.

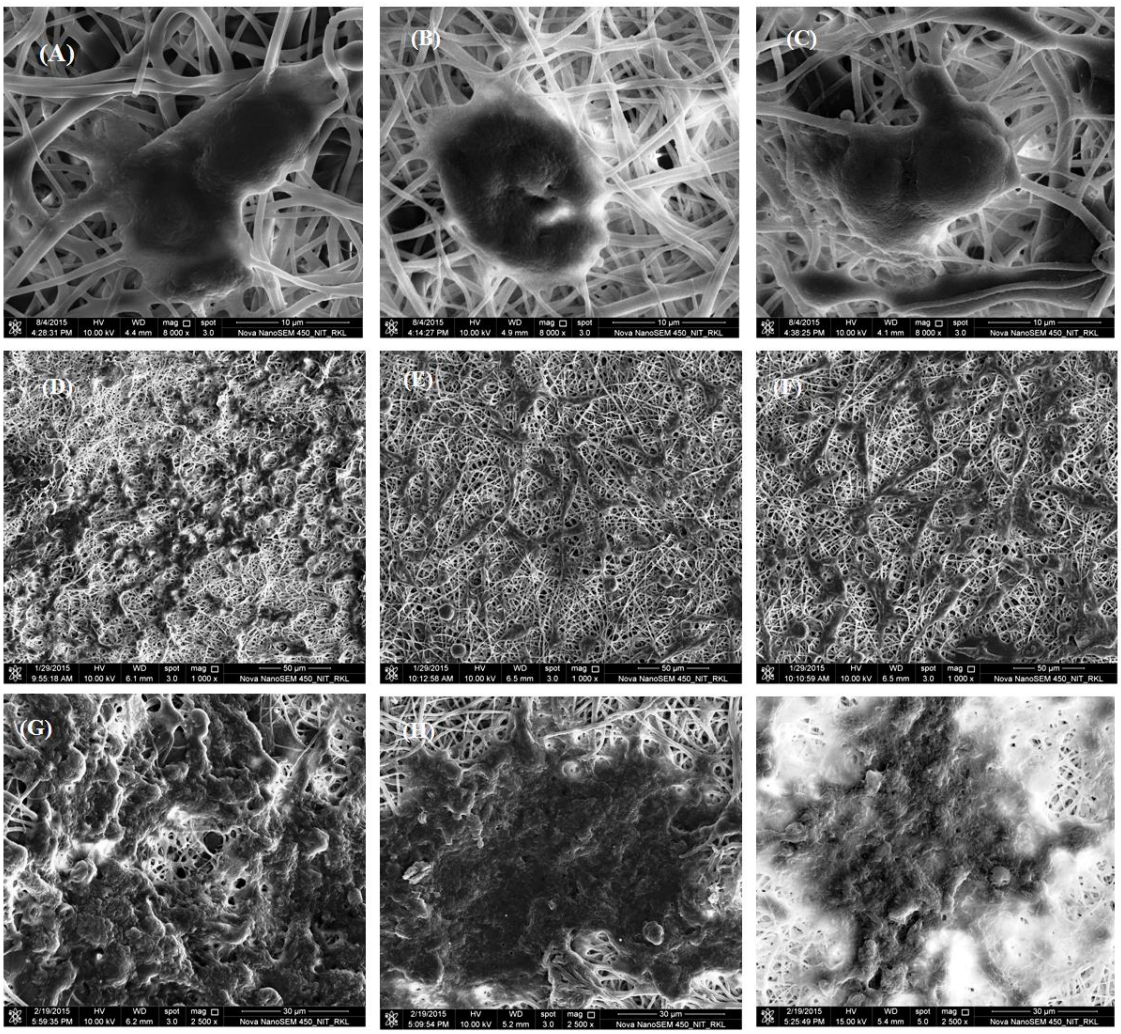

Figure 5.15: FESEM images of hMSCs on gelatin (A), SF (B) and calcified SF/CMC_2 (C) after 12 h of culture. FESEM micrographs of cells cultured on gelatin (D), SF (E) and calcified SF/CMC_2 (F) after 7 days. FESEM images of cells cultured on gelatin (G), SF (H) and calcified SF/CMC_2 (I) on day 14. Change in cell morphology from spherical to elongated is observed during the progress of the culture representing the cell supportive property of the scaffolds.

Cytoskeletal organization

Figure 5.16 shows the fluorescence images of cytoskeleton development and distribution after 7 and 14 days of cell culture on the electrospun gelatin (Figure 5.16A, D), SF (Figure 5.16B, E) and calcified SF/CMC_2 blend (Figure 5.16C, F) scaffolds. On day 7, it was observed that cells were attached and elongated, whereas cells were proliferated and monolayer coverage of scaffold surface was evident on day 14. Furthermore, SF and calcified SF/CMC_2 nanofibrous scaffolds showed better development of filamentous actins compared to gelatin.

The formation of stable thin filamentous actins and its termination at focal contact further help in cell spreading and osteogenic differentiation of hMSCs [310]. Similar trends with more aggregated cells and absence of gap between cell boundaries (interconnected cells) were noticed on day 14.

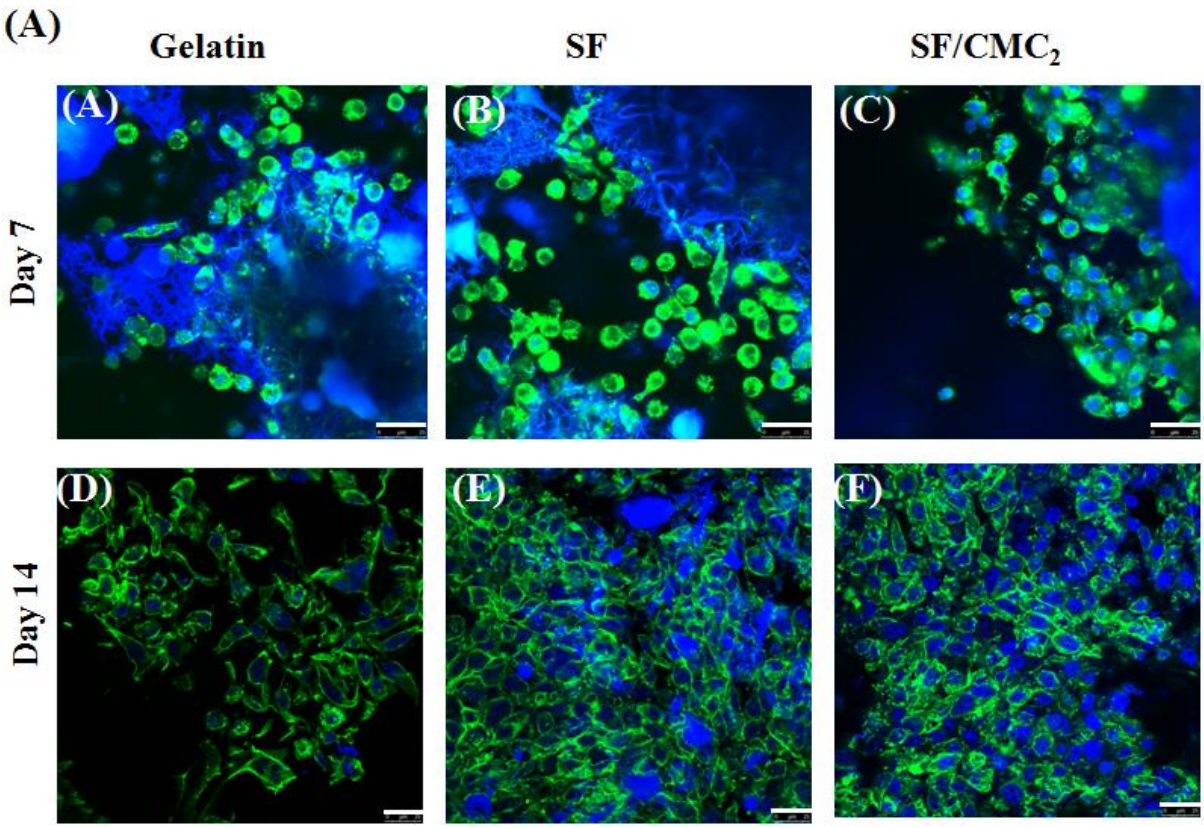

Figure 5.16: Cell proliferation and distribution are visualized under confocal microscope on gelatin (A), SF (B) and calcified SF/CMC_2 (C) after culture for 7 days, and gelatin (D), SF (E and calcified SF/CMC_2 (F) after culture for 14 days. Nuclei of the cells were stained with DAPI (blue) and actin filaments with phalloidin (green). Change in cell morphology from spherical to elongate is observed with increase in culture time. (Scale bar- 25µm)

Metabolic activity by MTT assay

The metabolic activity which represents the potentiality of cells to progress in the cell cycles was quantitatively estimated during 7 days of hMSCs cultured over the scaffolds by MTT assay [311]. As can be seen from Figure 5.17 that on day 3 the optical density (OD) measured with hMSCs seeded calcified SF/CMC_2 is higher than pure SF and gelatin ($p < 0.05$) scaffolds. The cell viability was gradually increased with time irrespective of the type of

scaffolds. However, maximum viability was obtained with blend scaffold up to 7 days of culture. On day 7, higher cell viability was shown by calcified SF/CMC_2 scaffold followed by SF and gelatin scaffolds. The overall trend of cell viability follows as-calcified SF/CMC_2 >SF>gelatin.

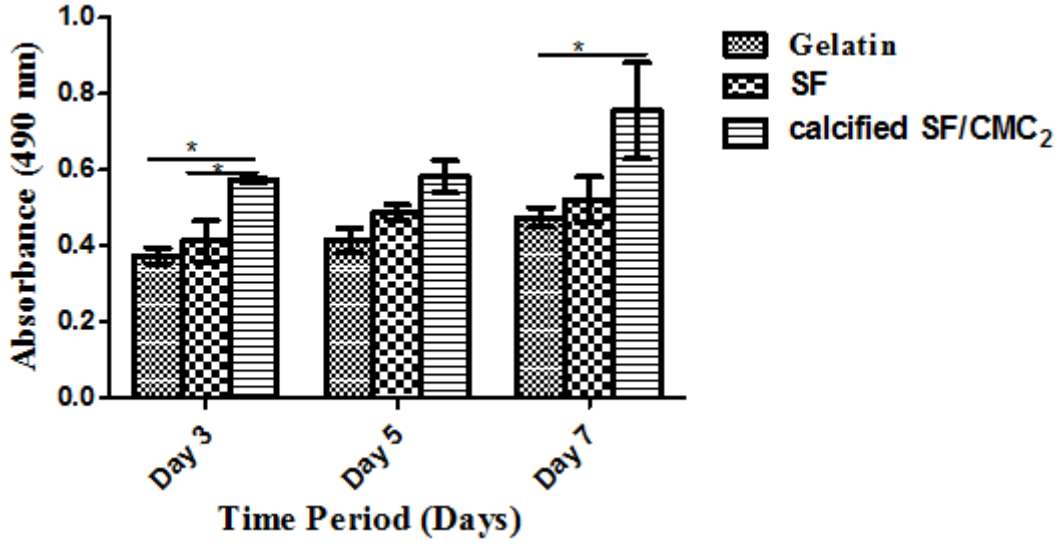

Figure 5.17: MTT assay of hMSCs cultured on gelatin, SF and calcified SF/CMC_2. The trend of cell viability over nanofibrous scaffolds follows as -calcified SF/CMC2 >SF>gelatin.

Live/dead assay and cellular distribution

The confocal images were taken to observe the viability of hMSCs cultured on the developed gelatin, SF and calcified SF/CMC_2. The cell viability of hMSCs seeded over scaffolds was done by live/dead staining solution (Calcein AM and EthD-1), where green signal indicates viable cells and red signal indicate dead cells. Figure 5.18A shows that the hMSCs are viable and healthy over the entire scaffold irrespective of their composition. However, cells were observed more elongated over SF and calcified SF/CMC_2 in comparison of gelatin.

The penetration and proliferation of hMSCs within the scaffolds were determined from the 3D-Z-stack images composed by arranging all Z-sections developed during the scanning of cell-seeded scaffolds under the confocal microscope. The images (Figure 5.18B) indicate that the cells were not only proliferated well over the scaffolds but also penetrated inside the scaffold at varying depth of penetration of hMSCs colonization. The highest penetration was occurred in gelatin up to 35- 40 µm and comparable intensity of cell penetration up to 30- 35

μm was shown by calcified SF/CMC_2 scaffold, while SF shows the lowest penetration depth of 15-20 μm. All these taken together, it has been observed that calcified SF/CMC_2 nanofibrous scaffold has the superior cellular activity than the other scaffold developed under study. The improved hydrophilicity, higher tensile strain (in wet state) and swelling property of calcified SF/CMC_2, along with its higher standard deviation in fiber diameter in comparison to pure SF, contribute to increased penetration and proliferation of hMSCs towards the interior of the scaffold without much affecting cell attachment and proliferation on the surface.

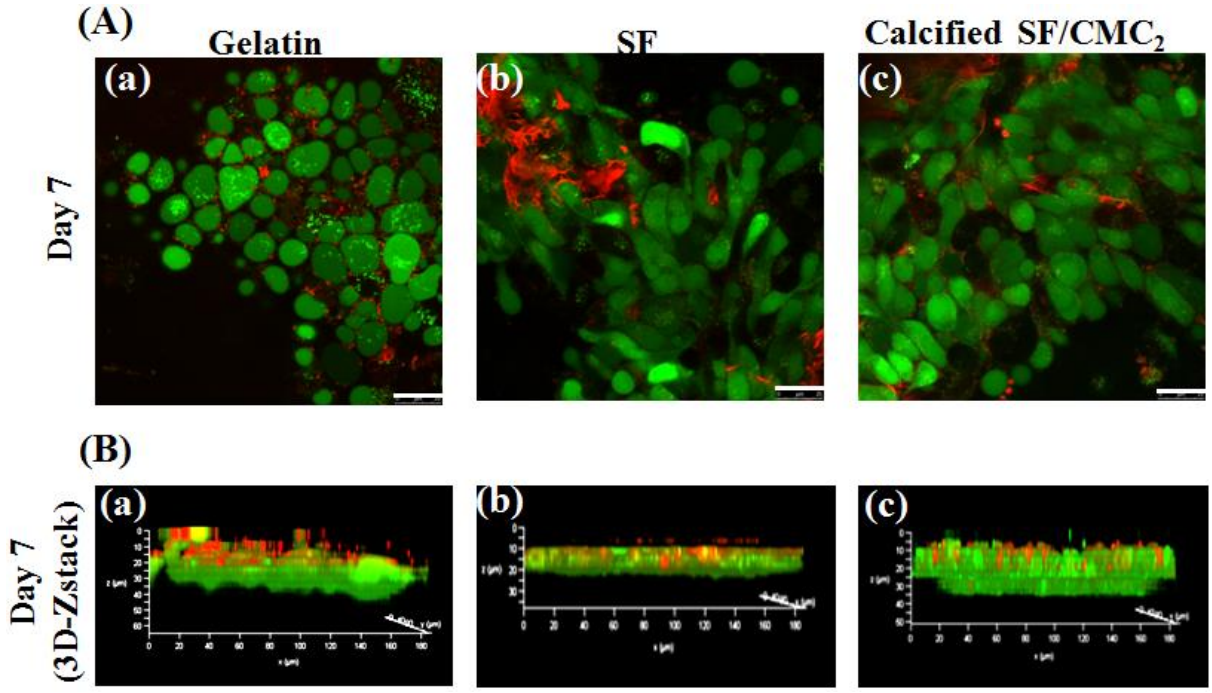

Figure 5.18: (A) Calcein AM and EthD-1 staining of hMSCs cultured for 7 days on Gelatin (a), SF (b) and calcified SF/CMC_2 (c). (B) 3D laser scanning confocal images were observed while live/dead staining (Z stacks) of hMSCs cultured for 7 days on Gelatin (a), SF (b) and calcified SF/CMC_2 (c). Green signals indicate viable cells and red signal for dead cells. (Scale bar = 25 μm)

Glucosamino glycan (GAG) analysis

The differentiation of hMSCs towards the osteogenic lineage is indicated by the synthesis and deposition of GAG over the scaffold [312]. GAG is also known to play a crucial role in sequestering growth factors in scaffold matrices [313]. Figure 5.19 shows GAG accumulation over Gelatin, SF and calcified SF/CMC_2 scaffold. The GAG production was shown to be

increased over culture period. The scaffolds used under study showed the formation of GAG with varied level of secretion. On day 7, the GAG content was slightly higher over calcified SF/CMC_2 than SF and gelatin scaffolds. On day 14, GAG content on calcified SF/CMC_2 (0.298 µg/mg) nanofibrous scaffold was 2.2 fold higher than day 7. Whereas, on day 14 GAG content (0.175 µg/mg) on SF nanofibrous scaffold was 1.8 fold higher than day 7. However, gelatine shows 1.9 fold higher GAG content (0.185µg/mg) on day 14 as compared of day 7. Thus, calcified SF/CMC_2 provides better GAG deposition reflecting its superior osteogenic differential than SF nanofibrous scaffold.

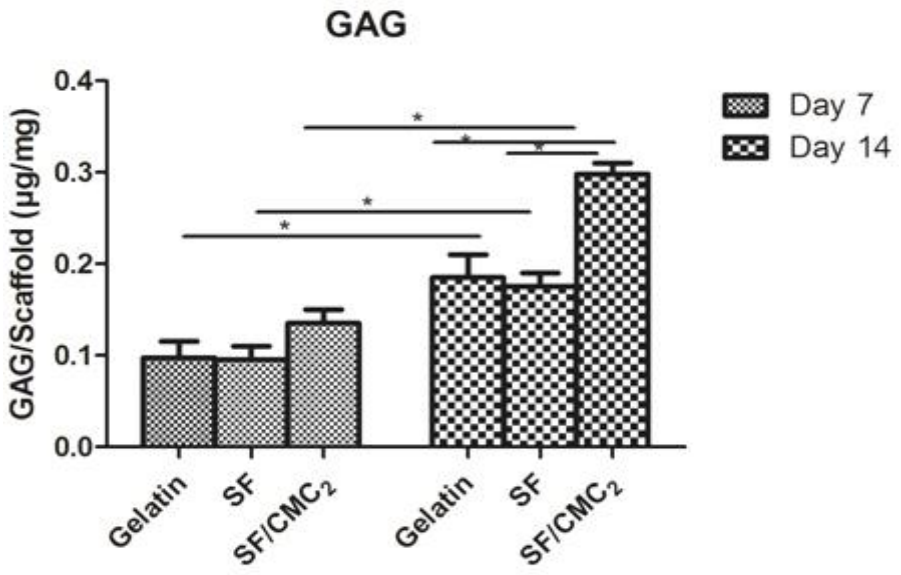

Figure 5.19: Estimation of intracellular GAG secreted by hMSCs cultured in the osteogenic media for 7 and 14 days of culture over gelatin, SF and calcified SF/CMC_2. Calcified SF/CMC_2 promotes better GAG deposition in comparison to SF nanofibrous scaffold is noticed.

5.1.7 Osteogenic differentiation

Alkaline Phosphatase assay

The alkaline phosphatase enzyme was assessed to evaluate the early osteogenic differentiation of hMSCs. The characteristic marker of early osteoblastic differentiation is attributed to the cellular secretion of ALP. ALP enzymes catalyse the hydrolysis of extracellular pyrophosphates and increase the local concentration of inorganic phosphates which facilitate biomineralization [314]. The ALP activity of hMSCs over the scaffolds was studied during 14 days of culture period. An increase in enzyme activity was observed with

all the scaffold with varied activity level with increasing culture period from 7 to 14days. This icrease in ALP activity represents the cells in a more differentiated stage (Figure 5.20). As compared to gelatin and SF, hMSCs show significantly higher ALP activity on calcified SF/CMC_2 on 14^{th} day ($p < 0.05$). Hence, calcified SF/CMC_2 is confirmed to provide a superior supportive platform for osteogenic differentiation of hMSCs. The superior ALP activity over calcified SF/CMC_2 was observed because of its superior Ca/P nucleation ability.

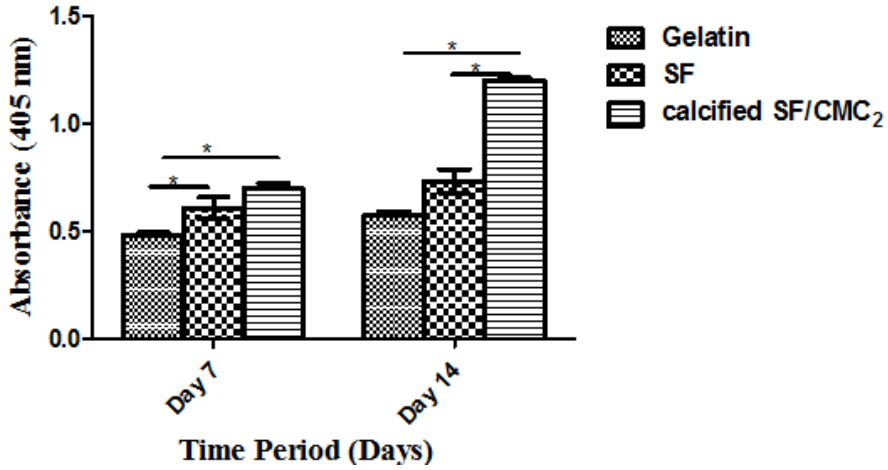

Figure 5.20: Alkaline phosphatase (ALP) activity in hMSCs cultured on the gelatin, SF and calcified SF/CMC_2 in osteogenic culture medium over time (n=3). From ALP activity analysis it has been observed that calcified SF/CMC_2 provides a better platform for osteogenic differentiation of hMSCs as compared to pure SF and gelatine scaffold.

Biomineralization of hMSCs seeded nanofibrous scaffold

The mineralization and formation of bioactive Ca/P like nodule over the surface of scaffold is the prime target to provide time dependent improved osteogenic environment for cultured cells. To assess the level of mineralized matrix produced by hMSCs over the developed scaffold after culturing for 14 days was assessed by ARS assay (Figure 5.21A). The uniform distribution of Ca/P was observed over calcified SF/CMC_2 nanofibrous scaffold surface which may promote better cell growth and differentiation as bone tissues exhibit orderly distribution of Ca/P over nanofibrous collagen matrix [169, 315]. As can be seen from the FESEM images (Figure 5.21B), the degree of biomineralization on day 7 is higher on calcified SF/CMC_2 than on SF. Further EDX analysis showed that hMSCs on pure SF formed a mineral phase with Ca/P ratio: 0.8-1.2 whereas on calcified SF/CMC_2, the Ca/P ratio was

1.4-1.5 which is similar to the mineral phase of the human bone that consists mostly of Ca and P in the ratio 1.4 - 1.7 [316]. The quantification of ECM mineralization was performed through ARS where it binds with calcium and forms ARS-calcium complex in a chelation process. It can be observed from the inverted phase contrast microscopic images (Figure 5.21A) that on day 7, the ARS-calcium complex (red colour) covered a greater percentage of calcified SF/CMC_2 surface than the other scaffolds. However on 14^{th} day of culture, all the scaffolds show higher level of formation of the ARS-calcium complex than that of day 7 but with varied degree of complex formation. However, the intensity of ARS complex was the highest in case of calcified SF/CMC_2. Also calcified SF/CMC_2, on day 14 (Figure 5.21C), showed greater OD as compared to gelatin and SF ($p < 0.05$). This suggests that the degree of ECM mineralization depends both on culture duration and the scaffold material. The analysis of EDX and ARS assay results demonstrate the ability of calcified SF/CMC_2 to mimic the osteogenic environment and found substantial superiority of calcified SF/CMC_2 over gelatin and SF scaffolds for bone tissue engineering application.

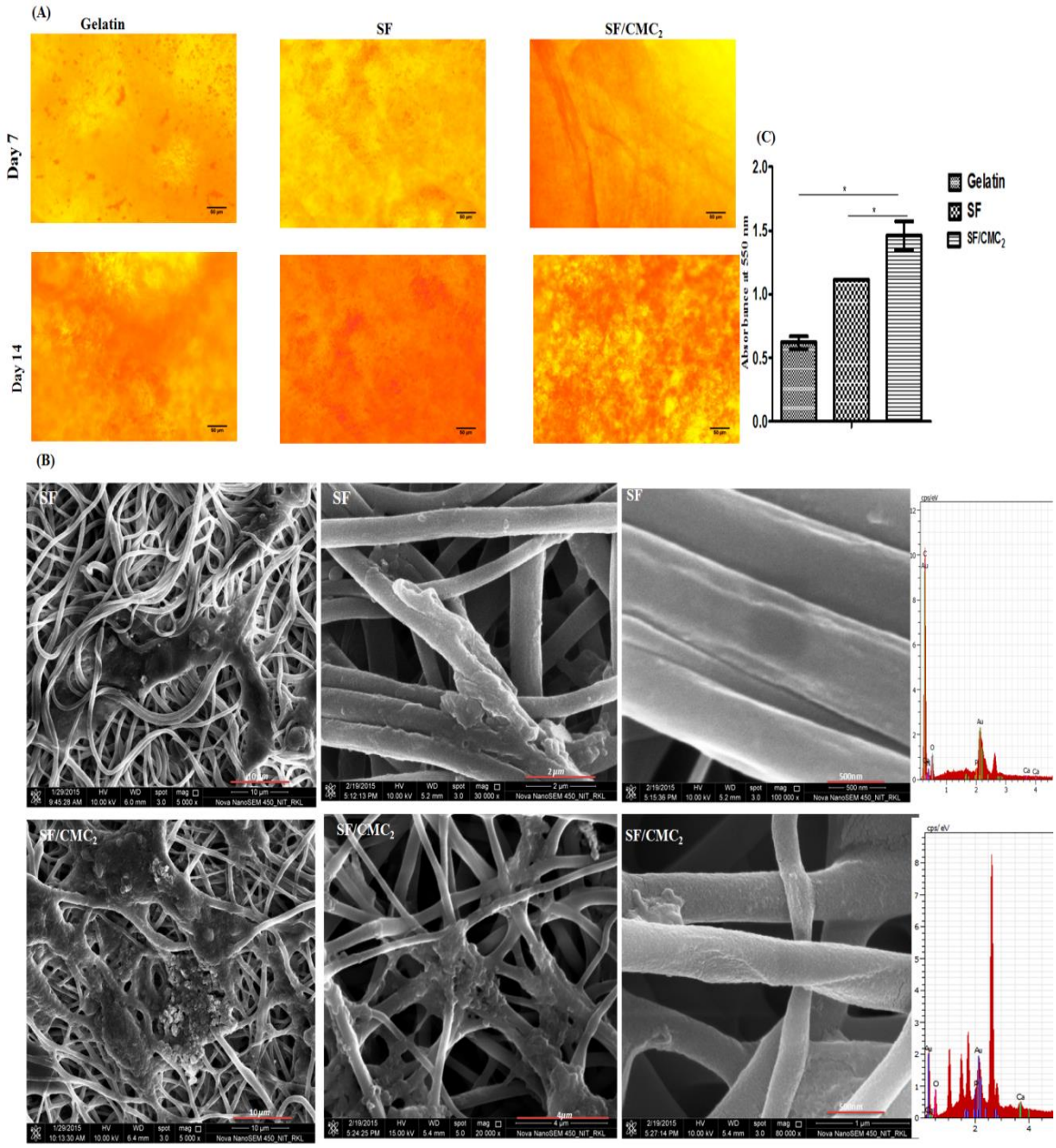

Figure 5.21: (A) Alizarin red S staining of hMSCs cultured over gelatin, SF and calcified SF/CMC_2 for 7 and 14 days. (B) FESEM images and EDX spectra of mineral deposition of SF and calcified SF/CMC_2 cultured for 7 days. (C) Alizarin Red S staining assay for quantitative evaluation of hMSCs mineralization on nanofibrous scaffolds after 14 days of culture. Calcified SF/CMC_2 shows enhanced biomineralization than pure SF and gelatin scaffolds.

Runx2, Osteocalcin and Collagen type I expression analysis

The osteogenic differentiation of hMSCs seeded on the scaffolds was further assessed by Runx2 transcription factor, osteocalcin and type1 collagen expression by the cells. The hMSCs seeded on the nanofibrous scaffolds tend to aggregate and form committed

osteoprogenitor cells. With time, they differentiate into pre-osteoblasts, early osteoblasts and mature osteoblasts. Runx2 is the key regulator for early osteoblastic differentiation of hMSCs [317]. With time, they differentiate into preosteoblasts, early osteoblasts and mature osteoblasts. Runx2 is the key regulator for early osteoblastic differentiation of hMSCs. Runx2 binds specific DNA sequences and regulates the transcription of various genes to orchestrate the osteogenic differentiation [318]. The immunocytochemistry for Runx2 transcription factor expression in hMSCs on the scaffolds for 7 (Figure 5.22A) and 14 days (Figure 5.22B) of culture depicted in the confocal images. As co-localization of Runx2 and DAPI immunostainning show that the expression of Runx2 was localized to the cell nuclei. From Integrated density (ID) evaluation, it was observed that the expression of RunX2 transcription factor at higher level on day 7 (Figure 5.22C) as compared to day 14. Runx2 is pro-terminal marker of osteogenesis and its level of expression on calcified SF/CMC_2 was the highest on day 7 and then decreased by day 14 as osteogenesis enhanced thereby, exhibiting the advantage of using calcified SF/CMC_2 composite scaffolds. The osteocalcin expression a late stage marker was studied over a period of 14 days to assess the osteogenic cell differentiation potential of the scaffold as shown in figure 5.22B. The confocal images revealed that hMSCs demonstrate the highest level of osteocalcin expression on calcified SF/CMC_2 on 14^{th} day. Moreover, the integrated density quantification of osteocalcin (Figure 5.22D) confirms that the calcified SF/CMC_2 shows significantly ($p < 0.05$) higher level of expression in comparison to other scaffolds at day 7 and day14.

On day 14, RT-PCR analysis shows significantly ($p < 0.05$) higher level of expression of OCN (1.67 fold) and Col1 (3.5 fold) on calcified SF/CMC_2 than SF (Figure 5.22E), whereas a decrease in Runx2 (1.7 fold) expression was observed on calcified SF/CMC_2 on day 14 (Figure 5.22E) with no significant difference at this point. Since osteocalcin is an abundant calcium binding protein and adsorbs Ca/P, calcified SF/CMC_2 facilitates higher degree of Ca/P nucleation sites and growth over the nanofibrous structure and cause the activation of calcium sensing receptor signalling leading to a higher level of osteocalcin expression in hMSCs. Thus, the in vitro stem cell study reveals the superior osteogenic potential of SF/CMC_2 with significantly higher ALP activity, biomineralization and expression of osteogenic marker such as OCN and Collagen type I. This might be due to the superior Ca/P nucleation ability and stiffness of developed SF/CMC_2 nanofibrous scaffold.

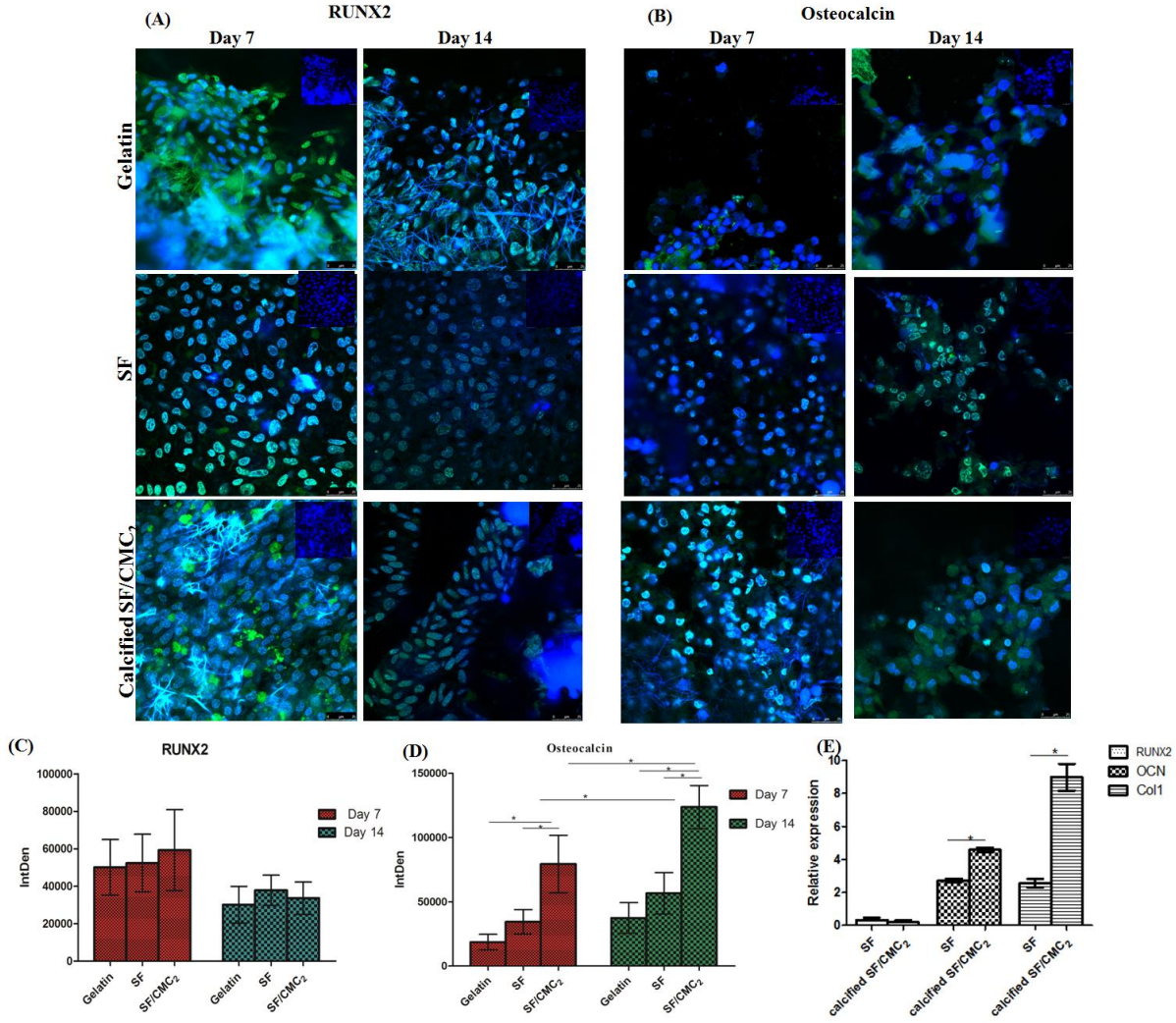

Figure 5.22: Immunocytochemistry for Runx2 and osteocalcin on hMSCs cultured on gelatin, pure SF and calcified SF/CMC$_2$ scaffolds. (A) Confocal images showing RunX2 expressions of hMSCs on day 7 and day 14 (B) Confocal images for osteocalcin expressions were observed in hMSCs on day 7 and day 14 in the osteogenic culture medium. Integrated density evaluation for RunX2 and osteocalcin are depicted in graphs (C) and (D) respectively. Scale bar = 25 µm. (E) The osteoblastic differentiation of hMSCs on nanofibrous scaffolds was assessed by measuring the mRNA expression of Runx2, osteocalcin and type1 collagen. The immunocytochemistry and gene expression study confirm the superior osteogenic potential of calcified SF/CMC$_2$ nanofibrous scaffold than SF scaffold.

CHAPTER-5B: Synthesis and Characterisation of nano-bioglas and Copper-doped nano-bioglass

Recent research has focused on the improvement of bioactivity and osteogenic property of polymeric biomaterial for bone tissue engineering applications. One of the promising ways to improve these properties by the addition of bioceramic to the biopolymer. Among the various bioceramics, bioactive bioglass has attracted much attention of the researchers for use in developing biopolymer- ceramic composites because of its several advantages like biodegradation, high apatite formation ability [319], osteoinductivity and osteoconductivity properties [135, 320]. It has also been demonstrated that there is a genetic control of human osteoblast cellular response to bioglass molecule [321]. Furthermore, the nanoscale structure is reported to be superior than its microscale counterpart [322] [323]. Therefore, this phase of research work focuses on the preparation of bioglass with nanoscale microstructure by sol-gel method. The prepared bioglass was characterized for morphology, structural and functional, bioactivity and ion release ability.

Very recently, it has been reported that the inorganic ions has the beneficial effect when these are added to the bioglass and enhances the osteogenic and angiogenic property of the polymer scaffold upon the incorporation of these components [324-325]. Furthermore, among the inorganic ionic components, Cu^{2+} seems to be the most attractive [324]. Therefore, research effort was also given to prepare and characterize Cu^{2+} doped nano-bioglass by following appropriate method.

The present chapter describes the above experimental result and discussion.

5.2.1 Synthesis and characterization of nano-bioglass

Bioactive bioglass in nano-size range was synthesised by acid-catalyzed sol-gel method. The choice of sol-gel process is based on its several advantages over the other conventional melt-quench method such as homogeneity, higher purity, higher surface area of the particles, superior degradation and high rate of apatite formation [326-327]. The molar composition of the prepared bioglass was 60% SiO_2, 36% CaO, and 4% P_2O_5.

Morphological Characterization of nano-bioglass

The FE-SEM images (Figure 5.23A) were used to assess the size, morphology and homogeneity of nano-bioglass (nBG) samples. The particle size distributions of nBG were observed to be in the range of 40 - 50 nm. Some of the conglomerated particles were also noticed in both FE-SEM and TEM images of nBG. The TEM images (Figure 5.23B) shows

the presence of particles with sizes ≤ 50 nm and conglomerated particle size was ≤100 nm. The selected area electron diffraction (SAED) pattern and HRTEM confirm their amorphous nature (Figure 5.23D, C) as SAED pattern lacks any ring like pattern and HRTEM images show absence of fringes.

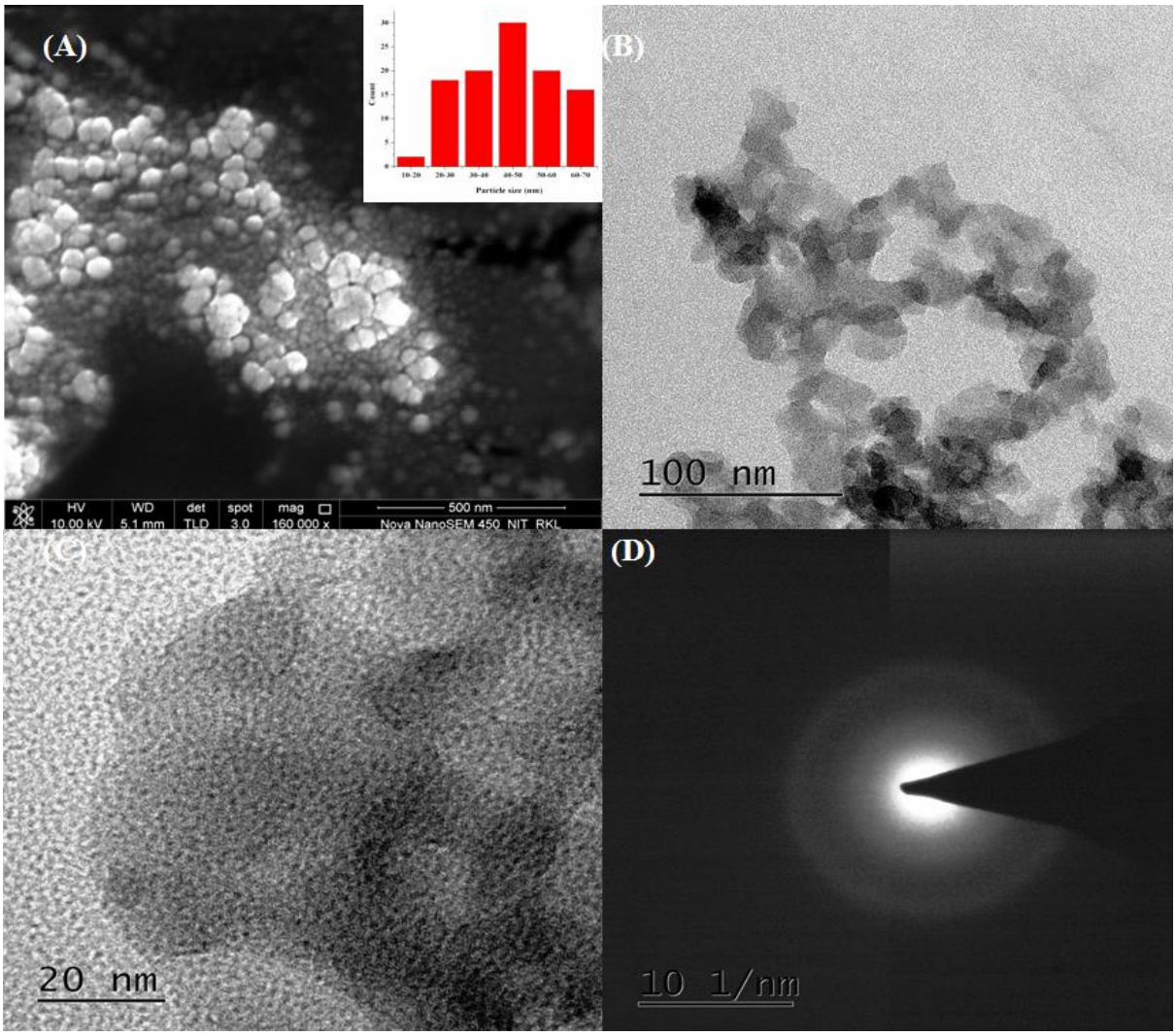

Figure 5.23: Showing the morphology of nBG by FESEM (A) and TEM images (B). HRTEM (C)images and SAED pattern(D) of nanobioglass. The presence of particles with sizes ≤ 50 nm and conglomerated particle size ≤100 nm was observed.

Structural and functional analysis of nBG

The structural and functional characteristics of synthesized nano-bioglass were assessed by XRD and FT-IR analysis. As observed from Figure 5.24A, the synthesized nano-bioglass shows wide diffraction peak (X-ray diffractogram) between 20° and 40°, which confirms

their amorphous feature [230]. The FT-IR (Figure 5.24B) spectrum of nBG shows the characteristic bands of Si-O-Si bonds at 1060 cm^{-1} (stretch vibration), 798 cm^{-1} (bending vibration) and 480 cm^{-1} (bending vibration). From the structural and functional analysis of nano-bioglass it has been confirmed that amorphous silicate based bioglass has been synthesised.

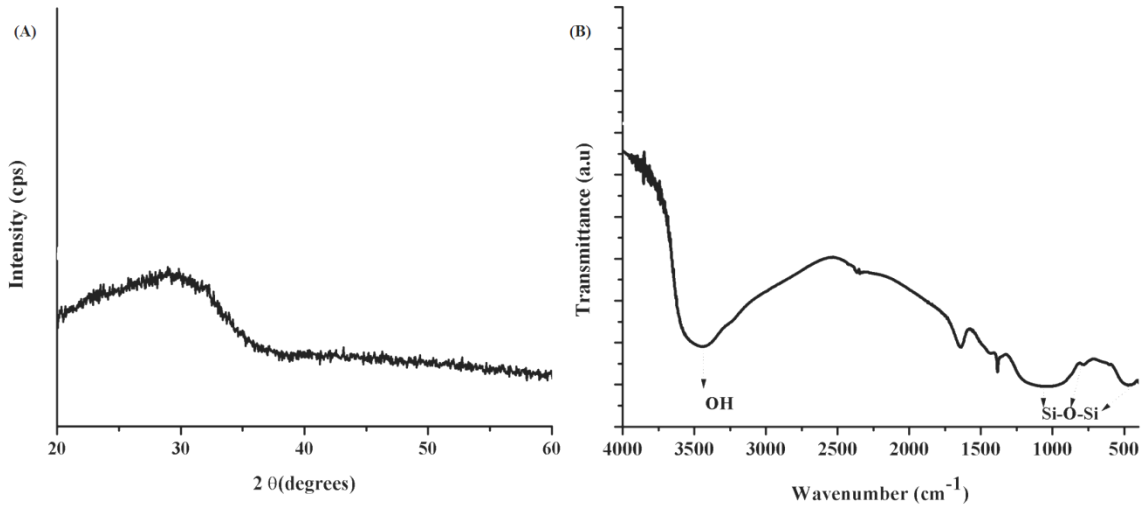

Figure 5.24: Showing the XRD diffractogram (A) and FT-IR spectra(B) of nano-bioglass. Synthesised nBG represents amorphous characteristics of glass system.

5.2.2 *In vitro* apatite forming ability of nano-bioglass

In vitro apatite forming ability is one of the important characteristic of bioactive glass. The bioactivity of bioglass was assessed by using simulated body fluid with ion concentration similar to human blood plasma [293]. Finally, SBF treated bioglass was characterized for morphological, structural and functional and ion release property.

Morphological analysis

After 7 days of soaking in SBF, FESEM analysis revealed the formation of fine granules like particles over the surface of the bioglasses (Figure 5.25A). Whereas, HR-TEM images as shown in Figure 5.25B depicts the amorphous as well as lattice fringes with d-spacing of 0.28 nm corresponding to the 211 plane for apatite formation over bioglass particles [328]. The SAED image (Figure 5.25C) of bioglasses shows visible diffraction ring formation. Thus, HR-TEM and SAED analysis support the bioactivity property of synthesized nano-bioglass.

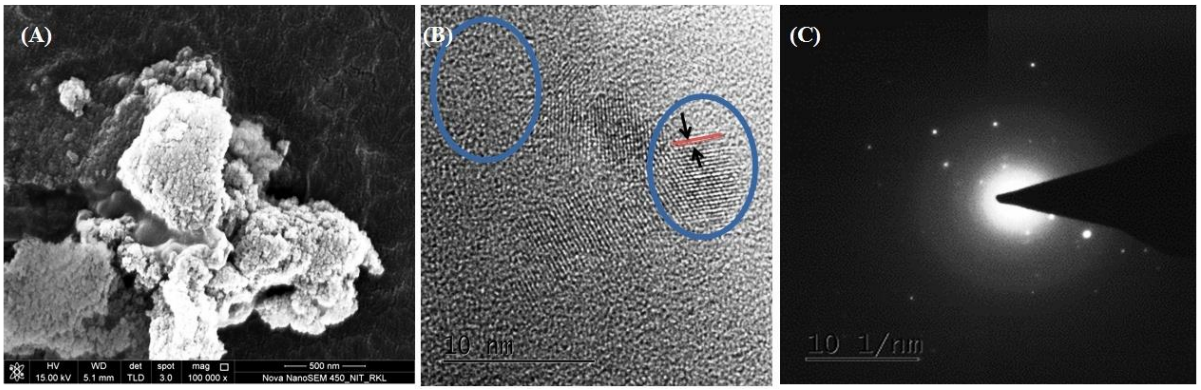

Figure 5.25: Showing the FESEM image (A), HRTEM image(B) and SAED pattern(C) for the developed nBG after SBF treatment. Formation of apatite like granules and its characteristic features (d-spacing of 0.28 nm corresponding to the 211 plane was observed from FESEM and TEM images respectively. The SAED image shows visible diffraction ring formation.

Structural and functional analysis

XRD diffractogram for nBG before and after SBF soaking is shown in Figure 5.26A. The new characteristic peaks were observed at 2θ = 26° (002), 32° (211), 39° (310), 46° (222), 49° (213) and 53° (004), which were assigned to hydroxyapatite[329-330]. The EDS studies showed the surface deposition of hydroxyapatite with Ca/P ratio of 1.80, suggesting the bioactivity characteristic of nBG in SBF (Figure 5.26C).

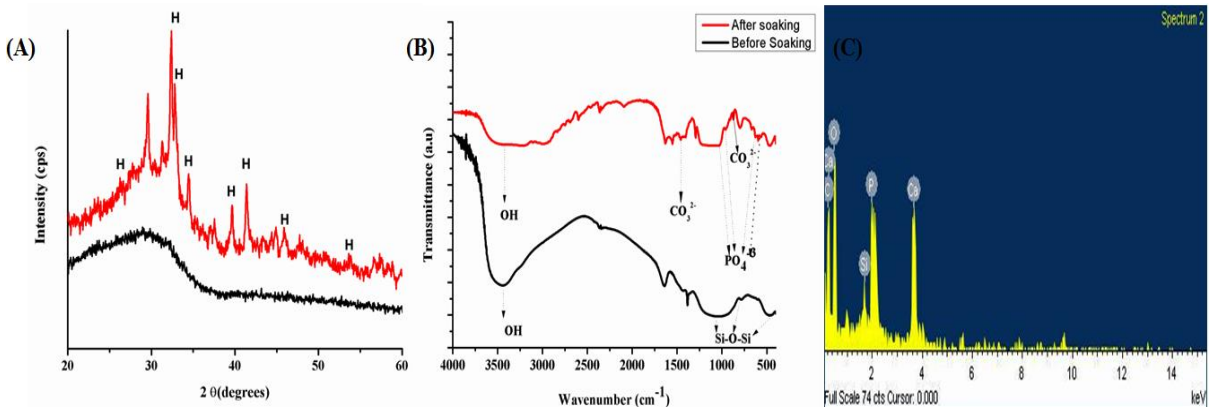

Figure 5.26: Showing the XRD diffractogram (A), FT-IR spectra(B) and EDS spectra(C) of nano-bioglass before and after SBF treatment. The characteristic hydroxyapatite peaks were observed at 2θ = 26° (002), 32° (211), 39° (310), 46° (222), 49° (213) and 53° (004). This was supported by FTIR analysis. The EDS studies showed the surface deposition of hydroxyapatite with Ca/P ratio of 1.80, suggesting the bioactivity characteristic of nBG.

The FT-IR (Figure 5.26B) spectrum of nBG shows the characteristic bands of Si-O-Si bonds at 1060 cm^{-1} (stretch vibration), 798 cm^{-1} (bending vibration) and 480 cm^{-1} (bending vibration). Whereas FT-IR spectra of nBG after SBF treatment shows the characteristic band of P-O bonds of PO_4^{3-} group of hydroxyapatite at 562 cm^{-1}, 595 cm^{-1} , 620 cm^{-1}, 962 cm^{-1} and 1026 cm^{-1}. The bands at 873 $cm^{-1}$and 1460 cm^{-1} were characteristic peaks of CO_3^{2-} group and band between 3300 cm^{-1} and 3600 cm^{-1} associated with the presence of hydroxyl groups [331].

Inductively coupled plasma atomic emission spectrophotometer (ICP-OES) analysis

The ion release behaviour of bioactive nano-bioglass was evaluated by the simulated body fluid treatment for 7 days followed by ICP-OES analysis. The dissolution experiments of nBG in SBF solution were performed to study its dissolution rate. The experimental results are depicted in Figure 5.27A. During dealkalinization process, Ca was rapidly released during the 3 day of soaking in SBF, reaching to 242.29 ± 3.44 ppm in SBF. This was followed by a decrease in the Ca^{2+} ion concentration with slower rate reaching to 215. 76 ± 3.82 ppm. The concentration of Si released from the nBG by breakdown of Si-O-Si bonds leading to 61.88 ± 1.14 ppm of Si, after 3 days and remained stable after soaking for 7 days (58.82 ± 1.4 ppm). Biodegradation and Si ion releases are the advantageous phenomenon of bioglass for bone tissue regeneration, as Si and Ca^{2+} ions having gene activating potential[83, 332]. This was followed by a decrease in the phosphorus ion concentration to 3.44 ± 0.464 ppm after 3 days of soaking in SBF, which shows the migration of Ca^{2+} and PO_4^{3-} through silica rich layer resulted in a formation of carbonated hydroxyapatite.

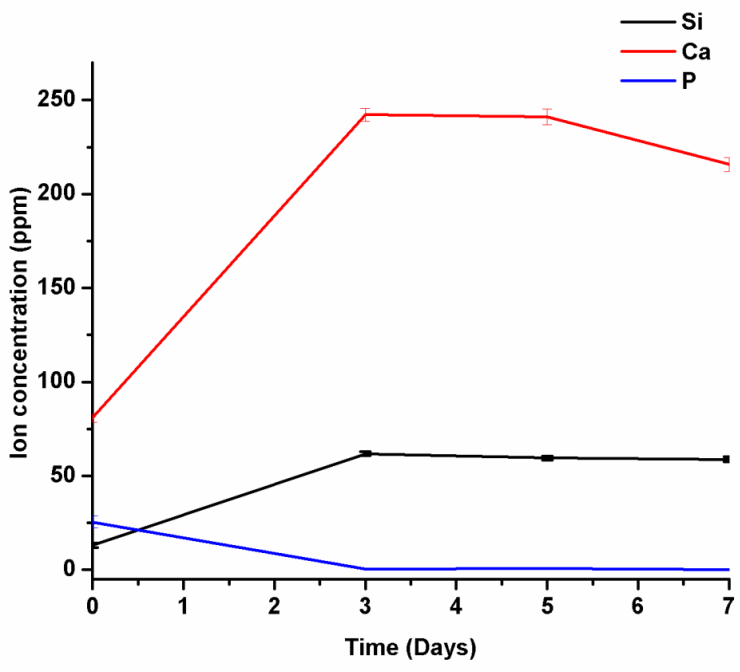

Figure 5.27: The graph showing the rate of ion release from nBG during the 7 days of SBF treatment

5.2.3 Synthesis and characterization of copper doped nano-bioglass

Bioactive bioglass in nano-size range was synthesised by acid-catalyzed sol-gel method. Different batches of copper doped nano–bioactive glass (Cu-nBG) with 0.5 mol% ($Cu_{0.5}$-nBG) and 1 mol% (Cu_1-nBG) based on 58S bioglass were prepared.

Morphological Characterization

The prepared copper doped nano-bioglasses ($Cu_{0.5}$-nBG and Cu_1-nBG) were successfully synthesised by using sol-gel method and their morphologies were observed under FESEM. The formation of agglomerated spherical shaped nano-bioglass with nanoscale sizes (< 100 nm) was evident from FESEM images as shown in Figure 5.28A. There is no significant change in morphology and particle size of nBG by the doping of Cu^{2+} ions as well as their concentration (0.5 % and 1 %). The TEM analysis of synthesized copper doped nBG further reveals that the bioglass particle size was in range of 50 nm (Figure 5.28C, D). Furthermore, the selected area electron diffraction (SAED) pattern (Figure 5.28C, D) obtained for all the synthesised nBG confirms their amorphous nature as SAED pattern lacks any ring like pattern and HRTEM images shows the absence of fringes.

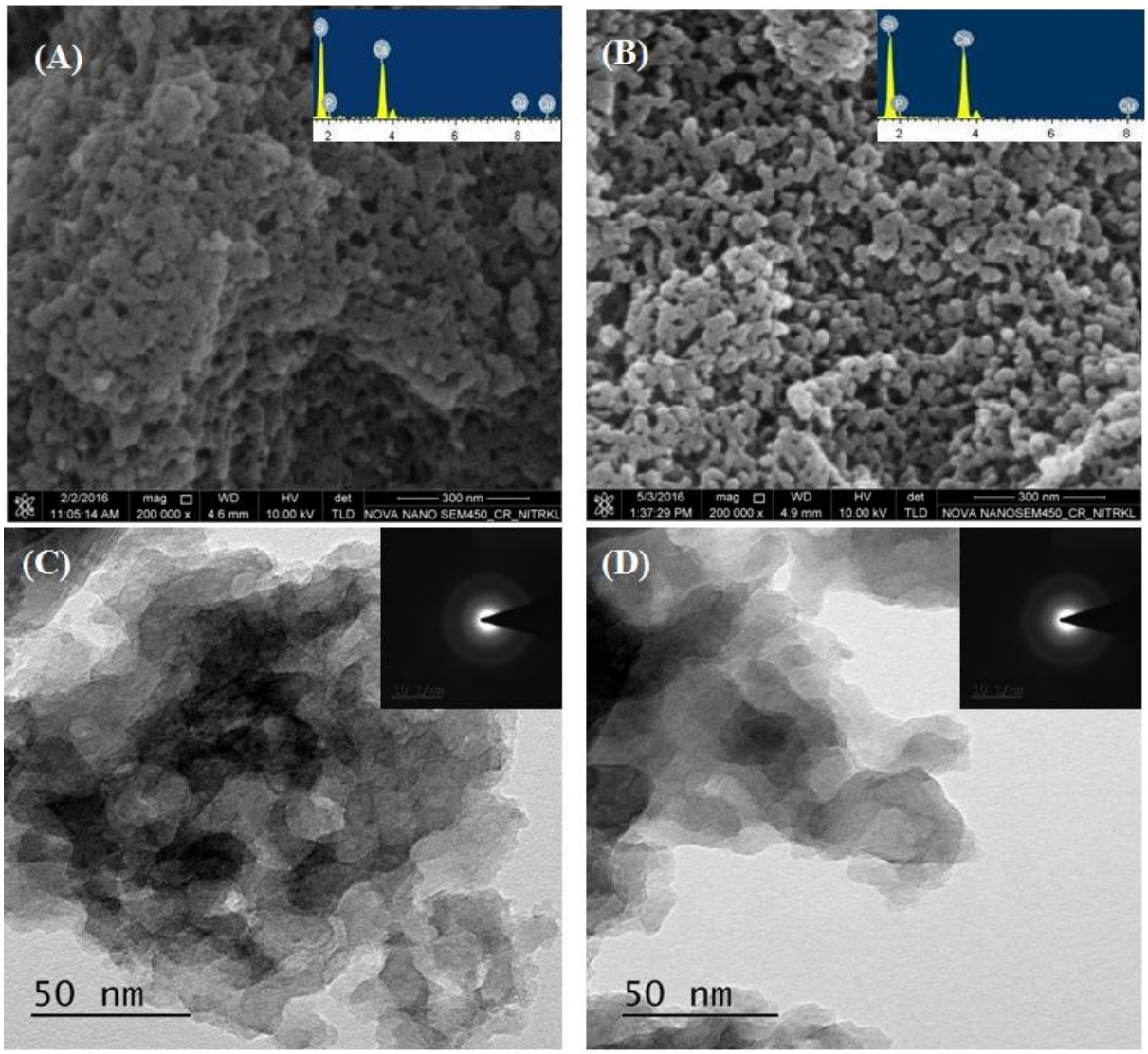

Figure 5.28: FESEM and EDX images showing the morphology and elemental composition of $Cu_{0.5}$-nBG (A) and Cu_1-nBG (B). TEM image and SAED pattern of $Cu_{0.5}$-nBG(C) and Cu_1-nBG(D)

Structural and functional analysis of copper doped nBG

The synthesized Cu^{2+} ion doped nano-bioglasses($Cu_{0.5}$-nBG and Cu_1-nBG) showing the (Figure 5.29A) wide diffraction peak between 20° and 40°, thereby confirms their amorphous features [230]. Also peaks at 2θ equal to 35.5° and 38.7° which correspond to copper oxide (CuO) is absent in XRD pattern of copper doped glasses, thus confirming the presence of copper ions (Cu^{2+}) in the silicate glass network [333-334]. The FT-IR (Figure 5.29B) spectrum of nBG shows the characteristic bands of Si-O-Si bonds at 1060 cm^{-1} (stretch vibration), 798 cm^{-1} (bending vibration) and 480 cm^{-1} (bending vibration). The P-O antisymmetric stretching was associated to a band at 1000-1100 cm^{-1}. However, the band for

P-O antisymmetric stretching was overlapped with that of Si-O-Si asymmetric stretching [335-336]. The antisymmetric bending of PO_4^{3-} was observed for both the glasses at 570 cm^{-1} – 600 cm^{-1} due to the interaction between calcium ion and orthophosphate [337]. The band at 3400 cm^{-1} was assigned to the O-H symmetric stretching vibration H_2O [338].

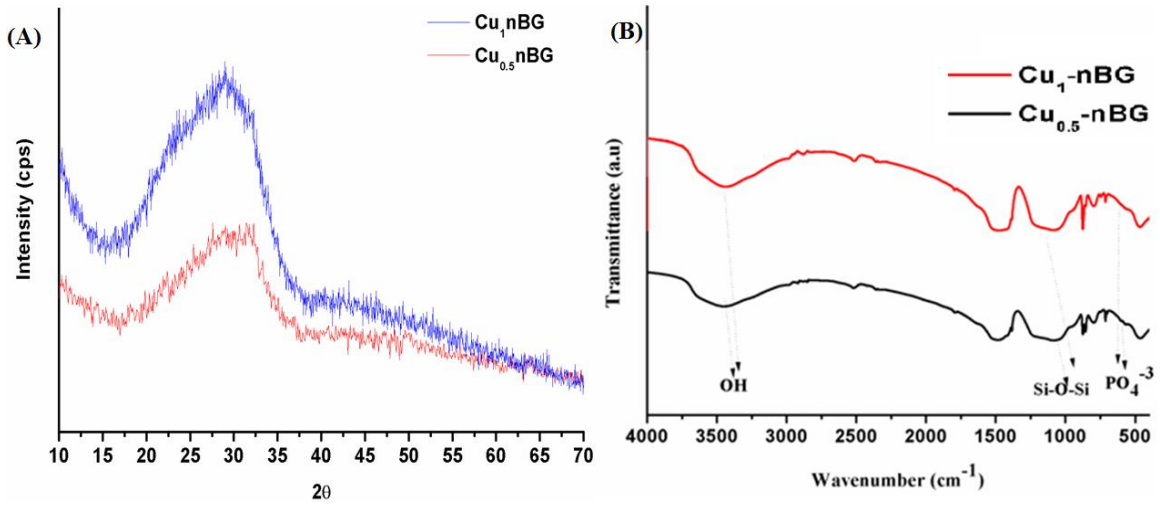

Figure 5.29: Showing the XRD diffractogram(A) and FT-IR spectra(B) of the synthesized two varieties of copper doped nanobioglasses. The presence of copper ions (Cu^{2+}) in the silicate glass network [333-334]and the amorphous characteristics of the modified nBG were confirmed.

5.2.4 *In vitro* apatite forming ability of copper doped nano-bioglass

Similar to nBG the *in vitro* apatite forming ability of the modofied nBGs was assessed by SBF treatment. The SBF treated bioglasses were characterized for morphological, structural and functional and ion release property.

Morphological Characterization

After 7 days of exposure in SBF, FESEM analysis revealed the formation of fine granules like particles over the surface of the bioglasses was observed (Figure 5.30A, B). The HR-TEM images (Figure 5.30C, D) of modified bioglasses ($Cu_{0.5}$-nBG and Cu_1-nBG) after soaking for 7 days shows well resolved lattice fringes with d-spacing of 0.285 nm correspond to 211 plane for nano-crystalline apatite formation over bioglasses particles [328]. The SAED image of bioglasses shows visible diffraction rings formation. The diffraction rings were observed to be more prominent in case of Cu_1-nBG as compared to $Cu_{0.5}$-nBG, representing

the improved bioactivity with copper doping of bioglass. Thus HR-TEM and SAED analysis support the bioactivity properties of synthesized nano-bioglasses.

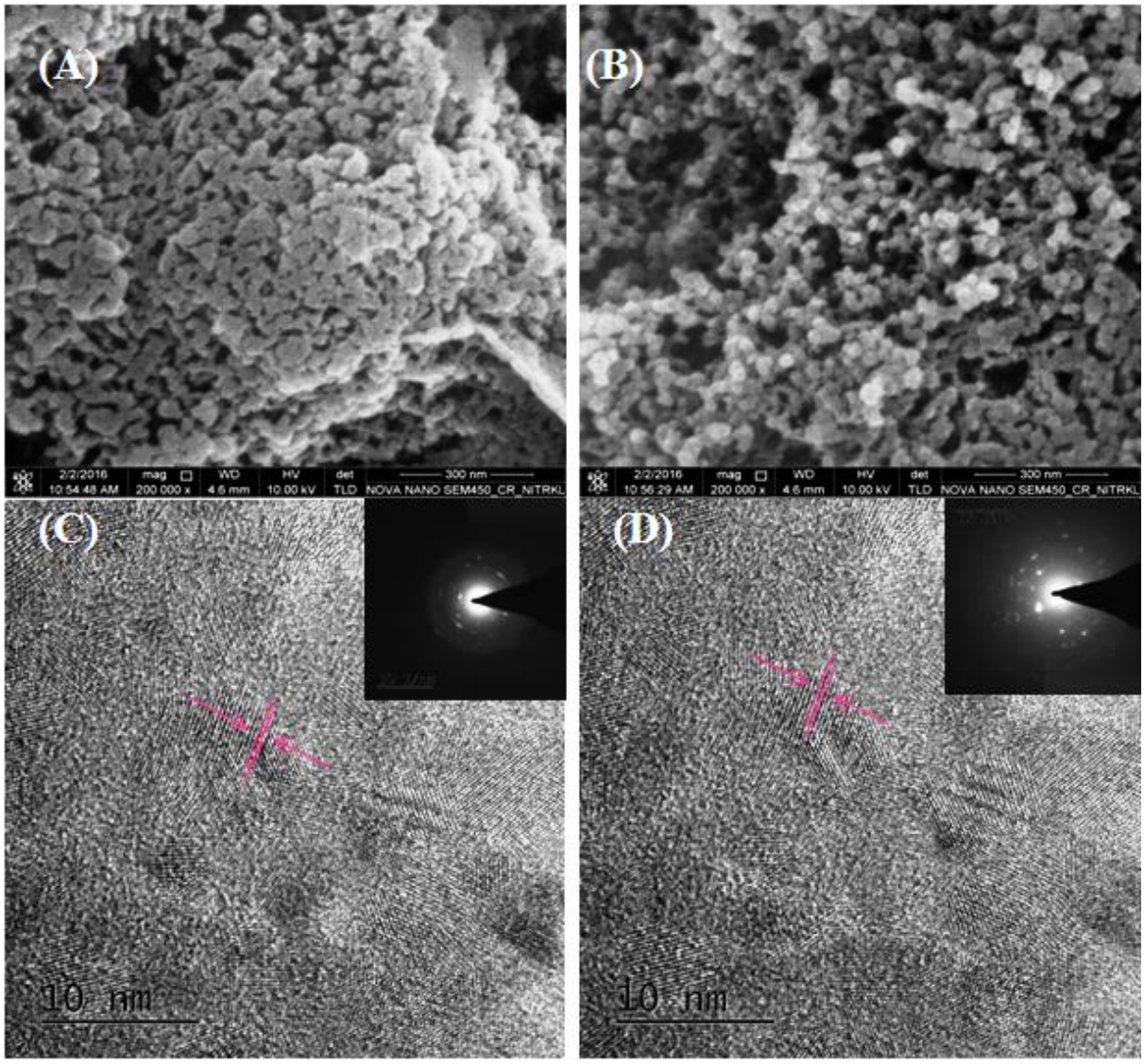

Figure 5.30: FESEM images showing the morphology of $Cu_{0.5}$-nBG (A) and Cu_1-nBG (B) after SBF treatment. HRTEM image and SAED pattern of $Cu_{0.5}$-nBG(C) and Cu_1-nBG (D) after SBF treatment

Structural and functional analysis

X-ray diffraction pattern of copper doped nBG was recorded after 7 days of treatment in SBF to investigate the *in vitro* apatite formation ability. Synthetic hydroxyapatite (Sigma-Aldrich) XRD pattern was used as a reference to analyse formation of apatite layer over the particles. X-ray diffractogram obtained for the modified bioglass samples treated with SBF shows the

peaks at 2θ equal to 25.8°, 31.8°, 32.8°, 46.6° and 53.2° correspond to hydroxyapatite (HA) as shown in Figure 5.31A [339]. The FT-IR (Figure 5.31B) spectrum shows the characteristic bands of Si-O-Si bonds at 1060 cm^{-1} (stretch vibration), 798 cm^{-1} (bending vibration) and 480 cm^{-1} (bending vibration). Whereas FT-IR spectra of Cu-nBG shows the characteristic band of P-O bonds of PO_4^{3-} group of hydroxyapatite at 562 cm^{-1}, 595 cm^{-1} , 620 cm^{-1}, 962 cm^{-1} and 1080 cm^{-1}. The bands at 873 $cm^{-1}$and 1460 cm^{-1} were characteristics of CO_3^{2-} group and band between 3300 cm^{-1} and 3600 cm^{-1} associated with the presence of hydroxyl groups [331].

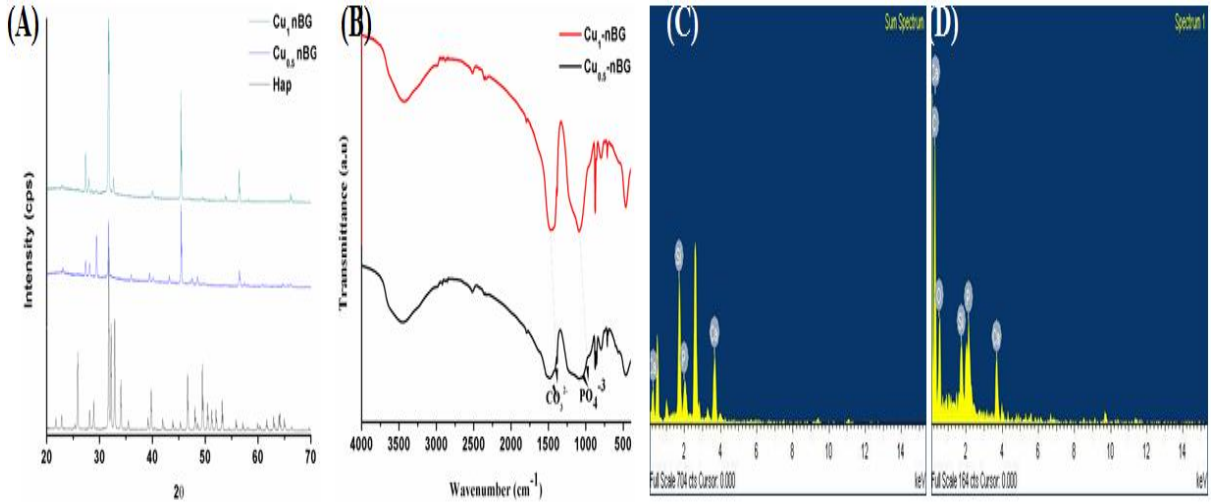

Figure 5.31: Showing the XRD diffractogram (A), FT-IR spectra (B), EDX analysis(C) and EDX analysis (D) of copper doped $Cu_{0.5}$-nBG and Cu_1-nBG bioglasses after 7 days of SBF treatment

Inductively coupled plasma atomic emission spectrophotometer (ICP-OES) analysis

The copper ion release behaviour of Cu-nBG was evaluated after treatment in simulated body fluid for 7 days and analysed by using ICP-OES. Figure 5.32 shows the ion release from the copper doped bioglass samples while soaking in SBF for a period of 3, 5 and 7 days at room temperature. During dealkalinization process, Ca was observed to be rapidly released from $Cu_{0.5}$-nBG and Cu_1-nBG on 3rd day of soaking in SBF, reaching to 158 ± 13.56 ppm and 353 ± 18.13 ppm in SBF. This was followed by a decrease in the Ca^{2+} ion concentration to 124 ± 2.32 ppm and 185 ± 13.8 ppm for $Cu_{0.5}$-nBG and Cu_1-nBG after 7 days of incubation respectively. However, the release of calcium ion from copper doped nano-bioglass is significantly higher as compared to nBG because of higher surface reactivity of copper doped bioglass than the undoped nBG during initial phase of reaction, which was also reported

earlier with different glass system [340].The concentration of Si released from $Cu_{0.5}$-nBG and Cu_1-nBG by breakdown of Si-O-Si bonds leading to 64 ± 2.21 ppm and 68 ± 3.5 ppm of Si, after soaking for 3 days in SBF and further reduced to 46 ± 3.89 ppm and 48 ± 1.35 ppm after soaking for 7 days.

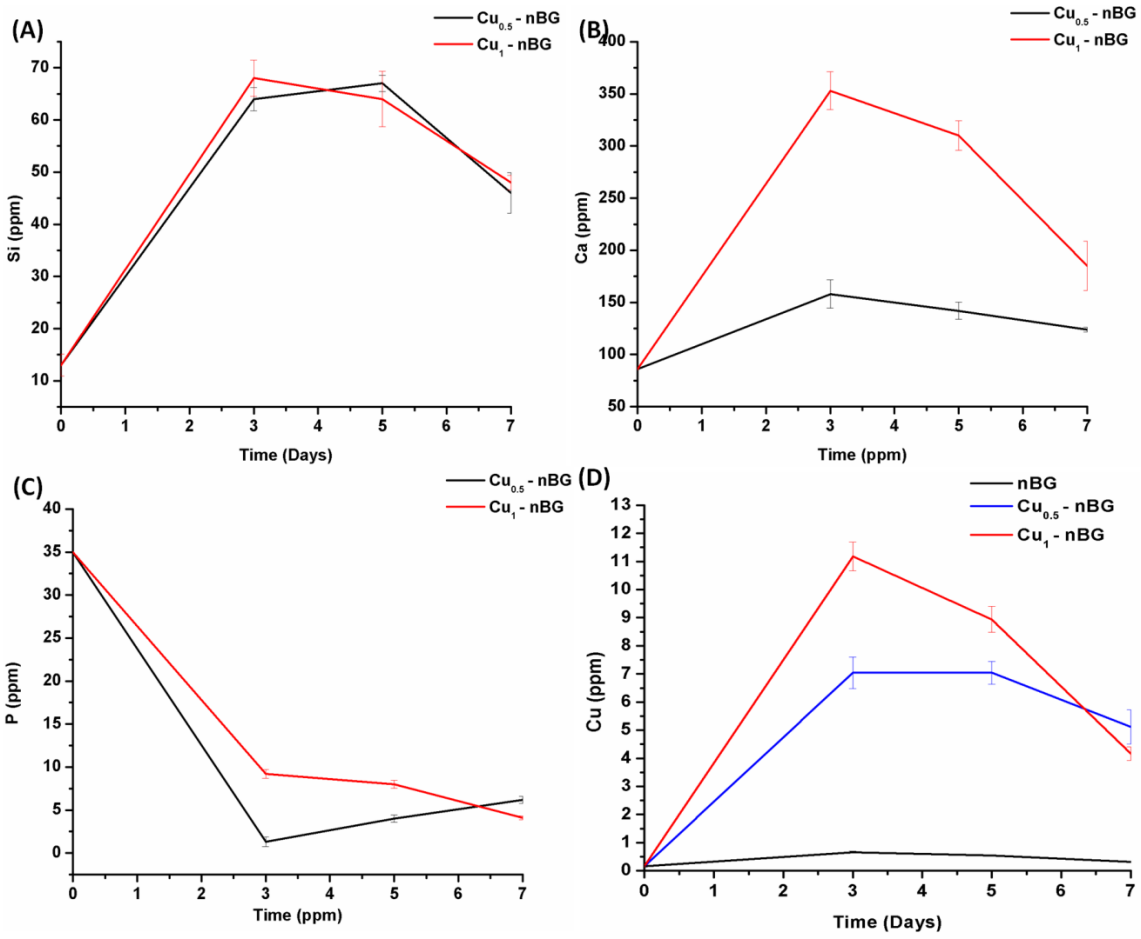

Figure 5.32: The graphs showing the rate of ion release from $Cu_{0.5}$-nBG and Cu_1-nBG during the 7 days of SBF treatment

Furthermore, a decrease in the phosphorus ion concentration was observed which shows the migration of Ca^{2+} and PO_4^{3-} through silica rich layer resulted in a formation of carbonated hydroxyapatite. However, the level of PO_4^{3-} in SBF collected from $Cu_{0.5}$-nBG and Cu_1-nBG treatment after soaking for 7 days was found to be 6.11± 0.41 ppm and 4.1 ± 0.24 ppm respectively. The bioglass sample without copper doped shows constant and negligible level of copper ion release during soaking period of 7 days in SBF. Whereas $Cu_{0.5}$-nBG was observed to release 7.06 ± 0.02 ppm of copper ion by 3 days, which was reduced to 6.09 ±

0.015 ppm by 7 days. In case of Cu_1-nBG, the copper ion release was observed to be 11.18 ± 0.51 ppm and 4.25 ± 0.24 ppm after 3 and 7 days respectively. The higher level of Cu ion release from Cu_1-nBG was due to higher surface reactivity; however it reduces rapidly as the apatite layer developed over the glass surfaces. Thus it has been concluded from the above study that doping of Cu ion in bioglass improves its bioactivity.

CHAPTER 5C: Development of nano-bioglass incorporated electrospun SF/CMC composite nanofibrous scaffold

In the previous chapter, a novel SF/CMC blend nanofibrous scaffold was developed which is proven to be a good substrate for bone tissue engineering application. It is further reported that the development of composite biopolymeric materials derived from natural or synthetic polymers and bioceramics like nanohydroxyapatite is a promising approach to overcome some of the limitations of the polymeric scaffold thereby improving the scaffold property [341-342]. These polymer-bioceramic matrices are proven to prompt the differentiation of mesenchymal stem cells to an osteogenic lineage and thus provides bone tissue like microenvironments [343]. Furthermore, nanofibrous polymeric composite scaffolds containing osteogenic inorganic phases, fabricated by electrospinning technique has been reported to be the most appropriate structures that mimic ECM of bone tissue [344-346]. Therefore, in this work, for the first time an attempt was made to fabricate natural biopolymer based composite nanofibrous scaffold by combining silk fibroin (SF)/carboxymethyl cellulose (CMC) and nano-bioglass as the promising bioactive ceramic with the intention to bring the mechanical property of silk fibroin, strong ability to absorb and transport fluids as well as chelation property of CMC and the bioactivity of nano-bioglass to a common template thereby developing a nanofibrous scaffold with robust property for bone tissue engineering applications.

Keeping in view of the multiple promising properties, bioactive glass in nanoscale was synthesised in the previous chapter and this was used to increase the apatite formation ability and osteogenic (osteoinductive and osteocounductive) properties of the polymeric SF/CMC blend in this phase of work. The developed nanofibrous nanocomposite scaffolds were evaluated for their various physicochemical, mechanical, biomineralization, *in vitro* biocompatibility and osteogenic differentiation ability using umbilical cord blood derived human mesenchymal stem cell. The result and discussion of this research work is described below-

5.3.1 Fabrication and characterization of SF/CMC/nBG nanofibrous composite scaffold

Various batches of SF/CMC/nBG composite mixtures with different nano-bioglass (5 wt% - 20 wt%) content were prepared by dissolving in formic acid as solvent. The prepared polymer-ceramic composite solutions were successfully electrospun. The effect of nBG concentration

on the viscosity of the electrospinnable composite solution and the electrospun nanofiber diameter is shown in Table 5.1. It is depicted that the increase in nBG concentration significantly increases the viscosity of the composite solution from 0.092 ± 0.0016 to 0.316 ± 0.018. This result is corroborated with the study reported earlier using different polymer system like poly-caprolactone/nano-bioglass [347]. This increase in viscosity may be attributed to the increase in shear viscosity due to the presence of nBG in the polymer suspension [347]. A significant effect of the viscosity change due to the combined effect of SF/CMC polymer blend and nBG as additive on the fiber diameter and morphology was also observed. These experimental findings are evident from Table 5.2 and FESEM images as in Figure 5.33A. The average fiber diameter was increased steadily from 233.60 ± 83 nm to 594.66 ± 157 nm, when nBG content was increased from 0 wt% to 20 wt%. An increased fiber diameter was also exhibited by SF/CMC/nBG composite solution containing higher nBG content of 20 wt% but the difference in fiber diameter obtained with SF/CMC/10%nBG and SF/CMC/20%nBG is statistically in significant, which is also due to the increased viscosity resulting from the addition of more nBG. As evident from published literature, at higher concentration of nBG greater interaction (hydrogen bonding and ionic bonding) between the fibers occurs which leads to the deposition of fused fibers [348]. The pore size of (4.51 ± 1.65 µm) of SF/CMC/0%nBG scaffold was gradually increases with increasing nBG content from 0 wt% to 20 wt%. The measured average pore size for SF/CMC/5%nBG, SF/CMC/10%nBG and SF/CMC/20%nBG are 4.57 ± 1.3 µm, 4.64 ± 2.1 µm and 5.4 ± 1.7 µm respectively.

The distribution of the nBG over the surface of fiber matrix was further examined by TEM images. The TEM images of SF/CMC/0%nBG, SF/CMC/5%nBG, SF/CMC/10%nBG and SF/CMC/20%nBG composite nanofibers are presented in Figure 5.33B. As indicated, SF/CMC/0%nBG (Figure 5.33B) shows the absence of nBG over the surface of blend nanofibrous scaffold. As revealed by TEM image (Figure 5.33B) nano-bioglass (≤ 100 nm) was successfully electrospun with SF/CMC and well incorporated over the surface of nanofibers. The TEM images clearly show the presence of nBG over the SF/CMC/nBG composite nanofibrous scaffold. However, the content of nano-bioglass over SF/CMC/5%nBG, SF/CMC/10%nBG and SF/CMC/20%nBG composite scaffold increases as the concentration of nano-bioglass increases from 5 to 20 wt%. The distribution of nBG in nanofibers was observed from FESEM and TEM images (Figure 5.33A, B) shows that nBG was uniformly distributed over SF/CMC/5%nBG and SF/CMC/10%nBG composite scaffolds. However, nBG was observed to be agglomerated and distributed as clumps over the composite

nanofibers with higher nBG content. Thus, at higher content of nBG, agglomeration of nanoparticle occurs.

Table.5.2. Fiber diameter of electrospun composite mats and viscosity of various solutions prepared for fabrication of the respective electrospun mats

Scaffolds	Fiber diameter(nm)	Viscosity (Pas)
SF/CMC/0%nBG	233.60 ± 83	0.09265 ± 0.00165
SF/CMC/5%nBG	350.39 ± 147	0.1557 ± 0.015608
SF/CMC/10%nBG	589.68 ± 161	0.249
SF/CMC/20%nBG	594.66 ± 157	0.316 ± 0.0185

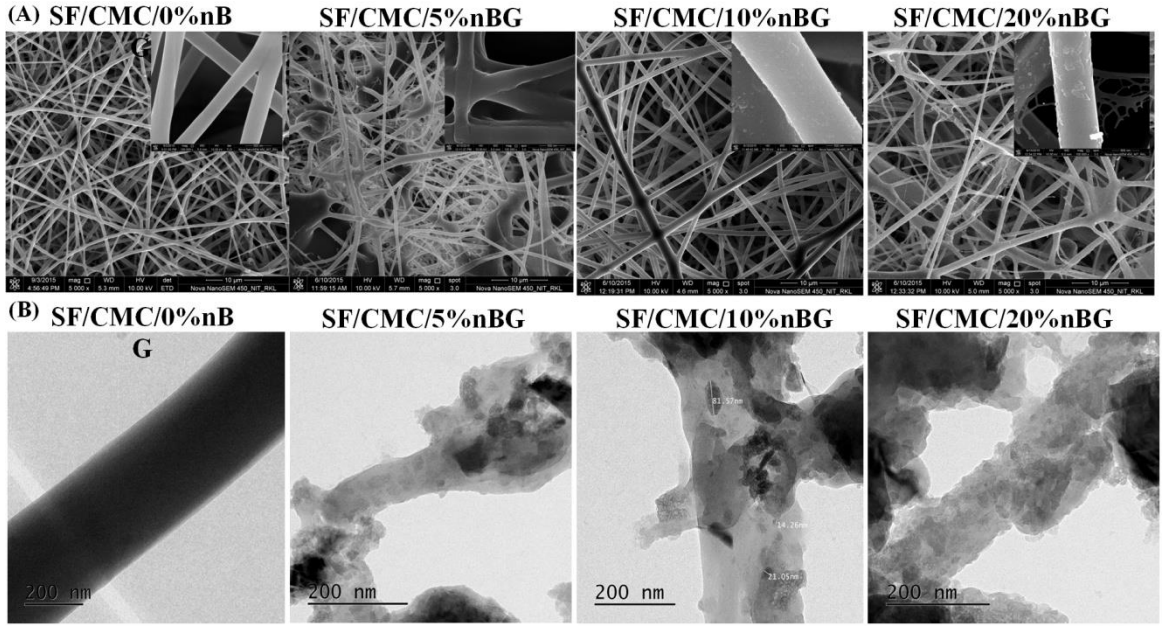

Figure 5.33: Showing the FESEM(A) and TEM(B) images of fabricated SF/CMC/0%nBG, SF/CMC/5%nBG, SF/CMC/10%nBG and SF/CMC/20%nBG nanofibrous scaffolds. Fiber diameter was found to increase from 233.60 ± 83 nm to 594.66 ± 157 nm as the nBG content increases from 0 wt% to 20 wt%. TEM images confirm the presence and well distribution of nano-bioglass (≤ 100 nm) throughout the SF/CMC blend nanofibrous mats.

Structural and functional analysis

XRD and FT-IR were used as efficient techniques to investigate the structural and functional characteristics of the modified SF/CMC/0%nBG scaffolds resulted by the incorporation of nBG thereby SF/CMC/nBG composite scaffold was developed. The X-ray diffractogram

pattern of SF/CMC/nBG composite scaffolds with different content of nBG is depicted in Figure 5.34A. As indicated, the diffraction peaks at 2θ values of 20.8° and 24.3° indicating β-sheet conformation of the SF/CMC nanofibrous scaffolds were intensified as nBG introduced (5 – 10 wt %) which may be due to the enrichment in the transformation of randomly arranged to crystalline β – sheet structure. Whereas at higher concentration of nBG (20 wt %) the amorphous glassy structure were dominant that led to reduced intensity at respective angle.

The change in structural and functional conformation that might have occurred in band position due to the incorporation of nBG was shown by FT-IR spectrum of SF/CMC/nBG nanofibrous scaffolds as depicted in Figure 5.34B. The FT-IR spectra of SF/CMC/nBG showed vibration bands at 470 cm^{-1}, 1060 cm^{-1} and 1100 cm^{-1} which are associated with Si-O-Si bending mode[331, 349]. The peak at 970 cm^{-1} was assigned to the non-bridging oxygen together with the surface active silanols (Si-OH) groups, which facilitate the enhanced rate of apatite formation. The shoulder peak at 958 cm^{-1} belongs to the Si-O-Ca vibration mode[230]. The peak at 920 cm^{-1} is the result of stretching vibration of the phosphate group (O-P-O)[349]. It has been noticed that as the nBG incorporated in SF/CMC/nBG scaffold peak for amide I, amide II and amide III get narrowed due to conformational change in SF/CMC in presence of nBG. However, in case of SF/CMC/20%nBG peaks were broader due to dominance of amorphous glassy structure of nBG [350]. Also peak at 1060 cm^{-1} associated with Si-O-Si bending mode get intensified and broader as the nBG content increases.

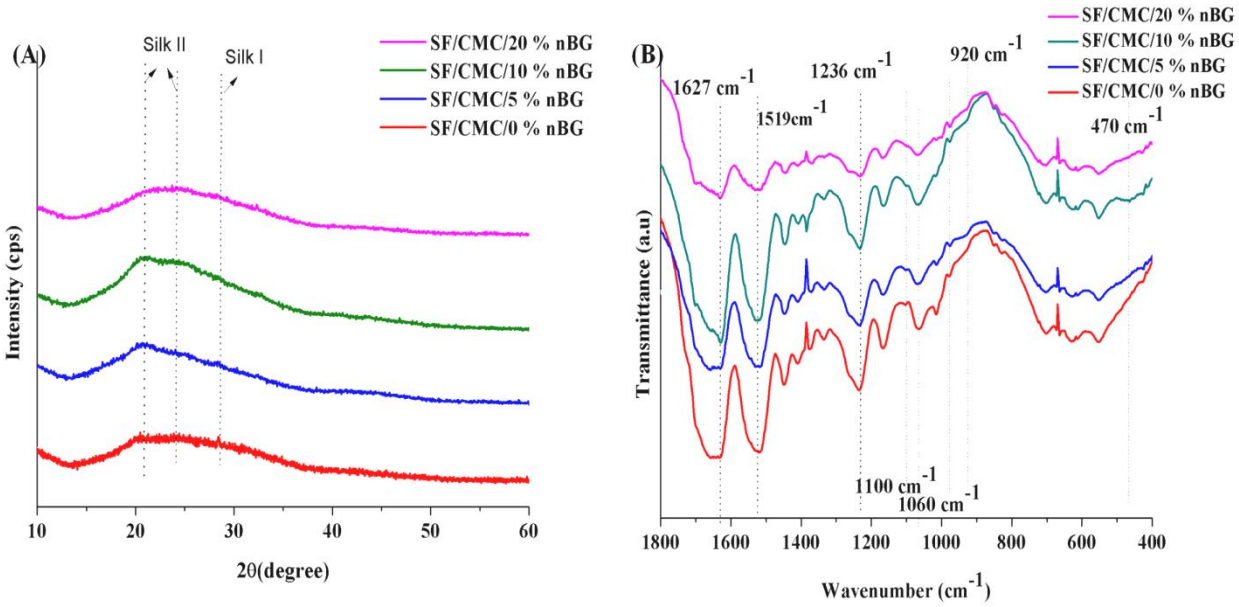

Figure 5.34: XRD diffractogram(A) and FT-IR spectrum (B) showing the change in structural and functional conformation of the fabricated SF/CMC/0%nBG, SF/CMC/5%nBG, SF/CMC/10%nBG and SF/CMC/20%nBG nanofibrous scaffolds due to the incorporation of nano-bioglass.

Mechanical property

The mechanical property of scaffold plays distinctive roles in modulation of cell behaviour and its lineage determination as well as also improve osteogenic property [351]. Therefore, the assessment of mechanical properties of the developed nBG incorporated SF/CMC/0%nBG nanofibrous scaffold both at dry and wet condition is essential for understanding the performance of the scaffold in bone tissue regeneration. The measured mechanical properties in term of tensile strength and tensile strain at break of SF/CMC/nBG composite scaffold are depicted in Figure 5.35 and compared with the SF/CMC blend scaffold. Figure 5.35A shows ultimate tensile strength (UTS) of SF/CMC/0%nBG and SF/CMC/nBG composite scaffolds in dry condition. The tensile strength and tensile strain at break were decreased with the addition of nBG. The tensile strength and tensile strain at break for SF/CMC/0%nBG composite scaffold was measured to be 9.49 ± 1.83 MPa and 8.54 ± 0.91 % respectively. Among the composite scaffolds the SF/CMC10%nBG composite nanofibrous scaffold shows higher tensile strength in comparison to scaffold with 5 and 20 wt % nBG. The SF/CMC/5%nBG scaffold posses tensile strength of 5.5 ± 1.8 MPa and tensile strain at break of 1.9 ± 0.5 %, whereas the SF/CMC/10%nBG shows tensile strength of 7.591 ± 1.23 MPa and tensile strain at break of 9.62 ± 0.85 %. Since SF/CMC/20%nBG composite

scaffold was highly fragile it broke apart immediately even at low load and thus exhibited lower tensile strength of 4.28 ± 0.76 MPa and tensile strain at break of 8.8 ± 2.5 %. The overall trend of the mechanical behaviour of the developed scaffolds is as follows SF/CMC/0%nBG> SF/CMC/10%nBG > SF/CMC/5%nBG > SF/CMC/20%nBG. This may be attributed to the improvement of interaction (hydrogen bonding or ionic bonding) with the increasing content of nBG [350] however the decrease in tensile strength of SF/CMC/20%nBG is attributed to the higher fiber diameter and weak link between continuum matrices because of the inclusion of nBG [352].

However, the trend for tensile strain at break was observed to be SF/CMC10%nBG > SF/CMC/20%nBG > SF/CMC/0%nBG> SF/CMC/5%nBG, which may be attributed to the improved ductility of composite nanofiber because of yielding phenomenon as a result of debonding between nBG particles and SF/CMC blend matrix [350]. Furthermore, a decrease in stiffness of SF/CMC scaffolds was observed when loaded with nBG and also increased nBG content. The stiffness of developed composite scaffold was measured to be 531.81 ± 17 MPa, 208.9 ± 83 MPa, and 149.8 ± 24 MPa for SF/CMC/0%nBG, SF/CMC/5%nBG, SF/CMC/10%nBG and SF/CMC/20%nBG respectively. The lower stiffness of developed composite scaffold with increasing nBG content might be due to the debonding between nBG and SF/CMC polymeric matrix [350]. Which may affect stem cell response during cell culture due to lower cell scaffold interaction [284]. Furthermore, in wet condition tensile strength recorded for SF/CMC/0%nBG, SF/CMC/5%nBG and SF/CMC/10%nBG are 3.46 ± 0.66 MPa, 2.49 ± 0.25 MPa and 3.6 ± 0.135 MPa respectively. However, due to highly fragile nature SF/CMC/20%nBG broke apart immediately upon applying force, thus values could not be measured [353]. Figure 5.35C and Figure 5.35D shows mechanical characteristic of developed scaffold in wet condition. These results indicate that 10 wt % nBG could be used to improve properties like biomineralization and osteogenic activity of SF/CMC composite nanofibrous scaffold.

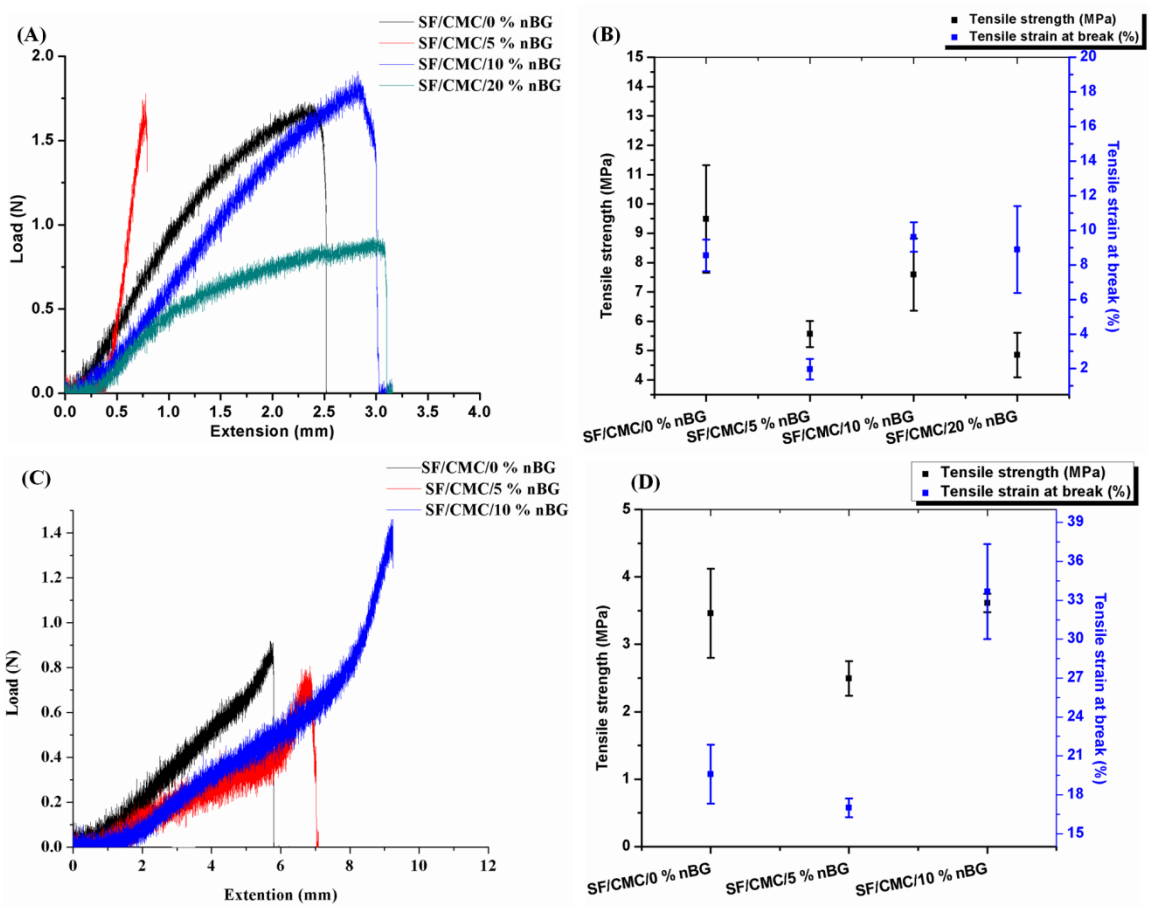

Figure 5.35: (A) Load Vs Extension curve for composite scaffolds in dry condition. (B) Distribution of tensile strength and tensile strength at break of SF/CMC/0%nBG, SF/CMC/5%nBG, SF/CMC/10%nBG and SF/CMC/20%nBG scaffolds in dry condition. (C) Load Vs Extension curve for composite scaffolds SF/CMC/0%nBG, SF/CMC/5%nBG, SF/CMC/10%nBG and SF/CMC/20%nBG in wet condition. (D) Distribution of tensile strength and tensile strength at break of SF/CMC/0%nBG, SF/CMC/5%nBG, SF/CMC/10%nBG and SF/CMC/20%nBG scaffolds in wet condition. The tensile strength of SF/CMC/10nBG composite scaffold was found to be more suitable in comparison to SF/CMC/0%nBG and other composite scaffolds.

Surface roughness analysis of composite scaffold

The analysis of surface roughness of SF/CMC/nBG scaffolds was performed to assess their performance towards cell supportive property and bone tissue regeneration. The roughness of SF/CMC/nBG (5-20 wt %) scaffold surfaces were improved gradually with the addition of nBG from 0.214 µm to 0.309 µm respectively (Figure 5.36). The obtained surface roughnes for developed composite scaffold follows trend as SF/CMC/0%nBG (0.101 µm) <

SF/CMC/5%nBG (0.214 µm) < SF/CMC/10%nBG (0.219 µm) < SF/CMC/20%nBG (0.309 µm).

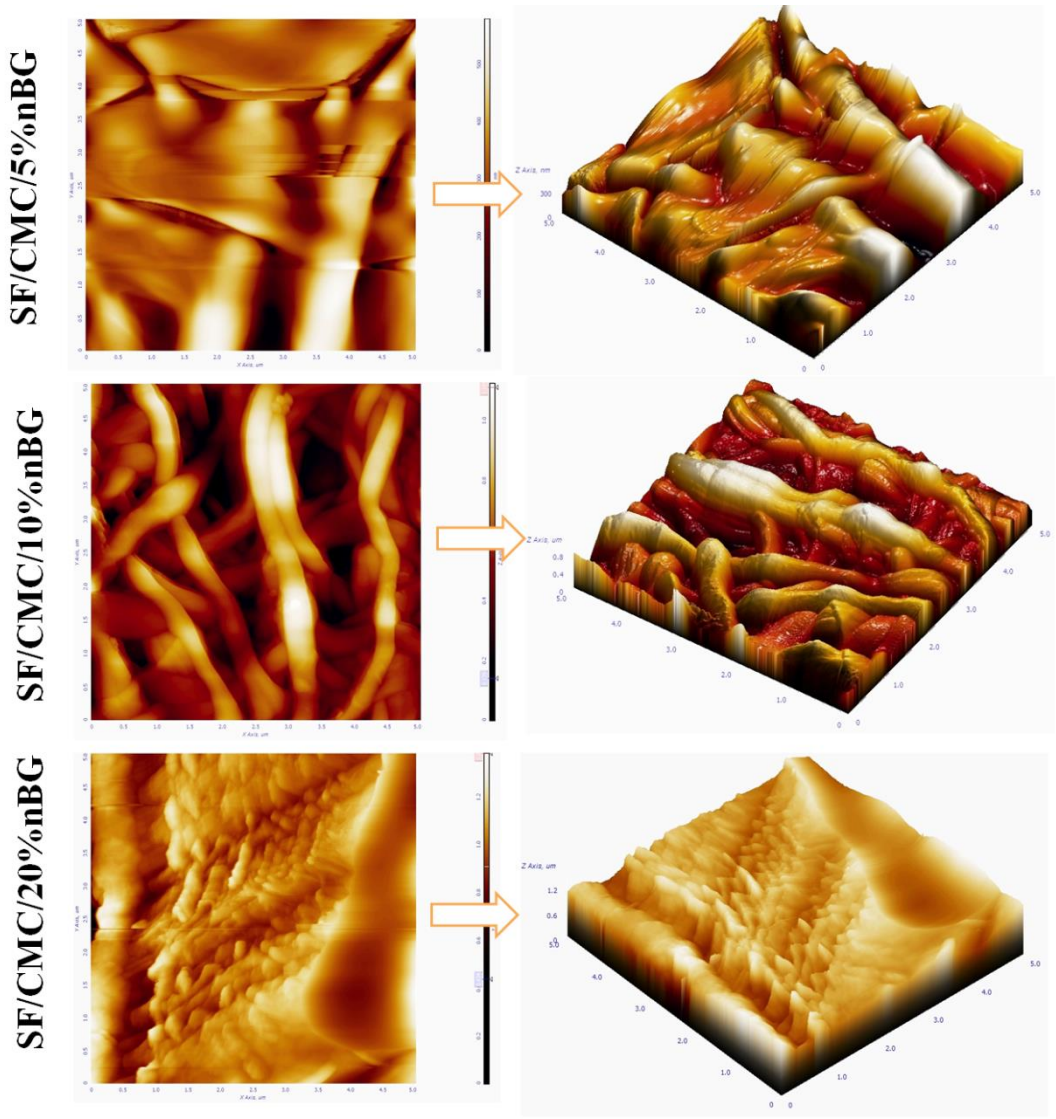

Figure 5.36: Surface roughness of fabricated SF/CMC/5%nBG, SF/CMC/10%nBG and SF/CMC/20%nBG composite nanofibrous scaffolds. An enhanced surface roughness of SF/CMC scaffold surfaces was obtained with the addition of nBG.

Thus, as the nBG content increases wrinkles, grooves and pits on the nanofibrous composite scaffold were found to be developed, which in turn resulted in improved surface roughness [354-355]. This study was in accordance with the result of FESEM analysis. Thus, the enhanced surface roughness of composite nanofibrous scaffold with addition of nBG is

expected to induce changes in cell membrane interaction and promote cell attachment, proliferation and direct differentiation of hMSCs, thereby favouring osteogenesis [356].

Hydrophilicity and swelling behaviour

The hydrophilicity of scaffold is important factor which determines its cell supportive property and ability for neo tissue regeneration. Thus, the contact angle of the developed SF/CMC scaffold loaded with nBG was measured and the values are shown in Table 5.2. As indicated, an decrease in contact angle representing the enhanced hydrophilicity of the scaffold was obtained by increasing the nBG content which is due to the hydrophilic nature of the later. The contact angle of SF/CMC/0%nBG, SF/CMC10%nBG and SF/CMC/5%nBG was $57.4^{\circ} \pm 0.3$, $55^{\circ} \pm 0.5$ and $52^{\circ} \pm 1.4$ respectively. The overall trend of these contact angle as follows SF/CMC10%nBG > SF/CMC/5%nBG > SF/CMC/0%nBG. However, SF/CMC/20%nBG get folded while coming into contact with water thus its contact angle value was not possible to be recorded in our study.

The swelling behaviour of SF/CMC/nBG composite scaffold is shown in Figure 5.37. The water uptake property of SF/CMC blend scaffold was observed to be in the range of 352 – 389 (%). The SF/CMC/nBG (5 wt%, 10wt% and 20 wt %) shows lower water uptake capacity than SF/CMC, which may be attributed to the structural stability of the composite scaffolds [357]. The water uptake capacity of SF/CMC/nBG was increased sharply up to 8 hr and then slightly decreased which is due to the occurrence of dissolution of nBG. The swelling ratio of SF/CMC/20%nBG was observed to be the lowest. However, swelling behaviour of composite scaffolds is not in coordination with the contact angle as the incorporation of bioglass results in maintaining structural integrity and inhibits excess swelling. This observation supports that SF/CMC/nBG composite scaffolds shall provide better uptake of nutrients to the interior of scaffold thereby facilitate cell migration and proliferation in the interior region of the composite scaffold without much affecting mechanical integrity of the scaffold [48, 357].

Table 5. 2: Mean contact angle measurement of nanofibrous scaffolds

Scaffolds	**MACA [°]**	**MRCA [°]**	**Hysteresis [°]**
SF/CMC/0%nBG	57.4 ± 0.3	18.5 ± 1.8	38.9 ± 3.2
SF/CMC/5%nBG	55 ± 0.5	30.0 ± 1.45	26.2 ± 2.1

SF/CMC/10%nBG	52 ± 1.4	41.7 ± 2.5	12.3 ± 1.8
SF/CMC/20%nBG	Failed to measure	Failed to measure	Failed to measure

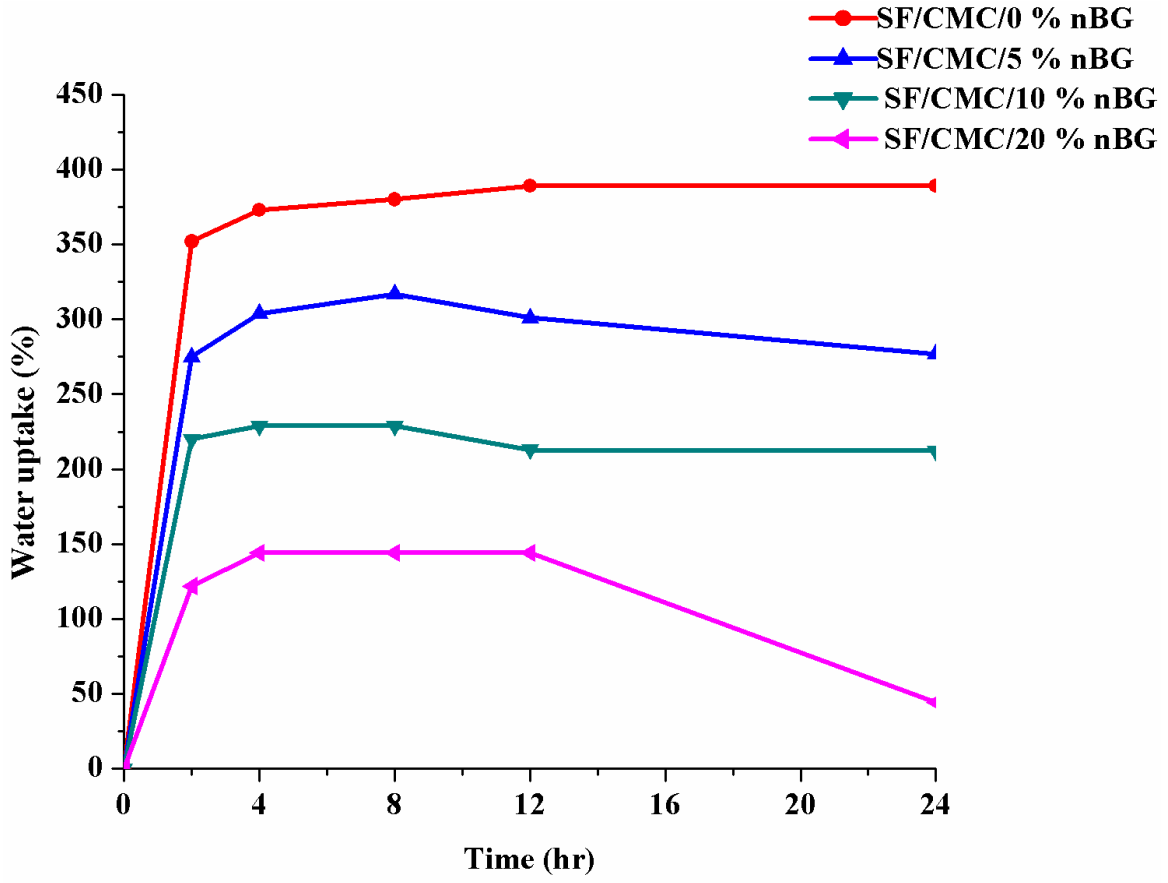

Figure 5.37: Swelling behaviour at different time interval observed with SF/CMC/0%nBG, SF/CMC/5%nBG, SF/CMC/10%nBG and SF/CMC/20%nBG composite nanofibrous scaffolds in PBS solution. Incorporation of nBG in composite scaffold resulted into improved hydrophilicity and structural stability.

5.3.2 *In vitro* bioactivity analysis

In chapter 5A, the bioactivity of SF scaffold was increased by the addition of CMC. In this study, the effect of incorporation of the nBG in SF/CMC blend was investigated. The ability of the composite scaffold containing different content of nBG to induce apatite formation on their surface was assessed by FESEM image analysis before and after soaking in SBF for 7 days. As expected, the nBG incorporated SF/CMC composite scaffold shows improved apatite like deposition throughout the surface, whereas SF/CMC/0%nBG shows less deposition as can be

seen from Figure 5.38A. Furthermore, as the concentration of nBG increases from 5 to 20 wt% the surface of composite scaffold shows improved mineral deposition as observed from FESEM images. Thus, as the concentration of nBG increases the formation of spherical nano-hydroxyapatite like nodule (size $\leq$ 50 nm as measured by using image J software) were improved. The negatively charged carboxyl groups of CMC interact with positively charged calcium ion released by the dissolution of nBG. As the calcium ions associated with carboxyl group, it further promotes adsorption of phosphate ions of SBF and leads to the growth of hydroxyapatite particle over composite scaffolds [358]. The EDX analysis showed that the mineral phase with Ca/P ratio: 0.8-1.3 was deposited over SF/CMC/0%nBG whereas on SF/CMC/nBG, the Ca/P ratio was 1.6-1.8 which is similar to the mineral phase of the human bone that consists mostly of Ca and P in the ratio 1.4 - 1.7 [316].

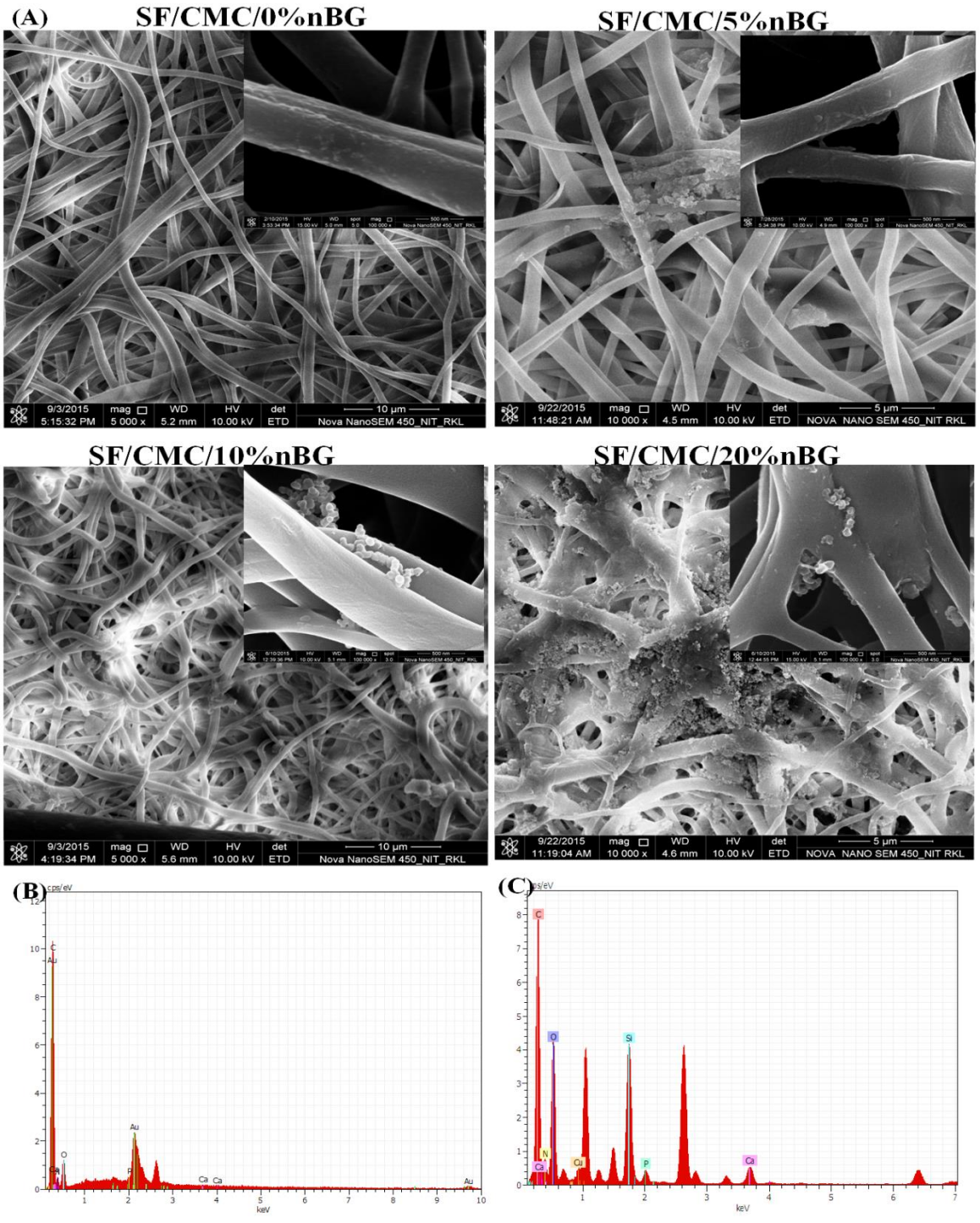

Figure 5.38: FESEM images of SF/CMC/0%nBG, SF/CMC/5%nBG, SF/CMC/10%nBG and SF/CMC/20%nBG composite matrices after SBF treatment for 7 days (A). EDX spectra depicts the mineral deposition over SF/CMC/0%nBG (B) and SF/CMC/10%nBG (C) after 7 days of SBF treatment. The apatite like mineral deposition over scaffold increases with increasing nBG content.

Structural and functional analysis of biomineralized scaffold

The formation of apatite on the surface of the nanofiberous scaffold was also examined by XRD and FT-IR study as shown in Figure 5.39. The diffractogram of SF/CMC (Figure 5.39A) shows the presence of peak at $2\theta = 28.4^{\circ}$ and broad weak scattering peak at 32° which implicates the presence of amorphous apatite to some extent. Whereas, in case of SF/CMC/nBG as the concentration of nBG increases the characteristic peaks of the apatite at 31.7° attributed to 211 plane got intensified thereby resulted in better biomineralization at higher concentration of nBG [359]. Thereby, the characteristic peak at 31.7° was observed to be broader and intense in case of SF/CMC/20%nBG as compared of SF/CMC/5%nBG and SF/CMC/10%nBG respectively.

After *in vitro* mineralization the prepared scaffolds were also characterized by FT-IR to analyse their ability towards in vitro apatite formation. As observed in FT-IR spectra (Figure 5.39B) the hydroxyapatite like deposition on the scaffolds is reflected by the characteristic peak at 1070 cm^{-1} which corresponds to the P-O asymmetric stretching mode of vibration for PO_4^{-3} group [300-301]. The P-O stretching mode has been observed at 1012 cm^{-1} and 976 cm^{-1} which correspond to major bands for phosphate group. The sharpening of peaks observed at 610 cm^{-1} and 556 cm^{-1} are due to O-P-O bending and stretching respectively [301-302]. The absorbed CO_2 corresponds to the 1400-1450 cm^{-1} peaks indicating the deposition of carbonated HAp on the nanofibers. Furthermore, the characteristic peaks of the apatite were improved at higher concentration of nBG. Thereby, the characteristic peak of PO_4^{-3} group at 1070 cm^{-1} was observed to be broader in case of SF/CMC/20%nBG as compared to SF/CMC/5%nBG and SF/CMC/10%nBG respectively.

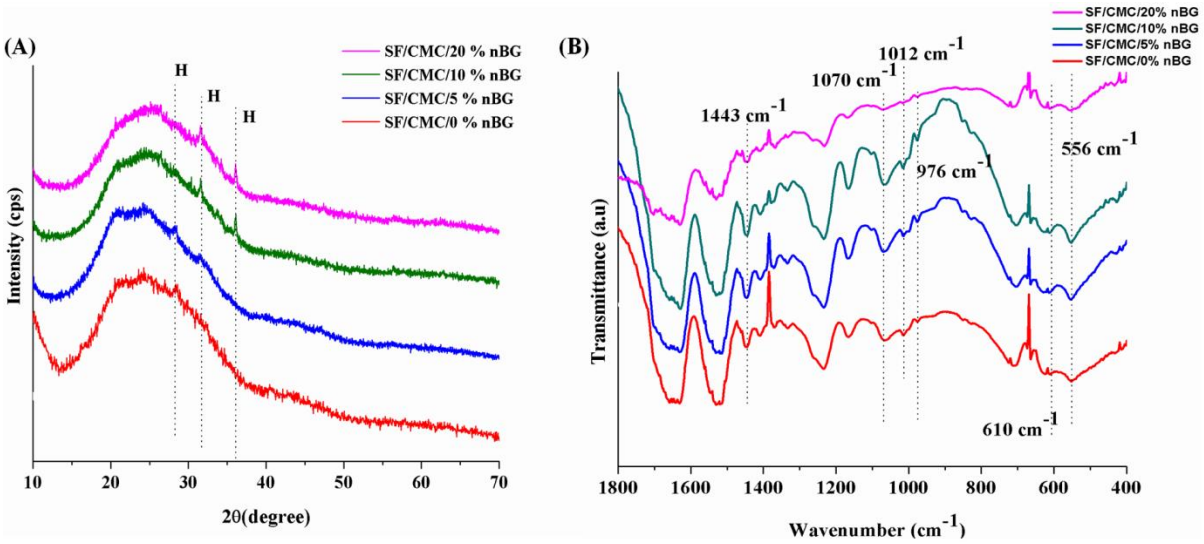

Figure 5.39: Showing the XRD spectrum (A) and FT-IR spectrum(B) of SF/CMC/0%nBG, SF/CMC/5%nBG, SF/CMC/10%nBG and SF/CMC/20%nBG after incubation in SBF for 7 days

5.3.3 *In vitro* biodegradation of scaffold

The *in vitro* biodegradation result of the bioglass loaded composite scaffolds obtained by measuring the loss of weight during exposure in PBS and protease XIV enzymatic solution for 28 days is presented in Figure 5.40. The study has shown that bioglass incorporated SF/CMC scaffold degraded faster as compared to the scaffold without bioglass. Furthermore, the extent of degradation was observed to be depended on the bioglass content. As expected the degradation rate of SF/CMC scaffold was remarkably enhanced by the increase of nBG concentration. The corresponding degradation was measured as 53% to 60% in presence of enzyme, where as 28% to 35% degradation was obtained in PBS. The increase in scaffold degradation by the incorporation of nBG may be attributed to the augmentation of hydrophilicity that resulted in the increase in hydrolytic degradation of composite polymer matrix thereby causing higher weight loss than that shown by SF/CMC scaffold without bioglass.

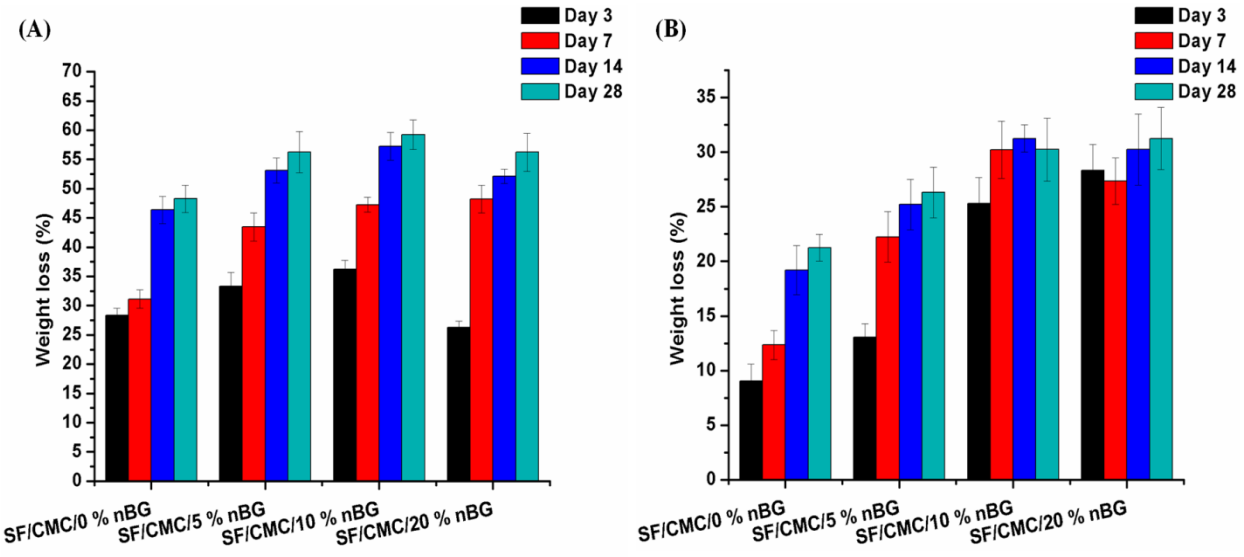

Figure 5.40: Observed degradation behaviour of SF/CMC/0%, SF/CMC/5%nBG, SF/CMC/10%nBG and SF/CMC/20%nBG scaffolds by soaking in enzyme (A) and PBS solution (B) for 28 days. The result shows that the bioglass incorporated SF/CMC scaffold degraded faster than the scaffold without bioglass. Furthermore, the extent of degradation was observed to be depended on the bioglass content.

5.3.4 In-vitro cell culture study

All the above assessments taken together, SF/CMC/10nBG composite scaffold found to possess a desired set of superior scaffold properties namely hydrophilicity, apatite forming ability, biodegradability and mechanical property and hence it was selected for in-vitro cell study to evaluate its potentiality for bone tissue regeneration.

hMSCs adhesion, morphology and spreading

The cellular affinity to the scaffold representing the indication of the ability towards the neo tissue regeneration was visualized through the observation of attached cells and the morphological changes during the culture of MSCs by FESEM image analysis. From Figure 5.41A, it has been observed that hMSCs seeded on SF/CMC/0%nBG and SF/CMC/10%nBG were more or less round in shape after 12 h with aspect ratio of 1.32 ± 0.078 and 1.59 ± 0.221 respectively. The higher aspect ratio shown by SF/CMC loaded with nBG reflects the slightly higher cellular attraction than SF/CMC scaffold. However, on day 7, the cells were found to gradually well attached and spread over all the scaffolds indicating the active cell

proliferation potential. Furthermore, the spindle shaped morphology of hMSCs was observed over the SF/CMC/0%nBG nanofibrous mats, whereas cells morphology was observed to be polygonal in shape when SF/CMC/10%nBG was used as the substrate.

The prominent development of outgrowths leading to the formation of filopodia as observed confirms the stronger interaction between the hMSCs and SF/CMC/10%nBG scaffold thereby favours strong cell attachment. The hMSCs morphology tends to changes in to polygonal shape is primary indication for osteogenic differentiation potential of SF/CMC/10%nBG [360]. Thus SF/CMC/0%nBG promotes cell growth and deposition of ECM to some extent, whereas SF/CMC/10%nBG possessed additional advantage of bioactive glass which promotes not only the growth and cellular attachment but also facilitates cell proliferation and differentiation. The cultured hMSCs are observed to be polygonal in shape (Figure 5.41) along with the formation of filopodia like extension from cell surface over SF/CMC/10%nBG indicating higher osteogenic differentiation potential of composite scaffold was partly because of higher surface roughness of the composite scaffold [350] and partly due to superior mineralization ability of scaffold containing nBG. Though the stiffness of composite scaffold decreases with increasing nBG, the dissolution of nBG favoured the deposition of apatite layer over the fibers, thereby improves the stiffness of scaffold which triggered cells towards osteogenic differentiation.

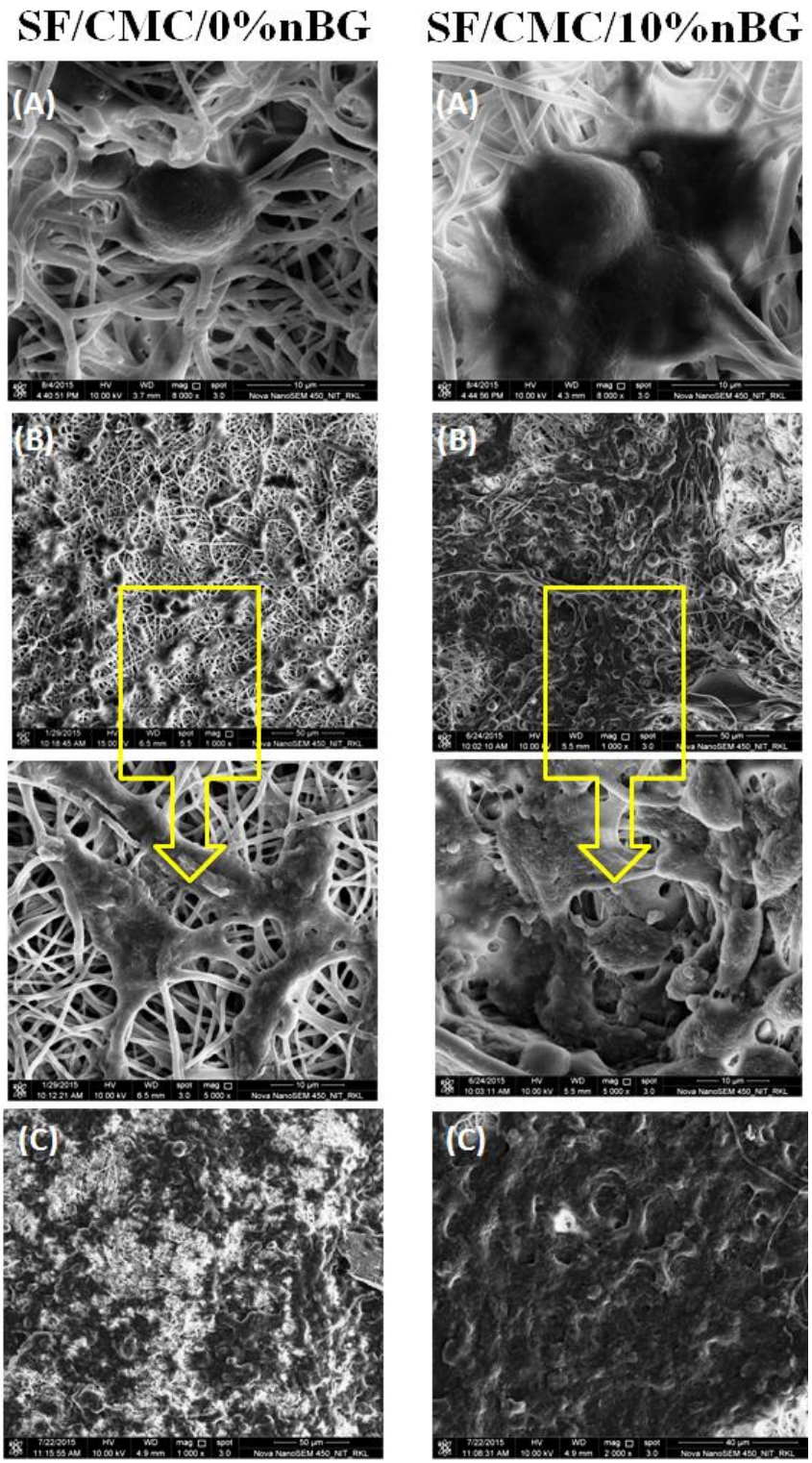

Figure 5.41:FESEM images of hMSCs cultured over the SF/CMC/0%nBG and SF/CMC/10%nBG scaffolds after 12 hour (A) ,7 days (B) and 14 days (C).

Cytoskeletal organization

Figure 5.42 shows the fluorescence images of cytoskeleton development and distribution after 7 and 14 days of cell culture on the electrospun SF/CMC/0%nBG (Figure 5.42A, C), and SF/CMC/10%nBG (Figure 5.42B, D) composite scaffolds. On day 7, it was observed that cells were attached and elongated, whereas cells were proliferated and monolayer coverage of scaffold surface was evident on day 14. However, the cells were polygonal in shape and show more spreading over SF/CMC/10%nBG as compared of SF/CMC/0%nBG counterpart. Furthermore, the development of filamentous actins was superior with the nBG incorporated composite scaffolds compared to SF/CMC/0%nBG. Thus, as expected developed composite scaffold provides superior cell supportive property then SF/CMC/0%nBG blend scaffold and maintaining the cytoskeletal organization of the hMSCs.

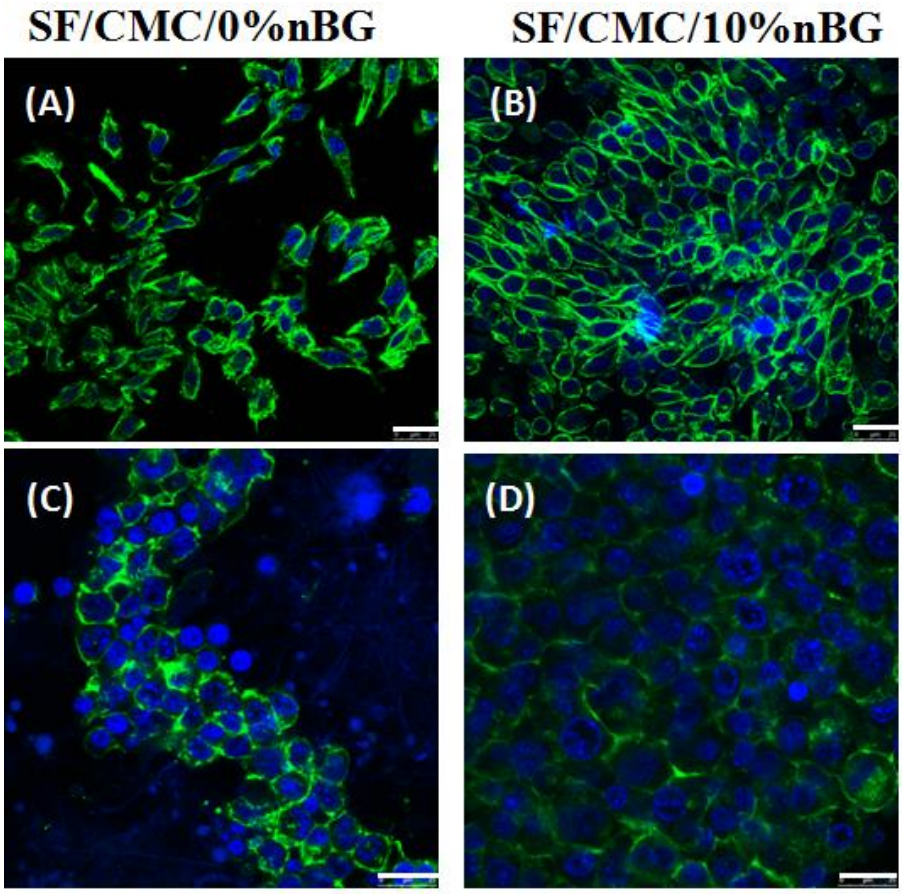

Figure 5.42: hMSCs proliferation and distribution are visualized under confocal microscope on SF/CMC/0%nBG (A and C) and SF/CMC/10%nBG (B and D) on 7 and 14 days of culture, Nuclei of the cells were stained with DAPI (blue) and actin filaments with phalloidin (green).

Composite scaffold SF/CMC/10nBG shows better elongation and spreading of cells in comparison to SF/CMC scaffold. (Scale bar = 25 µm)

Metabolic activity by MTT assay

The cytocompatibility and cell proliferation of the developed nano composite scaffold were assessed during 7 days of hMSCs culture over the scaffolds by MTT assay [311]. As can be seen from Figure 5.43B that, on day 3, the optical density (OD) measured with hMSCs seeded SF/CMC/10%nBG is higher than pure SF/CMC ($p<0.05$) scaffolds. However, during the progress of the culture OD values were observed to be steadily increased with both SF/CMC with and without nBG. However, the metabolic activity of hMSCs on SF/CMC/10%nBG was significantly higher ($p<0.05$) in comparison to SF/CMC/0%nBG blend scaffold throughout the culture period on day 14 in particular. Thus, the metabolic activity study shows superior biocompatibility of the developed SF/CMC/10%nBG composite scaffolds due to the presence of nBG. Overall, the result confirms that no toxic leachable from nBG loaded SF/CMC scaffold was released which could be detrimental to cellular activity.

Live/dead assay

The confocal images were used to assess the viability of hMSCs cultured for 24h on the developed SF/CMC/0%nBG and SF/CMC/10%nBG scaffolds. The live/dead staining solutions (calcein AM and EthD-1), where green signal indicates viable cells and red signal indicates dead cells as shown in Figure 5.43A. The images show that the hMSCs are viable and look healthy over the entire scaffold irrespective of their composition, however cells were observed to cover higher surface area of SF/CMC/10%nBG as compared to SF/CMC/0%nBG representing the superior hMSCs recruitment to the nBG loaded composite scaffold moiety.

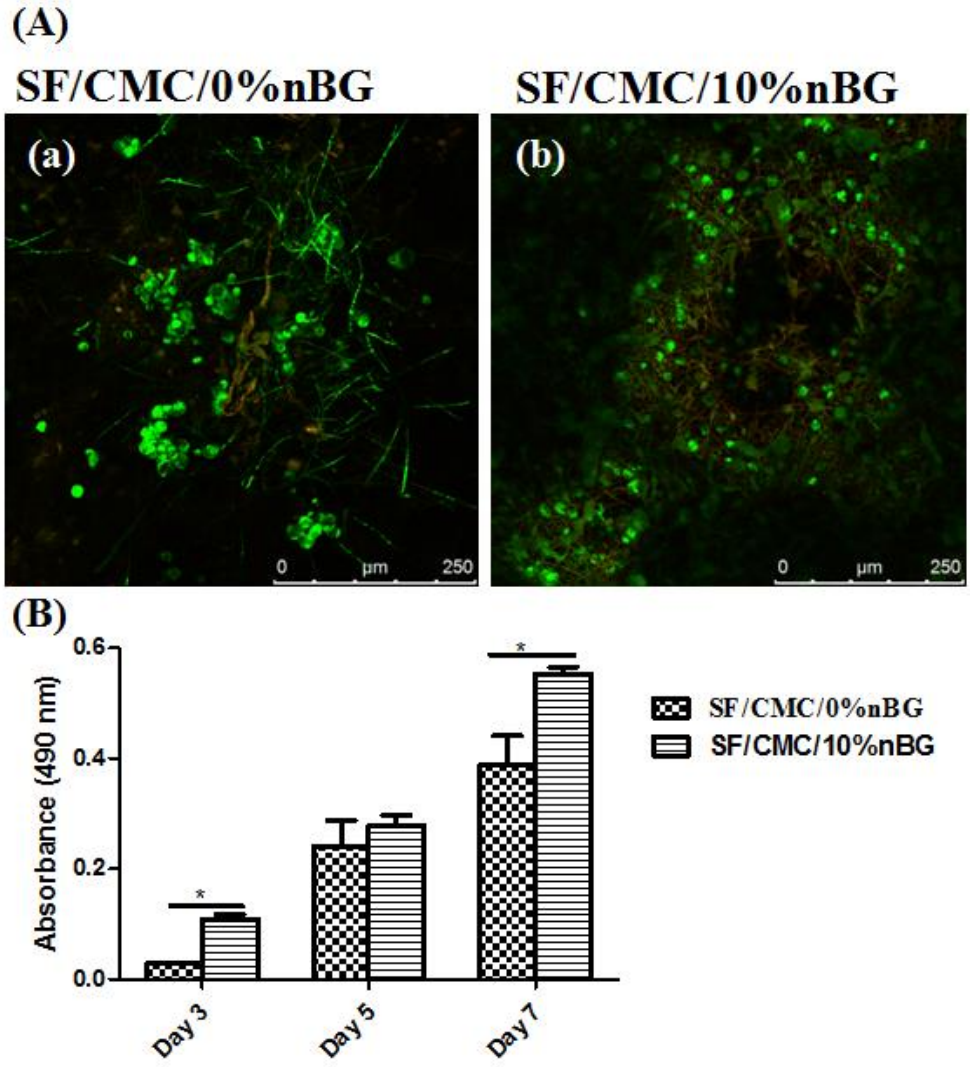

Figure 5.43: Live/dead confocal microscopy images (A) and MTT reduction assay(B) of hMSCs cultured on SF/CMC/0%nBG(control) and SF/CMC/10%nBG nanofibrous scaffolds. The cell viability over nano bioglass incorporated SF/CMC/10%nBG was higher than the control.

Glucosamino glycan (GAG) analysis

Figure 5.44 shows the GAG deposition over SF/CMC/0%nBG and SF/CMC/10%nBG scaffolds. The GAG production was shown to be increased over culture period irrespective of the scaffold composition but with a varied degree of GAG synthesis. On day 7, the GAG content was significantly higher over SF/CMC/10%nBG (0.317 µg/mg) than SF/CMC/0%nBG (0.109 µg/mg) scaffold. A drastic increase in GAG secretion on SF/CMC/10%nBG (0.714 µg/mg) composite nanofibrous scaffold was obtained which was 2.25 fold higher than day 7. Whereas, on day 14, the GAG content on SF/CMC/0%nBG (0.183 µg/mg) nanofibrous scaffold was only 1.6 fold higher than day 7. Thus,

SF/CMC/10%nBG has been proven to promote higher GAG deposition indicating the superior ECM production ability of SF/CMC/10%nBG [361].

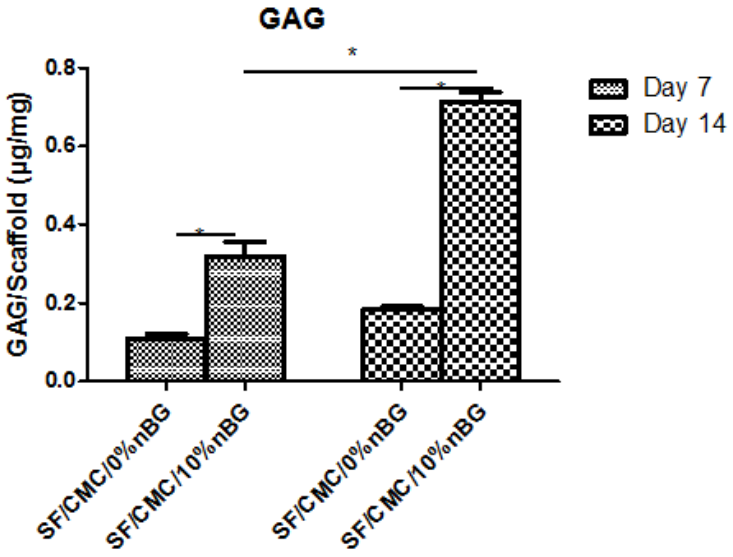

Figure 5.44: Estimation GAG secreted by hMSCs cultured in osteogenic media during 7 and 14 days of culture over SF/CMC/0%nBG and SF/CMC10%nBG nanofibrous scaffolds. The nano composite scaffold loaded with nano-bioglass (SF/CMC/10%nBG) promotes GAG secretion which is higher than SF/CMC scaffold without nano bioglass.

5.3.5 Osteogenic differentiation

Alkaline Phosphatase assay

The alkaline phosphatase enzyme is analysed to evaluate the early osteogenic differentiation of hMSCs. The characteristic marker of early osteoblastic differentiation is attributed to the cellular secretion of ALP. The ALP activities of hMSCs over the scaffolds were studied during 14 days of culture period and the obtained ALP result is shown as Figure 5.45. An increase in enzyme activity level with increasing culture period from 7 days to 14 days represents the more differentiated stage of hMSCs seeded on the scaffold. A gradual increase in ALP activity in all the scaffolds was shown during the 14 days of culture period which indicates the osteogenic differentiation of hMSCs. However, the ALP activity of hMSCs on SF/CMC/10%nBG was significantly ($p<0.05$) higher than SF/CMC/0%nBG throughout the culture period. Hence, it is confirmed that nano bioglass incorporated SM/CMC provides superior osteogenic platform for hMSCs than the SF/CMC scaffold containing no bioglass.

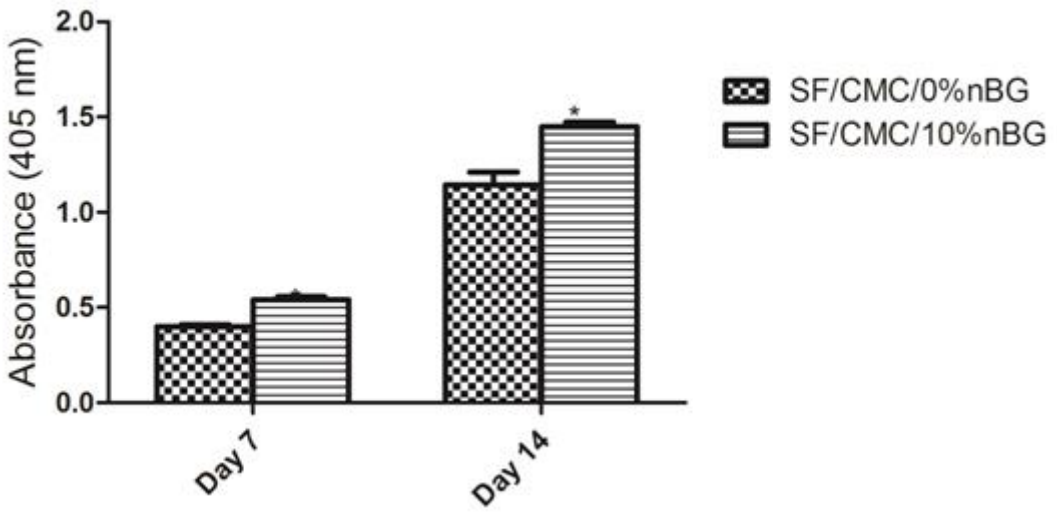

Figure 5.45: Alkaline phosphatase (ALP) activity in hMSCs on SF/CMC/0%nBG and SF/CMC/10%nBG in an osteogenic culture medium over time (n=3). From ALP activity analysis it has been observed that SF/CMC/10%nBG provides a better supportive platform for osteogenic differentiation of hMSCs than the SF/CMC scaffolds

Biomineralization of hMSCs seeded composite nanofibrous scaffold

The level of mineralized matrix produced by hMSCs over the developed scaffold after culturing for 14 days in osteogenic differentiation media was assessed by observation under inverted phase contrast microscope and further quantified by ARS assay. The inverted phase contrast microscopic image (Figure 5.46A) clearly shows that the biomineralization of scaffolds by hMSCs depends on both culture duration as well as scaffold composition. The extent of mineralization was observed to be increased with culture time over all the scaffolds. The intensity of stained calcium nodules was observed to be higher on SF/CMC/10%nBG compared to the control throughout the culture period which signifies the superior bioactivity of the nano composite scaffold.

The quantitative ARS assay shows that biomineralization increases with time from day 7 to day 14. As indicated from Figure 5.46B, the optical density (OD) for SF/CMC/10%nBG was significantly higher ($p < 0.05$) than SF/CMC/0%nBG on both 7 and 14 days of culture period. The higher degree of biomineralization on SF/CMC/10%nBG is due to the dissolution of bioglass, leading to the formation of osteoconductive hydroxyapatite. This also suggests that the degree of ECM mineralization depends on culture duration as well as the scaffold material. Thus, it demonstrates that nano-bioglass containing SF/CMC composite

nanofibrous scaffolds not only facilitate the hMSCs recruitment but also triggers hMSCs towards osteogenic lineages and invoke the biomineralization of scaffold.

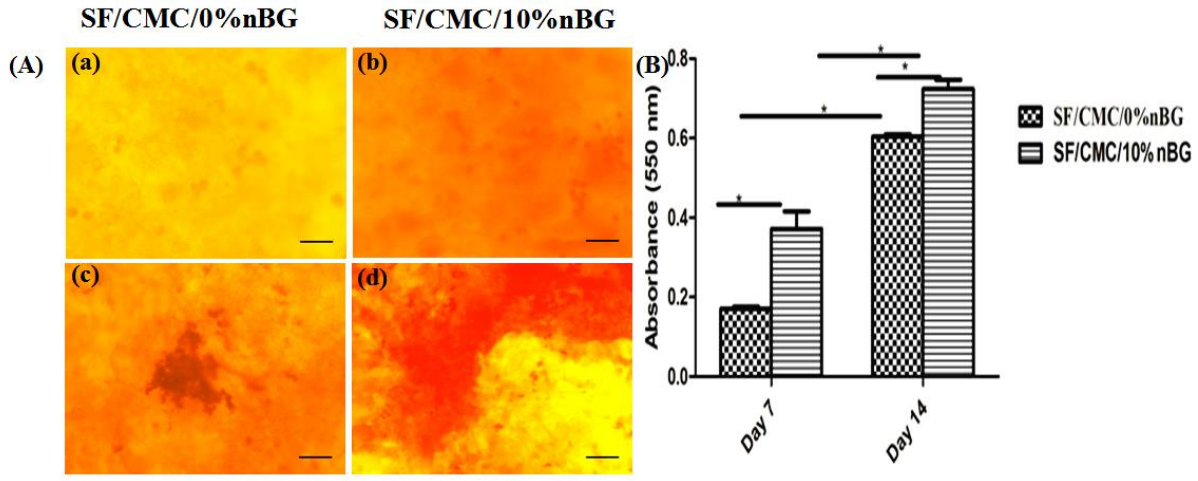

Figure 5.46: (A) Alizarin red S staining of SF/CMC/0%nBG and SF/CMC/10%nBG nanofibrous scaffolds cultured for day 7 (a) and day 14 (b). (B) Alizarin Red S staining assay for quantitative evaluation of hMSCs mineralization on SF/CMC/0%nBG and SF/CMC/10%nBG nanofibrous scaffolds after 14 days of culture. The nano-bioglass incorporated composite scaffold SF/CMC/10%nBG shows enhanced biomineralization than the control. (Scale bar = 50 µm)

Osteogenic differentiation of hMSCs seeded on composite nanofibrous scaffold

The expression of Runx2, osteocalcin and collagen type1, which are well known markers for osteogenic differentiation of human mesenchymal stem cells were investigated to confirm the bone tissue regeneration ability of the nanofibrous composite scaffold. Runx2 is an osteoblast specific transcription factor that acts intracellularly and controls the expression of bone tissue specific genes such as collagen 1 and osteocalcin respectively [362]. The immunocytochemistry for Runx2 expression during 7 and 14 days of culture (Figure 5.47A) was examined through the confocal microscopic laser assisted image analysis. As co-localization of Runx2 and DAPI immunostainning shows that the expression of Runx2 was localized mostly to the cell nuclei. The fluorescent signals for Runx2 immunostainning were quantified and statistically analyzed (Figure 5.47C). From integrated density plot (Figure 5.47C) it was observed that Runx2 expression level was higher on day 7 and down regulated further on day 14. Furthermore, the Runx2 expression level was significantly ($p<0.05$) higher

in hMSCs seeded on SF/CMC/10%nBG on day 7 and then decreased significantly ($p<0.05$) on day 14 as compared to SF/CMC/0%nBG. Thus the bioglass containing nanofibrous composite scaffolds shows improved bioactivity that triggers the differentiation of hMSCs toward osteogenic lineages through Runx2 dependent pathways. As Runx2 is an early stage marker of osteogenic differentiation and observed to be well expressed by hMSCs seeded on nanofibrous composite scaffolds, the OCN expression, as a late marker and depend on degree of mineralization was measured [363]. Figure 5.47B reveals that the OCN expressions were consecutively increased in hMSCs seeded on SF/CMC/0%nBG and SF/CMC/10%nBG scaffolds from day 7 to 14 of culture. The Integrated density plot (Figure 5.47D) shows that OCN expression level was significantly ($p<0.05$) higher in SF/CMC/10%nBG in comparison of other scaffolds at day 7 and day 14.

The osteoblastic differentiation of hMSCs on the scaffolds was further assessed by RT-PCR for Runx2, osteocalcin (OCN) and collagen type1 gene expressions. On day 14 of culture, RT-PCR analysis shows significantly ($p<0.05$) higher level of OCN expression on SF/CMC/10%nBG (Figure 5.47F) then SF/CMC/0%nBG nanofibrous scaffolds. The OCN expression on SF/CMC/10nBG was observed to be 4.1 fold higher than pure SF/CMC scaffold. The Runx2 gene expression (Figure 5.47E) was observed to be lower with insignificant difference among scaffolds after two weeks of culture. Whereas for collagen type1 SF/CMC/10%nBG shows 3.3 fold higher expressions than pure SF/CMC (Figure 5.47G). This can be explained as- the nano-bioglas dissolution resulted into higher silicon, Ca^{2+} and PO_4^{2-} ion concentration as observed by ICP-OES analysis, which were beneficial for osteogenic differentiation and extracellular matrix formulation.

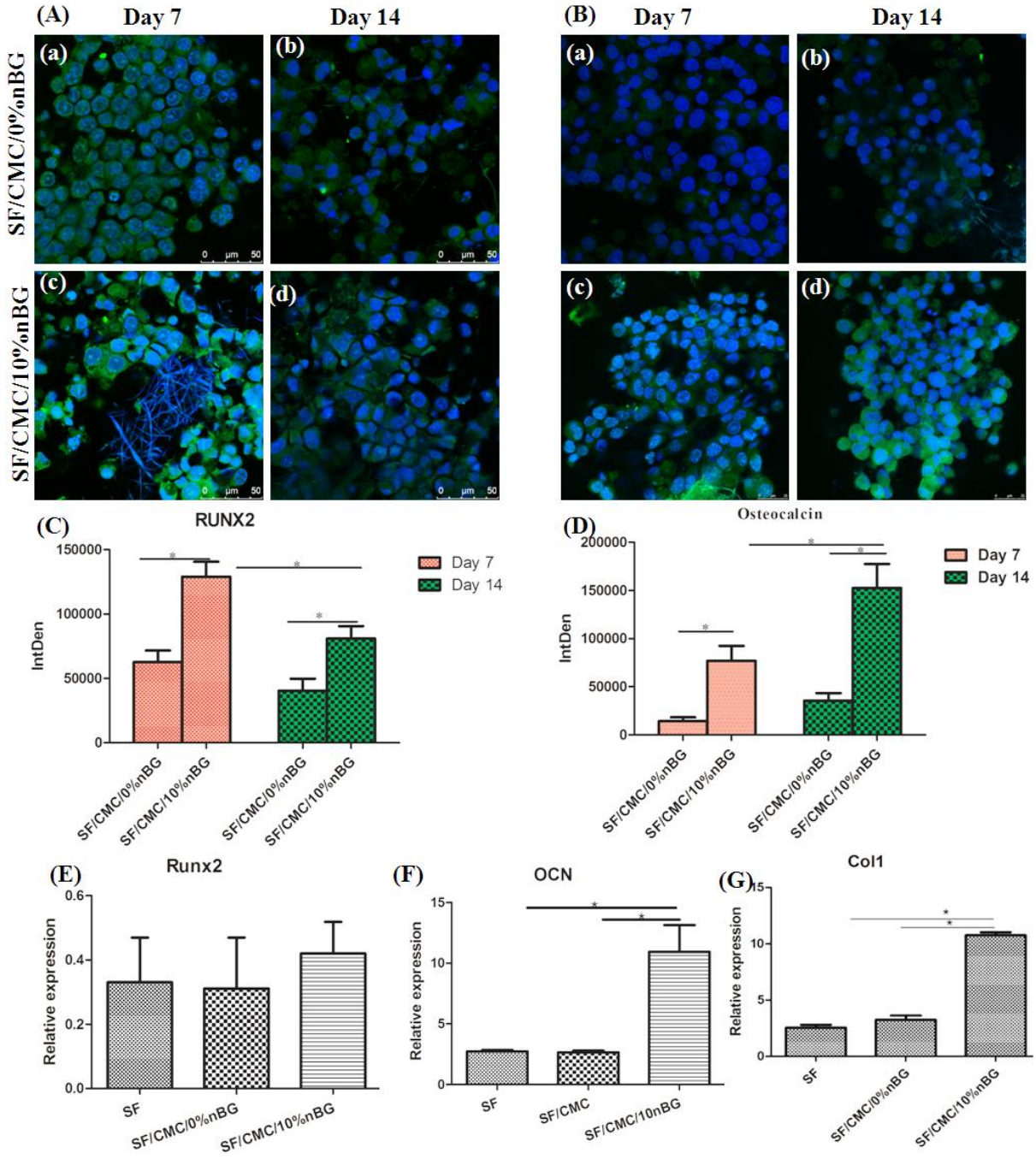

Figure 5.47: Immunocytochemistry for Runx2 and osteocalcin expression by hMSCs cultured on SF/CMC/0%nBG and SF/CMC/10%nBG nanofibrous scaffolds. (A) Confocal images for Runx2 expressions (scale bar = 50 µm) (A) and Confocal images for osteocalcin expressions of hMSCs (scale bar = 25 µm) on day 7 and day 14 in the osteogenic culture medium. Integrated density evaluation for RunX2 and osteocalcin were shown in graphs (C) and (D) respectively. The osteogenic differentiation of hMSCs on SF/CMC and SF/CMC/10nBG scaffolds was assessed by RT-PCR for Runx2 (E), osteocalcin (F) and collagen type1 (G) expression after 14 days of culture.

CHAPTER 5D

Development of copper doped nano bioglass incorporated SF/CMC composite scaffolds

Development of bioactive scaffold, which provides appropriate osteogenic and angiogenic microenvironment for osteogenic cells growth and bone tissue regeneration is important paradigms in current approaches of bone tissue engineering. To fulfil the needed requirement of organic and inorganic containing microenvironment for osteogenic cell growth, biopolymer -bioceramic composite scaffold proves to be beneficial. Therefore, in the previous chapter nanofibrous SF/CMC/nBG nanocomposite scaffold with appropriate composition was developed which has been proven to be a potential artificial ECM matrix with enhanced osteogenic and biomineralization (apatite formation ability) property. Angiogenesis is another crucial factor in bone tissue regeneration because blood vessels provide a means to supply nutrients and oxygen which are essential for growth of neo tissue formed. Therefore, vascularisation is essential for the survival of the cells seeded in the scaffold. In this context, different approaches have been advocated to stimulate angiogenesis in tissue engineering, e.g. the delivery of vasculogenic growth factor (VEGF). However, side effects of using the growth factor and high expenditure involved in this approach limit their uses[364]. Recently, the doping of inorganic ions has been considered as a novel approach to increase the intrinsic angiogenesis potential of the scaffold by stimulating angiogenesis. Furthermore, among the inorganic ions, Cu^{2+} is an attractive choice in enhancing vascularisation. Very recently, *in-vitro* and *in-vivo* studies has further reported the promising role of Cu^{2+} ions in enhancing angiogenesis and also osteogenesis thereby, increased bone tissue regeneration [365-366].

Therefore, efforts have been given in this phase of research work to improve the angiogenic potential of the SF/CMC scaffold by incorporating Cu^{2+} doped nano-bioglass prepared in the chapter 5B. In this study, several batches of SF/CMC scaffolds with varied percentage of Cu^{2+} doped nBG were prepared and the performance of the Cu doped scaffolds were evaluated for their various physiochemical features and biological functionality which are described in this chapter.

5.4.1 Fabrication and characterization of SF/CMC/Cu-nBG nanofibrous composite scaffold

Different batches of SF/CMC/Cu-nBG composite mixtures are prepared by dissolving SF/CMC blend and copper doped nano-bioglass with different compositions in formic acid as shown in Table 5.3. Electrospun nanofibers were successfully generated from the prepared

nano composite solutions. The effect of Cu-nBG concentration on the viscosity of the electrospinnable composite solution and the fiber diameter of the generated electrospun fiber were observed to be in similar trend to the nBG incorporated SF/CMC composite nanofibrous scaffolds developed in chapter 5C. The different composite solutions, there viscosity and the corresponding fiber diameter are shown in Table 5.4. These experimental findings are evident from FESEM images that are depicted in Figure 5.48. As indicated, the average fiber diameter was increased steadily from 233.60 ± 83 nm to 568.40 ± 172 nm and 233.60 ± 83 nm to 572.87 ± 158 nm with the incorporation of $Cu_{0.5}$-nBG and Cu_1-nBG at 5 wt% to 10 wt% respectively. The average pore size of SF/CMC/$Cu_{0.5}$-5%nBG, SF/CMC/$Cu_{0.5}$-10%nBG, SF/CMC/Cu_1-5%nBG and SF/CMC/Cu_1-10%nBG measured from FESEM images (Figure 5.48) are 4.55 ± 1.7 µm, 4.62 ± 2.3 µm, 4.49 ± 1.1 µm and 4.58 ± 1.5 µm respectively. However, the difference in pore size between SF/CMC/Cu-nBG and SF/CMC/nBG composite scaffolds is not statistically significant. As revealed by TEM image, the copper doped nano-bioglass (≤ 100 nm) was successfully electrospun with SF/CMC and well dispersed over the surface of nanofibers. Furthermore, the amorphous nature of both polymeric as well as copper doped nano-bioglass components of composite nanofibrous scaffold was confirmed by SAED pattern as no ring like pattern was found in obtained SAED images. Furthermore, FESEM and TEM images (Figure 5.48) reveal that Cu-nBG is uniformly distributed over all the Cu-nBG loaded composite scaffolds. However, agglomeration of Cu-nBG over SF/CMC/Cu_1-10%nBG scaffold is observed to a certain extent.

Table 5. 3: Composition of various composite nanofibrous scaffold

Scaffold	**SF/CMC (wt%)**	**$Cu_{0.5}$-nBG (wt%)**	**Cu_1-nBG(wt%)**
SF/CMC/0%nBG	100	0	0
SF/CMC/ $Cu_{0.5}$-5%nBG	95	5	0
SF/CMC/ Cu_1-5%nBG	95	0	5
SF/CMC/ $Cu_{0.5}$-10%nBG	90	10	0
SF/CMC/ Cu_1-10%nBG	90	0	10

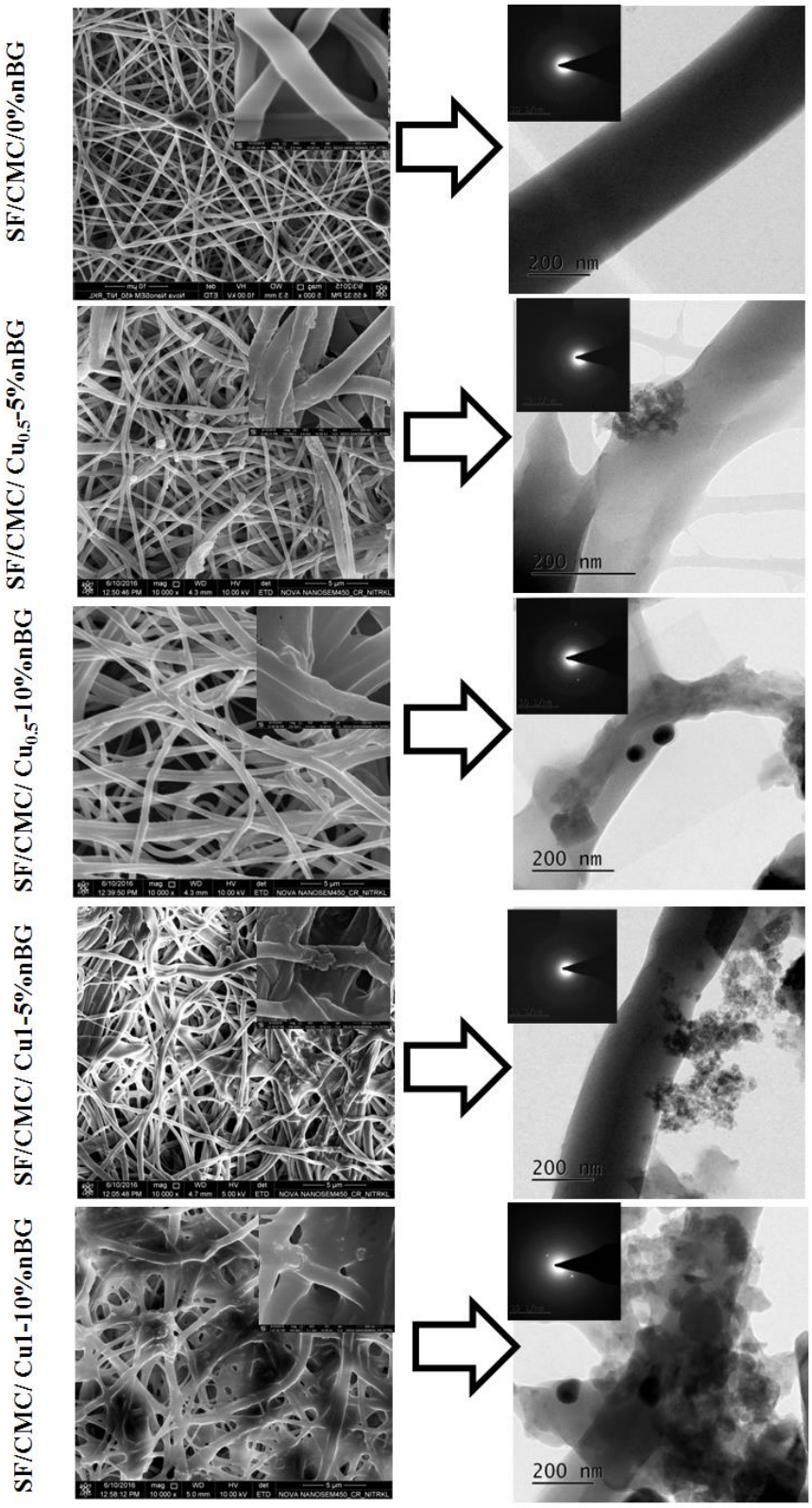

Figure 5.48: FESEM, TEM and SAED pattern images of fabricated SF/CMC/0%nBG, SF/CMC/$Cu_{0.5}$-5%nBG, SF/CMC/$Cu_{0.5}$-10%nBG, SF/CMC/Cu_1-5%nBG and SF/CMC/ Cu_1-10%nBG nanofibrous scaffolds.

Table 5. 4: Viscosity, average fiber diameter and average pore size of various composite nanofibrous scaffolds with and without Cu-nBG

Scaffold	Average fiber diameter (nm)	Average pore size (µm)
SF/CMC/0%nBG	233.60 ± 83	4.51 ± 1.6
SF/CMC/ $Cu_{0.5}$-5%nBG	362.23 ± 134	4.55 ± 1.7
SF/CMC/ $Cu_{0.5}$-10%nBG	568.40 ± 172	4.62 ± 2.3
SF/CMC/ Cu_1-5%nBG	347.53 ± 142	4.49 ± 1.1
SF/CMC/ Cu_1-10%nBG	572.87 ± 158	4.58 ± 1.5

Structural and functional analysis

The respective XRD (Figure 5.49A) and FT-IR (Figure 5.49B) patterns were used to investigate the structural and functional characteristics of the SF/CMC scaffolds modified by the incorporation of $Cu_{0.5}$-nBG and Cu_1-nBG respectively. The diffraction peaks at 2θ values of 20.8° and 24.3° indicating the β-sheet conformation of the developed nanofibrous scaffold were intensified as Cu-nBG introduced up to 5 wt%. This phenomenon may be attributed to the conformational transformation of randomly arranged coil to β – sheet structure. However, at 10wt% Cu-nBG incorporation, the amorphous nature of nBG was prominently noticed. The FT-IR spectra of SF/CMC/Cu-nBG showed vibration bands at 470 cm^{-1}, 1060 cm^{-1} and 1100 cm^{-1} which are associated with Si-O-Si bending mode[331, 349]. The peak at 970 cm^{-1} was assigned to the non-bridging oxygen together with the surface active silanols (Si-OH) groups, which facilitate apatite formation. The shoulder peak at 958 cm^{-1} belongs to the Si-O-Ca vibration mode [230]. The peak at 920 cm^{-1} is the result of stretching vibration of the phosphate group (O-P-O) [349]. From FT-IR spectra it has been observed that as the Cu-nBG content increases the peak at 1060 cm^{-1} which are associated with Si-O-Si bending mode became more broader due to the improvement in interaction such as hydrogen bonding or ionic bonding between the fibers and nano-bioglass [348]

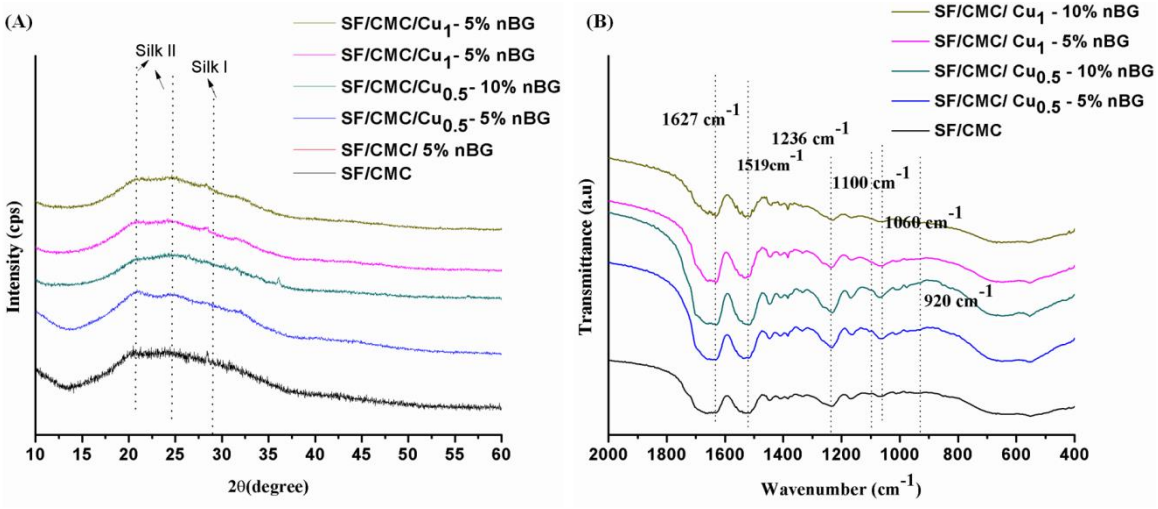

Figure 5.49: (A) XRD diffractogram and (B) FT-IR spectra of SF/CMC/0%nBG, SF/CMC/$Cu_{0.5}$-5%nBG, SF/CMC/$Cu_{0.5}$-10%nBG, SF/CMC/Cu_1-5%nBG and SF/CMC/ Cu_1-10%nBG nanofibrous scaffolds.

5.4.2 *In vitro* bioactivity

In this study, the effect of incorporated $Cu_{0.5}$-nBG and Cu_1-nBG at varying contents of each one from 5 to 10 wt% in SF/CMC blend (SF/CMC/$Cu_{0.5}$-5%nBG, SF/CMC/$Cu_{0.5}$-10%nBG, SF/CMC/ Cu_1-5%nBG and SF/CMC/ Cu_1-10%nBG) was investigated and the experimental results are depicted in Figure 5.50. The ability of the composite scaffold containing different Cu-nBG content to induce apatite formation on their surface was assessed by FESEM study after soaking in SBF for 7 days. In comparison, the SF/CMC/$Cu_{0.5}$-10%nBG shows better mineral deposition over the scaffold matrix than SF/CMC/$Cu_{0.5}$-5%nBG. Similarly, SF/CMC/ Cu_1-10%nBG shows greater extent of mineral deposition than that shown by SF/CMC/ Cu_1-5%nBG scaffold. Thus, as the concentration of Cu-nBG increases, the surface of the nano composite scaffold exhibited improved mineral deposition which is clearly seen in FESEM images. Furthermore, the extent of mineral deposition over SF/CMC/Cu_1-5%nBG scaffold matrix was similar to SF/CMC/$Cu_{0.5}$-5%nBG, whereas a slightly higher mineral deposition over the scaffold matrix was observed in SF/CMC/Cu_1-10%nBG in comparison to SF/CMC/$Cu_{0.5}$-10%nBG, the phenomena of which is attributed to the higher bioactivity of copper doped bioglass. Furthermore, the level of copper doping has independent effect on the apatite forming ability of copper doped nano-bioglass as reported earlier with other bioglass system (copper doped 45S5) [340].

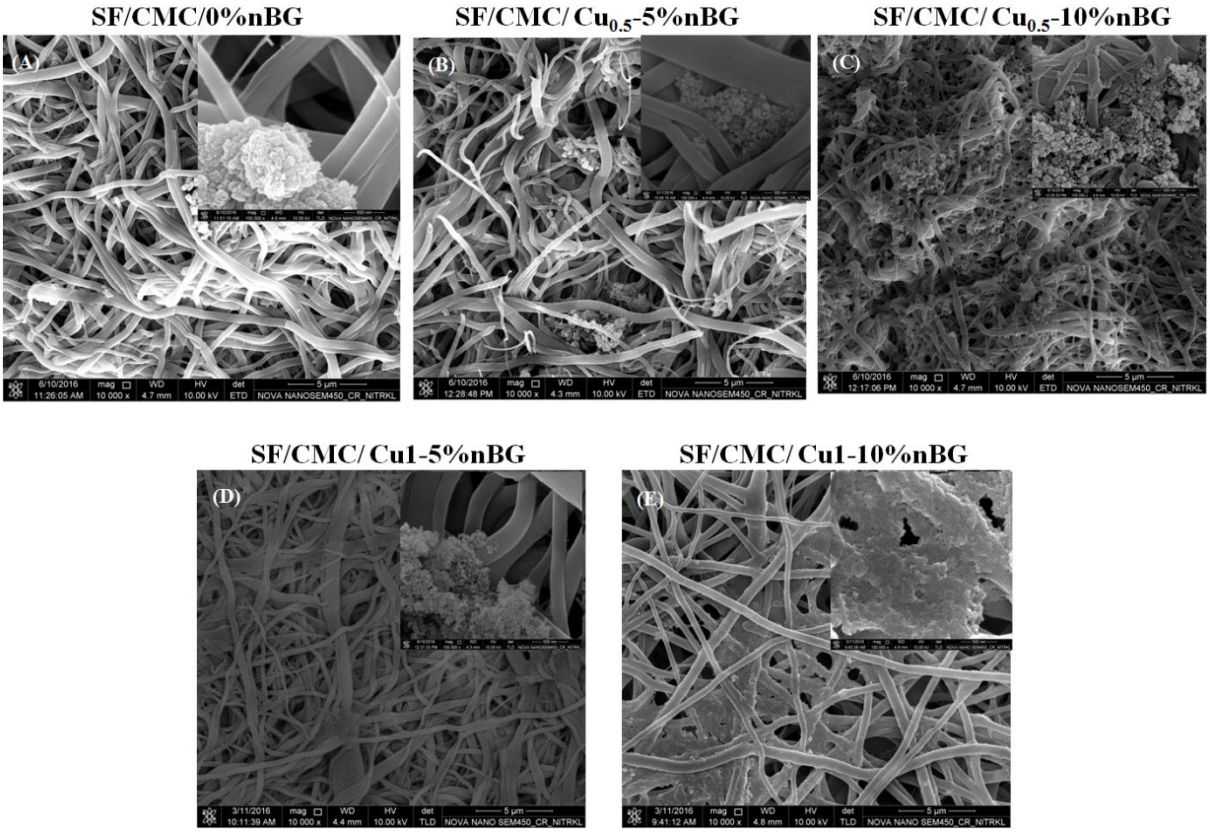

Figure 5.50: FESEM images of SF/CMC/0%nBG, SF/CMC/$Cu_{0.5}$-5%nBG, SF/CMC/$Cu_{0.5}$-10%nBG, SF/CMC/Cu_1-5%nBG and SF/CMC/Cu_1-10%nBG nanofibrous scaffolds after SBF treatment for 7 days (A-E).

Structural and functional analysis of biomineralized scaffold

The X-ray diffraction pattern of the developed Cu doped nanobioglass incorporated scaffolds were recorded after SBF treatment for 7 days to investigate the mineralization of scaffolds and compared with the standard XRD peak of synthetic hydroxyapatite as shown in Figure 5.51A. The diffractogram of SF/CMC/Cu-nBG shows that as the Cu-nBG content increases from 5 to 10wt% the characteristic peaks of the apatite at 31.8° attributed to 211 plane get intensified thereby resulted superior biomineralization at higher concentration of Cu-nBG [359]. Thus, the peak height and width were increased for SF/CMC/0.5Cu-10nBG and SF/CMC/1Cu-10nBG than those were shown by SF/CMC/0.5Cu-5nBG and SF/CMC/1Cu-5nBG respectively. Furthermore, the peak height and width at 31.8° was higher for SF/CMC/Cu_1-10%nBG than SF/CMC/$Cu_{0.5}$-10%nBG which is because of the improved bioactivity of Cu-nBG with increasing copper doping from 0.5 mol% to 1 mol%.

As observed in FT-IR spectra Figure 5.51B, the hydroxyapatite deposition on the scaffolds is reflected by the characteristic peak at 1070 cm^{-1} which corresponds to the P-O asymmetric stretching mode of vibration for PO_4^{-3} group [300-301]. However, the peak at 1070 cm^{-1} was broader in case of Cu-nBG loaded composite scaffold which may be due to the interaction between deposited hydroxyapatite and SF/CMC. The P-O stretching mode has been observed at 1012 cm^{-1} and 976 cm^{-1} which correspond to the major bands for phosphate group. The sharpening of peaks observed at 610 cm^{-1} and 556 cm^{-1} are because of O-P-O bending and stretching respectively[301-302]. The absorbed CO_2 corresponds to the 1400-1450 cm^{-1} peaks indicating the deposition of carbonated hydroxyapatite on the nanofibers. Furthermore, the peak intensity at 1070 cm^{-1} correspond to phosphate group was observed to be higher for SF/CMC/$Cu_{0.5}$-10%nBG and SF/CMC/Cu_1-10%nBG in comparison to SF/CMC/$Cu_{0.5}$-5%nBG and SF/CMC/Cu_1-5%nBG respectively which may be attributed to the increasing Cu-nBG content. However, SF/CMC/Cu_1-10%nBG shows prominent peak at 1070 cm^{-1} because of higher apatite forming ability as compared to SF/CMC/$Cu_{0.5}$-10%nBG composite scaffold. The FESEM, XRD and FT-IR analysis of nanofibrous scaffolds confirm re-precipitation of released ions after dissolution of Cu-nBG as carbonated nano hydroxyapatite on the composite scaffold matrix [367].

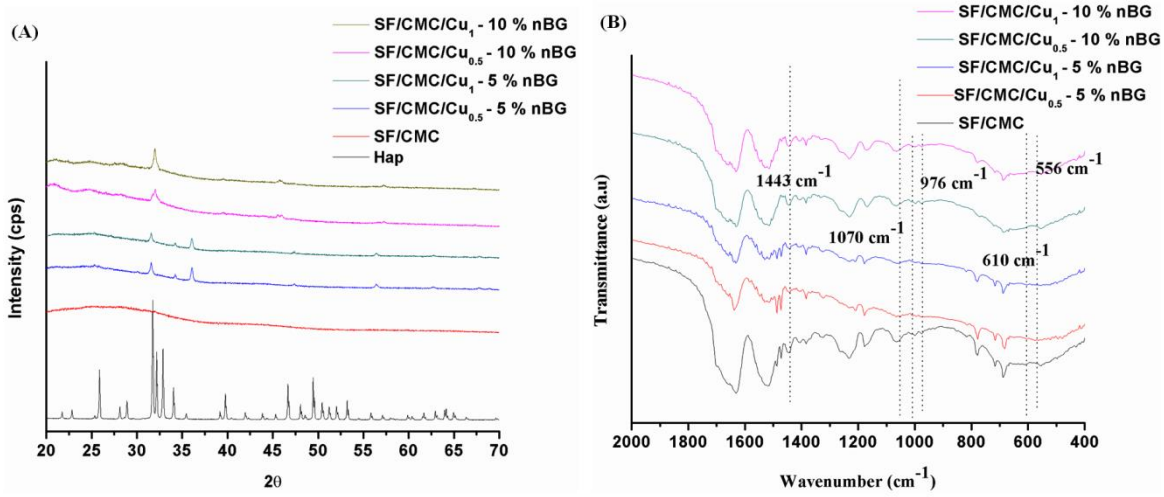

Figure 5.51: (A) **XRD diffractogram and (B) FTIR Spectra of SF/CMC/0%nBG, SF/CMC/$Cu_{0.5}$-5%nBG, SF/CMC/$Cu_{0.5}$-10%nBG, SF/CMC/Cu_1-5%nBG and SF/CMC/ Cu_1-10%nBG nanofibrous scaffolds after SBF treatment for 7 days.**

5.4.3 *In vitro* biodegradation of scaffold

The developed SF/CMC, SF/CMC/$Cu_{0.5}$-5%nBG, SF/CMC/$Cu_{0.5}$-10%nBG, SF/CMC/Cu_1-5%nBG and SF/CMC/Cu_1-10%nBG nanofibrous scaffolds were investigated for their biodegradation by treatment in PBS (Figure 5.52A) and protease XIV enzymatic (Figure 5.52B) solutions. The study has shown that the copper doped bioglass incorporated composite SF/CMC scaffold was degraded at higher rate than the scaffold without bioglass. Furthermore, an enhance rate degradation profile of scaffold occurs in presence of enzyme than the degradation obtained using PBS. The degradation was also found to be Cu-doped nano bioglass concentration dependent. The composite scaffold incorporated with Cu_1-nBG shows degradation of 54.12 ± 2.14 % for SF/CMC/Cu_1-5%nBG and 56.21 ± 2.34 % for SF/CMC/Cu_1-10%nBG, whereas $Cu_{0.5}$-nBG incorporated scaffold shows degradation of 53.21 ± 2.11 % for SF/CMC/$Cu_{0.5}$-5%nBG and 57.27 ± 3.21 % for SF/CMC/$Cu_{0.5}$-10%nBG in presence of enzyme after incubation for 28 days. However in presence of PBS, Cu_1-nBG incorporated scaffold shows degradation of 35.21 ± 3.25 % for SF/CMC/Cu_1-5%nBG and 36.43 ± 2.54 % for SF/CMC/Cu_1-10%nBG, whereas $Cu_{0.5}$-nBG shows degradation of 30.32 ± 2.31 % for SF/CMC/$Cu_{0.5}$-5%nBG and 33.25 ± 2.89 % for SF/CMC/$Cu_{0.5}$-10%nBG. Thus, an enhanced but controlled biodegradation of composite scaffold can be achieved by inclusion of Cu doped nano bioglass into the scaffold matrices.

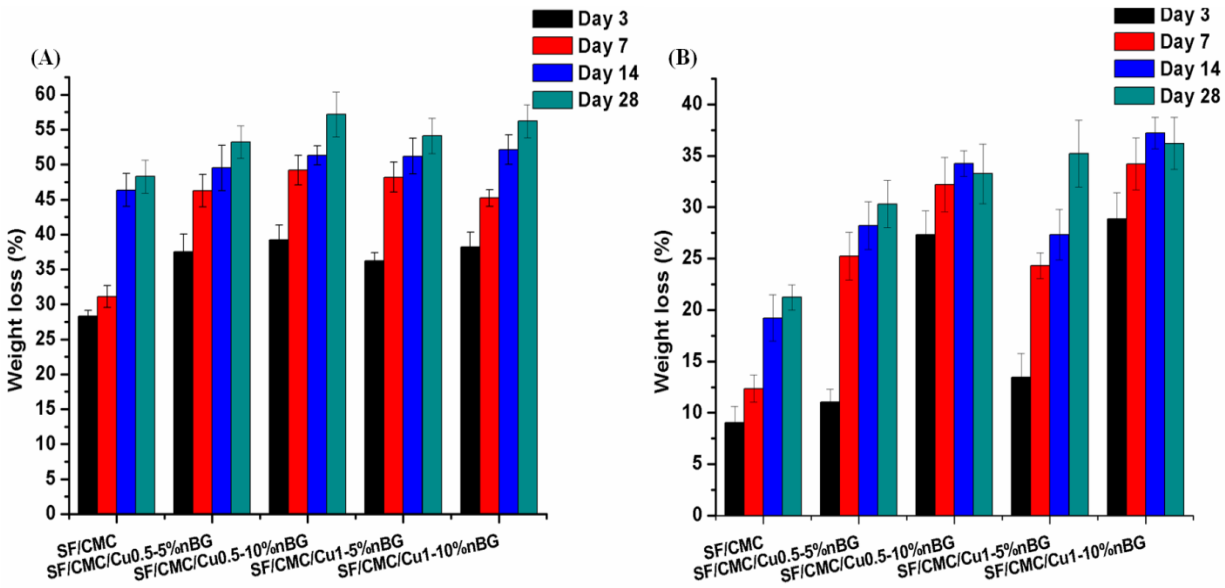

Figure 5.52: Observed degradation behaviour of *SF/CMC, SF/CMC/$Cu_{0.5}$-5%nBG, SF/CMC/$Cu_{0.5}$-10%nBG, SF/CMC/Cu_1-5%nBG and SF/CMC/ Cu_1-10%nBG* scaffolds by soaking in enzyme (A) and PBS solution (B) for 28 days.

5.4.4 In-vitro cell culture study

Metabolic activity

The metabolic activity represents the potential of cells to adhere and proliferate over scaffold surfaces, which was quantitatively estimated during the 7 days culture of hMSCs by MTT assay as shown in Figure 5.53B. The SF/CMC/$Cu_{0.5}$-5%nBG and SF/CMC/Cu_1-5%nBG composite nanofibrous scaffolds showed better metabolic activity or cell viability as comparison to SF/CMC/$Cu_{0.5}$-10%nBG and SF/CMC/Cu_1-10%nBG throughout the culture duration. This may be attributed to the higher copper ion concentration released from 10wt% of Cu-nBG modified SF/CMC blend scaffold.

Live/Dead assay

The viability of hMSCs seeded over scaffolds was further assessed by live/dead cell staining using confocal microscopy. Figure 5.53A shows that the hMSCs were well attached and viable after 1 day of culture over SF/CMC, SF/CMC/$Cu_{0.5}$-5%nBG and SF/CMC/Cu_1-5%nBG scaffolds, whereas SF/CMC/$Cu_{0.5}$-10%nBG and SF/CMC/1Cu-10%nBG was found to be less efficient showing lesser cell viability as most of the cells were found to be dead. hMSCs were also well attached and distributed over SF/CMC/$Cu_{0.5}$-5%nBG and SF/CMC/Cu_1-5%nBG in comparison to SF/CMC/$Cu_{0.5}$-10%nBG and SF/CMC/Cu_1-10%nBG. MTT assay (Figure 5.53B) shows significantly lower metabolic activity of hMSCs over SF/CMC/Cu_1-5%nBG than SF/CMC/$Cu_{0.5}$-5%nBG composite scaffold which may be due to higher copper ion release from Cu_1-nBG in comparison to $Cu_{0.5}$-nBG. Similar metabolic activity of hMSCs over SF/CMC/$Cu_{0.5}$-10%nBG and SF/CMC/1Cu-10%nBG composite scaffold was also observed. Thus, the cell metabolic activity and live/dead cell staining assays indicate that the SF/CMC/$Cu_{0.5}$-5%nBG and SF/CMC/Cu_1-5%nBG provide superior surface for cell attachment than SF/CMC/$Cu_{0.5}$-10%nBG and SF/CMC/Cu_1-10%nBG scaffolds. Thus SF/CMC, SF/CMC 5%nBG, SF/CMC/$Cu_{0.5}$-5%nBG and SF/CMC/Cu_1-5%nBG scaffolds were selected for further study.

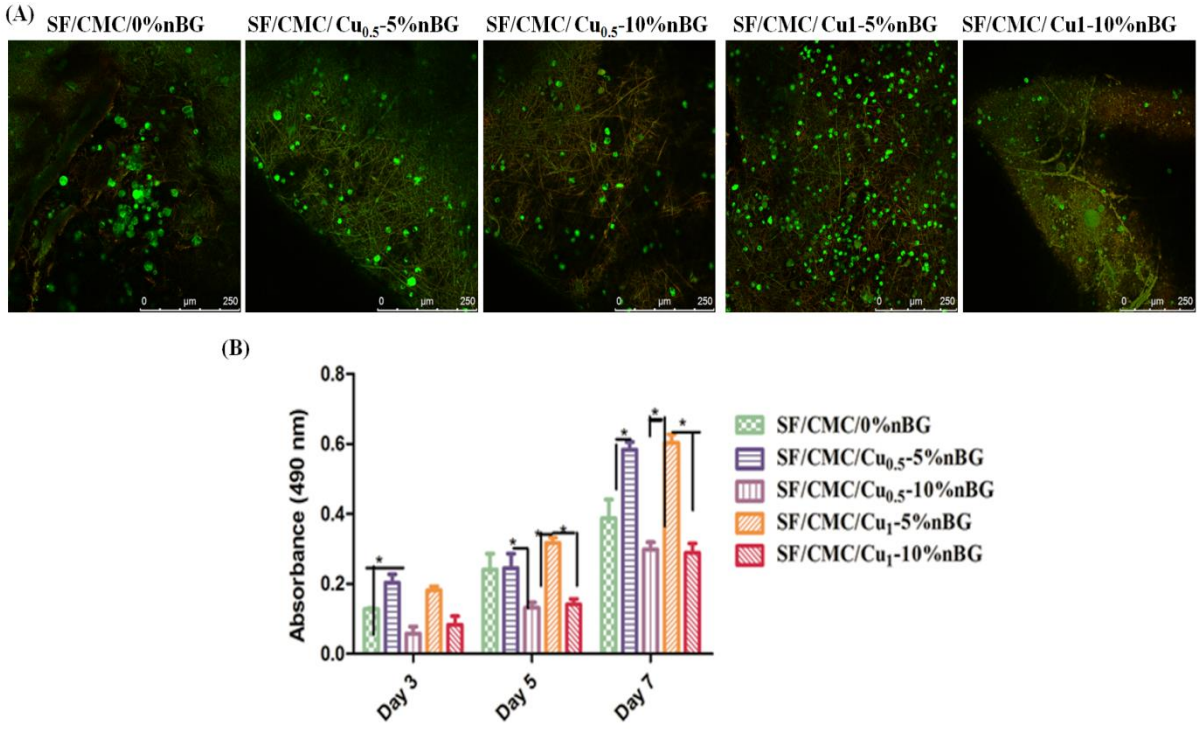

Figure 5.53: (A) Live/dead confocal microscopy images of hMSCs cultured on SF/CMC/0%nBG, SF/CMC/$Cu_{0.5}$-5%nBG, SF/CMC/$Cu_{0.5}$-10%nBG, SF/CMC/Cu_1-5%nBG and SF/CMC/ Cu_1-10%nBG nanofibrous scaffolds. (B) MTT reduction assay of hMSCs cultured on SF/CMC, SF/CMC/$Cu_{0.5}$-5%nBG, SF/CMC/$Cu_{0.5}$-10%nBG, SF/CMC/Cu_1-5%nBG and SF/CMC/ Cu_1-10%nBG nanofibrous scaffolds

hMSCs adhesion, morphology and spreading

Figure 5.54 shows the FESEM images of hMSCs seeded scaffold cultured for 14 days period. After 12 hour of cell seeding, the obtained aspect ratios for cells grown on SF/CMC, SF/CMC/5%nBG, SF/CMC/$Cu_{0.5}$-5%nBG and SF/CMC/Cu_1-5%nBG were 1.325 ± 0.078, 1.40 ± 0.12, 1.38 ± 0.45 and 1.29 ± 0.31 respectively. On day 7, cells were seen to be attached and proliferated over all types of scaffolds. The seeded hMSCs over the SF/CMC nanofibrous scaffold shows spindle shape like morphology. However, on SF/CMC/5%nBG, SF/CMC/0.5Cu-5nBG and SF/CMC/1Cu-5nBG, cell morphology was observed to be polygonal shape at the same time shows growth of filopodia that reflects the strong attachment and spreading of cells. The MSCs morphology tends to changes in to polygonal shape is primary indication for osteogenic differentiation potential of, SF/CMC/5%nBG, SF/CMC/0.5Cu-5nBG and SF/CMC/1Cu-5nBG [360]. However, by day 14, the proliferated cells were observed to cover the scaffold by formation of monolayer like structure.

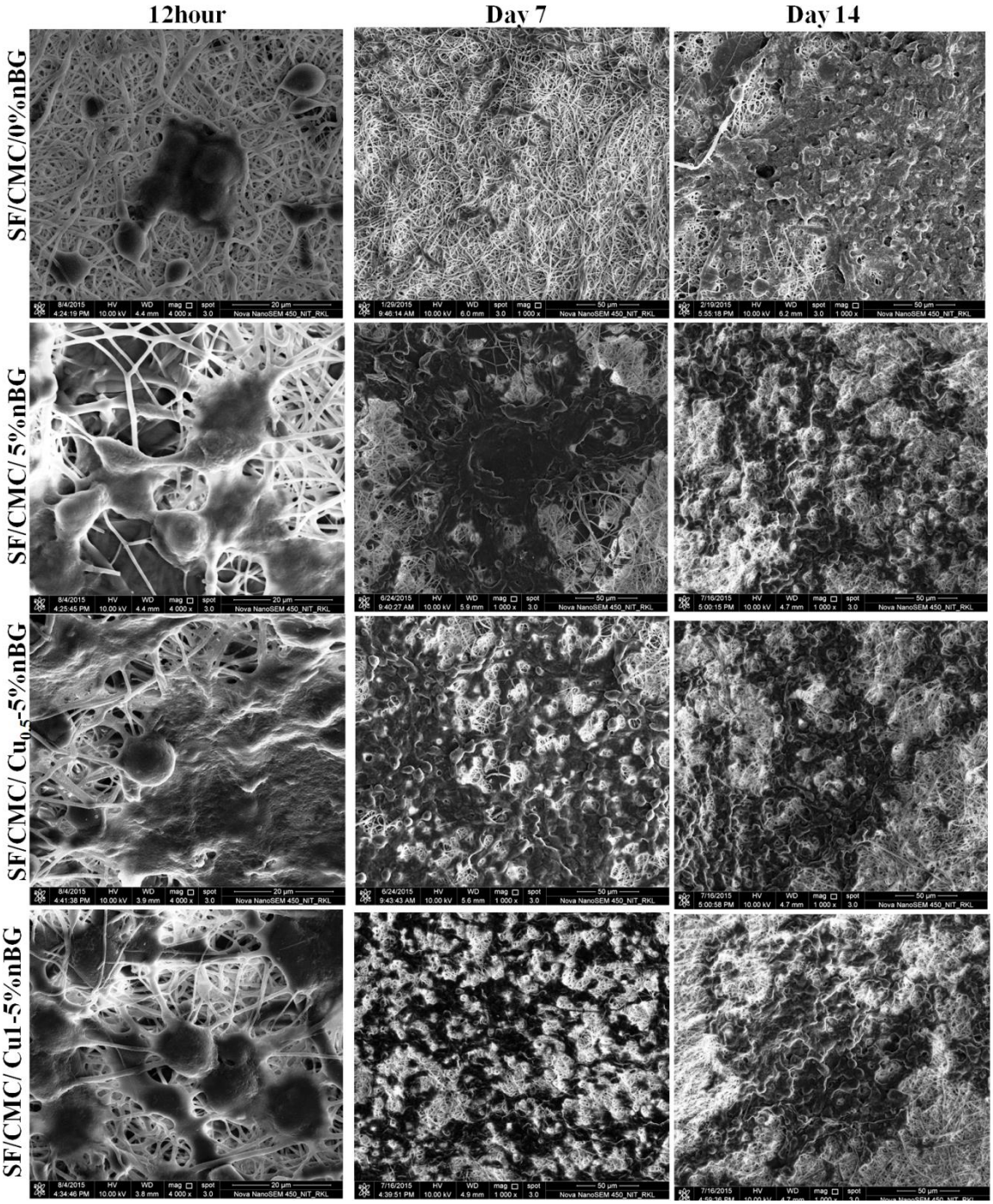

Figure 5.54: FESEM images of hMSCs cultured on the SF/CMC/0%nBG, SF/CMC/5%nBG, SF/CMC/$Cu_{0.5}$-5%nBG and SF/CMC/Cu_{1}-5%nBG scaffolds after 12 hour, 7 and 14 days of culture in DMEM media supplemented with FBS.

Cytoskeleton organization

Figure 5.55 shows the acquired fluorescence images of cytoskeleton development and their distribution after 14 days of cell culture on the electrospun SF/CMC/0%nBG, SF/CMC/5%nBG, SF/CMC/$Cu_{0.5}$-5%nBG and SF/CMC/Cu_1-5%nBG composite scaffolds. On day 14, it was observed that cells were proliferated and form monolayer like coverage over the scaffold surfaces. However, cells were more polygonal in shape and more cells were spread over SF/CMC/$Cu_{0.5}$-5%nBG and SF/CMC/Cu_1-5%nBG composite scaffolds as compared to SF/CMC/0%nBG and SF/CMC/5%nBG nanofibrous scaffolds Thus, the study demonstrates that the developed composite scaffold incorporated with copper doped nano-bioglass could be used as potential cell supportive matrix for neo bone tissue regeneration.

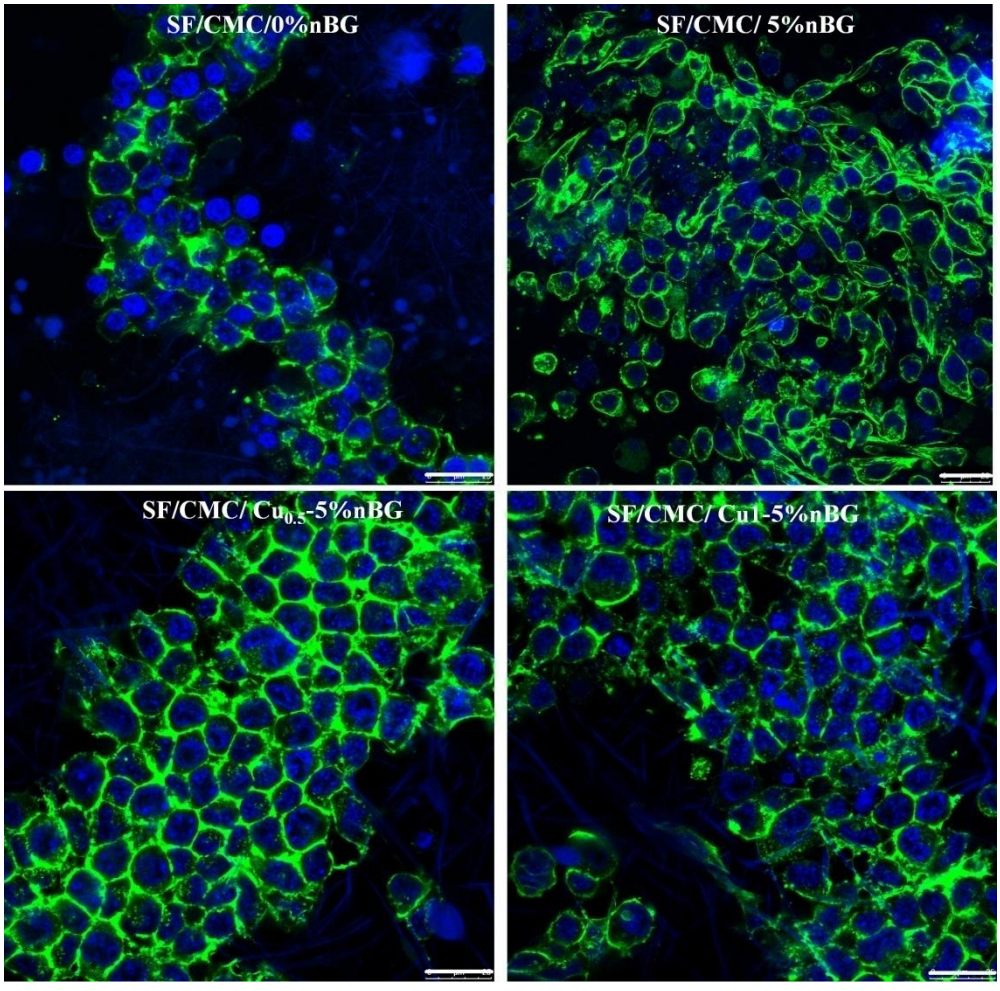

Figure 5.55: hMSCs proliferation and distribution are visualized under confocal microscope over SF/CMC/0%nBG, SF/CMC/5%nBG, SF/CMC/$Cu_{0.5}$-5%nBG and SF/CMC/Cu_1-5%nBG after 14 days of culture. Nuclei of the cells were stained with DAPI (blue) and actin filaments

with phalloidin (green). Overall, better elongation and spreading of cells were observed over SF/CMC/Cu0.5-5%nBG in comparison to SF/CMC and SF/CMC/5%nBG. (Scale bar = 25 µm)

Glucosamino glycan (GAG) estimation

The accumulation of synthesized GAG over SF/CMC/0%nBG, SF/CMC/5%nBG, and SF/CMC/Cu0.5-5%nBG and SF/CMC/Cu1-5% nBG composite scaffolds was evident from Figure 5.56. On day 7, GAG content was significantly higher over SF/CMC/$Cu_{0.5}$-5%nBG (0.311 ± 0.013 µg/mg) composite scaffold than SF/CMC/0%nBG (0.109 ± 0.011µg/mg), SF/CMC/5%nBG (0.209 ± 0.011 µg/mg) and SF/CMC/Cu_1-5%nBG (0.249 ± 0.004 µg/mg) scaffold. However, by day 14 of culture GAG content increases significantly for the entire set of scaffold. The production of GAG was increased with the progress of culture. The GAG content of 0.56 ± 0.02 µg/mg was estimated on SF/CMC/$Cu_{0.5}$-5%nBG scaffold which was 1.8 fold higher than day 7. Whereas, comparatively lesser amount of GAG was secreted over SF/CMC/0%nBG (0.1835 ± 0.008 µg/mg) and SF/CMC/Cu_1-5%nBG (0.405 ± 0.015 µg/mg) scaffolds which were also approximately 1.6 fold higher than day 7 respectively. However, SF/CMC/5%nBG significantly increased GAG production (0.318 ± 0.0065 µg/mg), which is 1.7 and 1.2 fold lower than SF/CMC/$Cu_{0.5}$-5%nBG and SF/CMC/Cu_1-5%nBG respectively. The Cu-nBG incorporated SF/CMC composite scaffold support superior cell viability and cell growth, which further augment the GAG deposition during the culture period. Thus, SF/CMC/$Cu_{0.5}$-5%nBG composite nanofibrous scaffold promoted better GAG deposition as compared to entire set of nanofibrous scaffolds.

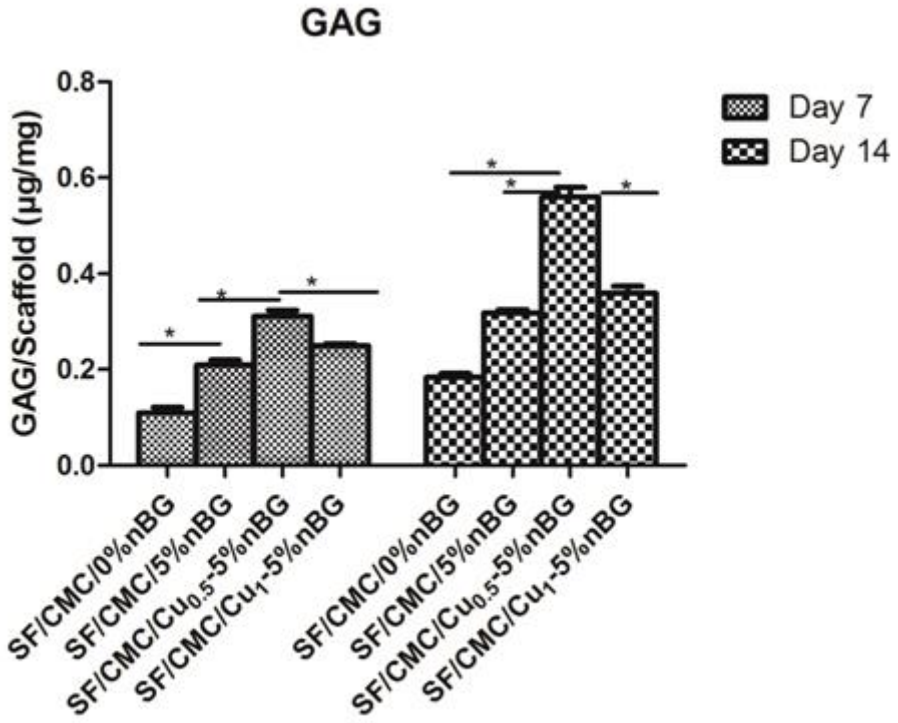

Figure 5.56: Estimation GAG secreted by hMSCs cultured in osteogenic media during 7 and 14 days of culture over over SF/CMC/0%nBG, SF/CMC/5%nBG, SF/CMC/$Cu_{0.5}$-5%nBG and SF/CMC/Cu_1-5%nBG. The SF/CMC/$Cu_{0.5}$-5%nBG composite nanofibrous scaffold shows significantly higher GAG deposition as compared of other set of scaffolds.

5.4.5 Osteogenic differentiation

Alkaline Phosphatase assay

Figure 5.57 shows that the ALP activities of hMSCs cultured over the scaffolds and indicate the progressive differentiation of hMSCs towards osteogenic lineages. The ALP activity of hMSCs on SF/CMC/5%nBG and SF/CMC/$Cu_{0.5}$-5%nBG was higher than SF/CMC/0%nBG and SF/CMC/Cu_1-5%nBG on day 7 of culture. However, by day 14 all the composite scaffolds containing nanobioglass showed higher bioactivity than SF/CMC scaffolds and the bioactivity level was comparable. Thus, it has been demonstrated that the addition of Cu^{2+} did not show any significant role in enhancing bioactivity. This finding is also corroborated with the published literature that reported the insignificant role of Cu^{2+} when it was doped with nanobioglass which was used as scaffold for bone tissue regeneration [325].

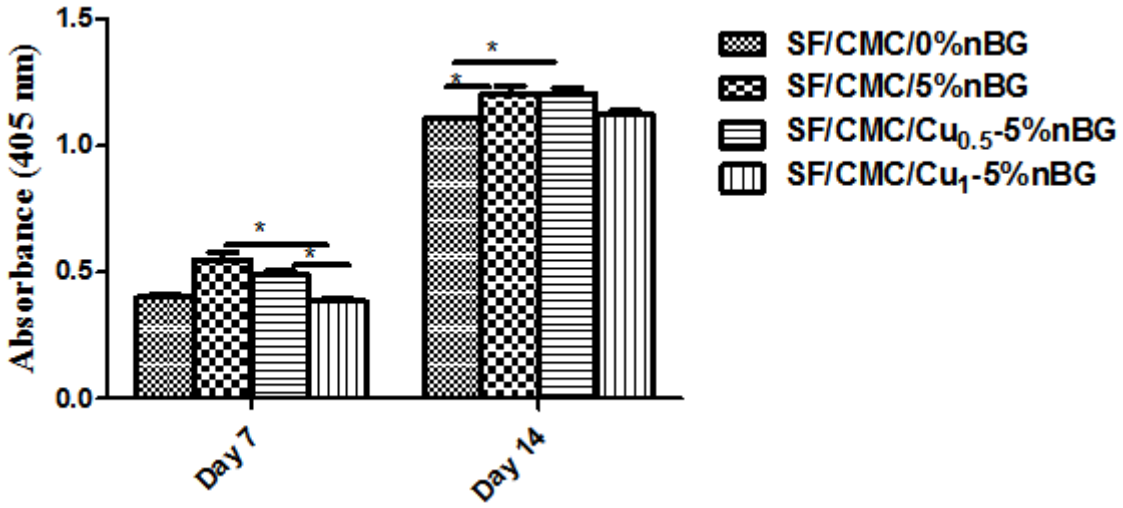

Figure 5.57: Alkaline phosphatase (ALP) activity in hMSCs on SF/CMC/0%nBG, SF/CMC/5%nBG, SF/CMC/$Cu_{0.5}$-5%nBG and SF/CMC/Cu_1-5%nBG nanofibrous scaffolds in an osteogenic culture medium over time (n=3).

Biomineralization of hMSCs seeded composite nanofibrous scaffold

The biomineralization of extracellular matrix deposited by hMSCs cultured on the scaffolds in osteogenic medium for two weeks were assessed by inverted phase contrast microscope and ARS assay. As revealed from Figure 5.58A, the biomineralization of scaffolds by hMSCs were varied depending upon time period of culture as well as scaffold composition. A gradual increase in the extent of mineralization was observed with culture time for all the scaffolds. The intensity of stained calcium nodules was observed to be higher on SF/CMC/Cu_1-5%nBG compared to SF/CMC/$Cu_{0.5}$-5%nBG by day7. However, the intensity for calcium nodules was observed to be almost similar to the intensity observed on day 14. The quantitative ARS assay shows that biomineralization increases with time from day 7 to day 14. Figure 5.58B shows the optical density (OD) for SF/CMC/0.5Cu-5nBG and SF/CMC/1Cu-5nBG was significantly higher than that of SF/CMC/0%nBG and SF/CMC/5%nBG on day14. The higher degree of biomineralization on SF/CMC/Cu_1-5%nBG and SF/CMC/$Cu_{0.5}$-5%nBG may be due to the synergistic action of copper ions with other ionic dissolution products released from bioglass.

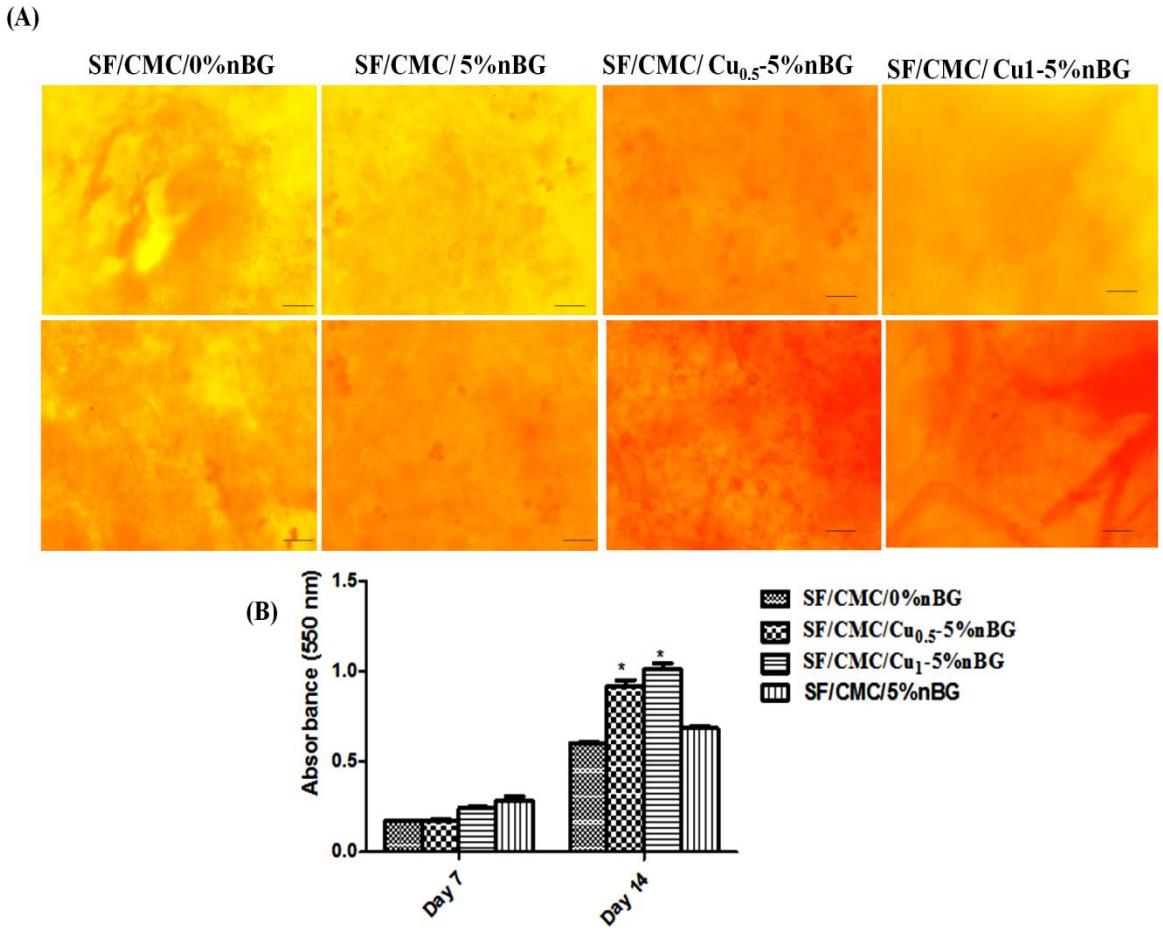

Figure 5.58: Showing the microscopic images of Alizarin red S staining of SF/CMC/0%nBG, SF/CMC/5%nBG, SF/CMC/$Cu_{0.5}$-5%nBG and SF/CMC/Cu_1-5%nBG nanofibrous scaffolds cultured for 14 days (A). Alizarin Red S staining assay for quantitative evaluation of mineralization on SF/CMC/0%nBG, SF/CMC/0.5Cu-5nBG and SF/CMC/1Cu-5nBG nanofibrous scaffolds after 14 days of culture. SF/CMC scaffold modified with Cu-nBG shows superior biomineralization as compared to other scaffolds due to its superior bioactivity potential. (Scale bar = 50 µm)

Osteogenic differentiation of hMSCs seeded on nanofibrous scaffold

Similar to the study in previous chapter, the immunocytochemistry for RUNX2 expression as shown in Figure 5.59A on the developed Cu-doped nanobioglass incorporated scaffolds was evaluated based on confocal microscopic. As co-localization of Runx2 and DAPI immunostainning shows that the expression of Runx2 was localized mostly to the cell nuclei. From confocal images and integrated density graph (Figure 5.59C) it has been observed that Runx2 expression was higher on SF/CMC/5%nBG, SF/CMC/$Cu_{0.5}$-5%nBG and SF/CMC/Cu_1-5%nBG composite scaffold on day 7 and 14 in comparison SF/CMC/0%nBG.

Furthermore, the expression of Runx2 was observed to be significantly higher on SF/CMC/5%nBG as compared of other set of scaffold while culture duration of 14 days. However, the florescence intensity was observed to be decreases by day 14 for the entire set of scaffold, this indicates the osteogenic differentiation of hMSCs seeded over the scaffold. Furthermore, the immunocytochemistry for OCN expression (Figure 5.59B) on the developed nanocomposite scaffold during 14 days culture period assessed by confocal microscopy study. OCN expression was observed to be significantly ($p<0.05$) higher on copper doped bioglass incorporated SF/CMC/$Cu_{0.5}$-5%nBG scaffold than the other scaffolds used under study on day 14. However, the expression of OCN over SF/CMC/5%nBG and SF/CMC/Cu_1-5%nBG was observed to be significantly higher ($p<0.05$) than SF/CMC/0%nBG on day 7 and 14.

The osteoblastic differentiation of hMSCs on the scaffolds was further assessed by RT-PCR for Runx2 and osteocalcin (OCN) gene expressions. On day 14 of culture, RT-PCR analysis shows insignificantly higher level of OCN expression on SF/CMC/$Cu_{0.5}$-5%nBG (Figure 5.59E) in comparison to SF/CMC/5%nBG and SF/CMC/Cu_1-5%nBG nanofibrous scaffolds respectively and significantly higher than SF/CMC/0%nBG. However, The Runx2 gene expression (Figure 5.59E) was observed to be significantly higher on SF/CMC/5%nBG, SF/CMC/$Cu_{0.5}$-5%nBG and SF/CMC/Cu_1-5%nBG in comparison of SF/CMC/0%nBG. Thus, copper doping at low level might not be sufficient to bring significant changes in osteogenic gene expression, however it might be useful to evaluate using culture media without adding osteogenic growth factors [325].

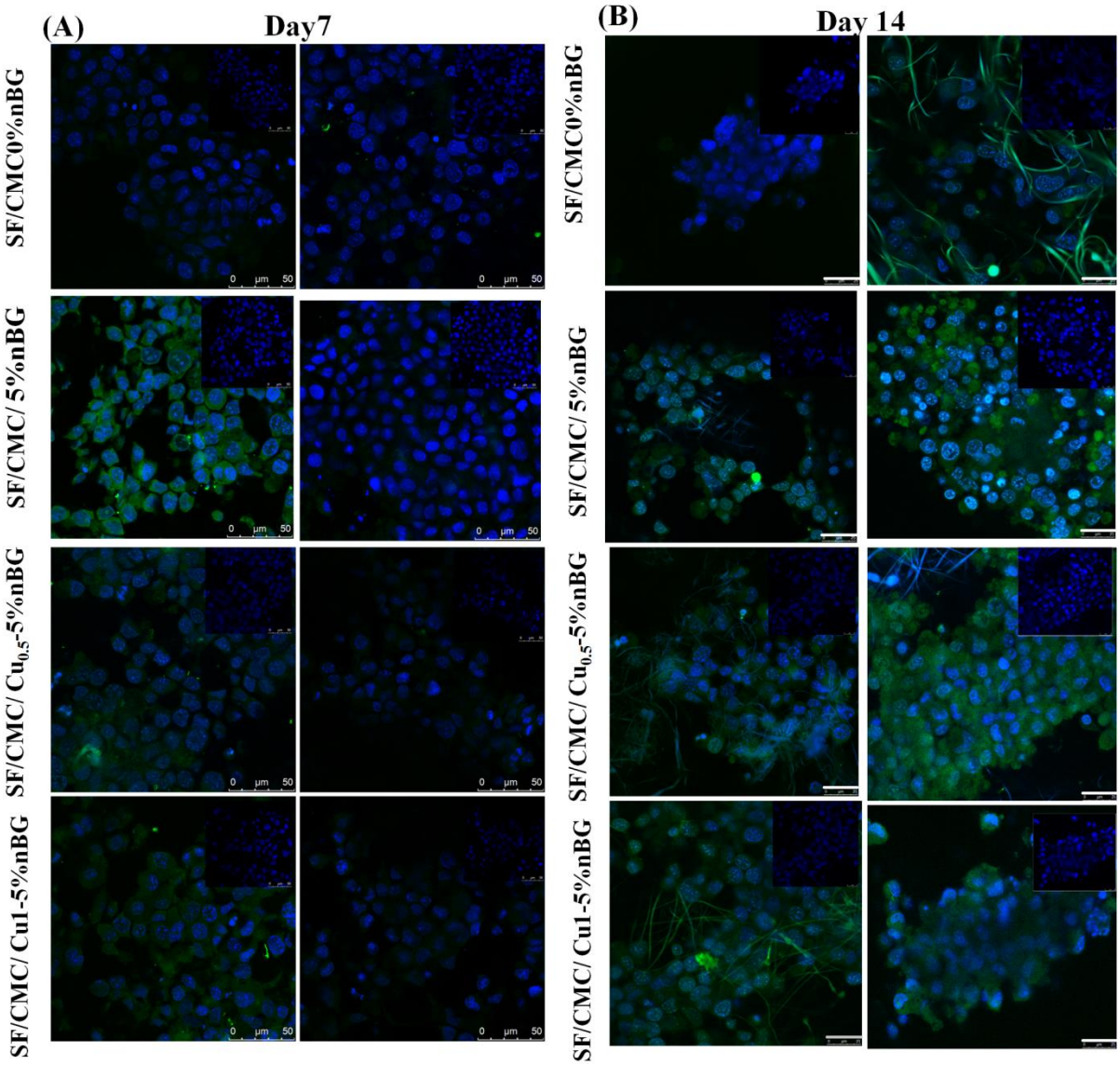
(A)
Day7
(B)
Day 14
SF/CMC0%nBG
SF/CMC/ 5%nBG
SF/CMC/ Cu0.5-5%nBG
SF/CMC/ Cu1-5%nBG
SF/CMC0%nBG
SF/CMC/ 5%nBG
SF/CMC/ Cu0.5-5%nBG
SF/CMC/ Cu1-5%nBG

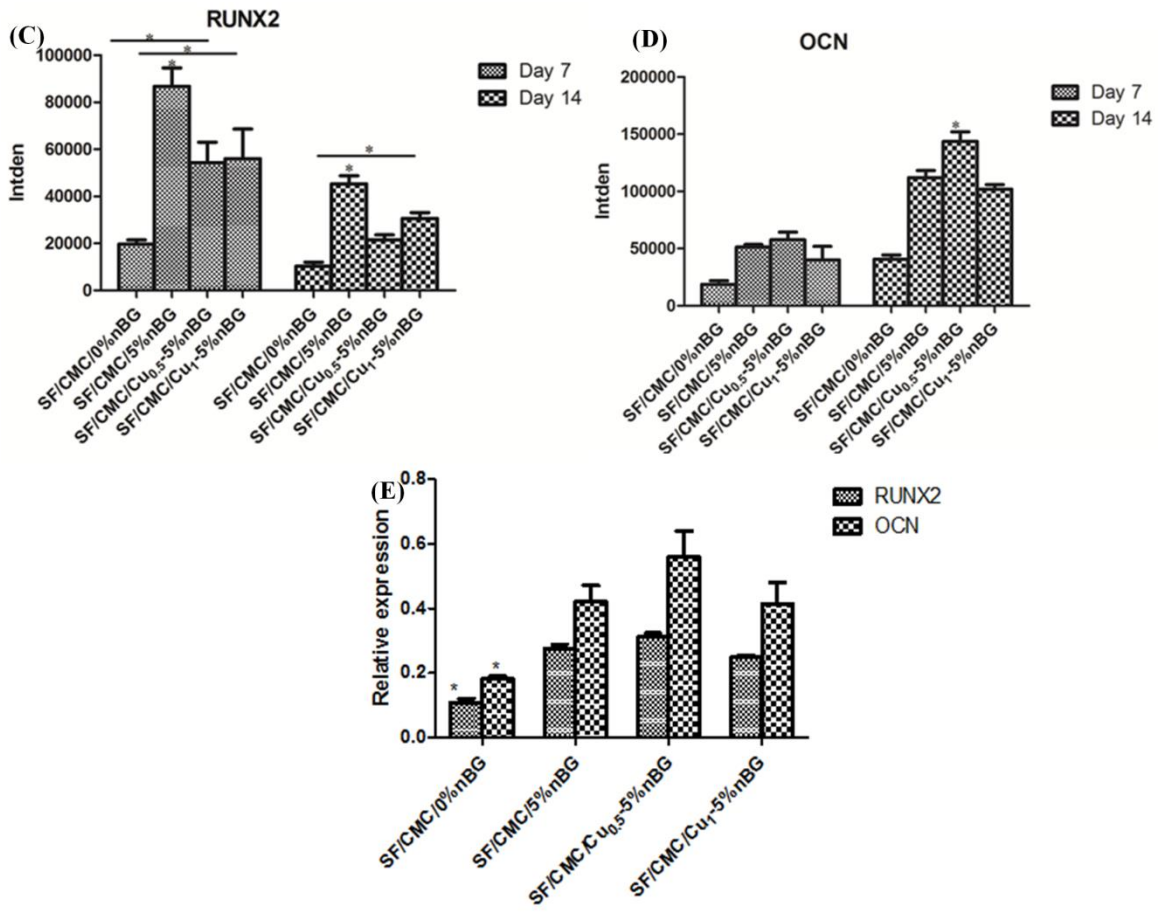

Figure 5.59: Immunocytochemistry for Runx2 and osteocalcin expression in hMSCs cultured on SF/CMC/0%nBG, SF/CMC/5%nBG, SF/CMC/$Cu_{0.5}$-5%nBG and SF/CMC/Cu_1-5%nBG scaffolds. Confocal images for Runx2 (Scale bar = 50 µm) (A) and osteocalcin expressions (Scale bar = 25 µm) (b) observed in hMSCs on day 7 and 14 in the osteogenic culture medium. Confocal images contain insets which represents distribution of cell nuclei stained with DAPI over the scaffold. Integrated density evaluation for RunX2 and osteocalcin were shown in graphs (C) and (D) respectively. (E) The osteogenic differentiation of hMSCs on the scaffolds was assessed by RT-PCR for Runx2 and osteocalcin expression after 14 days of culture

HIF-1α and VEGF expression analysis

The expression of hypoxia inducible factor was analysed by using confocal microscopy to determine the level of expression on various composite scaffolds developed in this study as shown in Figure 5.60. The expression of HIF-1α was observed to be higher over SF/CMC/Cu_1-5%nBG as compared of the entire scaffold on day 7. In comparison, the expression of HIF-1α by hMSCs seeded on SF/CMC/$Cu_{0.5}$-5%nBG and SF/CMC/Cu_1-5%nBG was significantly ($p < 0.05$) higher than SF/CMC/5%nBG and SF/CMC/0%nBG. Whereas, the expression level was decreased on both the scaffolds by 14th day of culture. Both on day 7 and 14, the expression of

HIF-1α was observed to be low on SF/CMC/0%nBG than SF/CMC/5%nBG. Furthermore, copper ion is reported to influence angiogenesis of bone tissue graft. The effect of release of copper ion from Cu-nBG on HIF-1α expression and VEGF secretion by hMSCs over developed composite scaffold was evaluated. The expression of HIF-1α was observed to be higher over SF/CMC/Cu_1-5%nBG as compared to other scaffold on day 7 due to higher copper ion release from Cu_1-nBG. The overall trend was observed to be SF/CMC/Cu_1-5%nBG > SF/CMC/$Cu_{0.5}$-5%nBG > SF/CMC/5%nBG > SF/CMC. This shows higher Cu ion releases from Cu_1-nBG than $Cu_{0.5}$-nBG, playing significant role in maintaining stable HIF-1α expression and higher VEGF expression by hMSCs [325]. Thus, it has been demonstrated that the release of copper ion from Cu-nBG plays significant role in expression of HIF-1α and the expression is dependent on the level of copper doping. Furthermore, nBG also trigger expression of HIF-1α but at low level thus this can be further enhanced by the doping of Cu^{2+} in nano-bioglass. However, Cu-nBG shows better stability of HIF-1α expression and maintained up to day 14 of culture, which will further augment VEGF expression thereby leading to superior angiogenic potential of SF/CMC/$Cu_{0.5}$-5%nBG and SF/CMC/Cu_1-5%nBG composite scaffolds [325].

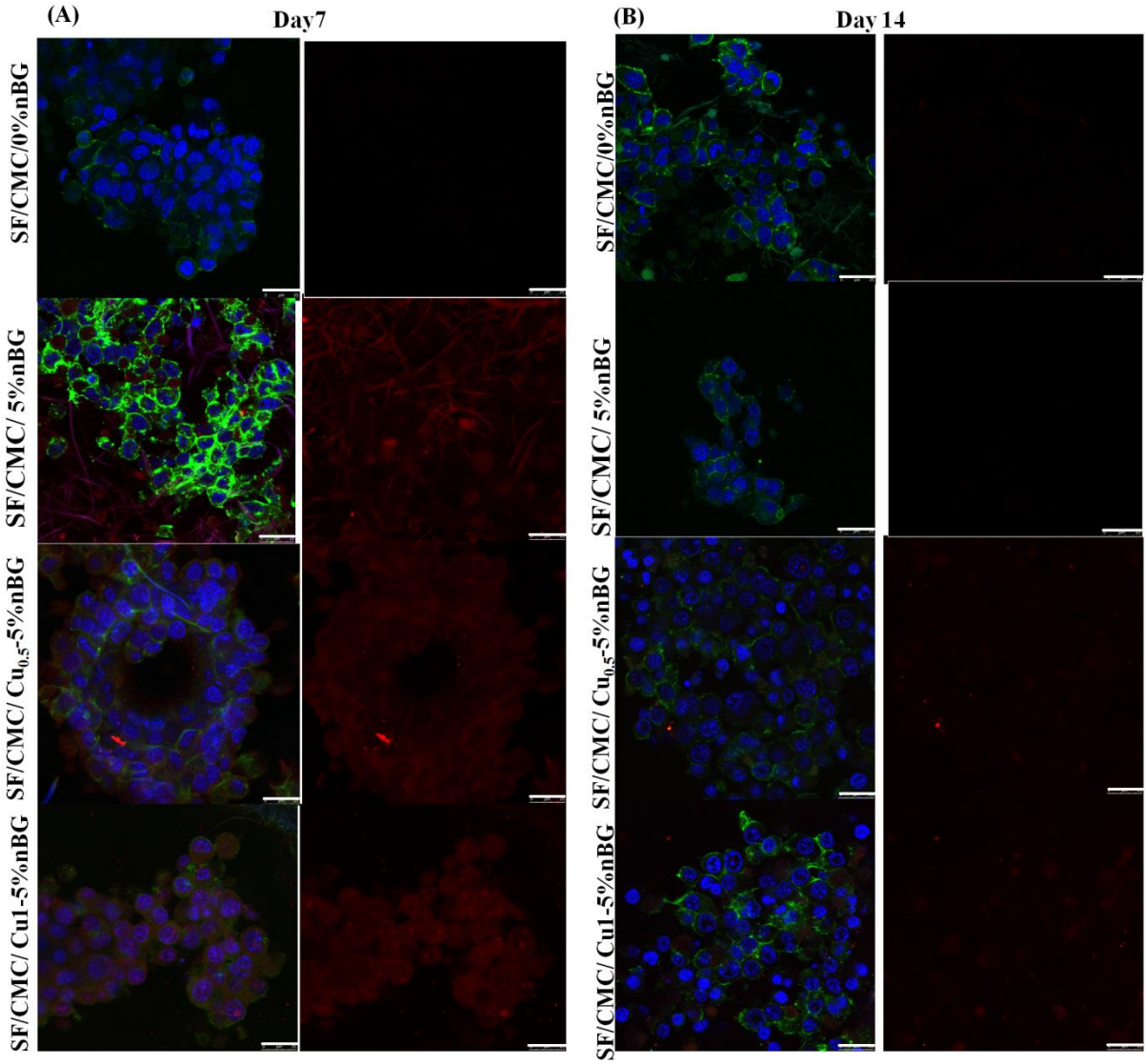

Figure 5.60: Confocal images for HIF-1α expression in hMSCs seeded on SF/CMC/0%nBG, SF/CMC/5%nBG, SF/CMC/$Cu_{0.5}$-5%nBG and SF/CMC/Cu_1-5%nBG nanofibrous nano composite scaffolds cultured for day 7 (A) and 14 (B). (Scale bar = 25 µm)

From the literature, it is evident that Cu^{2+} ions play important role not only in expression of HIF-1α, but also provides stability towards its expression, which further lead to the activation of VEGF expression. The study has revealed that the VEGF expression (Figure 5.61) in hMSCs on SF/CMC/Cu_1-5%nBG was 1.1 fold higher than SF/CMC/$Cu_{0.5}$-5%nBG. However, The VEGF expression over SF/CMC/Cu_1-5%nBG was observed to be 1.1, 1.65 and 1.9 folds higher than SF/CMC/$Cu_{0.5}$-5%nBG, SFCMC/5%nBG and SF/CMC/0%nBG respectively. Thus, copper doped bioglass incorporated composite nanofibrous scaffold is superior in terms of angiogenic potential as compared to composite scaffold incorporated with nano-bioglass.

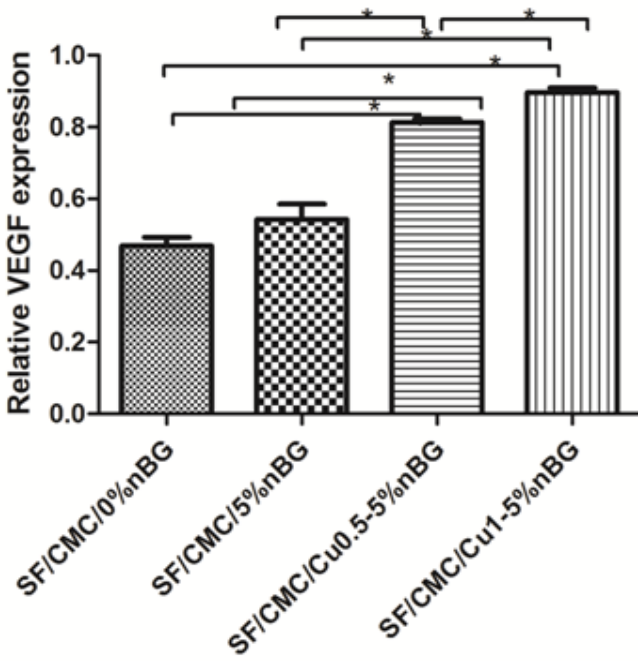

Figure 5.61: Relative VEGF expression in hMSCs seeded over SF/CMC/0%nBG, SF/CMC/5%nBG, SF/CMC/$Cu_{0.5}$-5%nBG and SF/CMC/Cu_1-5%nBG nanofibrous scaffolds during 7 days culture period. The study confirms that the copper doped bioglass incorporated composite nanofibrous scaffold is superior in terms of angiogenic potential as compared to composite scaffold incorporated with nano-bioglass.

Table 5.6: Comparison among the most potential scaffolds developed

Sl .No	Electrospun Scaffold	Average fiber diameter (nm)	Pore size (µm)	Tensile strength (MPa)	Contact angle (˚)	In-vitro Cell study
1.	SF/CMC blend scaffold	227.8 ± 87	4.7 ± 1.9	10.5 ± 1.3	57.4 ± 0.3	hMSCs, MTT, ALP, Alizarin red S assay, RT-PCR, Bone TE
2.	SF/CMC/10%nBG	589 ± 161	4.64	7.59 ± 1.23	52	hMSCs, MTT, ALP, Alizarin red S assay, RT-PCR, Bone TE
3.	SF/CMC/ Cu1-5%nBG	568.40 ± 172	4.62 ± 2.3	4.92 ± 0.14	56.28	hMSCs, MTT, ALP, Alizarin red S assay, RT-PCR, VEGF analysis, Bone TE

CHAPTER 6: Summary and Conclusion

Bone tissue engineering has emerged as an alternative promising approach for the repairing and/or replacing damaged and/or diseased bone tissue. In this technique, the design and development of bioactive functional scaffold with nanofibrous architecture from suitable biomaterial with desired properties like biocompatible, biodegradable, mechanical, surface and bone matrix formation ability is the key challenge to provide a suitable platform for the bone tissue regeneration. Silk fibron (SF) derived from Bombyx Mori silk cocoon is a potential biomaterial having various superior scaffold properties, however, use of SF alone cannot meet all the desirable properties required for bone tissue regeneration due to its poor bioactivity, lack of hydrophilicity, flexibility and osteoconductive property. In this context, the blending of SF with CMC seems to be an attractive biomaterial that can overcome many of the limitations associated with SF.

Besides material property, fabrication of scaffold with nanofiber architecture is another important aspect, which can mimic the body tissue and provide higher surface area. In this context, electrospinning has been evolved as the most suitable method for the generation of polymer nanofibers so far.

Therefore, the research in this dissertation work has been focussed on the development of novel SF/CMC based electrospun nanofibrous scaffolds for bone tissue engineering applications.

The most encouraging results achieved from this research is summarized as follows-

I. In the first phase of dissertation work, attempt has been given to develop SF/CMC blend nanofibrous scaffold by free liquid surface electrospinning process. The SF/CMC blend nanofibrous scaffolds were prepared by electrospinning with varied compositions of SF/CMC (100/0, 99/1, 98/2 and 97/3 (w/w)) blend solutions. The fabricated electrospun nanofibrous scaffolds were cross-linked with 3wt% EDC-NHS and calcified with 0.1M $CaCl_2$ solution. Significant improvement in various physico-chemical, mechanical and biological properties in comparison to the pure SF nanofibrous scaffold was achieved by blending of SF and CMC. Among the various blends, SF/CMC with blend ratio of 98:2w/w (SF/CMC_2) was found to be the most potential, possessing a set of superior

scaffold properties in comparison to pure SF scaffold. The scaffolds were characterized for morphological (SEM, AFM), structural (XRD, FT-IR), surface property (% water uptake and contact angle measurement), surface roughness (AFM) bioactivity (SBF treatment, ARS) and mechanical strength. The average fiber diameter of the blend scaffold was measured to be 227.8±87 nm. The scaffold exhibited improved water uptake capacity, hydrophilicity, surface roughness and bioactivity as compared to pure *Bombyx mori* SF. The tensile strength of SF (12.7±1.5 MPa) scaffold was slightly reduced by the addition of CMC. However, the scaffolds still possess sufficient strength (10.54±1.3 MPa) which can support many types of bone tissue regeneration. Whereas, the tensile strain at break of blend scaffold (18.37 ± 3.8 %) was significantly higher than SF (8.36 ± 3.3%) scaffold, which signifies its ability to facilitate cell penetration within the matrix. In vitro cell culture study has confirmed the cell supportive property of the scaffold as evident from cell attachment, cell proliferation, cell penetration and cellular metabolic activity of hMSCs derived from umbilical cord blood over the scaffold. The developed SF/CMC_2 scaffold further possess good osteogenic property as confirmed by ALP activity, biomineralization ability, GAG secretion, osteocalcin, Runx2 and collagen type1 expression. Thus, the developed SF/CMC_2 blend scaffold was selected for the further study.

II. In this phase of work, nano-bioglass and copper doped nano-bioglass were successfully prepared following sol-gel method with the expectation that the incorporation of these components will make the developed SF/CMC2 scaffold more potential by improving its bioactivity, osteogenic and angiogenic property, which are important aspects for bone tissue regeneration. The synthesised nano-bioglass and Cu2+ doped nano bioglass were characterized to assess their morphological, structural and physical properties. The developed nano-bioglass with and without copper doping were in nano size ≤ 100nm as revealed from FESEM and TEM analysis. Moreover, XRD and TEM (SAED) analysis further confirm their amorphous nature. The in-vitro bioactivity analysis by soaking in SBF, shows apatite forming ability of nano-bioglass with and without copper, which was further confirmed by FESEM, TEM (SAED), XRD and FT-IR analysis. The ion release from nano-bioglass with and without copper in SBF was measured through inductively coupled plasma atomic emission spectrophotometer **(**ICP-OES). ICP-OES analysis has shown the faster dissolution rate of copper doped nano-bioglass that resulted into release of calcium ion at higher level, which further augmented the apatite deposition over the

bioglass surfaces. The developed nano-bioglass with and without copper doping were used to develop SF/CMC composite scaffold.

III. Efforts have been given in this part of research work to improve the osteogenic potential of the developed SF/CMC_2 blend scaffold by incorporating nanobioglass (5-20 w/w%) that resulted in SF/CMC/nBG composite scaffolds with varying composition. The developed composite scaffolds were designated as SF/CMC/5%nBG, SF/CMC/10%nBG and SF/CMC/20%nBG. The developed composite scaffolds have shown increased average fiber diameter (233 ± 83 nm to 594 ± 157 nm), average pore size (4.5 ± 1.65 to 5.4 ± 1.7 µm), hydrophilicity (57° to 52° (contact angle)), surface roughness (0.101 to 0.309 µm), apatite forming ability and degradation (48.28 to 56.23 %) with increase in nano-bioglass content from 0 to 20 wt%. The improvement in pore size, hydrophilicity and surface roughness will augment cell supportive property of developed nano-bioglass incorporated SF/CMC composite scaffold.

Furthermore, among the SF/CMC/nBG scaffolds, SF/CMC/10%nBG exhibited superior tensile strength of 7.591 ± 1.23 MPa and tensile strain at break of 9.62 ± 0.85% as well as other properties such as hydrophilicity (52°), surface roughness (0.291 µm) and biodegradation (59.24 %). The *in-vitro* cell study over SF/CMC/10%nBG has shown significantly higher biocompatibility, GAG deposition and cell spreading through protrusion of filopodia to attain polygonal osteoblast like morphology than the other scaffolds. Moreover, hMSCs cultured over SF/CMC/10%nBG shows significantly higher ALP activity, biomineralization and gene expression for osteocalcin and collagen type I. Hence, SF/CMC/10nBG composite scaffold is proven to provide better osteogenic platform for hMSCs.

Besides osteogenic, angiogenic property of the engineered scaffold is another important factor which makes scaffold suitable for bone tissue regeneration. Therefore, in this phase of research work, effort has been given to improve the angiogenic property of SF/CMC/nBG composite scaffolds by incorporating Cu^{2+} ion in the form of Cu^{2+} doped nano bioglass prepared in the Chapter 5B. Various batches of copper doped nano-bioglass incorporated SF/CMC composite nanofibrous scaffolds (SF/CMC/$Cu_{0.5}$-5%nBG, SF/CMC/$Cu_{0.5}$-10%nBG, SF/CMC/Cu_1-5%nBG and SF/CMC/Cu_1-10%nBG) were prepared. Among the scaffolds with varied compositions, SF/CMC/Cu_1-5%nBG exhibited

superior osteogenic and angiogenic property. Though a slightly higher OCN expression was observed over SF/CMC/$Cu_{0.5}$-5%nBG composite scaffold than SF/CMC/Cu_1-5%nBG, the difference in the expression was not statistically significant. This signifies that osteogenic potential of both the composite scaffold is comparable.

Moreover, the angiogenic potential of the developed scaffold was analysed in terms of HIF-1α and VEGF expression. The developed SF/CMC/Cu_1-5%nBG shows higher angiogenic potential than SF/CMC/0.5Cu-5%nBG as evident from HIF-1α and VEGF expression. The VEGF expression by hMSCs over SF/CMC/Cu_1-5%nBG was observed to be 1.1, 1.65 and 1.9 folds higher than SF/CMC/$Cu_{0.5}$-5%nBG, SFCMC/5%nBG and SF/CMC/0%nBG respectively. Thus the developed composite scaffold incorporated with 5% Cu_1-nBG proved to be suitable candidate for bone tissue engineering and needs to be further assessed through *in-vivo* studies

Overall, in this dissertation work, a novel electrospun silk fibroin/carboxymethyl cellulose (SF/CMC) blend nanofibrous scaffold was developed which is proven to be a good substrate for bone tissue engineering application. The surface, bioactivity and osteogenic property of the scaffold was further augmented by the incorporation of nano-bioglass into the scaffold matrix which resulted in SF/CMC/nBG nano composite scaffold which prompted the recruitment and differentiation of mesenchymal stem cells derived from Umbilical Cord blood to osteogenic lineage. The angiogenic property of the developed scaffold was further improved by adding Cu^{2+} doped nano bioglass thereby novel SF/CMC/Cu_1-5%nBG was developed. In conclusion, the results demonstrated that the developed SF/CMC blend scaffold can be a potential base polymeric scaffold for tissue engineering application including bone tissue regeneration. Furthermore, electronspun nanofibrous SF/CMC/Cu_1-5%nBG nanocomposite scaffold developed in this study may provide an excellent platform for future bone tissue regeneration.

IV. Suggested Future Work

The following research work are suggested for future study with the developed composite scaffolds-

i. Detail *in-vivo* animal study can be undertaken for assessing its suitability for possible future clinical application.

ii. Three dimensional scaffolds with appropriate design and structure may be fabricated by adopting advanced scaffold fabrication technique like rapid prototyping technique.

iii. Research may be undertaken to develop aqueous based composite scaffolds rather than organic solvent to avoid risk of toxicity.

Electrospun nanofibrous scaffold possess suitable nano-architecture which mimics natural extracellular matrix of collagen fiber (50 – 500 nm). However, it is difficult to fabricate and achieve a 3D design of the scaffold with appropriate geometry and controlled pore size using electrospinning technique. In this context, RP technique is attractive and therefore, effort may be given to fabricate scaffold using rapid prototyping (RP) technique.

References

[1] V.C. Mow, R. Huiskes, Basic orthopaedic biomechanics & mechano-biology, Lippincott Williams & Wilkins2005.
[2] B.K. Timby, N.E. Smith, Introductory medical-surgical nursing, Lippincott Williams & Wilkins2013.
[3] A.R. Costa-Pinto, R.L. Reis, N.M. Neves, Scaffolds based bone tissue engineering: the role of chitosan, Tissue Engineering Part B: Reviews 17(5) (2011) 331-347.
[4] T.W. Bauer, G.F. Muschler, Bone Graft Materials: An Overview of the Basic Science, Clinical orthopaedics and related research 371 (2000) 10-27.
[5] K.C. Popat, L. Leoni, C.A. Grimes, T.A. Desai, Influence of engineered titania nanotubular surfaces on bone cells, Biomaterials 28(21) (2007) 3188-3197.
[6] A. Oryan, S. Alidadi, A. Moshiri, N. Maffulli, Bone regenerative medicine: classic options, novel strategies, and future directions, Journal of orthopaedic surgery and research 9(1) (2014) 1.
[7] G. Manivasagam, D. Dhinasekaran, A. Rajamanickam, Biomedical implants: Corrosion and its prevention-a review, Recent Patents on Corrosion Science 2(1) (2010) 40-54.
[8] L.G. Griffith, G. Naughton, Tissue engineering--current challenges and expanding opportunities, Science 295(5557) (2002) 1009-1014.
[9] K. Leong, C. Cheah, C. Chua, Solid freeform fabrication of three-dimensional scaffolds for engineering replacement tissues and organs, Biomaterials 24(13) (2003) 2363-2378.
[10] P.X. Ma, J. Elisseeff, Scaffolding in tissue engineering, CRC press2005.
[11] D.S. Katti, R. Vasita, K. Shanmugam, Improved biomaterials for tissue engineering applications: surface modification of polymers, Current topics in medicinal chemistry 8(4) (2008) 341-353.
[12] J.-H. Jang, O. Castano, H.-W. Kim, Electrospun materials as potential platforms for bone tissue engineering, Advanced drug delivery reviews 61(12) (2009) 1065-1083.
[13] Y. Cao, B. Wang, Biodegradation of silk biomaterials, International journal of molecular sciences 10(4) (2009) 1514-1524.
[14] C. Vepari, D.L. Kaplan, Silk as a biomaterial, Progress in polymer science 32(8) (2007) 991-1007.
[15] N. Kasoju, U. Bora, Silk fibroin based biomimetic artificial extracellular matrix for hepatic tissue engineering applications, Biomedical Materials 7(4) (2012) 045004.
[16] J. Zhao, Z. Zhang, S. Wang, X. Sun, X. Zhang, J. Chen, D.L. Kaplan, X. Jiang, Apatite-coated silk fibroin scaffolds to healing mandibular border defects in canines, Bone 45(3) (2009) 517-527.
[17] S. Wang, Y. Zhang, H. Wang, G. Yin, Z. Dong, Fabrication and properties of the electrospun polylactide/silk fibroin-gelatin composite tubular scaffold, Biomacromolecules 10(8) (2009) 2240-2244.

[18] Y. Gui-Bo, Z. You-Zhu, W. Shu-Dong, S. De-Bing, D. Zhi-Hui, F. Wei-Guo, Study of the electrospun PLA/silk fibroin-gelatin composite nanofibrous scaffold for tissue engineering, Journal of Biomedical Materials Research Part A 93(1) (2010) 158-163.
[19] N. Bhardwaj, S.C. Kundu, Silk fibroin protein and chitosan polyelectrolyte complex porous scaffolds for tissue engineering applications, Carbohydrate Polymers 85(2) (2011) 325-333.
[20] K. Sun, H. Li, R. Li, Z. Nian, D. Li, C. Xu, Silk fibroin/collagen and silk fibroin/chitosan blended three-dimensional scaffolds for tissue engineering, European Journal of Orthopaedic Surgery & Traumatology 25(2) (2015) 243-249.
[21] S. Van Vlierberghe, P. Dubruel, E. Schacht, Biopolymer-based hydrogels as scaffolds for tissue engineering applications: a review, Biomacromolecules 12(5) (2011) 1387-1408.
[22] M. Märtson, J. Viljanto, T. Hurme, P. Laippala, P. Saukko, Is cellulose sponge degradable or stable as implantation material? An in vivo subcutaneous study in the rat, Biomaterials 20(21) (1999) 1989-1995.
[23] J. Liuyun, L. Yubao, X. Chengdong, Preparation and biological properties of a novel composite scaffold of nano-hydroxyapatite/chitosan/carboxymethyl cellulose for bone tissue engineering, J Biomed Sci 16 (2009) 65.
[24] E. Entcheva, H. Bien, L. Yin, C.-Y. Chung, M. Farrell, Y. Kostov, Functional cardiac cell constructs on cellulose-based scaffolding, Biomaterials 25(26) (2004) 5753-5762.
[25] Y. Kino, M. Sawa, S. Kasai, M. Mito, Multiporous cellulose microcarrier for the development of a hybrid artificial liver using isolated hepatocytes, Journal of Surgical Research 79(1) (1998) 71-76.
[26] R. Langer, J. Vacanti, engenharia do Tecido, Ciência 260 (1993) 920-6.
[27] M.S. Chapekar, Tissue engineering: challenges and opportunities, Journal of biomedical materials research 53(6) (2000) 617-620.
[28] M.B. Prakash, M.K. Nag, A. Mohammed, K. Bhargavi, M.S. Ram, R. Rajkumar, Poly (ε-caprolactone) PCL Scaffolds Preparation and characterization for tissue engineering.
[29] Y.-M. Lee, Y.-J. Park, S.-J. Lee, Y. Ku, S.-B. Han, P.R. Klokkevold, S.-M. Choi, C.-P. Chung, Tissue engineered bone formation using chitosan/tricalcium phosphate sponges, Journal of periodontology 71(3) (2000) 410-417.
[30] S. Moeinzadeh, D. Barati, S.K. Sarvestani, T. Karimi, E. Jabbari, Experimental and Computational Investigation of the Effect of Hydrophobicity on Aggregation and Osteoinductive Potential of BMP-2-Derived Peptide in a Hydrogel Matrix, Tissue Engineering Part A 21(1-2) (2014) 134-146.
[31] A. Di Martino, M. Sittinger, M.V. Risbud, Chitosan: a versatile biopolymer for orthopaedic tissue-engineering, Biomaterials 26(30) (2005) 5983-5990.
[32] K.Y. Ching, O.G. Andriotis, S. Li, P. Basnett, B. Su, I. Roy, R.S. Tare, B.G. Sengers, M. Stolz, Nanofibrous poly (3-hydroxybutyrate)/poly (3-hydroxyoctanoate) scaffolds provide a functional

microenvironment for cartilage repair, Journal of biomaterials applications (2016) 0885328216639749.
[33] L. Ma, C. Gao, Z. Mao, J. Zhou, J. Shen, X. Hu, C. Han, Collagen/chitosan porous scaffolds with improved biostability for skin tissue engineering, Biomaterials 24(26) (2003) 4833-4841.
[34] S. Sahoo, S.L. Toh, J.C. Goh, A bFGF-releasing silk/PLGA-based biohybrid scaffold for ligament/tendon tissue engineering using mesenchymal progenitor cells, Biomaterials 31(11) (2010) 2990-2998.
[35] F. Yang, R. Murugan, S. Wang, S. Ramakrishna, Electrospinning of nano/micro scale poly (L-lactic acid) aligned fibers and their potential in neural tissue engineering, Biomaterials 26(15) (2005) 2603-2610.
[36] M. Dvir-Ginzberg, I. Gamlieli-Bonshtein, R. Agbaria, S. Cohen, Liver tissue engineering within alginate scaffolds: effects of cell-seeding density on hepatocyte viability, morphology, and function, Tissue engineering 9(4) (2003) 757-766.
[37] A. Mol, M.I. van Lieshout, C.G. Dam-de Veen, S. Neuenschwander, S.P. Hoerstrup, F.P. Baaijens, C.V. Bouten, Fibrin as a cell carrier in cardiovascular tissue engineering applications, Biomaterials 26(16) (2005) 3113-3121.
[38] S.A. Riboldi, M. Sampaolesi, P. Neuenschwander, G. Cossu, S. Mantero, Electrospun degradable polyesterurethane membranes: potential scaffolds for skeletal muscle tissue engineering, Biomaterials 26(22) (2005) 4606-4615.
[39] L. Labusca, M. O'Brien, K. Mashayekhi, A clinical perspective to mesenchymal stem cell-based musculoskeletal regeneration, OA Musculoskeletal Medicine 1(1) (2013) 8-13.
[40] K. Ikeda, A. Ito, M. Sato, S. Kanno, Y. Kawabe, M. Kamihira, Effects of heat stimulation and l-ascorbic acid 2-phosphate supplementation on myogenic differentiation of artificial skeletal muscle tissue constructs, Journal of tissue engineering and regenerative medicine (2015).
[41] M.K. Gunnewiek, A. Di Luca, H.Z. Bollemaat, C.A. van Blitterswijk, G.J. Vancso, L. Moroni, E.M. Benetti, Creeping Proteins in Microporous Structures: Polymer Brush-Assisted Fabrication of 3D Gradients for Tissue Engineering, Advanced healthcare materials 4(8) (2015) 1169-1174.
[42] C. Agrawal, R.B. Ray, Biodegradable polymeric scaffolds for musculoskeletal tissue engineering, Journal of biomedical materials research 55(2) (2001) 141-150.
[43] B. Brown, K. Lindberg, J. Reing, D.B. Stolz, S.F. Badylak, The basement membrane component of biologic scaffolds derived from extracellular matrix, Tissue engineering 12(3) (2006) 519-526.
[44] T.L. Sellaro, A.K. Ravindra, D.B. Stolz, S.F. Badylak, Maintenance of hepatic sinusoidal endothelial cell phenotype in vitro using organ-specific extracellular matrix scaffolds, Tissue engineering 13(9) (2007) 2301-2310.
[45] P. Fratzl, H. Gupta, E. Paschalis, P. Roschger, Structure and mechanical quality of the collagen–mineral nano-composite in bone, Journal of materials chemistry 14(14) (2004) 2115-2123.

[46] T. Jiang, S.P. Nukavarapu, M. Deng, E. Jabbarzadeh, M.D. Kofron, S.B. Doty, W.I. Abdel-Fattah, C.T. Laurencin, Chitosan–poly (lactide-co-glycolide) microsphere-based scaffolds for bone tissue engineering: In vitro degradation and in vivo bone regeneration studies, Acta biomaterialia 6(9) (2010) 3457-3470.

[47] C.M. Murphy, M.G. Haugh, F.J. O'Brien, The effect of mean pore size on cell attachment, proliferation and migration in collagen–glycosaminoglycan scaffolds for bone tissue engineering, Biomaterials 31(3) (2010) 461-466.

[48] H.-I. Chang, Y. Wang, Cell responses to surface and architecture of tissue engineering scaffolds, INTECH Open Access Publisher2011.

[49] S. Hulbert, F. Young, R. Mathews, J. Klawitter, C. Talbert, F. Stelling, Potential of ceramic materials as permanently implantable skeletal prostheses, Journal of biomedical materials research 4(3) (1970) 433-456.

[50] J. Klawitter, J. Bagwell, A. Weinstein, B. Sauer, J. Pruitt, An evaluation of bone growth into porous high density polyethylene, Journal of biomedical materials research 10(2) (1976) 311-323.

[51] I.V. Yannas, Tissue and organ regeneration in adults, Springer2015.

[52] I. Yannas, E. Lee, D. Orgill, E. Skrabut, G. Murphy, Synthesis and characterization of a model extracellular matrix that induces partial regeneration of adult mammalian skin, Proceedings of the National Academy of Sciences 86(3) (1989) 933-937.

[53] A.J. Salgado, O.P. Coutinho, R.L. Reis, Bone tissue engineering: state of the art and future trends, Macromolecular bioscience 4(8) (2004) 743-765.

[54] D.W. Hutmacher, Scaffolds in tissue engineering bone and cartilage, Biomaterials 21(24) (2000) 2529-2543.

[55] G. Marino, F. Rosso, G. Cafiero, C. Tortora, M. Moraci, M. Barbarisi, A. Barbarisi, β-Tricalcium phosphate 3D scaffold promote alone osteogenic differentiation of human adipose stem cells: in vitro study, Journal of Materials Science: Materials in Medicine 21(1) (2010) 353-363.

[56] R. Emadi, F. Tavangarian, S.R. Esfahani, Biodegradable and bioactive properties of a novel bone scaffold coated with nanocrystalline bioactive glass for bone tissue engineering, Materials letters 64(13) (2010) 1528-1531.

[57] S.A. Goldstein, P.V. Patil, M.R. Moalli, Perspectives on tissue engineering of bone, Clinical orthopaedics and related research 367 (1999) S419-S423.

[58] R.M. Day, A.R. Boccaccini, S. Shurey, J.A. Roether, A. Forbes, L.L. Hench, S.M. Gabe, Assessment of polyglycolic acid mesh and bioactive glass for soft-tissue engineering scaffolds, Biomaterials 25(27) (2004) 5857-5866.

[59] A. Remuzzi, S. Mantero, M. Colombo, M. Morigi, E. Binda, D. Camozzi, B. Imberti, Vascular smooth muscle cells on hyaluronic acid: culture and mechanical characterization of an engineered vascular construct, Tissue engineering 10(5-6) (2004) 699-710.

[60] C. Rodrigues, P. Serricella, A. Linhares, R. Guerdes, R. Borojevic, M. Rossi, M. Duarte, M. Farina, Characterization of a bovine collagen–hydroxyapatite composite scaffold for bone tissue engineering, Biomaterials 24(27) (2003) 4987-4997.
[61] W. Thein-Han, R. Misra, Biomimetic chitosan–nanohydroxyapatite composite scaffolds for bone tissue engineering, Acta biomaterialia 5(4) (2009) 1182-1197.
[62] P. Agarwal, P. Mishra, P. Srivastava, Statistical optimization of the electrospinning process for chitosan/polylactide nanofabrication using response surface methodology, Journal of Materials Science 47(10) (2012) 4262-4269.
[63] C. Li, C. Vepari, H.-J. Jin, H.J. Kim, D.L. Kaplan, Electrospun silk-BMP-2 scaffolds for bone tissue engineering, Biomaterials 27(16) (2006) 3115-3124.
[64] S. Midha, S. Murab, S. Ghosh, Osteogenic signaling on silk-based matrices, Biomaterials 97 (2016) 133-153.
[65] M. Barbosa, P. Granja, C. Barrias, I. Amaral, Polysaccharides as scaffolds for bone regeneration, Itbm-Rbm 26(3) (2005) 212-217.
[66] Y. Zhang, H. Ouyang, C.T. Lim, S. Ramakrishna, Z.M. Huang, Electrospinning of gelatin fibers and gelatin/PCL composite fibrous scaffolds, Journal of Biomedical Materials Research Part B: Applied Biomaterials 72(1) (2005) 156-165.
[67] D. Singh, A. Tripathi, S. Zo, D. Singh, S.S. Han, Synthesis of composite gelatin-hyaluronic acid-alginate porous scaffold and evaluation for in vitro stem cell growth and in vivo tissue integration, Colloids and Surfaces B: Biointerfaces 116 (2014) 502-509.
[68] P.A. Gunatillake, R. Adhikari, Biodegradable synthetic polymers for tissue engineering, Eur Cell Mater 5(1) (2003) 1-16.
[69] S. Srivastava, A. Chakraborty, R. Salunke, P. Roy, Development of a novel polygalacturonic acid-gelatin blend scaffold fabrication and biocompatibility studies for tissue-engineering applications, International Journal of Polymeric Materials 61(9) (2012) 679-698.
[70] H. Maachou, K. Bal, Y. Bal, A. Chagnes, G. Cote, D. Alliouche, Characterization and in vitro bioactivity of chitosan/hydroxyapatite composite membrane prepared by freeze-gelation method, Trends Biomater Artif Organs 22(1) (2008) 15-24.
[71] H. Cao, N. Kuboyama, A biodegradable porous composite scaffold of PGA/β-TCP for bone tissue engineering, Bone 46(2) (2010) 386-395.
[72] Y. Yin, F. Ye, J. Cui, F. Zhang, X. Li, K. Yao, Preparation and characterization of macroporous chitosan–gelatin/β-tricalcium phosphate composite scaffolds for bone tissue engineering, Journal of Biomedical Materials Research Part A 67(3) (2003) 844-855.
[73] C.-P. SCAFFOLD, Development of a collagen calcium-phosphate scaffold as a novel bone graft substitute, Medicine Meets Engineering: Proceedings of the 2nd Conference on Applied Biomechanics, Regensburg, IOS Press, 2008, p. 11.

[74] M.N. Rahaman, X. Liu, B.S. Bal, D.E. Day, L. Bi, L.F. Bonewald, Bioactive glass in bone tissue engineering, Biomaterials Science: Processing, Properties and Applications II: Ceramic Transactions, Volume 237 (2012) 73-82.
[75] L. Zhao, J. Chang, Preparation and characterization of macroporous chitosan/wollastonite composite scaffolds for tissue engineering, Journal of Materials Science: Materials in Medicine 15(5) (2004) 625-629.
[76] R. Jayasree, T.S. Kumar, Acrylic cement formulations modified with calcium deficient apatite nanoparticles for orthopaedic applications, Journal of Composite Materials 49(23) (2015) 2921-2933.
[77] H. Aoki, Medical applications of hydroxyapatite, Ishiyaku EuroAmerica, Incorporated1994.
[78] M. Bailey, S. Coe, D. Grant, G. Grime, C. Jeynes, Accurate determination of the Ca: P ratio in rough hydroxyapatite samples by SEM-EDS, PIXE and RBS—a comparative study, X-Ray Spectrometry 38(4) (2009) 343-347.
[79] M.M. Pereira, L.L. Hench, Mechanisms of hydroxyapatite formation on porous gel-silica substrates, Journal of Sol-Gel Science and Technology 7(1-2) (1996) 59-68.
[80] P. De Aza, A. De Aza, S. De Aza, Crystalline bioceramic materials, Bol. Soc. Esp. Ceram 44(3) (2005) 135-145.
[81] L.L. Hench, The story of Bioglass®, Journal of Materials Science: Materials in Medicine 17(11) (2006) 967-978.
[82] L.L. Hench, R.J. Splinter, W. Allen, T. Greenlee, Bonding mechanisms at the interface of ceramic prosthetic materials, Journal of biomedical materials research 5(6) (1971) 117-141.
[83] L.L. Hench, J.M. Polak, Third-generation biomedical materials, Science 295(5557) (2002) 1014-1017.
[84] B. Subia, J. Kundu, S. Kundu, Biomaterial scaffold fabrication techniques for potential tissue engineering applications, INTECH Open Access Publisher2010.
[85] B.B. Mandal, S.C. Kundu, Non-bioengineered silk gland fibroin protein: Characterization and evaluation of matrices for potential tissue engineering applications, Biotechnology and bioengineering 100(6) (2008) 1237-1250.
[86] D. Sin, X. Miao, G. Liu, F. Wei, G. Chadwick, C. Yan, T. Friis, Polyurethane (PU) scaffolds prepared by solvent casting/particulate leaching (SCPL) combined with centrifugation, Materials Science and Engineering: C 30(1) (2010) 78-85.
[87] N. Zhu, X. Chen, Biofabrication of tissue scaffolds, INTECH Open Access Publisher2013.
[88] T. Lu, Y. Li, T. Chen, Techniques for fabrication and construction of three-dimensional scaffolds for tissue engineering, International journal of nanomedicine 8 (2013) 337.
[89] Z. Xiang, R. Liao, M.S. Kelly, M. Spector, Collagen-GAG scaffolds grafted onto myocardial infarcts in a rat model: a delivery vehicle for mesenchymal stem cells, Tissue engineering 12(9) (2006) 2467-2478.

[90] J. Mano, Silva gA, Azevedo HS, Malafaya PB, Sousa RA, Silva SS, et al. Natural origin biodegradable systems in tissue engineering and regenerative medicine: present status and some moving trends, Journal of The Royal Society Interface 4(17) (2007) 999-1030.
[91] S. Zhang, Fabrication of novel biomaterials through molecular self-assembly, Nature biotechnology 21(10) (2003) 1171-1178.
[92] D. Liang, B.S. Hsiao, B. Chu, Functional electrospun nanofibrous scaffolds for biomedical applications, Advanced drug delivery reviews 59(14) (2007) 1392-1412.
[93] L.A. Smith, J.A. Beck, P.X. Ma, Nanofibrous scaffolds and their biological effects, Nanotechnologies for the Life Sciences (2006).
[94] D.W. Hutmacher, Scaffold design and fabrication technologies for engineering tissues—state of the art and future perspectives, Journal of Biomaterials Science, Polymer Edition 12(1) (2001) 107-124.
[95] G. Chen, T. Ushida, T. Tateishi, Development of biodegradable porous scaffolds for tissue engineering, Materials Science and Engineering: C 17(1) (2001) 63-69.
[96] D. Mooney, C. Mazzoni, C. Breuer, K. McNamara, D. Hern, J. Vacanti, R. Langer, Stabilized polyglycolic acid fibre-based tubes for tissue engineering, Biomaterials 17(2) (1996) 115-124.
[97] R. Thomson, M. Wake, M.J. Yaszemski, A. Mikos, Biodegradable polymer scaffolds to regenerate organs, Biopolymers Ii, Springer1995, pp. 245-274.
[98] R.C. Thomson, M.J. Yaszemski, J.M. Powers, T.P. Harrigan, A.G. Mikos, Poly (α-Hydroxy Ester)/Short Fiber Hydroxyapatite Composite Foams for Orthopedic Application, MRS Proceedings, Cambridge Univ Press, 1995, p. 25.
[99] V. Maquet, R. Jerome, Design of macroporous biodegradable polymer scaffolds for cell transplantation, Materials Science Forum, Trans Tech Publ, 1997, pp. 15-42.
[100] M.J. Yost, R.L. Price, D.G. Simpson, W. Yan, L. Terracio, G. Wnek, G. Bowlin, Encyclopedia of biomaterials and biomedical engineering, Taylor & Francis2004.
[101] K. Kim, G. Evans, Tissue engineering: the future of stem cells, Topics in tissue engineering 2 (2005) 1-21.
[102] D. Howard, L.D. Buttery, K.M. Shakesheff, S.J. Roberts, Tissue engineering: strategies, stem cells and scaffolds, Journal of anatomy 213(1) (2008) 66-72.
[103] P.C. Kreuz, J.P. Krüger, S. Metzlaff, U. Freymann, M. Endres, A. Pruss, W. Petersen, C. Kaps, Platelet-rich plasma preparation types show impact on chondrogenic differentiation, migration, and proliferation of human subchondral mesenchymal progenitor cells, Arthroscopy: The Journal of Arthroscopic & Related Surgery 31(10) (2015) 1951-1961.
[104] W. Zhao, X. Ji, F. Zhang, L. Li, L. Ma, Embryonic stem cell markers, Molecules 17(6) (2012) 6196-6236.
[105] S. Shi, C.-Y. Wang, Bone marrow stromal stem cells for repairing the skeleton, Biotechnology and Genetic Engineering Reviews 21(1) (2004) 133-146.

[106] X.-D. Chen, K. Akiyama, Y.-O. You, T. Yamaza, C. Chen, L. Tang, Y. Jin, S. Shi, Characterization of bone marrow derived mesenchymal stem cells in suspension, Stem Cell Res Ther 3(5) (2012) 40.
[107] L. Wang, L. Ott, K. Seshareddy, M.L. Weiss, M.S. Detamore, Musculoskeletal tissue engineering with human umbilical cord mesenchymal stromal cells, Regenerative medicine 6(1) (2011) 95-109.
[108] D.T. Harris, M. Badowski, N. Ahmad, M.A. Gaballa, The potential of cord blood stem cells for use in regenerative medicine, Expert opinion on biological therapy 7(9) (2007) 1311-1322.
[109] D. Sommerfeldt, C. Rubin, Biology of bone and how it orchestrates the form and function of the skeleton, European Spine Journal 10(2) (2001) S86-S95.
[110] Z. Xu, Y. Yang, W. Zhao, Z. Wang, W.J. Landis, Q. Cui, N. Sahai, Molecular mechanisms for intrafibrillar collagen mineralization in skeletal tissues, Biomaterials 39 (2015) 59-66.
[111] G. He, A. George, Dentin matrix protein 1 immobilized on type I collagen fibrils facilitates apatite deposition in vitro, Journal of Biological Chemistry 279(12) (2004) 11649-11656.
[112] H. Roach, WHY DOES BONE MATRIX CONTAIN NON-COLLAGENOUS PROTEINS? THE POSSIBLE ROLES OF OSTEOCALCIN, OSTEONECTIN, OSTEOPONTIN AND BONE SIALOPROTEIN IN BONE MINERALISATION AND RESORPTION, Cell biology international 18(6) (1994) 617-628.
[113] R. Tamma, C. Carbone, S. Colucci, Bone matrix proteins and mineralization process, Imaging of Prosthetic Joints, Springer2014, pp. 15-25.
[114] C. Wu, A.A. Skelton, M. Chen, L. Vlcek, P.T. Cummings, Modeling the interaction between integrin-binding peptide (RGD) and rutile surface: The effect of na+ on peptide adsorption, The Journal of Physical Chemistry C 115(45) (2011) 22375-22386.
[115] S.B. Kennedy, N.R. Washburn, C.G. Simon, E.J. Amis, Combinatorial screen of the effect of surface energy on fibronectin-mediated osteoblast adhesion, spreading and proliferation, Biomaterials 27(20) (2006) 3817-3824.
[116] J.E. Aubin, Regulation of osteoblast formation and function, Reviews in Endocrine and Metabolic Disorders 2(1) (2001) 81-94.
[117] S.-i. Harada, G.A. Rodan, Control of osteoblast function and regulation of bone mass, Nature 423(6937) (2003) 349-355.
[118] R. Florencio-Silva, G. Sasso, E. Sasso-Cerri, M.J. Simões, P.S. Cerri, Biology of bone tissue: structure, function, and factors that influence bone cells, BioMed research international 2015 (2015).
[119] A.G. Robling, A.B. Castillo, C.H. Turner, Biomechanical and molecular regulation of bone remodeling, Annu. Rev. Biomed. Eng. 8 (2006) 455-498.
[120] A.I. Alford, K.D. Hankenson, Matricellular proteins: extracellular modulators of bone development, remodeling, and regeneration, Bone 38(6) (2006) 749-757.

[121] B. Clarke, Normal bone anatomy and physiology, Clinical journal of the American Society of Nephrology 3(Supplement 3) (2008) S131-S139.
[122] H. Datta, W. Ng, J. Walker, S. Tuck, S. Varanasi, The cell biology of bone metabolism, Journal of clinical pathology 61(5) (2008) 577-587.
[123] H. Murakami, N. Takahashi, T. Sasaki, N. Udagawa, S. Tanaka, I. Nakamura, D. Zhang, A. Barbier, T. Suda, A possible mechanism of the specific action of bisphosphonates on osteoclasts: tiludronate preferentially affects polarized osteoclasts having ruffled borders, Bone 17(2) (1995) 137-144.
[124] J.M. McCOOL, Silk Fibroin-Based Scaffolds for Tissue Engineering Applications, Virginia Commonwealth University Richmond, Virginia, 2011.
[125] G.H. Altman, R.L. Horan, H.H. Lu, J. Moreau, I. Martin, J.C. Richmond, D.L. Kaplan, Silk matrix for tissue engineered anterior cruciate ligaments, Biomaterials 23(20) (2002) 4131-4141.
[126] U.-J. Kim, J. Park, H.J. Kim, M. Wada, D.L. Kaplan, Three-dimensional aqueous-derived biomaterial scaffolds from silk fibroin, Biomaterials 26(15) (2005) 2775-2785.
[127] M.J. Lysaght, J. Reyes, The growth of tissue engineering, Tissue engineering 7(5) (2001) 485-493.
[128] D.J. Berry, W.S. Harmsen, M.E. Cabanela, B.F. Morrey, Twenty-five-year survivorship of two thousand consecutive primary Charnley total hip replacements, J Bone Joint Surg Am 84(2) (2002) 171-177.
[129] M. Saccone, A.K. Jain, Fracture healing in India: Available therapies, indications, and protocols, Indian journal of orthopaedics 43(2) (2009) 175.
[130] C. Marya, C. Dhingra, Effect of Osteoporosis on Oral Health, Archives of Medicine (2016).
[131] R.C. Lawrence, D.T. Felson, C.G. Helmick, L.M. Arnold, H. Choi, R.A. Deyo, S. Gabriel, R. Hirsch, M.C. Hochberg, G.G. Hunder, Estimates of the prevalence of arthritis and other rheumatic conditions in the United States: Part II, Arthritis & Rheumatism 58(1) (2008) 26-35.
[132] S. Vijayan, G. Bentley, T. Briggs, J. Skinner, R. Carrington, R. Pollock, A. Flanagan, Cartilage repair: a review of Stanmore experience in the treatment of osteochondral defects in the knee with various surgical techniques, Indian journal of orthopaedics 44(3) (2010) 238.
[133] B.S. Dunkin, C. Lattermann, New and emerging techniques in cartilage repair: Matrix-induced autologous chondrocyte implantation, Operative techniques in sports medicine 21(2) (2013) 100-107.
[134] D. Tang, R.S. Tare, L.-Y. Yang, D.F. Williams, K.-L. Ou, R.O. Oreffo, Biofabrication of bone tissue: approaches, challenges and translation for bone regeneration, Biomaterials 83 (2016) 363-382.
[135] S. Bose, M. Roy, A. Bandyopadhyay, Recent advances in bone tissue engineering scaffolds, Trends in biotechnology 30(10) (2012) 546-554.
[136] J. Mano, G. Silva, H.S. Azevedo, P. Malafaya, R. Sousa, S. Silva, L. Boesel, J.M. Oliveira, T. Santos, A. Marques, Natural origin biodegradable systems in tissue engineering and regenerative

medicine: present status and some moving trends, Journal of The Royal Society Interface 4(17) (2007) 999-1030.
[137] Y. Zhang, C.T. Lim, S. Ramakrishna, Z.-M. Huang, Recent development of polymer nanofibers for biomedical and biotechnological applications, Journal of Materials Science: Materials in Medicine 16(10) (2005) 933-946.
[138] R.D. Bostrom, A.G. Mikos, Tissue engineering of bone, Synthetic biodegradable polymer scaffolds, Springer1997, pp. 215-234.
[139] B.C. Simionescu, D. Ivanov, Natural and Synthetic Polymers for Designing Composite Materials, Handbook of Bioceramics and Biocomposites (2016) 233-286.
[140] M. Ramalingam, X. Wang, G. Chen, P. Ma, F.-Z. Cui, Biomimetics: Advancing nanobiomaterials and tissue engineering, John Wiley & Sons2013.
[141] I. Armentano, M. Dottori, E. Fortunati, S. Mattioli, J. Kenny, Biodegradable polymer matrix nanocomposites for tissue engineering: a review, Polymer degradation and stability 95(11) (2010) 2126-2146.
[142] N. Minoura, M. Tsukada, M. Nagura, Physico-chemical properties of silk fibroin membrane as a biomaterial, Biomaterials 11(6) (1990) 430-434.
[143] J.-K.F. Suh, H.W. Matthew, Application of chitosan-based polysaccharide biomaterials in cartilage tissue engineering: a review, Biomaterials 21(24) (2000) 2589-2598.
[144] W. Friess, Collagen–biomaterial for drug delivery, European Journal of Pharmaceutics and Biopharmaceutics 45(2) (1998) 113-136.
[145] G. Gorrasi, V. Vittoria, M. Murariu, A.D.S. Ferreira, M. Alexandre, P. Dubois, Effect of filler content and size on transport properties of water vapor in PLA/calcium sulfate composites, Biomacromolecules 9(3) (2008) 984-990.
[146] R. Murugan, S. Ramakrishna, Development of nanocomposites for bone grafting, Composites Science and Technology 65(15) (2005) 2385-2406.
[147] S. Gautam, C.-F. Chou, A.K. Dinda, P.D. Potdar, N.C. Mishra, Surface modification of nanofibrous polycaprolactone/gelatin composite scaffold by collagen type I grafting for skin tissue engineering, Materials Science and Engineering: C 34 (2014) 402-409.
[148] P.K. Chu, J. Chen, L. Wang, N. Huang, Plasma-surface modification of biomaterials, Materials Science and Engineering: R: Reports 36(5) (2002) 143-206.
[149] Y. Yang, K.-H. Kim, J.L. Ong, A review on calcium phosphate coatings produced using a sputtering process—an alternative to plasma spraying, Biomaterials 26(3) (2005) 327-337.
[150] H. Iwata, A. Kishida, M. Suzuki, Y. Hata, Y. Ikada, Oxidation of polyethylene surface by corona discharge and the subsequent graft polymerization, Journal of Polymer Science Part A: Polymer Chemistry 26(12) (1988) 3309-3322.

[151] K. Rodríguez, S. Renneckar, P. Gatenholm, Biomimetic calcium phosphate crystal mineralization on electrospun cellulose-based scaffolds, ACS applied materials & interfaces 3(3) (2011) 681-689.
[152] U. Hersel, C. Dahmen, H. Kessler, RGD modified polymers: biomaterials for stimulated cell adhesion and beyond, Biomaterials 24(24) (2003) 4385-4415.
[153] T. Funakoshi, T. Majima, N. Iwasaki, S. Yamane, T. Masuko, A. Minami, K. Harada, H. Tamura, S. Tokura, S.I. Nishimura, Novel chitosan-based hyaluronan hybrid polymer fibers as a scaffold in ligament tissue engineering, Journal of Biomedical Materials Research Part A 74(3) (2005) 338-346.
[154] J. Chen, G.H. Altman, V. Karageorgiou, R. Horan, A. Collette, V. Volloch, T. Colabro, D.L. Kaplan, Human bone marrow stromal cell and ligament fibroblast responses on RGD-modified silk fibers, Journal of Biomedical Materials Research Part A 67(2) (2003) 559-570.
[155] G.H. Altman, F. Diaz, C. Jakuba, T. Calabro, R.L. Horan, J. Chen, H. Lu, J. Richmond, D.L. Kaplan, Silk-based biomaterials, Biomaterials 24(3) (2003) 401-416.
[156] L. Meinel, S. Hofmann, V. Karageorgiou, L. Zichner, R. Langer, D. Kaplan, G. Vunjak-Novakovic, Engineering cartilage-like tissue using human mesenchymal stem cells and silk protein scaffolds, Biotechnology and bioengineering 88(3) (2004) 379-391.
[157] E. Wenk, H.P. Merkle, L. Meinel, Silk fibroin as a vehicle for drug delivery applications, Journal of Controlled Release 150(2) (2011) 128-141.
[158] E. Khor, L.Y. Lim, Implantable applications of chitin and chitosan, Biomaterials 24(13) (2003) 2339-2349.
[159] R. Jayakumar, M. Prabaharan, S. Nair, H. Tamura, Novel chitin and chitosan nanofibers in biomedical applications, Biotechnology advances 28(1) (2010) 142-150.
[160] J. Synowiecki, N.A. Al-Khateeb, Production, properties, and some new applications of chitin and its derivatives, (2003).
[161] A. Martins, S. Chung, A.J. Pedro, R.A. Sousa, A.P. Marques, R.L. Reis, N.M. Neves, Hierarchical starch-based fibrous scaffold for bone tissue engineering applications, Journal of tissue engineering and regenerative medicine 3(1) (2009) 37-42.
[162] P.B. Malafaya, G.A. Silva, R.L. Reis, Natural–origin polymers as carriers and scaffolds for biomolecules and cell delivery in tissue engineering applications, Advanced drug delivery reviews 59(4) (2007) 207-233.
[163] F. Munarin, S. Guerreiro, M. Grellier, M. Tanzi, M. Barbosa, P. Petrini, P. Granja, Pectin-based injectable biomaterials for bone tissue engineering, Biomacromolecules 12(3) (2011) 568-577.
[164] L. Bacakova, K. Novotná, M. Parizek, Polysaccharides as cell carriers for tissue engineering: the use of cellulose in vascular wall reconstruction, Physiological Research 63 (2014) S29.

[165] N. Ninan, M. Muthiah, I.-K. Park, A. Elain, S. Thomas, Y. Grohens, Pectin/carboxymethyl cellulose/microfibrillated cellulose composite scaffolds for tissue engineering, Carbohydrate Polymers 98(1) (2013) 877-885.
[166] Y. Ogushi, S. Sakai, K. Kawakami, Synthesis of enzymatically-gellable carboxymethylcellulose for biomedical applications, Journal of bioscience and bioengineering 104(1) (2007) 30-33.
[167] L. Ghasemi-Mobarakeh, M.P. Prabhakaran, M. Morshed, M.-H. Nasr-Esfahani, S. Ramakrishna, Electrospun poly (ε-caprolactone)/gelatin nanofibrous scaffolds for nerve tissue engineering, Biomaterials 29(34) (2008) 4532-4539.
[168] W. Xia, W. Liu, L. Cui, Y. Liu, W. Zhong, D. Liu, J. Wu, K. Chua, Y. Cao, Tissue engineering of cartilage with the use of chitosan-gelatin complex scaffolds, Journal of Biomedical Materials Research Part B: Applied Biomaterials 71(2) (2004) 373-380.
[169] X. Liu, L.A. Smith, J. Hu, P.X. Ma, Biomimetic nanofibrous gelatin/apatite composite scaffolds for bone tissue engineering, Biomaterials 30(12) (2009) 2252-2258.
[170] M.I. Baker, S.P. Walsh, Z. Schwartz, B.D. Boyan, A review of polyvinyl alcohol and its uses in cartilage and orthopedic applications, Journal of Biomedical Materials Research Part B: Applied Biomaterials 100(5) (2012) 1451-1457.
[171] A. Coombes, S. Rizzi, M. Williamson, J. Barralet, S. Downes, W. Wallace, Precipitation casting of polycaprolactone for applications in tissue engineering and drug delivery, Biomaterials 25(2) (2004) 315-325.
[172] Y.-Z. Bian, Y. Wang, G. Aibaidoula, G.-Q. Chen, Q. Wu, Evaluation of poly (3-hydroxybutyrate-co-3-hydroxyhexanoate) conduits for peripheral nerve regeneration, Biomaterials 30(2) (2009) 217-225.
[173] G.-Q. Chen, Q. Wu, The application of polyhydroxyalkanoates as tissue engineering materials, Biomaterials 26(33) (2005) 6565-6578.
[174] M.J. Smith, M.J. McClure, S.A. Sell, C.P. Barnes, B.H. Walpoth, D.G. Simpson, G.L. Bowlin, Suture-reinforced electrospun polydioxanone–elastin small-diameter tubes for use in vascular tissue engineering: a feasibility study, Acta biomaterialia 4(1) (2008) 58-66.
[175] E.D. Boland, B.D. Coleman, C.P. Barnes, D.G. Simpson, G.E. Wnek, G.L. Bowlin, Electrospinning polydioxanone for biomedical applications, Acta biomaterialia 1(1) (2005) 115-123.
[176] W.J. Cho, J.H. Kim, S.H. Oh, H.H. Nam, J.M. Kim, J.H. Lee, Hydrophilized polycaprolactone nanofiber mesh-embedded poly (glycolic-co-lactic acid) membrane for effective guided bone regeneration, Journal of Biomedical Materials Research Part A 91(2) (2009) 400-407.
[177] C.R. Chu, R.D. Coutts, M. Yoshioka, F.L. Harwood, A.Z. Monosov, D. Amiel, Articular cartilage repair using allogeneic perichondrocyteseeded biodegradable porous polylactic acid (PLA): A tissue-engineering study, Journal of biomedical materials research 29(9) (1995) 1147-1154.
[178] M.E. Gomes, H.S. Azevedo, A. Moreira, V. Ellä, M. Kellomäki, R. Reis, Starch–poly (ε-caprolactone) and starch–poly (lactic acid) fibre-mesh scaffolds for bone tissue engineering

applications: structure, mechanical properties and degradation behaviour, Journal of tissue engineering and regenerative medicine 2(5) (2008) 243-252.
[179] Y. Cao, A. Rodriguez, M. Vacanti, C. Ibarra, C. Arevalo, C.A. Vacanti, Comparative study of the use of poly (glycolic acid), calcium alginate and pluronics in the engineering of autologous porcine cartilage, Journal of Biomaterials Science, Polymer Edition 9(5) (1998) 475-487.
[180] X. Liu, P.X. Ma, Polymeric scaffolds for bone tissue engineering, Annals of biomedical engineering 32(3) (2004) 477-486.
[181] N.K. Francis, H.S. Pawar, P. Ghosh, S. Dhara, In situ iodination cross-linking of silk for radio-opaque antimicrobial surgical sutures, ACS Biomaterials Science & Engineering 2(2) (2016) 188-196.
[182] A. Vasconcelos, G. Freddi, A. Cavaco-Paulo, Biodegradable materials based on silk fibroin and keratin, Biomacromolecules 9(4) (2008) 1299-1305.
[183] S. Keten, Z. Xu, B. Ihle, M.J. Buehler, Nanoconfinement controls stiffness, strength and mechanical toughness of [beta]-sheet crystals in silk, Nature materials 9(4) (2010) 359-367.
[184] B. Kundu, N.E. Kurland, S. Bano, C. Patra, F.B. Engel, V.K. Yadavalli, S.C. Kundu, Silk proteins for biomedical applications: bioengineering perspectives, Progress in polymer science 39(2) (2014) 251-267.
[185] R. Nazarov, H.-J. Jin, D.L. Kaplan, Porous 3-D scaffolds from regenerated silk fibroin, Biomacromolecules 5(3) (2004) 718-726.
[186] Y. Wang, H.-J. Kim, G. Vunjak-Novakovic, D.L. Kaplan, Stem cell-based tissue engineering with silk biomaterials, Biomaterials 27(36) (2006) 6064-6082.
[187] W.H. Park, L. Jeong, D.I. Yoo, S. Hudson, Effect of chitosan on morphology and conformation of electrospun silk fibroin nanofibers, Polymer 45(21) (2004) 7151-7157.
[188] J.-P. Chen, S.-H. Chen, G.-J. Lai, Preparation and characterization of biomimetic silk fibroin/chitosan composite nanofibers by electrospinning for osteoblasts culture, Nanoscale research letters 7(1) (2012) 1.
[189] H. Fan, H. Liu, S.L. Toh, J.C. Goh, Enhanced differentiation of mesenchymal stem cells co-cultured with ligament fibroblasts on gelatin/silk fibroin hybrid scaffold, Biomaterials 29(8) (2008) 1017-1027.
[190] C.T. Laurencin, J.W. Freeman, Ligament tissue engineering: an evolutionary materials science approach, Biomaterials 26(36) (2005) 7530-7536.
[191] G. Vunjak-Novakovic, G. Altman, R. Horan, D.L. Kaplan, Tissue engineering of ligaments, Annu. Rev. Biomed. Eng. 6 (2004) 131-156.
[192] S. De-bing, D. Zhi-hui, F. Wei-guo, Study on the properties of the electrospun silk fibroin/gelatin blend nanofibers for scaffolds, Journal of Applied Polymer Science 111(3) (2009) 1471-1477.

[193] I.-S. Yeo, J.-E. Oh, L. Jeong, T.S. Lee, S.J. Lee, W.H. Park, B.-M. Min, Collagen-based biomimetic nanofibrous scaffolds: preparation and characterization of collagen/silk fibroin bicomponent nanofibrous structures, Biomacromolecules 9(4) (2008) 1106-1116.
[194] X. Hu, Q. Lu, L. Sun, P. Cebe, X. Wang, X. Zhang, D.L. Kaplan, Biomaterials from ultrasonication-induced silk fibroin− hyaluronic acid hydrogels, Biomacromolecules 11(11) (2010) 3178-3188.
[195] F.A. Müller, L. Müller, I. Hofmann, P. Greil, M.M. Wenzel, R. Staudenmaier, Cellulose-based scaffold materials for cartilage tissue engineering, Biomaterials 27(21) (2006) 3955-3963.
[196] Z. Ma, S. Ramakrishna, Electrospun regenerated cellulose nanofiber affinity membrane functionalized with protein A/G for IgG purification, Journal of Membrane Science 319(1) (2008) 23-28.
[197] G. Fundueanu, M. Constantin, E. Esposito, R. Cortesi, C. Nastruzzi, E. Menegatti, Cellulose acetate butyrate microcapsules containing dextran ion-exchange resins as self-propelled drug release system, Biomaterials 26(20) (2005) 4337-4347.
[198] T. Miyamoto, S.i. Takahashi, H. Ito, H. Inagaki, Y. Noishiki, Tissue biocompatibility of cellulose and its derivatives, Journal of biomedical materials research 23(1) (1989) 125-133.
[199] J. Kundu, R. Mohapatra, S. Kundu, Silk fibroin/sodium carboxymethylcellulose blended films for biotechnological applications, Journal of Biomaterials Science, Polymer Edition 22(4-6) (2011) 519-539.
[200] K. Numata, S. Yamazaki, T. Katashima, J.A. Chuah, N. Naga, T. Sakai, Silk-Pectin Hydrogel with Superior Mechanical Properties, Biodegradability, and Biocompatibility, Macromolecular bioscience 14(6) (2014) 799-806.
[201] L. Soffer, X. Wang, X. Zhang, J. Kluge, L. Dorfmann, D.L. Kaplan, G. Leisk, Silk-based electrospun tubular scaffolds for tissue-engineered vascular grafts, Journal of Biomaterials Science, Polymer Edition 19(5) (2008) 653-664.
[202] B. Marelli, A. Alessandrino, S. Farè, G. Freddi, D. Mantovani, M.C. Tanzi, Compliant electrospun silk fibroin tubes for small vessel bypass grafting, Acta biomaterialia 6(10) (2010) 4019-4026.
[203] Y. Tamada, Sulfation of silk fibroin by chlorosulfonic acid and the anticoagulant activity, Biomaterials 25(3) (2004) 377-383.
[204] M. McClure, S. Sell, C. Ayres, D. Simpson, G. Bowlin, Electrospinning-aligned and random polydioxanone–polycaprolactone–silk fibroin-blended scaffolds: geometry for a vascular matrix, Biomedical Materials 4(5) (2009) 055010.
[205] P. Bhattacharjee, D. Naskar, H.-W. Kim, T.K. Maiti, D. Bhattacharya, S.C. Kundu, Non-mulberry silk fibroin grafted PCL nanofibrous scaffold: promising ECM for bone tissue engineering, European Polymer Journal 71 (2015) 490-509.

[206] S. Samavedi, A.R. Whittington, A.S. Goldstein, Calcium phosphate ceramics in bone tissue engineering: a review of properties and their influence on cell behavior, Acta biomaterialia 9(9) (2013) 8037-8045.
[207] M. Mehrjoo, J. Javadpour, M.A. Shokrgozar, M. Farokhi, S. Javadian, S. Bonakdar, Effect of magnesium substitution on structural and biological properties of synthetic hydroxyapatite powder, Materials Express 5(1) (2015) 41-48.
[208] A. Ambrosio, J.S. Sahota, Y. Khan, C.T. Laurencin, A novel amorphous calcium phosphate polymer ceramic for bone repair: I. Synthesis and characterization, Journal of biomedical materials research 58(3) (2001) 295-301.
[209] K.G. Marra, J.W. Szem, P.N. Kumta, P.A. DiMilla, L.E. Weiss, In vitro analysis of biodegradable polymer blend/hydroxyapatite composites for bone tissue engineering, Journal of biomedical materials research 47(3) (1999) 324-335.
[210] R. Liu, J. Ming, H. Zhang, B. Zuo, EDC/NHS crosslinked electrospun regenerated tussah silk fibroin nanofiber mats, Fibers and Polymers 13(5) (2012) 613-617.
[211] J.-H. Song, J.-H. Kim, S. Park, W. Kang, H.-W. Kim, H.-E. Kim, J.-H. Jang, Signaling responses of osteoblast cells to hydroxyapatite: the activation of ERK and SOX9, Journal of bone and mineral metabolism 26(2) (2008) 138-142.
[212] J. Melke, S. Midha, S. Ghosh, K. Ito, S. Hofmann, Silk fibroin as biomaterial for bone tissue engineering, Acta biomaterialia 31 (2016) 1-16.
[213] C. Cao, H. Li, J. Li, C. Liu, H. Yang, B. Li, Mechanical reinforcement of injectable calcium phosphate cement/silk fibroin (SF) composite by mineralized SF, Ceramics International 40(9) (2014) 13987-13993.
[214] A. Teimouri, M. Azadi, R. Emadi, J. Lari, A.N. Chermahini, Preparation, characterization, degradation and biocompatibility of different silk fibroin based composite scaffolds prepared by freeze-drying method for tissue engineering application, Polymer degradation and stability 121 (2015) 18-29.
[215] M. Ribeiro, M.A. de Moraes, M.M. Beppu, M.P. Garcia, M.H. Fernandes, F.J. Monteiro, M.P. Ferraz, Development of silk fibroin/nanohydroxyapatite composite hydrogels for bone tissue engineering, European Polymer Journal 67 (2015) 66-77.
[216] S.L. McNamara, J. Rnjak-Kovacina, D.F. Schmidt, T.J. Lo, D.L. Kaplan, Silk as a biocohesive sacrificial binder in the fabrication of hydroxyapatite load bearing scaffolds, Biomaterials 35(25) (2014) 6941-6953.
[217] H. Kim, L. Che, Y. Ha, W. Ryu, Mechanically-reinforced electrospun composite silk fibroin nanofibers containing hydroxyapatite nanoparticles, Materials Science and Engineering: C 40 (2014) 324-335.
[218] L.L. Hench, Bioceramics: from concept to clinic, Journal of the American Ceramic Society 74(7) (1991) 1487-1510.

[219] X. Yan, C. Yu, X. Zhou, J. Tang, D. Zhao, Highly Ordered Mesoporous Bioactive Glasses with Superior In Vitro Bone-Forming Bioactivities, Angewandte Chemie International Edition 43(44) (2004) 5980-5984.
[220] C. Wu, Y. Zhang, Y. Zhu, T. Friis, Y. Xiao, Structure–property relationships of silk-modified mesoporous bioglass scaffolds, Biomaterials 31(13) (2010) 3429-3438.
[221] C. Wu, Y. Zhou, M. Xu, P. Han, L. Chen, J. Chang, Y. Xiao, Copper-containing mesoporous bioactive glass scaffolds with multifunctional properties of angiogenesis capacity, osteostimulation and antibacterial activity, Biomaterials 34(2) (2013) 422-433.
[222] C. Wu, Y. Zhou, W. Fan, P. Han, J. Chang, J. Yuen, M. Zhang, Y. Xiao, Hypoxia-mimicking mesoporous bioactive glass scaffolds with controllable cobalt ion release for bone tissue engineering, Biomaterials 33(7) (2012) 2076-2085.
[223] E. Gentleman, Y.C. Fredholm, G. Jell, N. Lotfibakhshaiesh, M.D. O'Donnell, R.G. Hill, M.M. Stevens, The effects of strontium-substituted bioactive glasses on osteoblasts and osteoclasts in vitro, Biomaterials 31(14) (2010) 3949-3956.
[224] H. Xie, Z. Gu, C. Li, C. Franco, J. Wang, L. Li, N. Meredith, Q. Ye, C. Wan, A novel bioceramic scaffold integrating silk fibroin in calcium polyphosphate for bone tissue-engineering, Ceramics International 42(2) (2016) 2386-2392.
[225] L.-P. Yan, J. Silva-Correia, M.B. Oliveira, C. Vilela, H. Pereira, R.A. Sousa, J.F. Mano, A.L. Oliveira, J.M. Oliveira, R.L. Reis, Bilayered silk/silk-nanoCaP scaffolds for osteochondral tissue engineering: in vitro and in vivo assessment of biological performance, Acta biomaterialia 12 (2015) 227-241.
[226] A. Chandrasekaran, G. Novajra, I. Carmagnola, P. Gentile, S. Fiorilli, M. Miola, M. Boregowda, A. Dakshanamoorthy, G. Ciardelli, C. Vitale-Brovarone, Physico-chemical and biological studies on three-dimensional porous silk/spray-dried mesoporous bioactive glass scaffolds, Ceramics International (2016).
[227] A. Hoppe, B. Jokic, D. Janackovic, T. Fey, P. Greil, S. Romeis, J. Schmidt, W. Peukert, J. Lao, E. Jallot, Cobalt-releasing 1393 bioactive glass-derived scaffolds for bone tissue engineering applications, ACS applied materials & interfaces 6(4) (2014) 2865-2877.
[228] M. Sah, K. Pramanik, Regenerated Silk Fibroin from B. mori SilkCocoon for Tissue Engineering Applications, International journal of environmental science and development 1(5) (2010) 404.
[229] B. Singh, N. Panda, K. Pramanik, A novel electrospinning approach to fabricate high strength aqueous silk fibroin nanofibers, International journal of biological macromolecules 87 (2016) 201-207.
[230] W. Xia, J. Chang, Preparation and characterization of nano-bioactive-glasses (NBG) by a quick alkali-mediated sol–gel method, Materials letters 61(14) (2007) 3251-3253.

[231] P. Dey, S. Pal, R. Sarkar, Effect of Alumina Addition on 45S5 Bioglass, Transactions of the Indian Ceramic Society 73(2) (2014) 105-109.
[232] X.W. Gu, J.R. Greer, Ultra-strong architected Cu meso-lattices, Extreme Mechanics Letters 2 (2015) 7-14.
[233] T. Kokubo, H. Takadama, How useful is SBF in predicting in vivo bone bioactivity?, Biomaterials 27(15) (2006) 2907-2915.
[234] B. Lei, X. Chen, X. Han, J. Zhou, Versatile fabrication of nanoscale sol–gel bioactive glass particles for efficient bone tissue regeneration, Journal of materials chemistry 22(33) (2012) 16906-16913.
[235] L. Varila, T. Lehtonen, J. Tuominen, M. Hupa, L. Hupa, In vitro behaviour of three biocompatible glasses in composite implants, Journal of Materials Science: Materials in Medicine 23(10) (2012) 2425-2435.
[236] B. Singh, N. Panda, R. Mund, K. Pramanik, Carboxymethyl cellulose enables silk fibroin nanofibrous scaffold with enhanced biomimetic potential for bone tissue engineering application, Carbohydrate Polymers 151 (2016) 335-347.
[237] S. Udaseen, S. Asthana, N.T. Raveendran, K. Kumar, A. Samal, K. Pal, K. Pramanik, S.S. Ray, Optimization of process parameters for nozzle—free electrospinning of poly (vinyl alcohol) and alginate blend nano-fibrous scaffolds, Int J Enhanced Res Sci Technol Eng 3(1) (2014) 405-411.
[238] W.-S. Ma, L. Wu, F. Yang, S.-F. Wang, Non-covalently modified reduced graphene oxide/polyurethane nanocomposites with good mechanical and thermal properties, Journal of Materials Science 49(2) (2014) 562-571.
[239] Q. Fu, J.M. Ren, G.G. Qiao, Synthesis of novel cylindrical bottlebrush polypseudorotaxane via inclusion complexation of high density poly (ε-caprolactone) bottlebrush polymer and α-cyclodextrins, Polymer Chemistry 3(2) (2012) 343-351.
[240] Z. Zheng, L. Zhang, L. Kong, A. Wang, Y. Gong, X. Zhang, The behavior of MC3T3-E1 cells on chitosan/poly-L-lysine composite films: Effect of nanotopography, surface chemistry, and wettability, Journal of Biomedical Materials Research Part A 89(2) (2009) 453-465.
[241] F. Pati, H. Kalita, B. Adhikari, S. Dhara, Osteoblastic cellular responses on ionically crosslinked chitosan-tripolyphosphate fibrous 3-D mesh scaffolds, Journal of Biomedical Materials Research Part A 101(9) (2013) 2526-2537.
[242] R.L. Horan, K. Antle, A.L. Collette, Y. Wang, J. Huang, J.E. Moreau, V. Volloch, D.L. Kaplan, G.H. Altman, In vitro degradation of silk fibroin, Biomaterials 26(17) (2005) 3385-3393.
[243] T. Kokubo, H.-M. Kim, M. Kawashita, Novel bioactive materials with different mechanical properties, Biomaterials 24(13) (2003) 2161-2175.
[244] I.J. Fuss, M.E. Kanof, P.D. Smith, H. Zola, Isolation of whole mononuclear cells from peripheral blood and cord blood, Wiley Online Library2009.

[245] A. Bissoyi, K. Pramanik, N.N. Panda, S. Sarangi, Cryopreservation of hMSCs seeded silk nanofibers based tissue engineered constructs, Cryobiology 68(3) (2014) 332-342.
[246] V. Vishwanath, K. Pramanik, A. Biswas, Optimization and evaluation of silk fibroin-chitosan freeze-dried porous scaffolds for cartilage tissue engineering application, Journal of Biomaterials Science, Polymer Edition 27(7) (2016) 657-674.
[247] R. Secunda, R. Vennila, A. Mohanashankar, M. Rajasundari, S. Jeswanth, R. Surendran, Isolation, expansion and characterisation of mesenchymal stem cells from human bone marrow, adipose tissue, umbilical cord blood and matrix: a comparative study, Cytotechnology 67(5) (2015) 793-807.
[248] A. Biswas, K. Pramanik, S. Jonnalagadda, Enhanced osteogenic potential of human mesenchymal stem cells on electrospun nanofibrous scaffolds prepared from eri-tasar silk fibroin, Journal of Biomedical Materials Research Part B: Applied Biomaterials (2014).
[249] L. Ghasemi-Mobarakeh, M. Morshed, K. Karbalaie, M. Fesharaki, M.H. Nasr-Esfahani, H. Baharvand, Electrospun poly (ε-caprolactone) nanofiber mat as extracellular matrix, Yakhteh Medical Journal 10(3) (2008) 179-184.
[250] E. Gentleman, A.N. Lay, D.A. Dickerson, E.A. Nauman, G.A. Livesay, K.C. Dee, Mechanical characterization of collagen fibers and scaffolds for tissue engineering, Biomaterials 24(21) (2003) 3805-3813.
[251] C.A. Gregory, W.G. Gunn, A. Peister, D.J. Prockop, An Alizarin red-based assay of mineralization by adherent cells in culture: comparison with cetylpyridinium chloride extraction, Analytical biochemistry 329(1) (2004) 77-84.
[252] P. Karunanithi, M.R. Murali, S. Samuel, H.R.B. Raghavendran, A.A. Abbas, T. Kamarul, Three dimensional alginate-fucoidan composite hydrogel augments the chondrogenic differentiation of mesenchymal stromal cells, Carbohydrate Polymers 147 (2016) 294-303.
[253] J. Yang, Q.-D. Shi, T.-B. Song, G.-F. Feng, W.-J. Zang, C.-H. Zong, L. Chang, Vasoactive intestinal peptide increases VEGF expression to promote proliferation of brain vascular endothelial cells via the cAMP/PKA pathway after ischemic insult in vitro, Peptides 42 (2013) 105-111.
[254] Z. Shao, F. Vollrath, Materials: Surprising strength of silkworm silk, Nature 418(6899) (2002) 741-741.
[255] P. Amornsudthiwat, R. Mongkolnavin, S. Kanokpanont, J. Panpranot, C. San Wong, S. Damrongsakkul, Improvement of early cell adhesion on Thai silk fibroin surface by low energy plasma, Colloids and Surfaces B: Biointerfaces 111 (2013) 579-586.
[256] H. Yang, M. Sun, P. Zhou, L. Pan, C. Wu, Silk fibroins modify the atmospheric low temperature plasma-treated poly (3-hydroxybutyrate-co-3-hydroxyhexanoate) film for the application of cardiovascular tissue engineering, Journal of Biomedical Science and Engineering 3(12) (2010) 1146.

[257] S.-W. Ha, A.E. Tonelli, S.M. Hudson, Structural Studies of Bombyx m ori Silk Fibroin during Regeneration from Solutions and Wet Fiber Spinning, Biomacromolecules 6(3) (2005) 1722-1731.
[258] A.S. Gobin, V.E. Froude, A.B. Mathur, Structural and mechanical characteristics of silk fibroin and chitosan blend scaffolds for tissue regeneration, Journal of Biomedical Materials Research Part A 74(3) (2005) 465-473.
[259] B. Ghanbarzadeh, H. Almasi, Physical properties of edible emulsified films based on carboxymethyl cellulose and oleic acid, International journal of biological Macromolecules 48(1) (2011) 44-49.
[260] W. Wang, A. Wang, Nanocomposite of carboxymethyl cellulose and attapulgite as a novel pH-sensitive superabsorbent: Synthesis, characterization and properties, Carbohydrate Polymers 82(1) (2010) 83-91.
[261] R. Whistler, Industrial gums: polysaccharides and their derivatives, Elsevier2012.
[262] D. Bao, M. Chen, H. Wang, J. Wang, C. Liu, R. Sun, Preparation and characterization of double crosslinked hydrogel films from carboxymethylchitosan and carboxymethylcellulose, Carbohydrate Polymers 110 (2014) 113-120.
[263] D. Li, J.T. McCann, Y. Xia, M. Marquez, Electrospinning: a simple and versatile technique for producing ceramic nanofibers and nanotubes, Journal of the American Ceramic Society 89(6) (2006) 1861-1869.
[264] B. Veleirinho, M.F. Rei, J. Lopes-DA-Silva, Solvent and concentration effects on the properties of electrospun poly (ethylene terephthalate) nanofiber mats, Journal of Polymer Science Part B: Polymer Physics 46(5) (2008) 460-471.
[265] P. Fagerholm, N.S. Lagali, K. Merrett, W.B. Jackson, R. Munger, Y. Liu, J.W. Polarek, M. Söderqvist, M. Griffith, A biosynthetic alternative to human donor tissue for inducing corneal regeneration: 24-month follow-up of a phase 1 clinical study, Science translational medicine 2(46) (2010) 46ra61-46ra61.
[266] S. Edwards, W. Mitchell, J. Matthews, E. Ingham, S. Russell, Design of nonwoven scaffold structures for tissue engineering of the anterior cruciate ligament, AUTEX Research Journal 4(2) (2004) 86-94.
[267] S. Yang, K.-F. Leong, Z. Du, C.-K. Chua, The design of scaffolds for use in tissue engineering. Part I. Traditional factors, Tissue engineering 7(6) (2001) 679-689.
[268] I.C. Um, H. Kweon, Y.H. Park, S. Hudson, Structural characteristics and properties of the regenerated silk fibroin prepared from formic acid, International journal of biological Macromolecules 29(2) (2001) 91-97.
[269] S.-W. Ha, Y.H. Park, S.M. Hudson, Dissolution of Bombyx m ori Silk Fibroin in the Calcium Nitrate Tetrahydrate-Methanol System and Aspects of Wet Spinning of Fibroin Solution, Biomacromolecules 4(3) (2003) 488-496.

[270] J.-P. Chen, S.-H. Chen, G.-J. Lai, Preparation and characterization of biomimetic silk fibroin/chitosan composite nanofibers by electrospinning for osteoblasts culture, Nanoscale research letters 7(1) (2012) 1-11.
[271] R. Rošic, J. Pelipenko, P. Kocbek, S. Baumgartner, M. Bešter-Rogač, J. Kristl, The role of rheology of polymer solutions in predicting nanofiber formation by electrospinning, European Polymer Journal 48(8) (2012) 1374-1384.
[272] C. Holland, A. Terry, D. Porter, F. Vollrath, Comparing the rheology of native spider and silkworm spinning dope, Nature materials 5(11) (2006) 870-874.
[273] Q. Lu, Y. Huang, M. Li, B. Zuo, S. Lu, J. Wang, H. Zhu, D.L. Kaplan, Silk fibroin electrogelation mechanisms, Acta biomaterialia 7(6) (2011) 2394-2400.
[274] J. Zhu, Y. Zhang, H. Shao, X. Hu, Electrospinning and rheology of regenerated Bombyx mori silk fibroin aqueous solutions: The effects of pH and concentration, Polymer 49(12) (2008) 2880-2885.
[275] F. Zhang, B. Zuo, Z. Fan, Z. Xie, Q. Lu, X. Zhang, D.L. Kaplan, Mechanisms and control of silk-based electrospinning, Biomacromolecules 13(3) (2012) 798-804.
[276] C. Zhou, R. Chu, R. Wu, Q. Wu, Electrospun polyethylene oxide/cellulose nanocrystal composite nanofibrous mats with homogeneous and heterogeneous microstructures, Biomacromolecules 12(7) (2011) 2617-2625.
[277] J.V. Staros, R.W. Wright, D.M. Swingle, Enhancement by N-hydroxysulfosuccinimide of water-soluble carbodiimide-mediated coupling reactions, Analytical biochemistry 156(1) (1986) 220-222.
[278] G. Lu, L. Kong, B. Sheng, G. Wang, Y. Gong, X. Zhang, Degradation of covalently cross-linked carboxymethyl chitosan and its potential application for peripheral nerve regeneration, European Polymer Journal 43(9) (2007) 3807-3818.
[279] T. Asakura, R. Sugino, T. Okumura, Y. Nakazawa, The role of irregular unit, GAAS, on the secondary structure of Bombyx mori silk fibroin studied with 13C CP/MAS NMR and wide-angle X-ray scattering, Protein science 11(8) (2002) 1873-1877.
[280] M. Chai, M. Isa, The oleic acid composition effect on the carboxymethyl cellulose based biopolymer electrolyte, (2013).
[281] W. Ritcharoen, P. Supaphol, P. Pavasant, Development of polyelectrolyte multilayer-coated electrospun cellulose acetate fiber mat as composite membranes, European polymer journal 44(12) (2008) 3963-3968.
[282] H. Itagaki, M. Tokai, T. Kondo, Physical gelation process for cellulose whose hydroxyl groups are regioselectively substituted by fluorescent groups, Polymer 38(16) (1997) 4201-4205.
[283] S.-C. Wong, A. Baji, S. Leng, Effect of fiber diameter on tensile properties of electrospun poly (ε-caprolactone), Polymer 49(21) (2008) 4713-4722.

[284] N.R. Gandavarapu, D.L. Alge, K.S. Anseth, Osteogenic differentiation of human mesenchymal stem cells on α5 integrin binding peptide hydrogels is dependent on substrate elasticity, Biomaterials science 2(3) (2014) 352-361.
[285] A. Ranjan, T.J. Webster, Increased endothelial cell adhesion and elongation on micron-patterned nano-rough poly (dimethylsiloxane) films, Nanotechnology 20(30) (2009) 305102.
[286] A. Curtis, C. Wilkinson, Topographical control of cells, Biomaterials 18(24) (1997) 1573-1583.
[287] J.M. Goddard, J. Hotchkiss, Polymer surface modification for the attachment of bioactive compounds, Progress in polymer science 32(7) (2007) 698-725.
[288] Y.L. Cui, A. Di Qi, W.G. Liu, X.H. Wang, H. Wang, D.M. Ma, K. De Yao, Biomimetic surface modification of poly (L-lactic acid) with chitosan and its effects on articular chondrocytes in vitro, Biomaterials 24(21) (2003) 3859-3868.
[289] T. Groth, G. Altankov, Studies on cell-biomaterial interaction: role of tyrosine phosphorylation during fibroblast spreading on surfaces varying in wettability, Biomaterials 17(12) (1996) 1227-1234.
[290] G. Altankov, T. Groth, Reorganization of substratum-bound fibronectin on hydrophilic and hydrophobic materials is related to biocompatibility, Journal of Materials Science: Materials in Medicine 5(9-10) (1994) 732-737.
[291] P. Zahedi, I. Rezaeian, S.O. Ranaei-Siadat, S.H. Jafari, P. Supaphol, A review on wound dressings with an emphasis on electrospun nanofibrous polymeric bandages, Polymers for Advanced Technologies 21(2) (2010) 77-95.
[292] C. Wu, Y. Xiao, Evaluation of the in vitro bioactivity of bioceramics, Bone and Tissue Regeneration Insights 2 (2009) 25.
[293] S.K. Swain, D. Sarkar, Fabrication, bioactivity, in vitro cytotoxicity and cell viability of cryo-treated nanohydroxyapatite–gelatin–polyvinyl alcohol macroporous scaffold, Journal of Asian Ceramic Societies 2(3) (2014) 241-247.
[294] G.B. Schneider, A. English, M. Abraham, R. Zaharias, C. Stanford, J. Keller, The effect of hydrogel charge density on cell attachment, Biomaterials 25(15) (2004) 3023-3028.
[295] W.M. Hosny, A.K.A. Hadi, H. El-Saied, A.H. Basta, Metal chelates with some cellulose derivatives. Part III. Synthesis and structural chemistry of nickel (II) and copper (II) complexes with carboxymethyl cellulose, Polymer international 37(2) (1995) 93-96.
[296] T. Heinze, U. Heinze, The first approach to non-aqueous solutions of carboxymethylcellulose, Macromolecular rapid communications 18(12) (1997) 1033-1040.
[297] A. Salama, R.E. Abou-Zeid, M. El-Sakhawy, A. El-Gendy, Carboxymethyl cellulose/silica hybrids as templates for calcium phosphate biomimetic mineralization, International journal of biological macromolecules 74 (2015) 155-161.
[298] S. Agarwal, M. Burgard, A. Greiner, J. Wendorff, Electrospinning: A Practical Guide to Nanofibers, Walter de Gruyter GmbH & Co KG2016.

[299] S. Rungsiyanont, N. Dhanesuan, S. Swasdison, S. Kasugai, Evaluation of biomimetic scaffold of gelatin–hydroxyapatite crosslink as a novel scaffold for tissue engineering: Biocompatibility evaluation with human PDL fibroblasts, human mesenchymal stromal cells, and primary bone cells, Journal of biomaterials applications (2011) 0885328210391920.
[300] G. Stan, Adherent functional graded hydroxylapatite coatings produced by sputtering deposition techniques, Journal of optoelectronics and advanced materials 11(8) (2009) 1132-1138.
[301] H. Varma, S.S. Babu, Synthesis of calcium phosphate bioceramics by citrate gel pyrolysis method, Ceramics international 31(1) (2005) 109-114.
[302] Y. Greish, P. Brown, Chemically formed HAp-Ca poly (vinyl phosphonate) composites, Biomaterials 22(8) (2001) 807-816.
[303] N. Pramanik, D. Mishra, I. Banerjee, T.K. Maiti, P. Bhargava, P. Pramanik, Chemical synthesis, characterization, and biocompatibility study of hydroxyapatite/chitosan phosphate nanocomposite for bone tissue engineering applications, International journal of biomaterials 2009 (2009).
[304] A. El-Ghannam, P. Ducheyne, M. Risbud, C. Adams, I. Shapiro, D. Castner, S. Golledge, R. Composto, Model surfaces engineered with nanoscale roughness and RGD tripeptides promote osteoblast activity, Journal of Biomedical Materials Research Part A 68(4) (2004) 615-627.
[305] A.M. Martins, C.M. Alves, F.K. Kasper, A.G. Mikos, R.L. Reis, Responsive and in situ-forming chitosan scaffolds for bone tissue engineering applications: an overview of the last decade, Journal of Materials Chemistry 20(9) (2010) 1638-1645.
[306] X. Yuan, R. Tuan, Chondrogenic differentiation and functional maturation of bovine mesenchymal stem cells in long-term agarose culture, Osteoarthr. Cart 14(2) (2006) 179-189.
[307] T. Pirjali, N. Azarpira, M. Ayatollahi, M. Aghdaie, B. Geramizadeh, T. Talai, Isolation and characterization of human mesenchymal stem cells derived from human umbilical cord Wharton's jelly and amniotic membrane, International journal of organ transplantation medicine 4(3) (2013) 111.
[308] C.N. Salinas, K.S. Anseth, The enhancement of chondrogenic differentiation of human mesenchymal stem cells by enzymatically regulated RGD functionalities, Biomaterials 29(15) (2008) 2370-2377.
[309] Z. Li, H.R. Ramay, K.D. Hauch, D. Xiao, M. Zhang, Chitosan–alginate hybrid scaffolds for bone tissue engineering, Biomaterials 26(18) (2005) 3919-3928.
[310] I. Titushkin, M. Cho, Modulation of cellular mechanics during osteogenic differentiation of human mesenchymal stem cells, Biophysical journal 93(10) (2007) 3693-3702.
[311] C.G. Havens, A. Ho, N. Yoshioka, S.F. Dowdy, Regulation of late G1/S phase transition and APCCdh1 by reactive oxygen species, Molecular and cellular biology 26(12) (2006) 4701-4711.
[312] E. Arslan, M.O. Guler, A.B. Tekinay, Glycosaminoglycan-mimetic signals direct the osteo/chondrogenic differentiation of mesenchymal stem cells in a three-dimensional peptide nanofiber extracellular matrix mimetic environment, Biomacromolecules 17(4) (2016) 1280-1291.

[313] C. Bonnans, J. Chou, Z. Werb, Remodelling the extracellular matrix in development and disease, Nature reviews Molecular cell biology 15(12) (2014) 786-801.
[314] A.C. Allori, A.M. Sailon, S.M. Warren, Biological basis of bone formation, remodeling, and repair-part II: extracellular matrix, Tissue Engineering Part B: Reviews 14(3) (2008) 275-283.
[315] M. Akao, M. Sakatsume, H. Aoki, T. Takagi, S. Sasaki, In vitro mineralization in bovine tooth germ cell cultured with sintered hydroxyapatite, Journal of Materials Science: Materials in Medicine 4(6) (1993) 569-574.
[316] G.-J. Lai, K. Shalumon, J.-P. Chen, Response of human mesenchymal stem cells to intrafibrillar nanohydroxyapatite content and extrafibrillar nanohydroxyapatite in biomimetic chitosan/silk fibroin/nanohydroxyapatite nanofibrous membrane scaffolds, International journal of nanomedicine 10 (2015) 567.
[317] T. Komori, Regulation of osteoblast differentiation by transcription factors, Journal of cellular biochemistry 99(5) (2006) 1233-1239.
[318] M.B. Meyer, N.A. Benkusky, J.W. Pike, The RUNX2 Cistrome in Osteoblasts CHARACTERIZATION, DOWN-REGULATION FOLLOWING DIFFERENTIATION, AND RELATIONSHIP TO GENE EXPRESSION, Journal of Biological Chemistry 289(23) (2014) 16016-16031.
[319] L.L. Hench, Bioceramics, a clinical success, American Ceramic Society Bulletin 77(7) (1998) 67-74.
[320] A. Doostmohammadi, A. Monshi, R. Salehi, M.H. Fathi, Z. Golniya, A.U. Daniels, Bioactive glass nanoparticles with negative zeta potential, Ceramics International 37(7) (2011) 2311-2316.
[321] I.D. Xynos, A.J. Edgar, L.D. Buttery, L.L. Hench, J.M. Polak, Gene-expression profiling of human osteoblasts following treatment with the ionic products of Bioglass® 45S5 dissolution, Journal of biomedical materials research 55(2) (2001) 151-157.
[322] Z. Chen, T. Klein, R.Z. Murray, R. Crawford, J. Chang, C. Wu, Y. Xiao, Osteoimmunomodulation for the development of advanced bone biomaterials, Materials Today (2015).
[323] M.J. Dalby, N. Gadegaard, R. Tare, A. Andar, M.O. Riehle, P. Herzyk, C.D. Wilkinson, R.O. Oreffo, The control of human mesenchymal cell differentiation using nanoscale symmetry and disorder, Nature materials 6(12) (2007) 997-1003.
[324] M. Shi, Z. Chen, S. Farnaghi, T. Friis, X. Mao, Y. Xiao, C. Wu, Copper-doped mesoporous silica nanospheres, a promising immunomodulatory agent for inducing osteogenesis, Acta Biomaterialia 30 (2016) 334-344.
[325] S.N. Rath, A. Brandl, D. Hiller, A. Hoppe, U. Gbureck, R.E. Horch, A.R. Boccaccini, U. Kneser, Bioactive copper-doped glass scaffolds can stimulate endothelial cells in co-culture in combination with mesenchymal stem cells, PloS one 9(12) (2014) e113319.

[326] P. Sepulveda, J. Jones, L. Hench, In vitro dissolution of melt-derived 45S5 and sol-gel derived 58S bioactive glasses, Journal of biomedical materials research 61(2) (2002) 301-311.
[327] R. Li, A. Clark, L. Hench, An investigation of bioactive glass powders by sol-gel processing, Journal of Applied Biomaterials 2(4) (1991) 231-239.
[328] M. Yang, Y. Shuai, C. Zhang, Y. Chen, L. Zhu, C. Mao, H. OuYang, Biomimetic nucleation of hydroxyapatite crystals mediated by Antheraea pernyi silk sericin promotes osteogenic differentiation of human bone marrow derived mesenchymal stem cells, Biomacromolecules 15(4) (2014) 1185-1193.
[329] B. Lei, X. Chen, Y. Wang, N. Zhao, Synthesis and in vitro bioactivity of novel mesoporous hollow bioactive glass microspheres, Materials Letters 63(20) (2009) 1719-1721.
[330] C. Gao, T. Liu, C. Shuai, S. Peng, Enhancement mechanisms of graphene in nano-58S bioactive glass scaffold: mechanical and biological performance, Scientific reports 4 (2014).
[331] X. Chen, B. Lei, Y. Wang, N. Zhao, Morphological control and in vitro bioactivity of nanoscale bioactive glasses, Journal of Non-Crystalline Solids 355(13) (2009) 791-796.
[332] J.R. Jones, P.D. Lee, L.L. Hench, Hierarchical porous materials for tissue engineering, Philosophical Transactions of the Royal Society of London A: Mathematical, Physical and Engineering Sciences 364(1838) (2006) 263-281.
[333] J. Bejarano, P. Caviedes, H. Palza, Sol–gel synthesis and in vitro bioactivity of copper and zinc-doped silicate bioactive glasses and glass-ceramics, Biomedical Materials 10(2) (2015) 025001.
[334] Y.F. Goh, A.Z. Alshemary, M. Akram, A. Kadir, M. Rafiq, R. Hussain, Bioactive Glass: An In-Vitro Comparative Study of Doping with Nanoscale Copper and Silver Particles, International Journal of Applied Glass Science 5(3) (2014) 255-266.
[335] X. Yan, X. Huang, C. Yu, H. Deng, Y. Wang, Z. Zhang, S. Qiao, G. Lu, D. Zhao, The in-vitro bioactivity of mesoporous bioactive glasses, Biomaterials 27(18) (2006) 3396-3403.
[336] Q. Williams, E. Knittle, Infrared and Raman spectra of Ca 5 (PO 4) 3 F 2-fluorapatite at high pressures: compression-induced changes in phosphate site and Davydov splittings, Journal of Physics and Chemistry of Solids 57(4) (1996) 417-422.
[337] H. Aguiar, E. Solla, J. Serra, P. González, B. León, N. Almeida, S. Cachinho, E. Davim, R. Correia, J. Oliveira, Orthophosphate nanostructures in SiO 2–P 2 O 5–CaO–Na 2 O–MgO bioactive glasses, Journal of Non-Crystalline Solids 354(34) (2008) 4075-4080.
[338] Y. Li, J. Ho, C.P. Ooi, Antibacterial efficacy and cytotoxicity studies of copper (II) and titanium (IV) substituted hydroxyapatite nanoparticles, Materials Science and Engineering: C 30(8) (2010) 1137-1144.
[339] C.J. Grande, F.G. Torres, C.M. Gomez, M.C. Bañó, Nanocomposites of bacterial cellulose/hydroxyapatite for biomedical applications, Acta biomaterialia 5(5) (2009) 1605-1615.

[340] A. Hoppe, R. Meszaros, C. Stähli, S. Romeis, J. Schmidt, W. Peukert, B. Marelli, S.N. Nazhat, L. Wondraczek, J. Lao, In vitro reactivity of Cu doped 45S5 Bioglass® derived scaffolds for bone tissue engineering, Journal of Materials Chemistry B 1(41) (2013) 5659-5674.
[341] M.E. Frohbergh, A. Katsman, G.P. Botta, P. Lazarovici, C.L. Schauer, U.G. Wegst, P.I. Lelkes, Electrospun hydroxyapatite-containing chitosan nanofibers crosslinked with genipin for bone tissue engineering, Biomaterials 33(36) (2012) 9167-9178.
[342] S. Catledge, W. Clem, N. Shrikishen, S. Chowdhury, A. Stanishevsky, M. Koopman, Y. Vohra, An electrospun triphasic nanofibrous scaffold for bone tissue engineering, Biomedical Materials 2(2) (2007) 142.
[343] I. Wheeldon, A. Farhadi, A.G. Bick, E. Jabbari, A. Khademhosseini, Nanoscale tissue engineering: spatial control over cell-materials interactions, Nanotechnology 22(21) (2011) 212001.
[344] T. Cordonnier, J. Sohier, P. Rosset, P. Layrolle, Biomimetic materials for bone tissue engineering–state of the art and future trends, Advanced Engineering Materials 13(5) (2011) B135-B150.
[345] A. Tripathi, S. Saravanan, S. Pattnaik, A. Moorthi, N.C. Partridge, N. Selvamurugan, Bio-composite scaffolds containing chitosan/nano-hydroxyapatite/nano-copper–zinc for bone tissue engineering, International journal of biological macromolecules 50(1) (2012) 294-299.
[346] H. Yoshimoto, Y. Shin, H. Terai, J. Vacanti, A biodegradable nanofiber scaffold by electrospinning and its potential for bone tissue engineering, Biomaterials 24(12) (2003) 2077-2082.
[347] M. Kouhi, M. Morshed, J. Varshosaz, M.H. Fathi, Poly (ε-caprolactone) incorporated bioactive glass nanoparticles and simvastatin nanocomposite nanofibers: preparation, characterization and in vitro drug release for bone regeneration applications, Chemical engineering journal 228 (2013) 1057-1065.
[348] S. Talebian, M. Mehrali, S. Mohan, M. Mehrali, H.M. Khanlou, T. Kamarul, A.M. Afifi, A.A. Abass, Chitosan (PEO)/bioactive glass hybrid nanofibers for bone tissue engineering, RSC Adv. 4(90) (2014) 49144-49152.
[349] C. Ohtsuki, T. Kokubo, T. Yamamuro, Mechanism of apatite formation on CaO SiO 2 P 2 O 5 glasses in a simulated body fluid, Journal of Non-Crystalline Solids 143 (1992) 84-92.
[350] S. Talebian, M. Mehrali, S. Mohan, M. Mehrali, H.M. Khanlou, T. Kamarul, A.M. Afifi, A.A. Abass, Chitosan (PEO)/bioactive glass hybrid nanofibers for bone tissue engineering, Rsc Advances 4(90) (2014) 49144-49152.
[351] K. Rezwan, Q. Chen, J. Blaker, A.R. Boccaccini, Biodegradable and bioactive porous polymer/inorganic composite scaffolds for bone tissue engineering, Biomaterials 27(18) (2006) 3413-3431.
[352] I. Rajzer, Fabrication of bioactive polycaprolactone/hydroxyapatite scaffolds with final bilayer nano-/micro-fibrous structures for tissue engineering application, Journal of Materials Science 49(16) (2014) 5799-5807.

[353] M.C. Phipps, W.C. Clem, S.A. Catledge, Y. Xu, K.M. Hennessy, V. Thomas, M.J. Jablonsky, S. Chowdhury, A.V. Stanishevsky, Y.K. Vohra, Mesenchymal stem cell responses to bone-mimetic electrospun matrices composed of polycaprolactone, collagen I and nanoparticulate hydroxyapatite, PloS one 6(2) (2011) e16813.
[354] Y. Miyauchi, B. Ding, S. Shiratori, Fabrication of a silver-ragwort-leaf-like super-hydrophobic micro/nanoporous fibrous mat surface by electrospinning, Nanotechnology 17(20) (2006) 5151.
[355] J.H. Lee, N.G. Rim, H.S. Jung, H. Shin, Control of Osteogenic Differentiation and Mineralization of Human Mesenchymal Stem Cells on Composite Nanofibers Containing Poly [lactic-co-(glycolic acid)] and Hydroxyapatite, Macromolecular bioscience 10(2) (2010) 173-182.
[356] A. Polini, D. Pisignano, M. Parodi, R. Quarto, S. Scaglione, Osteoinduction of human mesenchymal stem cells by bioactive composite scaffolds without supplemental osteogenic growth factors, PloS one 6(10) (2011) e26211.
[357] T. Long, J. Yang, S.S. Shi, Y.P. Guo, Q.F. Ke, Z.A. Zhu, Fabrication of three-dimensional porous scaffold based on collagen fiber and bioglass for bone tissue engineering, Journal of Biomedical Materials Research Part B: Applied Biomaterials 103(7) (2015) 1455-1464.
[358] J. Song, E. Saiz, C.R. Bertozzi, Preparation of pHEMA–CP composites with high interfacial adhesion via template-driven mineralization, Journal of the European Ceramic Society 23(15) (2003) 2905-2919.
[359] M. Peter, P.T.S. Kumar, N.S. Binulal, S.V. Nair, H. Tamura, R. Jayakumar, Development of novel α-chitin/nanobioactive glass ceramic composite scaffolds for tissue engineering applications, Carbohydrate Polymers 78(4) (2009) 926-931.
[360] S. Ichinose, M. Tagami, T. Muneta, H. Mukohyama, I. Sekiya, Comparative sequential morphological analyses during in vitro chondrogenesis and osteogenesis of mesenchymal stem cells embedded in collagen gels, Medical molecular morphology 46(1) (2013) 24-33.
[361] W. Helen, J.E. Gough, Cell viability, proliferation and extracellular matrix production of human annulus fibrosus cells cultured within PDLLA/Bioglass® composite foam scaffolds in vitro, Acta Biomaterialia 4(2) (2008) 230-243.
[362] T. Komori, Regulation of osteoblast differentiation by Runx2, Osteoimmunology, Springer2009, pp. 43-49.
[363] J.B. Lian, G.S. Stein, Development of the osteoblast phenotype: molecular mechanisms mediating osteoblast growth and differentiation, The Iowa orthopaedic journal 15 (1995) 118.
[364] H. Wang, S. Zhao, J. Zhou, Y. Shen, W. Huang, C. Zhang, M.N. Rahaman, D. Wang, Evaluation of borate bioactive glass scaffolds as a controlled delivery system for copper ions in stimulating osteogenesis and angiogenesis in bone healing, Journal of Materials Chemistry B 2(48) (2014) 8547-8557.
[365] C. Gérard, L.-J. Bordeleau, J. Barralet, C.J. Doillon, The stimulation of angiogenesis and collagen deposition by copper, Biomaterials 31(5) (2010) 824-831.

[366] G.f. Hu, Copper stimulates proliferation of human endothelial cells under culture, Journal of cellular biochemistry 69(3) (1998) 326-335.
[367] A. Barradas, H. Yuan, C.A. Blitterswijk, P. Habibovic, Osteoinductive biomaterials: current knowledge of properties, experimental models and biological mechanisms, European cells & materials 21 (2011) 407-429.

Bhisham Narayan Singh is a PhD candidate in the Department of Biotechnology and Medical Engineering at National Institute of Technology Rourkela, India. He received his B.Tech (Biotechnology) in 2009 from Vellore Institute of Technology (VIT), Vellore, Tamilnadu (India). He joined NIT Rourkela in the year of 2009 and completed his M.Tech (Biotechnology) in 2011. He started his Ph.D in NIT Rourkela in the year of 2012. His interests include biomaterials processing and application for bone and cartilage tissue engineering, nanotechnology and stem cell research for efficient and improved tissue regeneration.

Personal Details:

Father's Name	Mr. Ram Prabin Singh
Mother's Name	Mrs. Bas Devi
Date of Birth	30th March, 1984
Gender	Male
Nationality	Indian
Language Known	English, Hindi
Permanent Address	S/O Ram Prabin Singh Village- Garahtha Khurd Dist- Buxar, 802112 Bihar, India
E.Mail:	bhisham6@gmail.com

JOURNAL PUBLICATIONS

Published:

1. Singh, B., Panda, N., Mund, R., & Pramanik, K. (2016). Carboxymethyl cellulose enables silk fibroin nanofibrous scaffold with enhanced biomimetic potential for bone tissue engineering application. Carbohydrate Polymers 151 (2016) 335–347.

2. Singh, B., Panda, N., & Pramanik, K. (2016). A novel electrospinning approach to fabricate high strength aqueous silk fibroin nanofibers. International Journal of Biological Macromolecules 87 (2016) 201–207.

Under Review:

Singh, B., & Pramanik, K. Development of an engineered tissue construct from nano-bioglass loaded biomimetic composite scaffold and mesenchymal stem cells for bone tissue engineering. *Scientific report*.

Conference proceeding:

1. B. N. Singh and K. Pramanik, Isolation and Characterization of Mesenchymal Stem Cell from Umbilical Cord Blood for Tissue Engineering Application. International Journal of Biological Sciences and Engineering ISSN 0976-1519, Vol. 02, No 01 - Spl issue, April 2011, pp. 25-29.

2. B. N. Singh, P. Manjhi, K. Pramanik, "Fabrication and characterization of Chitosan Nanofibers for tissue engineering applications", Proceedings of Emerging issues in Chitin and Chitosan Research, Institute of Himalayan Bioresource Technology, Palampur June 7-8 2013

3. B. N. Singh and K. Pramanik, "A Novel Approach To Fabricate Aqueous Silk Fibroin Based Nanofibrous Mats With Enhanced Mechanical Properties" in International conference on Biomaterial, Biodignostics, Tissue Engineering, Drug Delivery and Regenerative Medicine" April 15-17 2016 at IIT Delhi, India